

The Electronic Structure and Spectroscopy of
Diarylidene – Cycloalkanones and Their Protonated
Cations

by
Mine Gunes Ucak-Astarlioglu

A Dissertation Submitted to the Faculty of the WORCESTER POLYTECHNIC
INSTITUTE in partial fulfillment of the requirements for the
Degree of Doctor of Philosophy in Chemistry

by

May 2003

Approved

Professor Robert E. Connors, Advisor
Worcester Polytechnic Institute

Professor William D. Hobey
Worcester Polytechnic Institute

Professor W. Grant McGimpsey
Worcester Polytechnic Institute

Professor Harry A. Frank
University of Connecticut

ABSTRACT

A series of 2,5-diarylidene-cyclopentanones (ndbcp), their protonated cations (ndbcp- H^+), and a substituted compound, 2,5-bis-[3-(4-dimethylamino-phenyl)-allylidene-cyclopentanone (2dbma) have been synthesized. Their electronic absorption and fluorescence spectra have been measured. The absorption spectra have been assigned with the aid of INDO/S calculations. Molecular structures used for the INDO/S calculations were computed with the PM3 Hamiltonian. Polarized excitation spectra have been measured for 2dbcp and 3dbcp at 77 K in ethanol/methanol glass and used as an aid for the assignments of electronic transitions. Absorption and fluorescence spectra have been measured in solvents of varying polarity for all compounds synthesized. The influence of hydrogen bonding on the excitation spectra of compounds has been investigated. Solvent induced shifts in the absorption and fluorescence spectra of 3dbcp and 2dbma in combination with the PM3 calculated ground state dipole moment have been used to determine the excited state dipole moment of these compounds. Fluorescence quantum yields have been obtained to analyze the changes in the nonradiative rate of decay from S_1 . The protonated cations have been prepared in acids of different strength. The influence of acid strength on the excitation and emission spectra has been analyzed by gradually diluting acid solution. Evidence for excited state proton transfer in weak acids has been obtained for 2dbcp and 3dbcp. Brief photochemical studies of 1dbcp and 1dbcp- H^+ have been carried out and analyzed by HPLC.

ACKNOWLEDGEMENTS

"Study of The Electronic Structure and Spectroscopy of Diarylidene-Cycloalknones and
Their Protonated Cations"
Ph.D. thesis by Mine Gunes Ucak-Astarlioglu, dedicated

To My family, committee members, and friends

TABLE OF CONTENTS

ABSTRACT.....	i
ACKNOWLEDGEMENTS.....	ii
LIST OF FIGURES.....	v
LIST OF TABLES.....	ix
1 INTRODUCTION.....	1
1.1 Introduction.....	1
1.2 Objective and Scope.....	3
1.3 Thesis Layout.....	4
2 LITERATURE REVIEW.....	6
2.1 Introduction.....	6
2.2 Review of Applications, Electronic and Spectroscopic Properties of Arylpolyene Ketones.....	6
2.3 Review of Electronic Properties of Linear Polyenes.....	17
2.4 Review of Electronic and Spectroscopic Properties of Polyene Aldehydes.....	20
2.5 Solvent Effects on Ground and Excited State Properties.....	26
2.5.1 General Effects of the Solvent.....	26
2.5.2 Electronic State Dipole Moment Calculation - Lippert Plots.....	30
2.5.3 Electronic State Acidity – Forster Cycle.....	31
3 EXPERIMENTAL.....	34
3.1 Synthesis of Compounds.....	34
3.1.1 RuCl ₃ Catalyzed Aldol Condensation of Aldehydes and Ketones to Synthesize Diarylidene-Cycloalkanones ³³	35
3.1.2 Synthesis of Dimethylamino Substituted Polyene Ketones.....	39
3.1.3 Synthesis of 2,5-Bis-(5-phenyl-penta-2,4-dienylidene)-cyclopentanone.....	42
3.1.4 Synthesis of 2,5-dibenzylidene-cyclopent-3-enone.....	46
3.1.5 General Procedures for Purification and Characterization.....	50
3.2 Spectroscopic Measurement.....	50
3.2.1 Quantum Yield Calculation.....	52
3.2.2 Extinction Coefficient Calculation.....	53
3.2.3 Polarized Excitation Spectra.....	54
3.3 Preparation of Protonated Cations.....	54
3.3.1 Investigation of Reversibility of Protonation/ Deprotonation.....	57
3.3.2 Photochemistry of 1dbcp and 1dbcp-H ⁺ Protonated Cation.....	57
3.4 HPLC Analysis.....	57
3.5 Computational Studies.....	58
4 RESULTS AND DISCUSSION.....	60
4.1 Section 1: Electronic Absorption and Fluorescence Properties of 2,5-Diarylidene-cyclopentanones.....	60
4.1.1 Introduction.....	60
4.1.2 PM3 Optimized Geometries.....	60
4.1.3 Absorption Spectra and INDO/S Calculations.....	70
4.1.4 Fluorescence Properties.....	88
4.1.5 Additional Spectral Data.....	107
4.1.6 Summary.....	113

4.2	Section 2: Ground and Excited State Properties in Acidic Media : Excited State Proton Transfer for 2,5-Diarylidene-Cyclopentanones.....	115
4.2.1	Introduction.....	115
4.2.2	Spectroscopic Investigations in Acidic Media.....	115
4.2.3	PM3 Optimized Geometries of Protonated Cations.....	134
4.2.4	Absorption Spectra and INDO/S Calculations	136
4.2.5	Photochemistry Studies of 1dbcp and 1dbcp-H ⁺	161
4.2.6	Summary	163
4.3	Section 3: Absorption and Fluorescence Properties of 2,5-bis-[3-(4-dimethylamino-phenyl)-allylidene-cyclopentanone	168
4.3.1	Introduction.....	168
4.3.2	Absorption Properties	168
4.3.3	Fluorescence Properties	169
4.3.4	Summary	182
5	SUMMARY AND RECOMMENDATIONS FOR FUTURE WORK	183
5.1	Summary	183
5.2	Recommendation for Future Research.....	185
5.2.1	Experimental Investigations of Lifetimes.....	185
5.2.2	Photochemistry Study	188
5.2.3	Optimized Geometry of 2dbma	188
	REFERENCES	189
	APPENDIX.....	192

LIST OF FIGURES

Figure 1: (a) Structure of 2,5-diarylidene-cyclopentanones (abbreviated as ndbcp), (b) protonated cations of 2,5-diarylidene-cyclopentanones (abbreviated as ndbcp-H ⁺), (c) 2,5-bis-[3-(4-dimethylamino-phenyl)-allylidene-cyclopentanone (abbreviated as 2dbma).	2
Figure 2: Polyene ketones studied in the literature.	8
Figure 3: Probe solvation process. ²	15
Figure 4: Formation of probable alcohol-probe complexes. ²	16
Figure 5: Linear polyene p atomic orbitals. ¹⁶	18
Figure 6: Absorption, fluorescence, and fluorescence excitation spectra of decatetraenal in (a) ethanol/methanol glass, (b) trifluoroethanol (TFE), and (c) hexafluoroisopropanol (HFIP) at 10K. ²⁷	24
Figure 7: Decatetraenal/ HFIP alcohol fluorescence and fluorescence excitation as a function of temperature. ²⁷	25
Figure 8: Jablonski diagram for fluorescence with solvent relaxation. ²⁹	28
Figure 9: The effect of solvent polarity on the order of (π , π^*) and (n , π^*) states. ²⁸	29
Figure 10: Forster Cycle. Electronic energy levels of an acid (BH ⁺) and its conjugate base (B) in the ground and excited states. ²⁹	33
Figure 11: Synthesis of unsubstituted compounds. ³³	36
Figure 12: Synthesis of 2,5-bis-[3-(4-dimethylamino-phenyl)-allylidene-cyclopentanone (2dbma). ³⁴	40
Figure 13: a) Synthesis of 5-phenyl-penta-2,4-dienal ³⁵ and b) 2,5-Bis-(5-phenyl-penta-2,4-dienylidene)-cyclopentanone (3dbcp).	43
Figure 14: Synthesis of 2,5-dibenzylidene-cyclopent-3-enone (1dbcp u). ³⁶	49
Figure 15: Emission spectrometer (adapted V. Chynwat Ph D thesis ³⁷).	51
Figure 16: The protonated cations of arylpolyene ketones.	56
Figure 17: Molecular structures of 1dbcp, 2dbcp, and 3dbcp.	62
Figure 18: Optimized geometry of 1dbcp ($\Delta H_f = 35.78$ kcal/mol).	63
Figure 19: Optimized geometry of 2dbcp ($\Delta H_f = 62.05$ kcal/mol).	66
Figure 20: Optimized geometry of 3dbcp ($\Delta H_f = 89.85$ kcal/mol).	68
Figure 21: Room temperature absorption spectra of 1dbcp in cyclohexane and INDO/S-CIS calculated results. The diamond on the wavelength axis indicates the computed location of the forbidden $^1A_2 \leftarrow ^1A_1$ transition.	73
Figure 22: Room temperature absorption spectra of 2dbcp in cyclohexane and INDO/S-CIS calculated results. The diamond on the wavelength axis indicates the computed location of the forbidden $^1A_2 \leftarrow ^1A_1$ transition.	74
Figure 23: Room temperature absorption spectra of 3dbcp in cyclohexane and INDO/S-CIS calculated results. The diamond on the wavelength axis indicates the computed location of the forbidden $^1A_2 \leftarrow ^1A_1$ transition.	75
Figure 24: Absorption (dashed line), excitation (left), and fluorescence (right) spectra of 2dbcp in alcohols: (a) 1-octanol ($\lambda_{Ex\ max}: 431$ nm); (b) 1-butanol ($\lambda_{Ex\ max}: 428$ nm); (c) 1-propanol ($\lambda_{Ex\ max}: 430$ nm); (d) ethanol ($\lambda_{Ex\ max}: 420$ nm); (e) methanol ($\lambda_{Ex\ max}: 416$ nm); (f) TFE ($\lambda_{Ex\ max}: 430$ nm); (g) HFIP ($\lambda_{Ex\ max}: 434$ nm).	97

Figure 25: Absorption (dashed line), excitation (left), and fluorescence (right) spectra of 3dbcp in alcohols: (a) 1-octanol ($\lambda_{\text{Ex max}}$: 452 nm); (b) 1-butanol ($\lambda_{\text{Ex max}}$: 450 nm); (c) 1-propanol ($\lambda_{\text{Ex max}}$: 445 nm); (d) ethanol ($\lambda_{\text{Ex max}}$: 445 nm); (e) methanol ($\lambda_{\text{Ex max}}$: 451 nm); (f) TFE ($\lambda_{\text{Ex max}}$: 464 nm); (g) HFIP ($\lambda_{\text{Ex max}}$: 477 nm).	98
Figure 26: Absorption (dashed line), excitation (left), and fluorescence (right) spectra and fluorescence quantum yield as a function of excitation wavelength for 2dbcp in methanol (multiple excitation from 340 nm to 460 nm with increments of 20 nm).....	99
Figure 27: Absorption (dashed line), excitation (left), and fluorescence (right) spectra of 3dbcp in various solvents I: (a) acetonitrile ($\lambda_{\text{Ex max}}$: 434 nm); (b) acetone ($\lambda_{\text{Ex max}}$: 435 nm); (c) dichloromethane ($\lambda_{\text{Ex max}}$: 447 nm); (d) pyridine ($\lambda_{\text{Ex max}}$: 449 nm); (e) ethyl acetate ($\lambda_{\text{Ex max}}$: 425 nm); (f) ether ($\lambda_{\text{Ex max}}$: 409 nm).....	100
Figure 28: Absorption (dashed line), excitation (left), and fluorescence (right) spectra of 3dbcp in various solvents II: (g) chloroform ($\lambda_{\text{Ex max}}$: 450 nm); (h) carbon tetrachloride ($\lambda_{\text{Ex max}}$: 427 nm); (i) toluene ($\lambda_{\text{Ex max}}$: 445 nm); (j) benzene ($\lambda_{\text{Ex max}}$: 480 nm); (k) carbon disulfide ($\lambda_{\text{Ex max}}$: 443 nm).	101
Figure 29: Plot of (a) absorption frequency; (b) fluorescence frequency; (c) Stokes' shift against solvent orientation polarization of 3dbcp. Open symbols for protic solvents; solid symbols for aprotic solvents.	102
Figure 30: Fluorescence quantum yield of 3dbcp in different solvents plotted against the frequency of fluorescence.	103
Figure 31: (a) Fluorescence, fluorescence excitation, and polarized excitation spectra of 2dbcp in ethanol/methanol (4:1) glass at 77 K ($\lambda_{\text{Ex max}}$: 460 nm) (b) Fluorescence, fluorescence excitation, and polarized excitation spectra of 3dbcp in ethanol/methanol (4:1) glass at 77 K ($\lambda_{\text{Ex max}}$: 470 nm).....	104
Figure 32: Absorption spectra of 1dbcp_u in solvents: (a) cyclohexane; (b) acetonitrile; (c) methanol.	109
Figure 33: Absorption spectra of 1dbcp in solvents: (a) cyclohexane; (b) acetonitrile, and (c) methanol.	110
Figure 34: Absorption spectra of 2dbcp spectra in solvents: (a) cyclohexane; (c) acetonitrile, and (c) methanol.	111
Figure 35: Absorption (dashed line), excitation (left), and fluorescence (right) spectra of (a) 2dbcp ($\lambda_{\text{Ex max}}$: 415 nm) and (b) 3dbcp in acetic acid ($\lambda_{\text{Ex max}}$: 455 nm).	122
Figure 36: Titration study of 2dbcp in acetic acid: absorption (dashed line), fluorescence, and fluorescence excitation spectra (solid lines): (a) pH=1.8 and (b) pH=2.5 (in each case, excitation wavelengths: 415 nm).	123
Figure 37: Titration study of 2dbcp in sulfuric acid: absorption (dashed line), fluorescence, and fluorescence excitation spectra (solid lines): (a) pH=96%; (b) pH=1; (c) pH=1.4; and (d) pH=1.6 (in each case, excitation wavelengths: 580 and 430 nm).....	124
Figure 38: Absorption (dashed line), fluorescence, and fluorescence excitation spectra of (a) 1dbcp-H ⁺ ($\lambda_{\text{Ex max}}$: 475 nm) and (b) 2dbcp-H ⁺ in sulfuric acid ($\lambda_{\text{Ex max}}$: 580 nm) and (c) 3dbcp-H ⁺ ($\lambda_{\text{Ex max}}$: 660 nm) in sulfuric acid/acetic acid (1:3) mixture.	125
Figure 39: Absorption (dashed line), fluorescence, and fluorescence excitation spectra (solid lines) of 2dbcp in solvents: (a) methanol; (b) acetic acid; and (c) sulfuric acid... ..	126
Figure 40: Absorption (dashed line), fluorescence, and fluorescence excitation spectra (solid lines) 3dbcp in solvents: (a) methanol; (b) acetic acid; and (c) sulfuric acid.	127

Figure 41: Fluorescence and fluorescence excitation spectra (solid lines) of 2dbcp in (a) acetic and (b) deuterated acetic acid (in each case, excitation wavelength: 415 nm).....	128
Figure 42: Fluorescence and fluorescence excitation spectra (solid lines) of 3dbcp in (a) acetic and (b) deuterated acetic acid (in each case, excitation wavelength: 455 nm).....	129
Figure 43: Concentration study of 2dbcp in acetic acid (concentrations from top to bottom: 4.79×10^{-4} M, 2.39×10^{-4} M, 1.20×10^{-4} M, 5.99×10^{-5} M).....	130
Figure 44: Fluorescence and fluorescence excitation spectra of (a) 2dbcp ($\lambda_{\text{EX max}}$: 430 nm) and (b) 3dbcp in acetic acid ($\lambda_{\text{EX max}}$: 455 nm) at 77K.....	131
Figure 45: Fluorescence and fluorescence excitation spectra of (a) 1dbcp-H ⁺ ($\lambda_{\text{EX max}}$: 505 nm) and (b) 2bcp-H ⁺ in sulfuric acid ($\lambda_{\text{EX max}}$: 585 nm) and (c) 3dbcp-H ⁺ in sulfuric/ acetic acid mixture (1:3) ($\lambda_{\text{EX max}}$: 630 nm) at 77K.	132
Figure 46: Optimized geometry of 1dbcp-H ⁺ ($\Delta H_f = 196.71$ kcal/mol).	138
Figure 47: Optimized geometry of 2dbcp-H ⁺ ($\Delta H_f = 217.55$ kcal/mol).	140
Figure 48: Optimized geometry of 3dbcp-H ⁺ ($\Delta H_f = 243.35$ kcal/mol).	142
Figure 49: Three-dimensional optimized geometry of 1dbcp and 1dbcp-H ⁺	144
Figure 50: Three-dimensional optimized geometry of 2dbcp and 2dbcp-H ⁺	145
Figure 51: Atomic charges of 1dbcp and 1dbcp-H ⁺	146
Figure 52: Bond lengths of 1dbcp and 1dbcp-H ⁺	147
Figure 53: Bond orders of 1dbcp and 1dbcp-H ⁺	148
Figure 54: Resonance structures of 1dbcp-H ⁺	149
Figure 55: Room temperature absorption spectra of 1dbcp-H ⁺ in sulfuric acid and INDO/S-CIS calculated results.	150
Figure 56: Room temperature absorption spectra of 2bcp-H ⁺ in sulfuric acid and INDO/S-CIS calculated results.	151
Figure 57: Room temperature absorption spectra of 3dbcp-H ⁺ in sulfuric acid/ acetic acid (1:3) and INDO/S-CIS calculated results.	152
Figure 58: LUMO, HOMO, and HOMO-1 for 3dbcp-H ⁺ as calculated by INDO/S.....	153
Figure 59: HPLC of 1dbcp in THF: (a) 0 and (b) 5 min irradiation.	164
Figure 60: HPLC of 1dbcp-H ⁺ in THF: (a) 0 and (b) 5 min irradiation.	166
Figure 61: Absorption spectra of 2dbma in various solvents: (a) 2,2,2_trifluoroethanol; (b) methanol; (c) n_butanol; (d) 1,2_dichlorobenzene; (e) acetonitrile; (f) ether; (g) cyclohexane.....	173
Figure 62: Absorption (dashed line), fluorescence, and fluorescence excitation spectra (solid lines) of 2dbma in alcohols: (a) 2,2,2_trifluoroethanol ($\lambda_{\text{EX max}}$: 535 nm); (b) methanol ($\lambda_{\text{EX max}}$: 525 nm); (c) ethanol ($\lambda_{\text{EX max}}$: 510 nm); (d) isopropanol ($\lambda_{\text{EX max}}$: 510 nm); (e) n_propanol ($\lambda_{\text{EX max}}$: 515 nm); (f) n_butanol ($\lambda_{\text{EX max}}$: 515 nm).....	174
Figure 63: Absorption (dashed line), fluorescence, and fluorescence excitation spectra (solid lines) of 2dbma in solvents I: (a) acetonitrile ($\lambda_{\text{EX max}}$: 478 nm); (b) acetone ($\lambda_{\text{EX max}}$: 475 nm); (c) n,n_dimethylformamide ($\lambda_{\text{EX max}}$: 507 nm); (d) dimethyl sulfoxide ($\lambda_{\text{EX max}}$: 515 nm); (e) pyridine ($\lambda_{\text{EX max}}$: 506 nm); (f) ethyl acetate ($\lambda_{\text{EX max}}$: 480 nm).	175
Figure 64: Absorption (dashed line), fluorescence, and fluorescence excitation spectra (solid lines) of 2dbma in solvents II: (g) 1,2_dichlorobenzene ($\lambda_{\text{EX max}}$: 505 nm); (h) ether ($\lambda_{\text{EX max}}$: 475 nm); (i) carbon tetrachloride ($\lambda_{\text{EX max}}$: 470 nm); (j) benzene ($\lambda_{\text{EX max}}$: 474 nm); (k) hexane ($\lambda_{\text{EX max}}$: 480 nm); (l) carbon disulfide ($\lambda_{\text{EX max}}$: 480 nm).	176

Figure 65: Fluorescence and fluorescence excitation spectra of 2dbma in ethanol/methanol (4:1) ($\lambda_{\text{Ex max}}$: 580 nm) at 77K.....	177
Figure 66: 2dbma plot of (a) absorption frequency, (b) fluorescence frequency, (c) Stokes' shift against solvent orientation polarization. Open symbols for protic solvents, solid symbols for aprotic polar solvents, and semi-filled symbols for nonpolar solvents.	180
Figure 67: Fluorescence quantum yield of 2dbma plotted against orientation polarization. The solvents used are shown by the numbers: 1) Acetone, 2) ACN, 3) N,N_dimethylformamide, 4) DMSO, 5) CH ₂ Cl ₂ , 6) pyridine, 7) ethyl acetate, 8) 1,2_dichloro benzene, 9) ether, 10) CHCl ₃ , 11) toluene, 12) CCl ₄ , 13) benzene, 14) heptane, 15) hexane, 16) cyclohexane, 17) CS ₂ , 18) TFE, 19) MeOH, 20) EtOH, 21) isopropanol, 22) n_propanol, 23) n_butanol.....	181
Figure 68: Schematic for time-correlated single photon counting. ²⁹	187

LIST OF TABLES

Table 1 Maximum Absorption Wavelengths Reported for 1dbcp, 1dbch, 2dbcp, and 2dbch. ^{14,15}	10
Table 2 ¹ H_NMR, ¹³ C_NMR, and IR Data for 1dbcp, 2dbcp, 1dbch, and 2dbch.....	38
Table 3 ¹ H_NMR, ¹³ C_NMR, and IR data for 2dbma.....	41
Table 4 ¹ H_NMR, ¹³ C_NMR, and IR data for 3dbcp.....	45
Table 5 ¹ H_NMR, ¹³ C_NMR, and IR data for 1dbcp_u.....	47
Table 6 Calculated and Experimental Geometry of 1dbcp.....	64
Table 7 Calculated Ground State Equilibrium Geometry of 1dbcp by PM3 Method.	65
Table 8 Calculated Ground State Equilibrium Geometry of 2dbcp by PM3 Method.	67
Table 9 Calculated Ground State Equilibrium Geometry of 3dbcp by PM3 Method.	69
Table 10 INDO/S Energies (eV) and Symmetries of MO's Important in Configuration Interaction (CI) for 1dbcp.	76
Table 11 INDO/S-CIS Computed Singlet State Excitations for 1dbcp.....	77
Table 12 INDO/S Energies (eV) and Symmetries of MO's Important in Configuration Interaction (CI) for 2dbcp.	79
Table 13 INDO/S-CIS Computed Singlet State Excitations for 2dbcp.....	80
Table 14 INDO/S Energies (eV) and Symmetries of MO's Important in Configuration Interaction (CI) for 3dbcp.	82
Table 15 INDO/S-CIS Computed Singlet State Excitations for 3dbcp.....	83
Table 16 Absorption Spectral Data for 1dbcp, 2dbcp, and 3dbcp in Cyclohexane at Room Temperature and INDO/S Calculated Results.....	86
Table 17 Extinction Coefficients of Compounds in Cyclohexane and Methanol.	87
Table 18 Alcohol Acidity.....	96
Table 19 Absorption, Excitation, and Fluorescence Spectral Data and Fluorescence Quantum Yields for 2dbcp in Alcohols.	105
Table 20 Absorption and Fluorescence Spectral Data and Fluorescence Quantum Yields for 3dbcp.....	106
Table 21 Maximum Absorption Energy of Compounds in Various Solvents.....	112
Table 22 Properties of 2,5-diarylidene Cyclopentanones in Acidic Media and Differences in the Electronic State Acidities in Acetic Acid at Room Temperature.	133
Table 23 Calculated Ground State Equilibrium Geometry of 1dbcp-H ⁺ by PM3 Method.	139
Table 24 Calculated Ground State Equilibrium Geometry of 2dbcp-H ⁺ by PM3 Method.	141
Table 25 Calculated Ground State Equilibrium Geometry of 3dbcp-H ⁺ by PM3 Method.	143
Table 26 INDO/S-CIS Computed Singlet State Excitations for 1dbcp-H ⁺	154
Table 27 INDO/S-CIS Computed Singlet State Excitations for 2dbcp-H ⁺	156
Table 28 INDO/S-CIS Computed Singlet State Excitations for 3dbcp-H ⁺	158
Table 29 2dbma Absorption and Fluorescence Characteristics in Various Solvents and Solvent Polarity Functions.....	178

1 INTRODUCTION

1.1 Introduction

Substituted and unsubstituted 2,5-diarylidene-cyclopentanones (Figure 1), a class of diarylpolyene ketones, have received recent attention for potential applications in a variety of areas. These include use as photosensitizers and photopolymer imagers¹, solvent polarity probes^{2,3}, fluoroionophores⁴, and nonlinear optical materials.⁵ In addition, interesting photodimerization reactions that have implications for crystal engineering have been reported for crystalline 2,5-dibenzylidene-cyclopentanone (R = H, n = 1, Figure 1).⁶⁻¹⁰ Despite the considerable interest in applications related to their photoexcited state properties, little has been reported¹¹⁻¹³ describing the electronic structure and spectroscopy of these molecules.^{14,15}

This thesis reports the electronic structure, absorption and luminescence properties of the molecules represented in Figure 1. The focus of this research is on the all-E configurations of the unsubstituted parent compounds (R = H) with n = 1, 2, and 3: 2,5-dibenzylidene-cyclopentanone (1dbc), 2,5-bis-(3-phenyl-allylidene)-cyclopentanone (2dbc), and 2,5-bis-(5-phenyl-penta-2,4-dienylidene)-cyclopentanone (3dbc) (see Figure 1). The combination of aryl, carbonyl, and polyene chromophores presents an interesting challenge for molecular orbital methods to provide insight as to the nature of the spectral transitions. Any discussion of the electronic structure and spectroscopy of molecules containing polyene chains brings to mind the considerable body of work regarding the relative location of the symmetry forbidden 2^1A_g state (under C_{2h} symmetry) and the strongly allowed 1^1B_u state.^{16,17} Comparison with previous work on polyene aldehydes and ketones will be given where pertinent throughout the thesis.

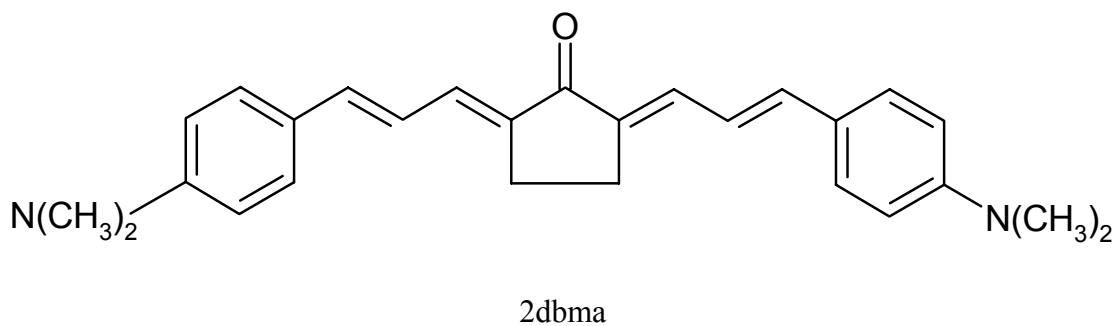
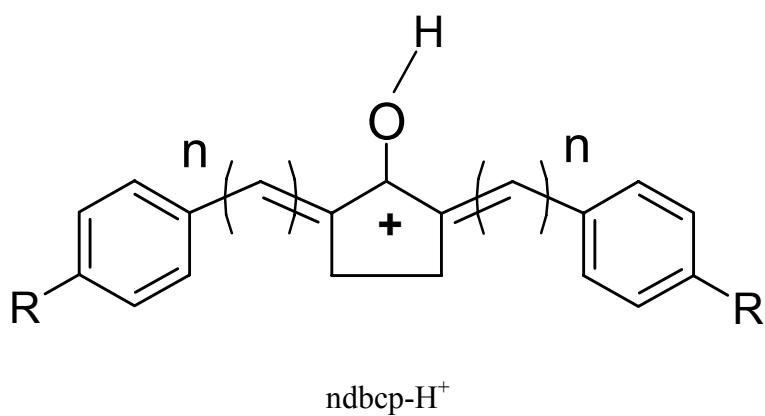
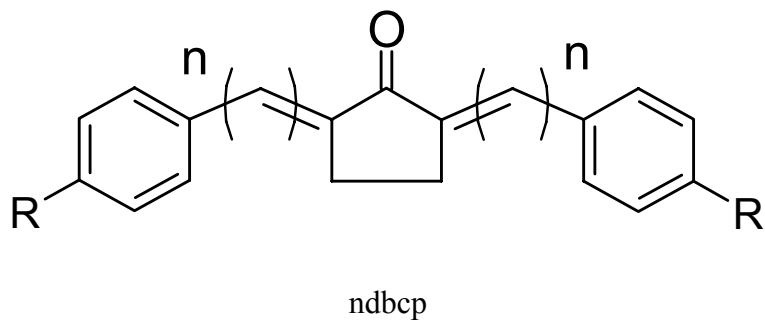


Figure 1: (a) Structure of 2,5-diarylidene-cyclopentanones (abbreviated as ndbcp), (b) protonated cations of 2,5-diarylidene-cyclopentanones (abbreviated as ndbcp-H⁺), (c) 2,5-bis-[3-(4-dimethylamino-phenyl)-allylidene]-cyclopentanone (abbreviated as 2dbma).

1.2 Objective and Scope

The electronic spectroscopy and excited state dynamics of polyene and polyene aldehydes have been the subjects of numerous studies. The reasons for this attention can be attributed to the development of molecular orbital theory, distinctive photochemistry of these compounds (cis-trans photoisomerization), and the important roles polyenes play in photobiology (such as, vision, photosynthesis).^{16,18,19}

The studies conducted to date explore polyene and polyene aldehyde chemistry using many experimental techniques and theoretical models. However, there has been little reported on the optical properties of polyene ketones. In this study, the spectroscopic and electronic properties of a class of arylpolyene ketones will be investigated. This study will bring a new perspective to polyene chemistry with the investigation of polyene ketones with higher symmetry than those previously studied. The objective will be achieved within the following scope.

1. To determine electronic and spectroscopic properties of a class of arylpolyene ketones.
2. To analyze hydrogen-bonding effects on the low lying electronic states of these arylpolyene ketones.
3. To investigate the influence of polyene length on electronic and spectroscopic properties of the arylpolyene ketones.
4. To investigate the effect of substituted electron donating groups on the aryl units of the polyene ketones.

1.3 Thesis Layout

This thesis on “the electronic structure and spectroscopy of diarylidene-cycloalkanones and their protonated cations” is divided into five sections. The objective and scope of this study are presented in Chapter 1.

A review of literature is presented in four main sections in Chapter 2. First section starts with an introduction to the limited number of studies presented in the literature on spectroscopic and electronic behaviors of unsubstituted and substituted aryl polyene ketone compounds. The reviews concentrated are the most relevant compounds to the ones studied in this research. Second section presents a review of electronic properties of linear polyenes, ever since their characteristic electronic state symmetries are applicable throughout polyene chemistry. Third section concentrates on a review of the electronic and spectroscopic properties of polyene aldehydes due to their applicability of some of the results presented in Chapter 4. Fourth section gives a review on the effects of solvent in the ground and excited state properties of the compounds. This section also describes the methods to determine the differences in ground and excited state dipole moments and acidities.

Chapter 3 starts with an introduction of syntheses applied to obtain targeted compounds along with characterization techniques. In the continuation of this Chapter, spectroscopic and computational methods used are presented.

Chapter 4 presents the results and discussion of the findings. This chapter investigates the electronic and spectroscopic properties of the compounds in three sections: in the first section, 2,5-diarylidene- cyclopentanone; in the second section,

protonated cations of 2,5-diarylidene-cyclopentanones; and in the third section 2,5-bis-[3-(4-dimethylamino-phenyl)-allylidene-cyclopentanone.

Finally, Chapter 5 summarizes the major conclusions reached and recommendations for future research.

2 LITERATURE REVIEW

2.1 Introduction

In the literature, polyene and polyene aldehyde chemistry has been the subject of numerous studies; whereas, there has been little reported on the optical properties of polyene ketones.

In this Chapter, firstly a review will be given on the spectroscopic and electronic properties of arylpolyene ketones, which are closely related to the molecules of this research. Secondly, a brief review will be given on linear polyene electronic properties; since, their electronic state symmetries are being used throughout polyene chemistry. Thirdly, polyene aldehyde electronic and spectroscopic properties will be briefly investigated due to their applicability to the results found in this research, as will be later discussed in Chapter 4. Finally, a review will be given in determining the differences of ground and excited state dipole moments and acidities.

2.2 Review of Applications, Electronic and Spectroscopic Properties of Arylpolyene Ketones

The applications of the arylpolyene ketones studied throughout this research will not be discussed in detail, since it is not within the scope of this thesis. Briefly, these compounds with electron donor amino and acceptor carbonyl groups at different ends of a conjugated π -system cause long wavelength emission and show spectral sensitivity towards environment.²⁰ Such arylpolyene ketones derived from ketocyanine dyes (such as, organic amino-carbonyl compounds) have been reported to function as solvent polarity probes, laser dyes or photosensitizers, and non linear optical materials.^{21,22}

Employing crown-ether group containing ketocyanine dyes, optical metal sensing, such as; metal ion concentrations, and membrane surface potential can be determined which have implications in biological, ecological, and medical fields. These ketocyanine dyes with crown-ether groups exhibit spectral properties that change dramatically in the presence of certain metal ions.⁴ Upon binding with a metal ion the dye symmetry is broken, which induces a change in the UV - Visible spectrum, and as a result dye can be used as a sensor for cation analysis in solution.²³ These groups, lead to a considerable charge separation upon excitation with a subsequently increased dipole moment in the excited state.⁴ A limited number of ketocyanine dyes containing two electron donating groups and a single acceptor group on the same conjugated system have been reported to have distinctive solvatochromic properties in both absorption and emission.³

In the rest of this section, a brief literature overview will be given to summarize the spectral properties of the compounds that are shown in Figure 2.

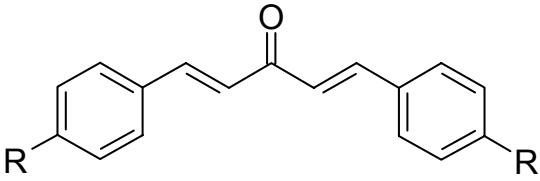
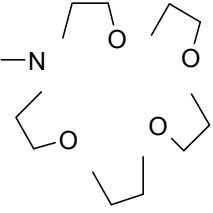
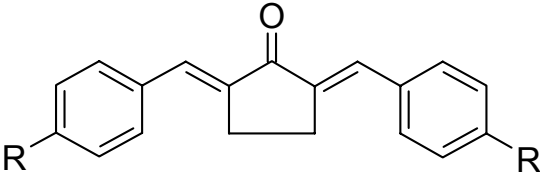
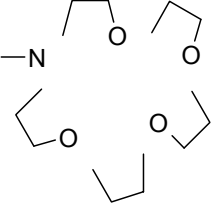
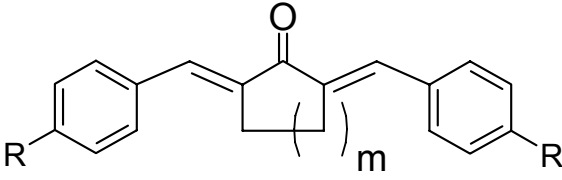
 <p>I) bis-amino-dibenzylidene-acetone</p>	<p>a) $R = N(CH_3)_2$ b) $R = N(C_2H_5)_2$ c) $R =$</p> 
 <p>II) bis-amino-dibenzylidene-ketone</p>	<p>a) $R = N(CH_3)_2$ b) $R = N(C_2H_5)_2$ c) $R = (\text{aza-15-crown-5})$</p> 
 <p>III) bis-amino-dibenzylidene-cycloalkanone</p>	<p>a) $R = H, m = 5 - 10$ b) $R = N(CH_3)_2, m=1$</p>

Figure 2: Polyene ketones studied in the literature.

Farrell and Read studied unsubstituted bis-dibenzylidene-cycloalkanone compounds from $m = 5$ to 10, where m is the number of carbon atoms in the cycloalkanone ring.¹⁵ They reported a shift of an intense long wavelength transition to shorter wavelength as m increases. This finding was attributed to a twisting of part of the conjugated system (decreasing planarity) with increasing ring size, so that effective conjugation extends over only one-half of the compound. Issa et al, also reported electronic absorption spectra of some diarylidenecyclopentanones and diarylidene cyclohexanones.¹⁴ It was found that the cyclopentanone derivatives absorb at longer wavelength compared to cyclohexanones. Farrell and Read reported the maximum absorption wavelengths of 1dbcp, 1dbch, 2dbcp, and 2dbch in n -hexane; whereas, Issa et al reported 1dbcp and 1dbch in a number of solvents other than n -hexane as presented in Table 1.^{14,15} The assignments for the absorption spectra were for a longer wavelength band, π - π^* intramolecular charge transfer and for shorter wavelength band π - π^* centered on the aromatic system. The charge transfer assignment was based on the high extinction coefficient and broad absorption band. This band red shifted with increasing solvent polarity, and going from cyclohexanone to cyclopentanone derivatives. An overall shift towards red was observed in the absorption spectra with electron donor substituents, whereas a blue shift was observed with electron acceptor substituents for both the cyclopentanone and cyclohexanone derivatives.¹⁴

Table 1 Maximum Absorption Wavelengths Reported for 1dbcp, 1dbch, 2dbcp, and 2dbch.^{14,15}

Compound	Property	Solvents				
		CCl ₄	CHCl ₃	Ether	Ethanol	*n Hexane
1dbcp	λ_{\max} (nm)	343	350	230, 338	230, 354	337
	ϵ (M ⁻¹ cm ⁻¹)	41,700	35,900	23,900, 46,500	16,600, 43,800	32,000
1dbch	λ_{\max} (nm)	332	322	230, 320	230, 330	315
	ϵ (M ⁻¹ cm ⁻¹)	37,300	24,500	19,400, 36,200	6,600, 9,400	25,000
2dbcp	λ_{\max} (nm)	-	-	-	-	380
	ϵ (M ⁻¹ cm ⁻¹)	-	-	-	-	58,000
2dbch	λ_{\max} (nm)	-	-	-	-	369
	ϵ (M ⁻¹ cm ⁻¹)	-	-	-	-	58,000

* shows n_{hexane} results taken from Farrell and Read.¹⁵

In a study by Marcotte and Ferry-Forgues, diethyl amino substituted compounds of Figure 2, I-b and II-b were studied in a number of polar and apolar solvents. I-b was found to have a twisted structure with rotamers of cis, cis (11 %) and cis, trans (89%) in solution; whereas, II-b has pure cis, cis conformer.²⁰ In another paper, by Barnabas¹ on II-b, similar findings to Marcotte paper were reported.²⁰ In both papers a structured intense long wavelength band was found between 400 and 500 nm in nonpolar solvents. This structured band disappeared in polar solvents due to the dipole dipole interaction of intramolecular charge transfer transition (ICT) originating from the electron donor amino groups to the electron acceptor carbonyl group. This ICT band was found to shift towards the red with increasing solvent polarity and acidity. This finding indicates a less stabilized ground state compared to excited state in polar solvents, resulting in a lower energy gap. Absorption transition of π - π^* at 275 nm was assigned to be a characteristic transition of aromatic ketones, which did not shift much with changing solvent polarity. A n - π^* transition was assumed to be buried in the ICT band, since ICT band and n - π^* lie close to each other and appears to be a shoulder in the absorption spectra. In various solvents, absorption maxima of II-b were found to be higher than I-b and interpreted due to the planarity of II-b, which makes π -electron delocalization easier. In apolar solvents both molecules exhibited vibronic structure; however, absorption spectra of II-b showed a more defined vibronic structure compared to I-b due to its higher rigidity.²⁰

A lack of agreement was found between the absorption and excitation spectra of I-b. This finding of I-b was attributed to the presence of both rotamers in the absorption spectrum; whereas only the cis, cis rotamer appears in the excitation spectrum. Rigid compound, II-b exhibited a perfectly superimposed absorption and excitation spectrum,

since it only has cis-cis structure in both ground and excited states. Each molecule displayed an intense emission band in a number of solvents due to pure cis, cis structure of II-b and cis, cis rotamer of I-b. In general, absorption and emission spectra were found to be strongly dependent on solvent acidity. In the same apolar solvents, both compounds exhibited the same maximum emission wavelength, however, with increasing solvent polarity a widening occurred between the emission spectra of the two compounds. In the same protic solvents, I-b was found more sensitive to solvent polarity in the excited state; which yielded to the conclusion of the lesser rigidity of the compound the higher sensitivity to the solvent. In general, the two amino groups of I-b and II-b transfer their charge to the carbonyl group making it as a negative pole and thus maintain strongly localized charges in their excited states.²⁰

Using solvatochromic shifts (absorption and emission) the excited state dipole moment was calculated for II-b and found to be 14D. The ground state dipole moment was calculated from PC Model calculations, to be 5D. Quantum yield values were calculated with increasing solvent polarity among hydrocarbons and apolar solvents and fell in a range of 0.005-0.290 from cyclohexane to acetonitrile, respectively. However, in protic solvents, an opposite trend was observed with increasing solvent polarity, indicating a different nature of the emitting state in alcohols compared to other solvents.²⁰ The crown group substituted derivative, I-c, shows a blue shifted absorption spectrum compared to the diethyl amino substituted derivative, I-b (maximum absorption bands are at 446 nm for I-b and at 438 nm for I-c), as reported in Marcotte paper.²³ The blue shift observed in the absorption spectra of I-c compared to I-b was explained to be due to decreased donor strength of the nitrogen atom in addition to the electron-withdrawing

effect of the crown oxygen atoms. The transitions of I-c were similar to the ones assigned for I-b and II-b derivatives; π - π^* transition at 262 nm with a weak intensity and a charge transfer band at 438 nm.

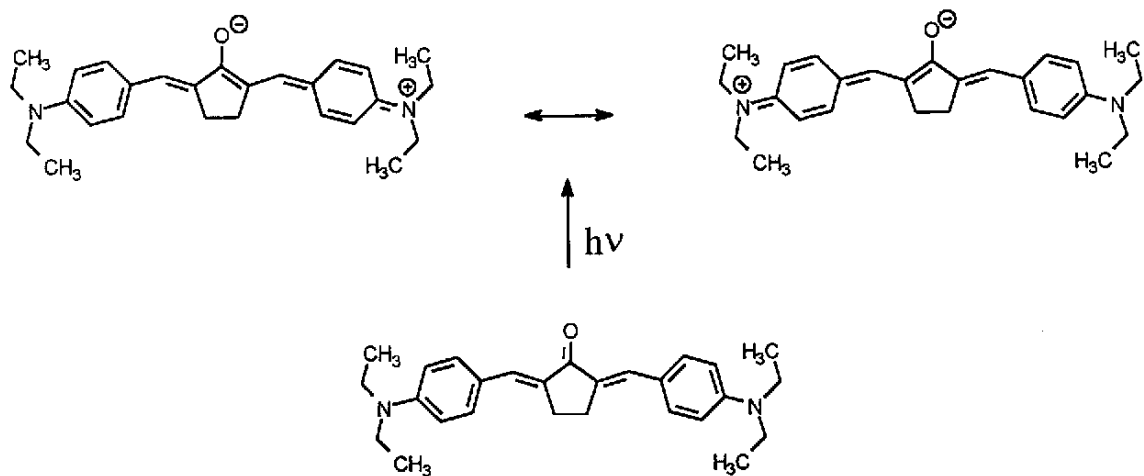
In a paper by Demchenko² compounds of Figure 2 II-a, c were studied as polarity probes due to their high quantum yield and solvent sensitive fluorescence spectra. II-a and II-c were studied in binary mixtures of solvents (nonpolar, toluene-and polar, alcohols) that differ in polarity and hydrogen bonding ability. At low alcohol concentrations, besides the common solvent effects, such as band shift with increased polarity; new, well resolved discrete bands were observed in the fluorescence spectra, indicating 1:1 and 1:2 hydrogen bonded complexes of II-a and II-c with alcohols. This finding indicates that in hydrophobic media it is possible to detect small amounts of protic polar molecules. At high alcohol concentrations, II-a and II-c make specific complex with alcohol molecules and as a result gradual shifts in the spectra with varying intensities were observed. II-a was also investigated in a paper by Das.³ Study was conducted in n-hexane/ ethanol (1:1) solvent mixture and a ground state complex formation was found due to the hydrogen bonding interaction of the solute and alcohol. Increasing solvent polarity was found to cause a red shift in the fluorescence spectra because of an increase in the dipole moment upon excitation.

The probe molecule can have a redistribution of electronic density upon excitation, which can form new interactions in the excited state and cause reorganization of the hydrogen bonds existing in the ground state.² To identify if preexisting ground state complexes were giving rise to fluorescence bands, excitation spectra were measured by monitoring emission at the maximum of fluorescence bands. Unlike the excitation

spectra in pure solvents, the probes were found to depend on emission wavelength. This was explained to be due to an equilibrium, which takes place relatively slowly between the excited state of the dye and its dielectric environment. In neat solvents, dielectric relaxations, rotations of solvent dipoles, can occur 10^{-10} - 10^{-12} s. In a mixed solvent, preferential solvation by a polar component requires translational diffusion of proton donor molecules in 10^{-9} s. As a result, in the ground state, preexisting probe-alcohol complexes were found with the observation of a new band in the excitation spectrum and a dramatic Stokes' shift. Considering the findings observed with titration in binary solvents with increasing alcohol concentration, four spectral emissive forms were found and a probe solvation process was proposed as shown in Figure 3.² According to this proposal; initially, upon electronic excitation, charge transfer takes place and makes the carbonyl oxygen more basic compared to its ground state form (Figure 3-a).

Subsequently, vibrational relaxation occurs in Frank Condon S_1 state and molecules break hydrogen bonds with solvent molecules. Followed by relaxation, the highly basic carbonyl group binds with an alcohol molecule (Figure 3-b).² In Figure 14, formation of probable alcohol-probe complexes is shown. These alcohol-probe complexes have different level of carbonyl oxygen interaction; therefore it was assumed that the emission band positions should vary.

In the next section, a brief review will be given on linear polyene electronic properties; due to their characteristic electronic state symmetries that are being used throughout polyene chemistry.

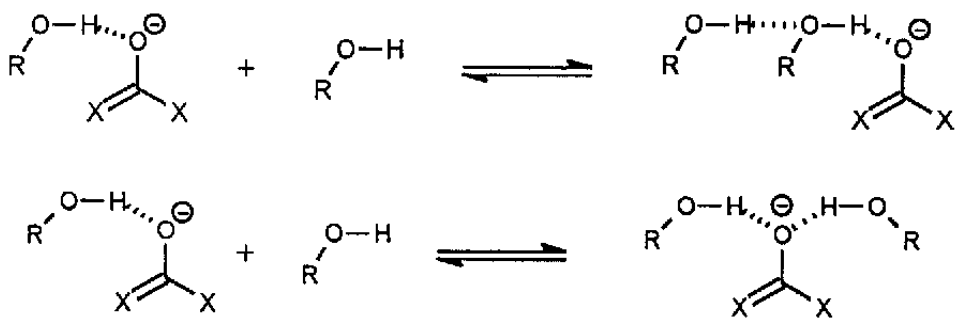


a) charge transfer upon electronic excitation (top level: resonance structure of S_1) making carbonyl oxygen more basic compared to its ground state form.

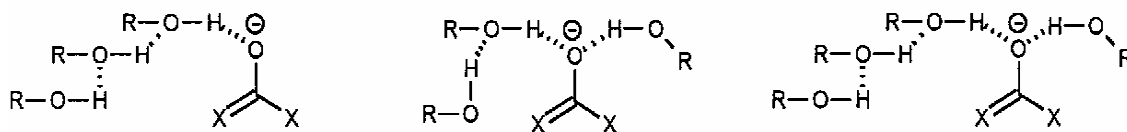


b) followed by relaxation, highly basic carbonyl group binds with an alcohol molecule

Figure 3: Probe solvation process.²



a) Probable organization of ketocyanine-alcohol complex (1:2)



b) Probable organization of ketocyanine-alcohol complex (1:3, 1:4)

Figure 4: Formation of probable alcohol-probe complexes.²

2.3 Review of Electronic Properties of Linear Polyenes

Polyenes are linear conjugated chains of carbon atoms joined by alternating double and single bonds. The carbon atoms in the polyene are sp^2 hybridized. The hybrid orbitals along with hydrogen 1s orbitals provide bonding molecular orbitals of sigma symmetry. The remaining electrons (one π electron per carbon atom) can move freely in the $2p\pi$ system as shown in Figure 5.¹⁶ The delocalization of π -electrons along this backbone gives polyenes their characteristic optical spectra, which are largely responsible for photophysical and photochemical responses of these molecules including cis - trans isomerization.¹⁶

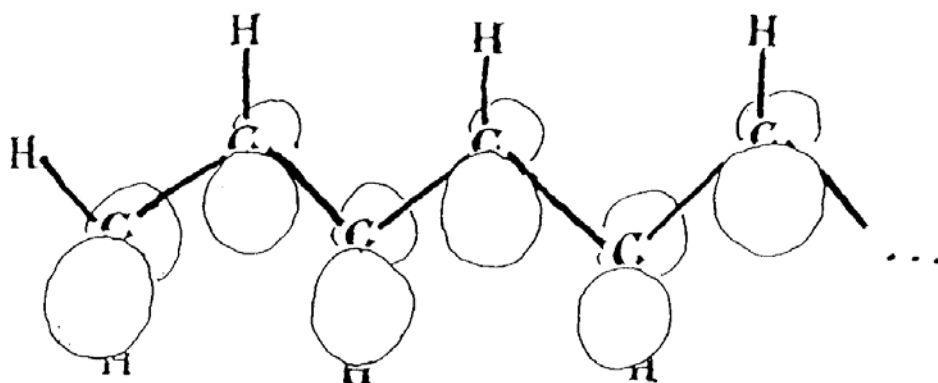


Figure 5: Linear polyene p atomic orbitals.¹⁶

The motion of π electrons conforms to the symmetry properties of the polyenes, and is classified according to how they transform under C_{2h} . A classification is made depending on whether the orbitals change sign under inversion at the symmetry center or under 180° rotation around the symmetry axis. The symmetry labeling is shown as follows ¹⁶:

u and g \rightarrow Inversion

b and a \rightarrow Rotation

2p orbitals change sign under reflection in the symmetry plane, therefore, the character of π electron orbitals is restricted to two symmetry classes: a_u and b_g . The symmetry character of p electron orbitals alternate between a_u and b_g when ordered with respect to increase in energy starting with a_u . Since, the general formula for a polyene hydrocarbon is C_nH_{2n+2} and $2n\pi$ electrons, where n shows the number of double bonds. The overall symmetry of $2n\pi$ electron states is determined from the multiplication rules for the C_{2h} group as follows:

$$a \times a = b \times b = a \qquad g \times g = u \times u = g$$

$$a \times b = b \times a = b \qquad g \times u = u \times g = u$$

According to these rules, π electron states have either A_g or B_u symmetry. Here, $2n$ electron states are shown with capital A and B. If excitations involve σ electrons or Rydberg orbitals, electronic states may also assume A_u and B_g symmetry. The ground state for octatetraene has A_g symmetry, since the π electron molecular orbitals are all doubly occupied. Promoting one electron from the highest occupied molecular orbital (HOMO) to the lowest unoccupied molecular orbital (LUMO) leads to an excited state symmetry of B_u . The selection rules for C_{2h} symmetry is as follows:

One-photon	$A_g \rightarrow B_u$	Allowed
absorption	$A_g \rightarrow A_g$	Forbidden
Two-photon	$A_g \rightarrow A_g$	Allowed
absorption	$A_g \rightarrow B_u$	Forbidden

Studies have shown that S_1 is B_u for shorter polyenes but that the A_g state drops in energy faster than does B_u as the polyene chain length increases. As a result, the forbidden A_g state is found to be S_1 for longer polyenes (four or more conjugate double bonds).¹⁶

In the next section, a review on the electronic and spectroscopic properties of polyene aldehydes will be given due to their applicability of some of the results obtained in this research and further discussed in Chapter 4.

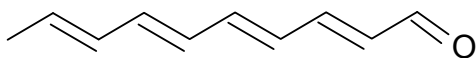
2.4 Review of Electronic and Spectroscopic Properties of Polyene Aldehydes

Previous studies have shown the excited energy states of polyene aldehydes as summarized below^{24,25} :

Energy State Order	Number of Double Bonds
$E(^1n\pi^*) < E(^1\pi\pi^*)$	≤ 3
$E(^1n\pi^*) \cong E(^1\pi\pi^*)$	$= 4$
$E(^1\pi\pi^*) < E(^1n\pi^*)$	> 5 , fluorescence even in nonhydrogen-bonded solvents

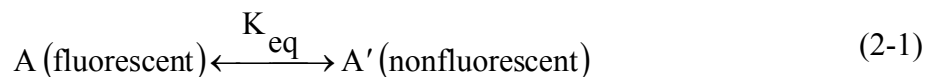
Due to the complexity of computational and experimental investigations of naturally occurring polyenes, model systems with similar but simpler chromophores and

analogous photochemical behaviors are investigated in the literature.²⁶ In this section the spectroscopic findings and accurate location of electronic origins of decatetraenal (as shown below) will be summarized due to their applicability to the results found in this research.²⁷



In dry hydrocarbon glasses well-resolved absorption spectra were obtained for decatetraenal and no emission was observed. Additions of hydrogen bonding solvent to the hydrocarbon resulted in emission and broader absorption spectra. However, the lack of the correspondence of the absorption and the fluorescence excitation spectra, and the dependence of excitation wavelength on fluorescence suggested a complicated equilibrium between emitting and non-emitting species. Furthermore, low-lying $n\pi^*$ states were found to cause a hindered spectroscopy of polyene aldehydes by spectral broadening and reduced or eliminated fluorescence. Therefore, to identify excited state energy levels, similar to their analogous hydrocarbons, spectral studies of decatetraenal were performed in alcohols with pK_a values ranging from 4.7 to 17.0.²⁷ Figure 6 shows the absorption, fluorescence, and fluorescence excitation spectra of decatetraenal in 10K, in a) ethanol/methanol glass (Et/Me) ($pK_a=15$), b) trifluoroethanol (TFE) ($pK_a=12.4$), and c) hexafluoroisopropanol (HFIP) ($pK_a=9.3$). In all three alcohols, fluorescence was observed at 380 nm, excitation was monitored at 500nm. As seen from Figure 6-a, there is a lack of agreement between the absorption and the fluorescence excitation spectra due to a significant fraction of decatetraenal remaining non-emitting in Et/Me. Parts b) and c) show that when the solvents are stronger hydrogen-bonders the absorption and the excitation spectra are found in good agreement with an indication of a much higher

fraction of emitting species relative to part a). These differences brought up the equilibrium below:



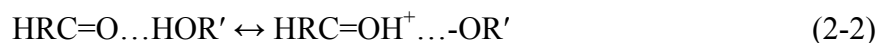
As seen from Figure 6, in the hydrogen-bonded complexes the low-lying $n\pi^*$ states are shifted above low-lying $\pi\pi^*$ states resulting in fluorescence spectra. Thus, free aldehydes (non-hydrogen-bonded) stay as the dominant non-fluorescing group and have $n\pi^*$ as the lowest energy excited state.²⁷

Stronger hydrogen-bonders complete inversion of $n\pi^*$ / $\pi\pi^*$ state ordering as similar to their analogues hydrocarbons. This effect of strong hydrogen-bonders in the spectra can be explained due to the oxygen electron density: increasing electron density results in a shift to the red ($\pi\pi^*$) and decreasing electron density results in a blue shift ($n\pi^*$) by weakening or breaking the hydrogen bond in such a way that the energy is unaffected by the hydrogen bond.²⁷

Figure 7 shows that the fluorescence and fluorescence excitation spectra of decatetraenal in HFIP as a function of temperature. It was observed that the spectra do not change for a given hydrogen-bonder with changing temperature, while, decreasing temperature leads to an increase in the net fluorescence yield. At 10K, HFIP and TFE alcohols had four to five times higher fluorescence intensity than Et/Me alcohol showing that the net fluorescence yield of decatetraenal is sensitive to the hydrogen bonder. However, the highest fluorescence intensity is found to be at lower temperatures (< 77K). Thus, the fluorescence intensities observed can be divided into two²⁷:

1. High temperature ($T > 77\text{K}$) (non-emitting), in weaker hydrogen bonding systems, complicated mixture of hydrogen-bonded and free polyene aldehyde species exist.
2. Low temperature ($T < 77\text{K}$) (emitting), the equilibrium between a hydrogen-bonded adduct and a protonated adduct does not require a significant geometry change and could occur in a low temperature matrix.

The suggested equilibrium for hydrogen-bonded and a protonated complex is shown in Eq. (2-2). If all the fluorescent species are protonated a similar fluorescence spectra should be observed with in three alcohol solvents (HFIP, Et/Me, TFE). Small differences may arise in the fluorescence maxima due to the association of proton with alcohol anion.



According to calculations, ionic 1^1B_u excited state is found to have sufficient electron density on carbonyl oxygen to compete for the alcohol protons. Thus, $1^1\text{n}\pi^* < 2^1\text{A}_g < 1^1\text{B}_u$ energy state order in free aldehyde would be reversed and protonation would take place from $\pi\pi^*$ lowest excited state.²⁷

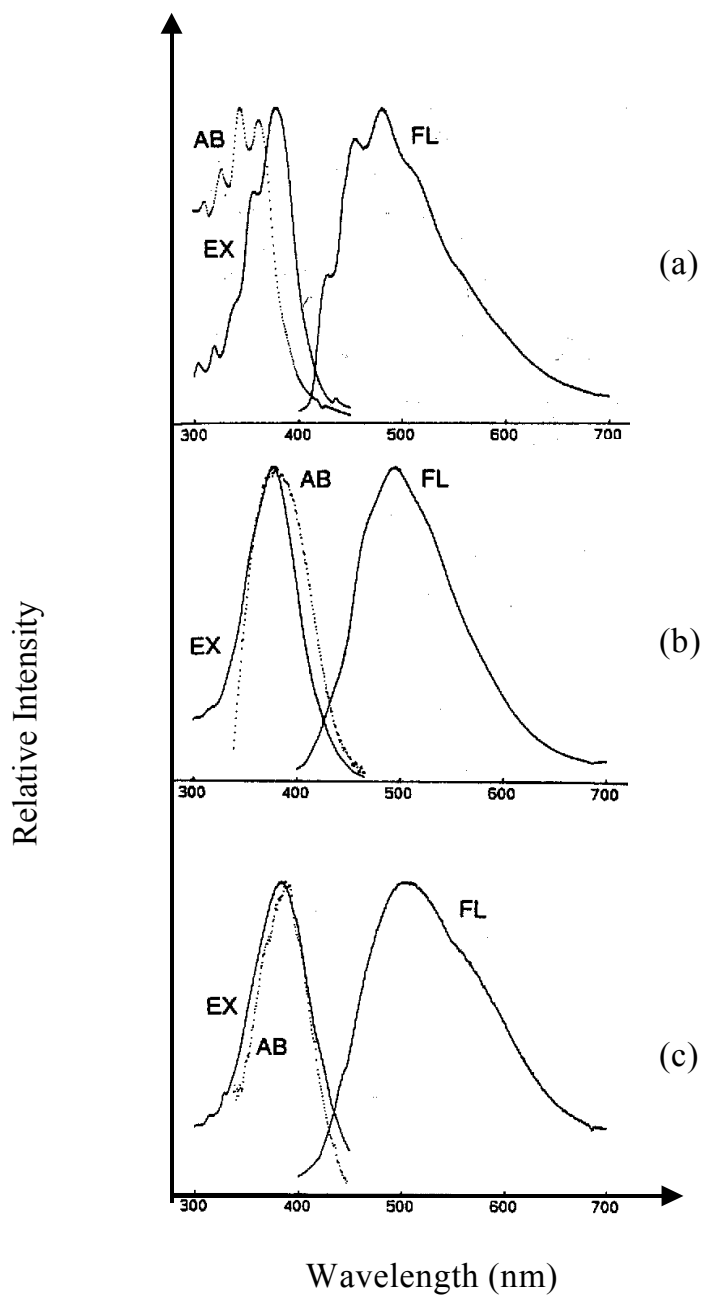


Figure 6: Absorption, fluorescence, and fluorescence excitation spectra of decatetraenal in (a) ethanol/methanol glass, (b) trifluoroethanol (TFE), and (c) hexafluoroisopropanol (HFIP) at 10K.²⁷

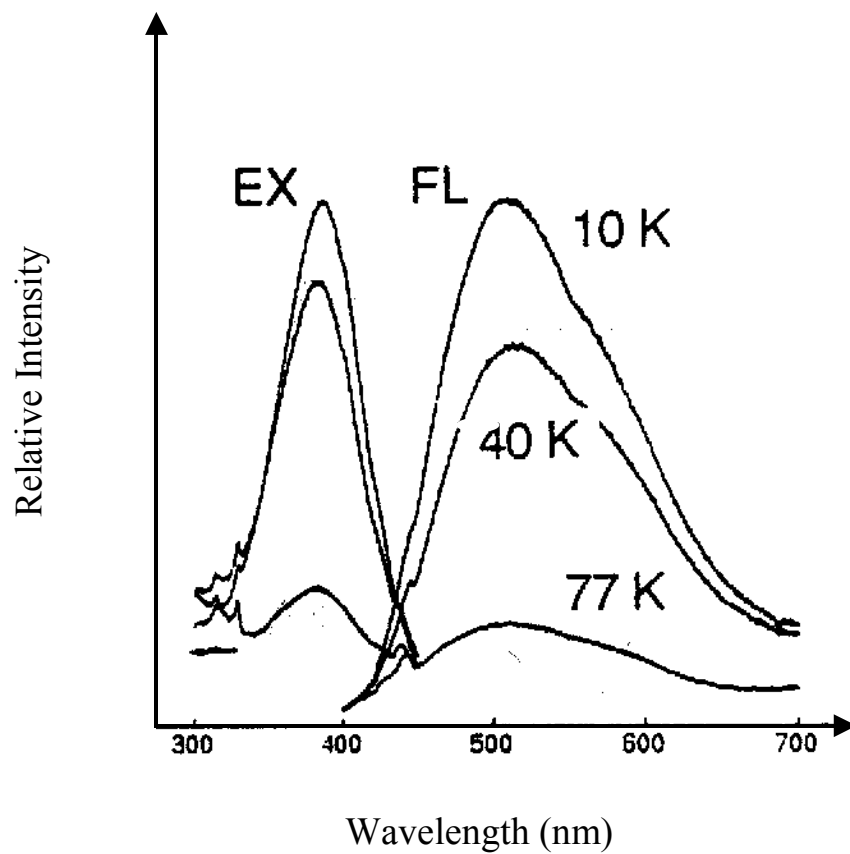


Figure 7: Decatetraenal/ HFIP alcohol fluorescence and fluorescence excitation as a function of temperature.²⁷

2.5 Solvent Effects on Ground and Excited State Properties

2.5.1 General Effects of the Solvent

In solvents of increasing polarity, a solute with an excited state that is more polar than the ground state is stabilized in the excited state better than a solute with a less polar excited state. A red shift is observed in the electronic absorption spectrum of a solute with an excited state that is more polar than the ground state in solvents of increasing polarity. Solvent molecules are organized in such a way to surround the solute to minimize the total free energy of the system in the ground state. Upon electronic excitation, the excited solute may have a different charge distribution than the ground state. The Franck-Condon principle states that nuclei do not move during an electronic transition, 10^{-15} s. However, the solvent molecules can redistribute and orient themselves around the new excited state dipole during the lifetime of the excited state prior to emission. Therefore, a red shift or Stoke's shift is generally observed between the origin of absorption and the origin of fluorescence.²⁸

In Figure 8, a Jablonski diagram of fluorescence with solvent relaxation is shown.²⁹ As Kasha's rule specifies, fluorescence takes place from the lowest excited singlet state. This state (S_1) may have excess vibrational energy. This vibrational energy can rapidly dissipate to the solvent. If S_2 is excited, an internal conversion takes place and decays to S_1 within 10^{-12} s. According to Kasha's rule, deactivation of higher lying excited states take place through the lowest excited electronic states such as, S_1 and T_1 , in general. However, there are some instances, anomalous emission (violation of Kasha's rule) is observed from higher lying excited states rather than the lowest excited energy states. These cases may arise due to decreased internal conversion rates as a result of

weaker Frank Condon factor for radiationless transitions (eg. in azulene a large energy gap exists between S_2 and S_1).¹⁹

In many fluorophores, where an electron donor and an acceptor group exist (for example amino and carbonyl) the excited state has a larger dipole moment than the ground state. Increasing solvent polarity causes even a greater dipole moment difference between the two states. Sometimes the polarity of a solvent not only stabilizes the excited state but also governs the nature of the excited state that is the lowest energy. For example S_1 may be: 1) in a polar solvent, a species with charge separation (internal charge transfer state, ICT) and 2) in a nonpolar solvent, a species with no charge separation (locally excited state, LE).²⁹ The dipole moment of a carbonyl molecule is predicted to decrease when excited to an $n\pi^*$ state. It is well established that polar solvents cause a small shift towards the red (bathochromic shift) for $\pi \rightarrow \pi^*$ transitions and a shift towards the blue (hypsochromic shift) for $n \rightarrow \pi^*$ transitions.²⁸ The blue shift for $n \rightarrow \pi^*$ is greatest in protic solvents. In cases where $\pi\pi^*$ and $n\pi^*$ states have similar energies, changing solvent polarity may invert the order of energy states as shown in Figure 9.

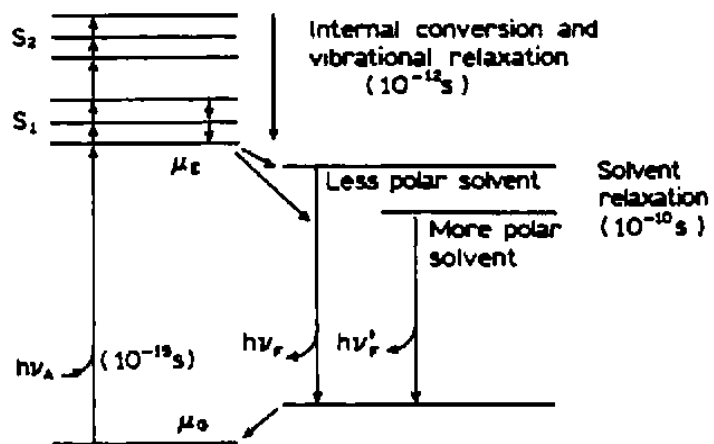


Figure 8: Jablonski diagram for fluorescence with solvent relaxation.²⁹

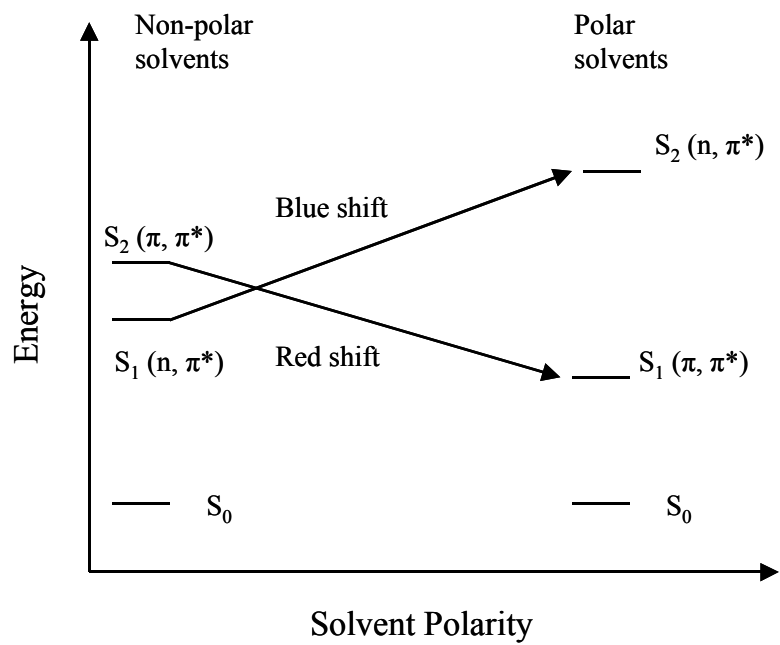


Figure 9: The effect of solvent polarity on the order of (π, π^*) and (n, π^*) states.²⁸

2.5.2 Electronic State Dipole Moment Calculation - Lippert Plots

By measuring spectral shifts, in a number of solvents of various polarities, Lippert plots can be constructed and the dipole moment change between the ground and excited state can be determined. The Lippert method employs the energy difference between the fluorescence and absorption bands as shown in Eq. (2-3) and plots this difference against orientation polarizability as shown in Eq. (2-4).^{29,30} The slope of this plot gives the dipole moment difference between the excited and ground states with a dependence on the Onsager Cavity radius (a). In general and in this research, to eliminate the dependence on the Onsager radius, another method, the Ratio Method as given in Eq. (2-5) is used. The Ratio Method employs the ratio of solvatochromic shift of the fluorescence band to that of the absorption band to determine the excited state dipole moment. These methods use the assumptions shown below^{29,30}:

- 1) No change in molecular geometry in going from ground state to the excited state.
- 2) In Frank-Condon and relaxed excited states dipole moments stay the same.
- 3) In ground and excited states the cavity radius remains the same.
- 4) The solvent shift should be measured in solvents of similar refractive indices solvents having different dielectric constants.

$$h.c.\Delta\bar{\nu} = hc(\bar{\nu}_A - \bar{\nu}_F) = \frac{2.\Delta f}{a^3} \cdot (\mu_E - \mu_G)^2 + \text{constant} \quad (2-3)$$

$$\Delta f = \frac{\varepsilon - 1}{2.\varepsilon + 1} - \frac{n^2 - 1}{2.n^2 + 1} \quad (2-4)$$

$$\bar{\mu}_E = \bar{\mu}_G \cdot \frac{\Delta\bar{\nu}_{\text{flu}}}{\Delta\bar{\nu}_{\text{abs}}} \text{ (Ratio Method)} \quad (2-5)$$

The symbols used throughout the equations are as follows:

$\Delta\bar{\nu}$: energy difference in absorption and emission frequency shift (cm^{-1}),

$\bar{\mu}_E$ and $\bar{\mu}_G$: excited and ground state dipole moments, respectively,

h : 6.6256×10^{-27} erg.sec, Plank's constant,

c : 2.99×10^{10} cm/sec, speed of the light,

a : cavity radius (\AA)

n : refractive index,

ε : dielectric constant

2.5.3 Electronic State Acidity – Forster Cycle

Photon absorption by a hydrogen bonding chromophore changes ground state solvation equilibrium and makes protonation or deprotonation necessary to reach an excited state equilibrium.³¹ The protonation of a series of unsubstituted and substituted diarylidene cycloalkanones and its effects on the molecular absorption and emission spectra can be determined by the Forster cycle³², which is based on the thermally equilibrated states existing between the ground state of the base and the lowest excited singlet state of the conjugated acid as shown in Figure 10. Upon electronic excitation, the pKa of the molecule changes and results in a dual emission.³² Forster cycle can

calculate this change in pKa between the ground and excited states by employing the spectral shifts that occur upon dissociation of the excited state. Since the energies of the ground and excited states depend on ionization, the dissociated form of the acid is observed at a higher energy due to its low dissociation constant.²⁹ If the excited state pKa is lower than the ground state pKa, a smaller increase in energy ($\Delta H^* < \Delta H$) is attained upon dissociation of the excited state. Assuming no entropy change for dissociation in the ground and excited states, the energy difference of the states of the acid (BH^+ , protonated form) and its conjugated base (B, neutral form) can be correlated to pKa as ²⁹:

$$\Delta pKa = pKa - pKa^* = \frac{E_{BH^+} - E_B}{2.303RT} \quad (2-6)$$

where,

pKa and pKa*: ground and excited state acidity, respectively;

R = Universal gas constant,

T = absolute temperature.

The energies of the protonated and dissociated forms are calculated averaging the absorption and emission maxima of the forms as:

$$E_i = Nhc \frac{\bar{\nu}_A + \bar{\nu}_F}{2}; \text{ where,} \quad (2-7)$$

E_i : the energies of the protonated and dissociated forms,

$\bar{\nu}_A$ and $\bar{\nu}_F$: absorption and emission maxima of species in wavenumbers,

N: Avogadro's number,

h: Planck's constant,

c : the speed of the light.

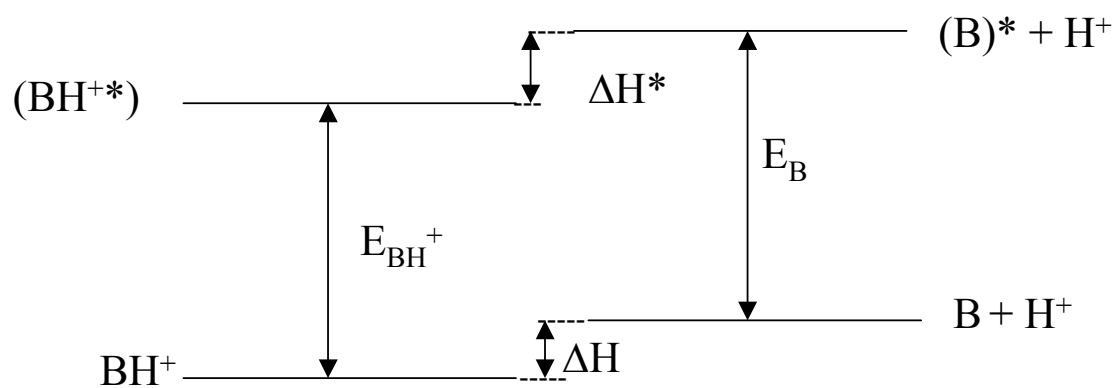


Figure 10: Forster Cycle. Electronic energy levels of an acid (BH^+) and its conjugate base (B) in the ground and excited states.²⁹

3 EXPERIMENTAL

3.1 Synthesis of Compounds

In this section, the syntheses applied to obtain targeted compounds along with characterization techniques are presented within the order given below:

- 1) Syntheses of 2,5-dibenzylidene-cyclopentanone (1dbcp), 2,5-bis-(3-phenyl-allylidene)-cyclopentanone (2dbcp), and their cyclohexanone analogs (1dbch and 2dbch) were performed by RuCl_3 catalyzed aldol condensations of aldehydes and ketones. This method yields symmetric (E,E) isomers of the products.
- 2) Synthesis of 2,5-bis-[3-(4-dimethylamino-phenyl)-allylidene]-cyclopentanone (2dbma) was achieved by base catalyzed aldol condensation.
- 3) Synthesis of 2,5-Bis-(5-phenyl-penta-2,4-dienylidene)-cyclopentanone (3dbcp) was accomplished by first synthesizing its starting compound, 5-phenyl-penta-2,4-dienal and followed by base catalyzed aldol condensation with cyclopentanone.
- 4) Synthesis of 2,5-dibenzylidene-cyclopent-3-enone, (1dbcp_u) was attained by first synthesizing the starting material by bromination to yield the 3,4-dibromo derivative of 1dbcp, which was followed by debromination with zinc/methanol.

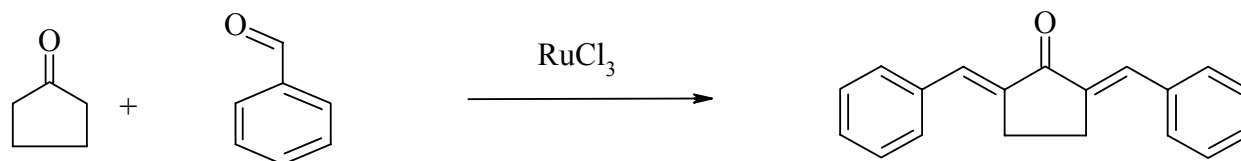
3.1.1 RuCl₃ Catalyzed Aldol Condensation of Aldehydes and Ketones to Synthesize Diarylidene-Cycloalkanones³³

As shown in Figure 11, the appropriate cycloalkanone (5mmol), aldehyde (10.1mmol), and anhydrous RuCl₃ (0.1mmol) were placed in a glass tube and sealed. The sealed tube was placed in an oven overnight at 120°C. After cooling to room temperature, the sealed tube was opened. The reaction mixture was powdered and poured into (25ml) cold ethanol and stirred for 3-4 minutes, followed by suction filtration. At this point the crystalline material was washed with water (~10 ml), 10% aqueous NaHCO₃ (~5ml), and cold ethanol (~10ml) and left on the suction filter to dry. The product was recrystallized from ethanol. Further purification was achieved by flash column chromatography. For this purpose a silica gel (wetted by hexane for uniformity) column was prepared. Then the product was dissolved in ethyl acetate/ hexane solution (1/10, v/v) and added to the column and a pressure of N₂ was applied to the column. TLC confirmed sample purity.

The compounds were yellow in color with melting points showing good agreement with the literature values. The melting points for 1dbcp, 2dbcp, 1dbch, and 2dbch were 188.0°C (188.5°C³³), 223.5°C (223.0°C³³), 116.0°C (116-117°C³³), and 179.5°C (179.0°C³³), respectively. The yields obtained for these compounds were around 70%.

¹H_NMR, ¹³C_NMR in CDCl₃, and IR (KBr) data for the compounds are given in Table 1. The reported results in the literature³³ for 1dbcp, 2dbcp, 1dbch, and 2dbch match well with our experimental results given in Table 2.

(a) Synthesis of 2,5-dibenzylidene-cyclopentanone (1dbcp)



(b) Synthesis of 2,5-bis-(3-phenyl-allylidene)-cyclopentanone (2dbcp)

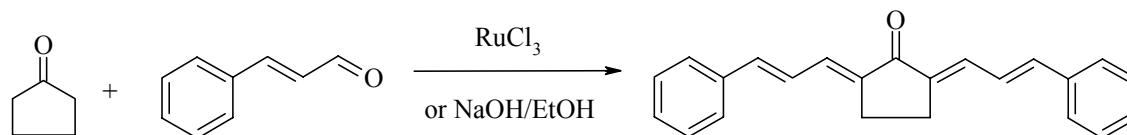
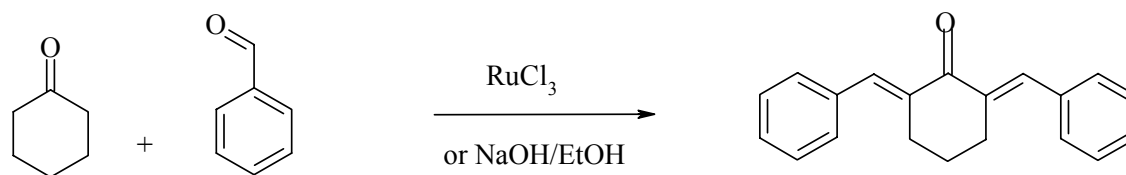


Figure 11: Synthesis of unsubstituted compounds.³³

(c) Synthesis of 2,6-dibenzylidene-cyclohexanone (1dbch)



(d) Synthesis of 2,6-bis-(3-phenyl-allylidene)-cyclohexanone (2dbch)

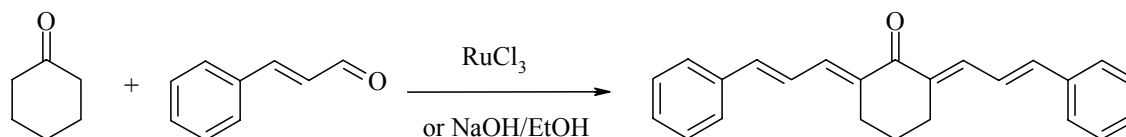


Figure 11 Cont'd: Synthesis of unsubstituted compounds.³³

Table 2 ¹H_NMR, ¹³C_NMR, and IR Data for 1dbcp, 2dbcp, 1dbch, and 2dbch.

Compounds	¹ H_NMR δ (ppm)	¹³ C_NMR δ (ppm)	IR (cm ⁻¹)
1dbcp	7.6-7.2 (m, 16H) 3.7-2.9 (m, 4H)	196.4, 137.3, 135.8, 133.8, 130.7, 129.4, 128.7, 26.5,	3439, 3020, 1691, 1626, 1603, 1570, 1490, 1447, 1284, 1253, 1181, 982
2dbcp	7.5-7.3 (m, 16H) 3.0-2.9 (m, 4H)	195, 141.3, 139.8, 136.5, 132.7, 129.2, 128.8, 127.2, 124.7, 23.9	2925, 1674, 1616, 1583, 1446, 1282, 1205, 1153, 968
1dbch	7.81 (s, 2H) 7.4-7.0 (m, 10H) 2.95-2.88 (t, 4H) 2.1 (m, 2H)	190.4, 136.9, 136.1, 135.9, 130.3, 128.6, 128.4, 30.9, 28.5, 23.0	3451, 2934, 1662, 1608, 1575, 1486, 1440, 1275, 1170, 1145, 970
2dbch	7.5-6.5 (m, 16H) 2.9-2.2 (m, 6H)	188.8, 140.7, 136.7, 136.3, 135.3, 128.8, 128.7, 127.1, 123.6, 26.6, 22.6	3432, 2922, 1654, 1610, 1582, 1450, 1285, 1174, 1148, 970

In Appendix A and Appendix B, ^1H _NMR and ^{13}C _NMR along with IR spectra are given, respectively.

3.1.2 Synthesis of Dimethylamino Substituted Polyene Ketones

Base catalyzed aldol condensation was used to synthesize dimethylamino substituted polyene ketones as shown in Figure 12.³⁴ In a round bottom flask, 4-dimethylamino-cinnamaldehyde (25 mmol), cyclopentanone (12.5 mmol), NaOH (50 mmol) and ethanol (100 ml) were mixed and allowed to stir for 2h at room temperature. The product was collected by suction filtration and recrystallized from benzene. A burgundy colored 2,5-bis-[3-(4-dimethylamino-phenyl)-allylidene-cyclopentanone (2dbma) was obtained with a 75% yield.

^1H _NMR, ^{13}C _NMR and IR spectra of 2dbma can be seen in and their results are reported in Table 3. The melting point of 2dbma was found to be 265°C.

Synthesis of 2,5-bis-[3-(4-dimethylamino-phenyl)-allylidene-cyclopentanone (2dbma)

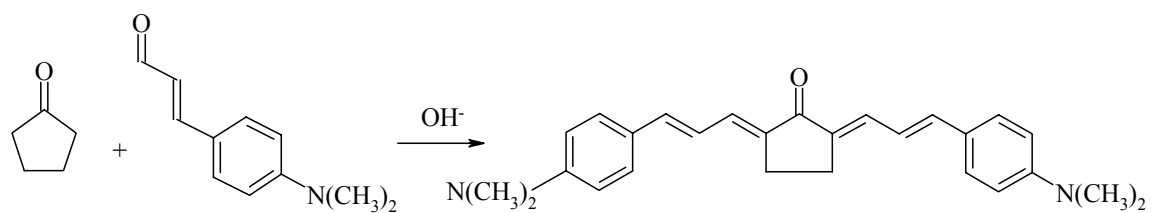


Figure 12: Synthesis of 2,5-bis-[3-(4-dimethylamino-phenyl)-allylidene-cyclopentanone (2dbma).³⁴

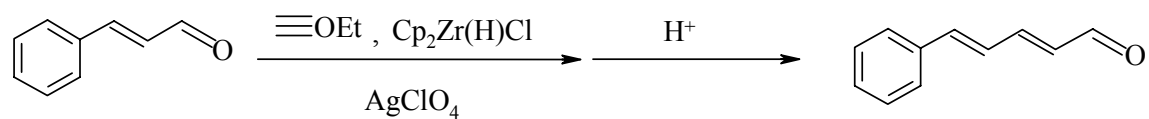
Table 3 ¹H_NMR, ¹³C_NMR, and IR data for 2dbma.

Compound	¹ H_NMR δ (ppm)	¹³ C_NMR δ (ppm)	IR (cm ⁻¹)
2dbma	7.5-7.2 (m, 6H) 6.9-6.5 (m, 8H) 3.0 (s, 12H) 2.8 (s, 4H)	195.1, 151.3, 142.1, 138.3, 133.8, 129.1, 125.3, 121.0, 112.4, 40.7, 24.4	3446, 2347, 1579, 1525, 1368, 1282, 1212, 1151, 949, 807

3.1.3 Synthesis of 2,5-Bis-(5-phenyl-penta-2,4-dienylidene)-cyclopentanone

Synthesis of 3dbcp was accomplished by first synthesizing 5-phenyl-penta-2,4-dienal followed by base catalyzed aldol condensation with cyclopentanone. The dienal was synthesized by two carbon homologation of cinnamaldehyde using the AgClO_4 catalyzed addition of the zirconocene complex derived from the hydrozirconation of 1-ethoxyethyne (Aldrich) with bis(cyclopentadienyl)zirconium chloride hydride (Strem) followed by acidic hydrolysis, as shown in Figure 13(a).³⁵ For the homologation of the aldehyde, a thermometer and N_2 gas inlet were attached to a three neck round bottom flask. The third neck of the flask was used to introduce the chemicals starting with the dissolved zirconium salt (17.62 g, 0.0713 mol) in (60 ml) distilled CH_2Cl_2 and (5g, 0.0713 mol) ethoxyethyne. 10 min later a red solution was formed. To this solution cinnamaldehyde (5.86 ml, 0.0464 mol) and AgClO_4 (0.48g, 2.36 mmol) were added. After 10 min the reaction mixture was diluted with ethanol (30 ml) and aqueous NaHCO_3 (5 ml). The reaction mixture was filtered through a celite pad followed by washing of the pad with ethyl ether to recover the product. After separation, the organic phase was refluxed in 3N HCl (100 ml) for 1.5 h at 50°C in an oil bath. The organic layer was washed with NaHCO_3 (aq) and brine and dried over Na_2SO_4 . After removing the solvent, a red oily-solid (5.23 g, 0.0331 mol), was obtained. To this product, cyclopentanone (1.46 ml, 0.0165 mol), NaOH (3.31 ml, 0.0331 mol), and ethanol (250 ml) were added as shown in Figure 13(b). The reaction mixture was allowed to stir for 2h at room temperature followed by suction filtration.

(a) Synthesis of 5-phenyl-penta-2,4-dienal



(b) Synthesis of 2,5-Bis-(5-phenyl-penta-2,4-dienylidene)-cyclopentanone (3dbcp)

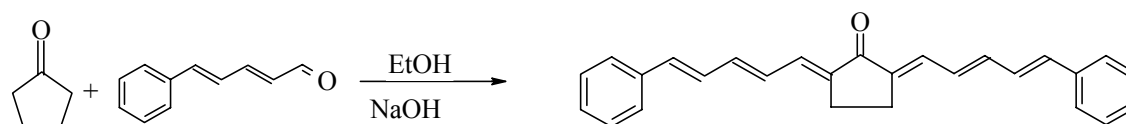


Figure 13: a) Synthesis of 5-phenyl-penta-2,4-dienal ³⁵ and b) 2,5-Bis-(5-phenyl-penta-2,4-dienylidene)-cyclopentanone (3dbcp).

The product was recrystallized from ethanol. Although one spot was observed on the TLC plate, further purification by flash column chromatography was applied. A 55 % of 3dbcp yield was attained. 3dbcp was identified by characterization with NMR and IR. Since 3dbcp could be a reactive compound, it was left in a vacuum desiccator overnight and then stored in the refrigerator in an amber bottle. $^1\text{H-NMR}$, $^{13}\text{C-NMR}$ in CDCl_3 , and IR (KBr) data for 3dbcp are given in Table 4.

The synthesis of 3dbcp has not been previously reported. 3dbcp $^1\text{H-NMR}$, $^{13}\text{C-NMR}$, and IR spectra are shown in Appendix A and B, respectively. The melting point of 3dbcp was found to be 190°C .

Table 4 ^1H _NMR, ^{13}C _NMR, and IR data for 3dbcp.

Compounds	^1H _NMR δ (ppm)	^{13}C _NMR δ (ppm)	IR (cm^{-1})
3dbcp	7.8-6.5 (m, 20H) 2.9-2.8 (m, 4H)	195.4, 142.4, 140.6, 137.4, 137.2, 133.1, 129.8, 129.4, 129.3, 129.1, 127.5, 24.5	3434, 3024, 1674, 1622, 1586, 1494, 1447, 1277, 1233, 1138, 993, 954

3.1.4 Synthesis of 2,5-dibenzylidene-cyclopent-3-enone

The synthesis of 2,5-dibenzylidene-cyclopent-3-enone, (1dbcp_u) took place in two steps as shown in Figure 14.³⁶ The first step was the bromination of 1dbcp with NBS/CCl₄ to yield the 3,4-dibromo derivative of 1dbcp. In the second step the product was debrominated with zinc/methanol. In the first step of the synthesis, 1dbcp (0.019 mol) and NBS (0.038 mol) in CCl₄ (300 ml) were refluxed for 4h. Following cooling of the reaction mixture to 0°C, suction filtration was applied, and the material remaining on the Buchner funnel was washed with CCl₄. The filtrate and washings were washed with cold aqueous NaHCO₃ and dried with MgSO₄. In the second step, a mixture of the debrominated compound (0.015 mol) and zinc (0.019 mol) in methanol (250 ml) was refluxed for 6 h. After the mixture was cooled to 25°C, methanol was removed under vacuum. The yellow product was stirred in HCl (3M) for 2 h. After suction filtration and washing with water, the compound was allowed to dry. The crude product was dissolved in dichloromethane and purified by flash chromatography using hexane: ethyl acetate (5:1). The yield of 1dbcp_u was found to be 60%.

In Table 5, experimental ¹H_NMR, ¹³C_NMR, and IR results are shown for 1dbcp_u. In the literature, there is no report on ¹³C_NMR for this compound. However, existing literature values of ¹H_NMR and IR³⁶ agree with our experimental data. The melting point of 1dbcp_u was found to be 150°C (lit. 146-147°C³⁶). The ¹H_NMR, ¹³C_NMR, and IR spectra of 1dbcp_u are given in Appendix A and Appendix B, respectively.

Table 5 ¹H_NMR, ¹³C_NMR, and IR data for 1dbcp_u.

Compounds	¹ H_NMR δ (ppm)	¹³ C_NMR δ (ppm)	IR (cm ⁻¹)
1dbcp_u	7.6-7.2 (m, 7H)	194.9, 136.0, 134.6, 133.5, 131.6, 130.4, 129.8, 128.6	3450, 3056, 1714, 1694, 1615, 1494, 1447, 1385, 1322, 1242, 1178, 987, 923, 828, 769, 729, 694

An attempt was made to synthesize 2,5-bis-(3-phenyl-allylidene)-cyclopent-3-enone (2dbcp_u) by the same method. Although, the first step, bromination of 2dbcp was successful, in the second step removal of bromines was unsuccessful to yield 2dbcp_u.

Synthesis of 2,5-dibenzylidene-cyclopent-3-enone (1dbcp_u)

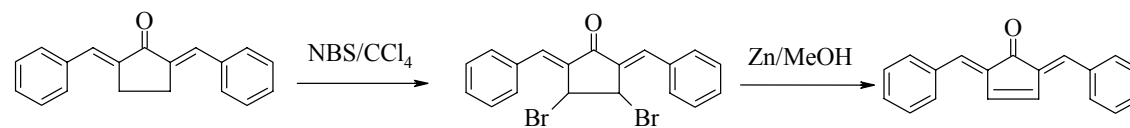


Figure 14: Synthesis of 2,5-dibenzylidene-cyclopent-3-enone (1dbcp_u).³⁶

3.1.5 General Procedures for Purification and Characterization

For characterization purposes, NMR spectra were taken with a BRUKER Avance 400 MHz spectrometer with chloroform-d employed as the solvent. A Perkin Elmer FT-IR model 1600 was used to measure the IR spectra. Melting point measurements were determined by a Uni-melt Thomas Hoover Capillary Melting Point Apparatus.

For purification, JT Baker 400 Mesh silica gel was used as the stationary phase in all flash column chromatographic separations. The mobile phase solvents/ or solvent systems were chosen by trial and error. All reactions were monitored during the reaction by thin layer chromatography (TLC). A BUCHI rotovapor was used for solvent evaporation at reduced pressure. All glassware was dried in the oven prior to use and, depending on air sensitivity of the reaction; the glassware was purged with dry nitrogen. Syntheses were carried out under dim light to prevent isomerization about double bonds.

3.2 Spectroscopic Measurement

All solutions were freshly prepared prior to spectroscopic measurements. Room temperature absorption spectra were measured using a Shimadzu UV2100 UV-Visible spectrophotometer. A Perkin-Elmer LS-50B luminescence spectrometer equipped with a R928 phototube was used to measure fluorescence excitation and fluorescence spectra at room temperature and 77K.

In addition to the LS50B, fluorescence spectra were also measured with a home-built apparatus as shown in Figure 15.

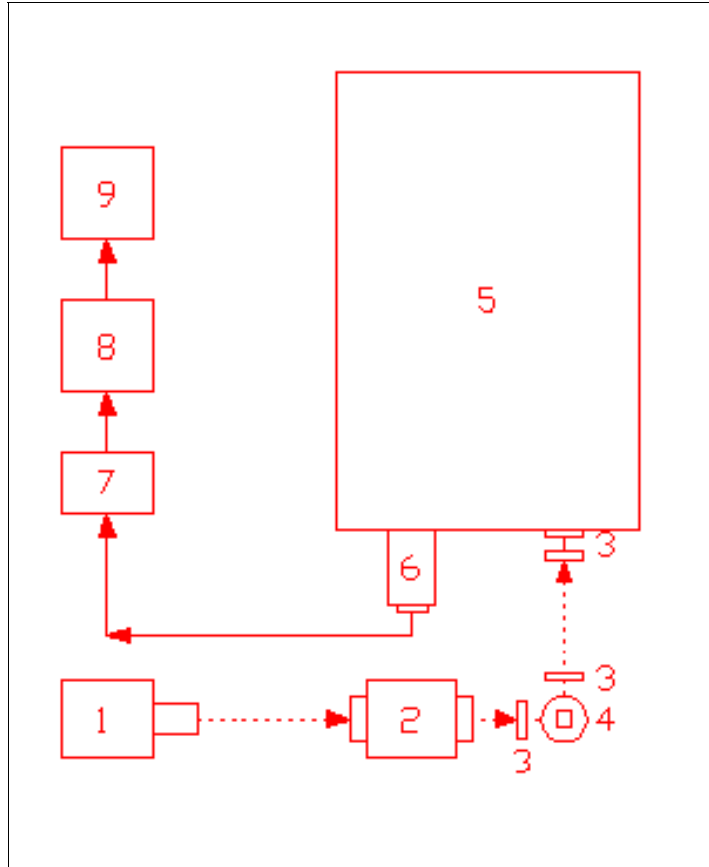


Figure 15: Emission spectrometer
(adapted V. Chynwat Ph D thesis ³⁷).

- 1) 150 W Xenon arc lamp
- 2) Jarrell-Ash 82-410, ¼ meter monochromator
- 3) Lens
- 4) Sample compartment
- 5) Spex 1702, ¾ meter

- monochromator
- 6) EMI 9659QB photomultiplier tube
- 7) Keitly Instrument 602 electrometer
- 8) Recorder
- 9) Computer and interface system

Excitation was provided by radiation from a 150W Xenon arc lamp filtered through a Jarrell-Ash 82-410, ¼ meter monochromator. Fluorescence was dispersed by a SPEX 1702 ¾ monochromator and detected with an EMI 9558QB photomultiplier tube. Amplification was conducted with a Keitly Instrument 602 electrometer. The analog output was digitized with a Data Translation A to D converter. Spectra were plotted with Grapher 3 software.

3.2.1 Quantum Yield Calculation

To determine quantum yields (Φ_f), the fluorescence spectra was corrected and integrated and compared with that of a standard with known Φ_f value. MathCAD was employed as the appropriate software for all the corrections and integration of spectra. To correct fluorescence spectra, the literature emission spectrum of N,N-dimethylamino-m-nitrobenzene (N,N-DMANB)²⁹ (Aldrich) was compared to the spectrum of N,N-DMANB measured with the LS50B. A set of scale factors were determined every 50 cm⁻¹ between 450 and 770 nm. The correction calculations can be seen in Appendix C. For Φ_f calculations of 2bcp and 3dbcp, coumarin 481 (Exciton, also known as coumarin 35), $\Phi_f=0.11$, in acetonitrile³⁸ and for 2dbma, fluorescein (Exciton), $\Phi_f=0.90$, in 0.1N NaOH¹¹ were used as standards. After the fluorescence measurements were conducted, solutions were purged with N₂ for 5 min and measurements were retaken. It was found that degassing had no measurable affect on the Φ_f values. All measurements were made with the LS50B for Φ_f determinations and Eq. (3-1) was used to calculate the Φ_f .

$$\Phi_C = \Phi_S \cdot \frac{A_S}{A_C} \cdot \frac{n_C^2}{n_S^2} \cdot \frac{D_C}{D_S} \quad (3-1)$$

where;

- Φ : quantum yield
- A: absorbance at excitation wavelength
- n: refractive index of solvent
- D: area under corrected emission curve
- C: compound
- S: standard

10^{-6} M and 10^{-7} M were used as standard concentrations. The absorbances were kept lower than 0.05 at the wavelengths of excitation. A sample Φ_f calculation is given in Appendix D.

3.2.2 Extinction Coefficient Calculation

Extinction coefficients were determined for 1dbcp, 2dbcp, and 3dbcp in cyclohexane and methanol. The weighed amount of compound was dissolved in a known volume of solvent to prepare the stock solution. Once this stock solution was ready a series of dilutions were prepared from it and UV absorption measurements of these solutions were taken. Employing the Beer-Lambert equation as shown in Eq. (3-2), a graph of absorbance versus concentration was drawn and from the slope of the plot, the extinction coefficient was determined.

$$A = \varepsilon \cdot b \cdot C \tag{3-2}$$

where;

- A: absorbance
- ε : extinction coefficient ($M^{-1}.cm^{-1}$)
- b: cell length (1cm)
- C: concentration of solution (M)

3.2.3 Polarized Excitation Spectra

Polarization was maintained by placing 3M Polacoat 150 UV linear polarizers in front of excitation and emission optical pathways. A Karl Lambrecht Corporation quartz scrambler was placed in front of the SPEX monochromator to eliminate the possibility of unequally transmitted polarized light. The emission polarizer was kept in a fixed position and transmitted only vertically polarized light (vertical plane). However, by rotating the excitation polarizer either vertically or horizontally polarized light could be selected for excitation. The sample was placed in a quartz cell and kept in a quartz dewar at 77K. Spectral data were digitized and the degree of polarization, P, was calculated according to Eq. (3-3).

$$P = \frac{I_{\parallel} - I_{\perp}}{I_{\parallel} + I_{\perp}} \quad (3-3)$$

where,

I_{\parallel} : fluorescence intensity when polarizers are parallel,

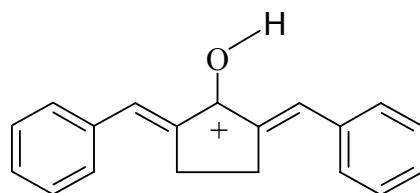
I_{\perp} : fluorescence intensity when polarizers are perpendicular.

P with positive values shows that the transition moments of the absorbing and emitting states are of the same symmetry (parallel), whereas, P with negative values show that these states are not of the same symmetry (perpendicular).

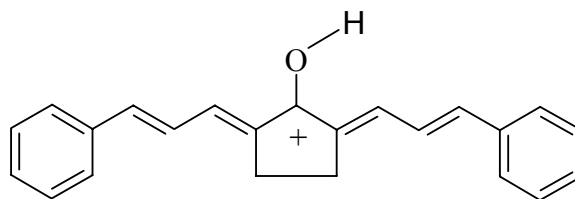
3.3 Preparation of Protonated Cations

Neutral unsubstituted arylpolyene compounds of 1dbcp, 2dbcp, and 3dbcp were dissolved in 96% sulfuric acid to obtain their protonated cations. In the case of 3dbcp, in sulfuric acid, a reaction other than protonation appeared to occur. Therefore for 3dbcp- H^+ , acidic solvents with lesser strength than sulfuric acid (e.g., trifluoroacetic acid, and

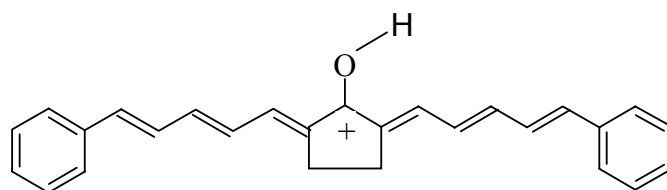
different ratios of acetic and sulfuric acids) were tried and among these an acetic acid:
sulfuric acid mixture of 3:1 ratio was found to be the appropriate one for our purposes.



1dbcp-H⁺



2dbcp-H⁺



3dbcp-H⁺

Figure 16: The protonated cations of arylpolyene ketones.

3.3.1 Investigation of Reversibility of Protonation/ Deprotonation

To determine if any side reactions were occurring, 1dbcp and 2dbcp were acidified with sulfuric acid and 3dbcp was acidified with acetic acid: sulfuric acid mixture (3:1). To these acidic solutions, saturated aqueous NaHCO₃ was added for neutralization. The neutralized compounds were extracted with ether and dried over MgSO₄. The ether was evaporated and the solid was collected. IR spectra of the recovered material were recorded and found to agree with the spectra of the compounds prior to treatment with acid. HPLC was also used to show that protonation followed by neutralization generated the starting compounds and no side products were observed.

3.3.2 Photochemistry of 1dbcp and 1dbcp-H⁺ Protonated Cation

Two sets of photochemical studies were carried out. First 1dbcp in tetrahydrofuran was irradiated for various intervals (5, 15, 45, 60 s) with a 150W xenon arc lamp filtered through 15 cm of distilled water. This procedure was repeated for 1dbcp-H⁺ (dissolved in 96% H₂SO₄). After each irradiation, the acid solutions were neutralized with aqueous NaHCO₃ and the organic compounds extracted with ethyl ether. The ether solutions were dried over MgSO₄ and analyzed by HPLC to determine the extent of any photochemical reaction that may have occurred.

3.4 HPLC Analysis

A Hewlett-Packard HPLC 1100 was used to analyze the purity of synthesized compounds and to follow the course of photochemical studies. HPLC utilizes the fact that certain compounds have different migration rates in a given particular column and phase. Reverse phase was used as the stationary phase, which consists of silica-based

packing with n-alkyl chains covalently bound. With this phase hydrophilic compounds elute more quickly than hydrophobic compounds. As for the mobile phase, different percentages of acetonitrile and water mixtures were tried for various time durations to obtain a good separation between peaks. A diode array was used for the detector. Gradient method was employed for the analyses and the methodology is given in Appendix H.

In the purity analysis, the liquid chromatography of a synthesized compound was taken at five selectively chosen wavelengths, (including wavelength of maximum absorption). The compound is pronounced to be pure if all the peaks observed at five different wavelengths appear at the same retention time. Purity percentages were calculated from peak areas. In photochemistry studies, sample solutions were irradiated with a 150W xenon arc lamp filtered through distilled water for various time (0, 5, 15, 45, 60 s...etc.) intervals. The analysis was finalized by comparing each peaks retention time and absorption spectra to that of non-irradiated compound.

3.5 Computational Studies

Computational studies were initiated by drawing the molecular structures with the PCMODEL program. Following the drawings, MOPAC 2000 was employed for optimization of these structures¹² In MOPAC 2000, for the neutral compounds (1dbcp, 2dbcp, and 3dbcp), the keywords PM3, precise, and bonds were employed, whereas, for the protonated cation structures an additional keyword of charge = 1 was used. In addition, the normal modes of vibration were computed and all positive force constants were obtained indicating that the structures were fully optimized. After optimization, MOPLLOT 95 was used to visualize the optimized structures. Spectral properties of the

optimized structures were calculated with the INDO/S Hamiltonian. Configuration interaction (CI) with singly excited configurations (INDO/S-CIS) and CI with singly and doubly excited configurations (INDO/S-C/S D) were employed in calculations.

4 RESULTS AND DISCUSSION

4.1 Section 1: Electronic Absorption and Fluorescence Properties of 2,5-Diarylidene-cyclopentanones

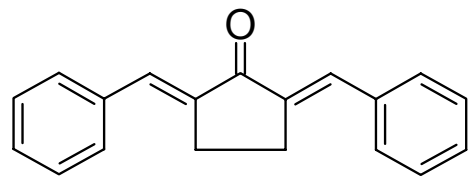
4.1.1 Introduction

This section starts with an investigation of PM3 Hamiltonian computed optimized structures of 2,5-diarylidene-cyclopentanones along with their INDO/S calculated and assigned absorption spectra. The electronic and spectroscopic properties of compounds and the influence of polyene length on those are determined by measurements of the absorption and fluorescence spectra. The influences of hydrogen bonding on the excitation spectra of compounds are investigated. Solvent induced shifts in the absorption and fluorescence spectra of 3dbcp are used with the PM3 calculated ground state dipole moment to determine the excited state dipole moment of 3dbcp. Polarized excitation spectra are measured for 2dbcp and 3dbcp at 77 K in ethanol/methanol glass and used as an aid for the assignments of electronic transitions. Fluorescence quantum yields are obtained to analyze the changes in the nonradiative rate of decay from S_1 .

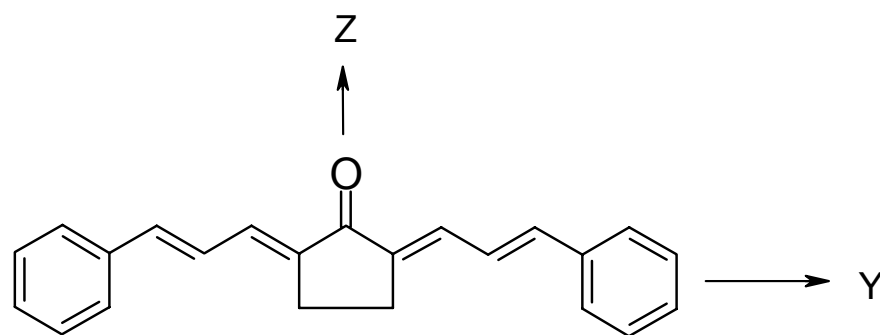
4.1.2 PM3 Optimized Geometries

Initial structures for geometry optimization were drawn with all carbon and oxygen atoms in, or nearly in the same plane. The molecular structures of the unsubstituted parent compounds (R = H) with $n = 1, 2,$ and 3 : 2,5-dibenzylidene-cyclopentanone (1dbcp), 2,5-bis-(3-phenyl-allylidene)-cyclopentanone (2dbcp), and 2,5-bis-(5-phenyl-penta-2,4-dienylidene)-cyclopentanone (3dbcp) are shown in Figure 17. The optimized structures of 1dbcp, 2dbcp, and 3dbcp are shown in Figure 18 - Figure 20.

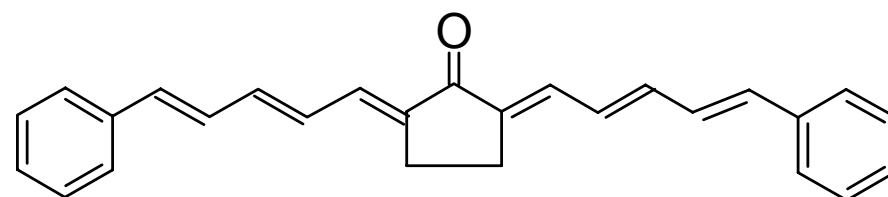
PM3 calculated ground state equilibrium geometries of these compounds are given in Table 7 - Table 9, respectively. After minimization it was found that 1dbcp had adopted a structure with C_s symmetry and 2dbcp and 3dbcp had found minima of C_{2v} symmetry. The major difference between the C_s and C_{2v} forms is the degree to which the phenyl rings are rotated out-of-plane. PM3 predicts that the phenyl groups of 1dbcp are rotated 35° out-of-plane relative to the cyclopentanone ring whereas 2dbcp and 3dbcp have nearly planar structures. A crystallographic structure determination has been reported for 1dbcp.⁹ The results of this study along with the PM3 calculated results are presented in Table 6. In general the agreement is good except for the out-of-plane rotation angle of the phenyl group, which is 3.0° in the crystal phase. However, crystal packing forces may be responsible for the deviation of this experimental structural parameter from the calculated value.¹³ Most of the computed structural parameters for 2dbcp and 3dbcp are similar to those of 1dbcp. All three compounds are predicted to have a carbonyl group bond length of 1.216 Å. The single bond connected to the phenyl group is predicted to have a bond length of 1.460 Å for 1dbcp and 1.458 Å for both 2dbcp and 3dbcp. The other exocyclic C-C single bond lengths fall in the range 1.448-1.449 Å for 2dbcp and 3dbcp. The exocyclic double bond lengths fall in the relatively narrow range of 1.340-1.344 Å for 1dbcp, 2dbcp, and 3dbcp. Rotation of the phenyl rings out of the plane of the cyclopentanone ring is predicted by PM3 to be less than 0.5° for 2dbcp and 3dbcp.



1dbcp



2dbcp



3dbcp

Figure 17: Molecular structures of 1dbcp, 2dbcp, and 3dbcp.

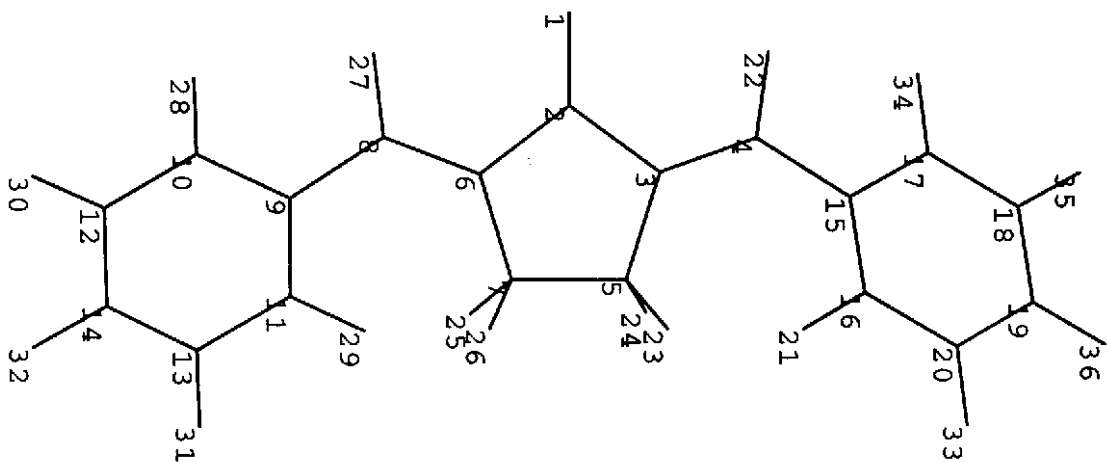


Figure 18: Optimized geometry of 1dbcp ($\Delta H_f = 35.78$ kcal/mol).

Table 6 Calculated and Experimental Geometry of 1dbcp.

	PM3	expt. ^a	PM3
	<u>bond lengths (Å)</u>		
O ₁ -C ₂	1.216	1.210	1.88
C ₂ -C ₃	1.491	1.474	0.95
C ₃ -C ₄	1.493	1.493	0.99
C ₃ -C ₅	1.340	1.341	1.84
C ₅ -C ₆	1.460	1.461	1.03
C ₆ -C ₇	1.400	1.389	1.38
C ₇ -C ₈	1.389	1.387	1.44
C ₈ -C ₉	1.391	1.356	1.41
C ₉ -C ₁₀	1.390	1.373	1.42
C ₁₀ -C ₁₁	1.390	1.385	1.43
C ₁₁ -C ₆	1.397	1.377	1.39
	<u>bond angles (°)</u>		
C ₁ -C ₂ -C ₃	126.1	125.6	
C ₂ -C ₃ -C ₄	109.0	108.8	
C ₄ -C ₃ -C ₅	127.8	130.6	
C ₃ -C ₅ -C ₆	126.6	131.1	
C ₅ -C ₆ -C ₇	118.3	118.4	
C ₆ -C ₇ -C ₈	120.2	121.4	
C ₇ -C ₈ -C ₉	120.2	120.1	
C ₈ -C ₉ -C ₁₀	119.9	119.8	
C ₉ -C ₁₀ -C ₁₁	120.2	120.1	
C ₁₀ -C ₁₁ -C ₆	120.2	121.4	
C ₁₁ -C ₆ -C ₇	119.2	117.2	
	<u>dihedral angle (°)</u>		
C ₃ -C ₅ -C ₆ -C ₁₁	35.5	3.0	

* from ref.⁹

Table 7 Calculated Ground State Equilibrium Geometry of 1dbcp by PM3 Method.

	Bond Lengths (Å)	Bond Orders
O ₁ -C ₂	1.21	1.88
C ₂ -C ₃	1.49	0.95
C ₂ -C ₆	1.49	0.95
C ₃ -C ₅	1.49	0.99
C ₅ -C ₇	1.53	0.98
C ₇ -C ₆	1.49	0.99
C ₃ -C ₄	1.34	1.84
C ₄ -C ₁₅	1.46	1.03
C ₁₅ -C ₁₇	1.40	1.38
C ₁₇ -C ₁₈	1.39	1.44
C ₁₈ -C ₁₉	1.39	1.41
C ₁₉ -C ₂₀	1.39	1.42
C ₁₆ -C ₂₀	1.39	1.43
C ₁₅ -C ₁₆	1.40	1.39

Bond Angles (°)	
O ₁ -C ₂ -C ₃	126.10
C ₂ -C ₃ -C ₄	123.20
C ₄ -C ₁₅ -C ₁₇	118.30
C ₁₇ -C ₁₈ -C ₁₉	120.20

Dihedral Angles (°)	
C ₁₁ -C ₉ -C ₈ -C ₆	-35.50
C ₁₆ -C ₁₅ -C ₄ -C ₃	35.60

Atomic Charges	
O ₁	-0.31
C ₂	0.36
C ₃	-0.20
C ₄	-0.01
C ₅	-0.05
C ₆	-0.20
C ₇	-0.05
C ₈	-0.01
C ₉	-0.06
C ₁₀	-0.08
C ₁₁	-0.10
C ₁₂	-0.10
C ₁₃	-0.10
C ₁₄	-0.09

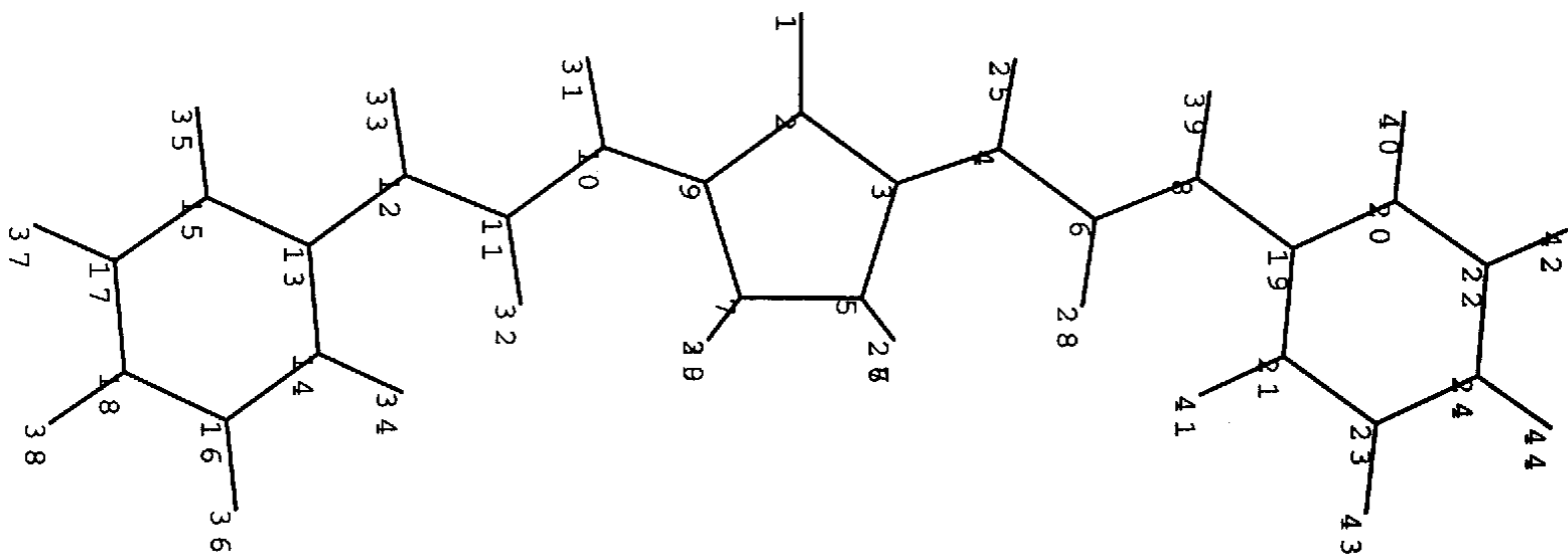


Figure 19: Optimized geometry of 2dbcp ($\Delta H_f = 62.05$ kcal/mol).

Table 8 Calculated Ground State Equilibrium Geometry of 2dbcp by PM3 Method.

	Bond Lengths (Å)	Bond Orders
O ₁ -C ₂	1.21	1.88
C ₂ -C ₃	1.49	0.95
C ₂ -C ₉	1.49	0.95
C ₃ -C ₅	1.49	0.99
C ₅ -C ₇	1.53	0.99
C ₇ -C ₉	1.49	0.99
C ₃ -C ₄	1.34	1.82
C ₄ -C ₆	1.45	1.06
C ₆ -C ₈	1.34	1.83
C ₈ -C ₁₉	1.46	1.04
C ₁₉ -C ₂₀	1.40	1.38
C ₂₀ -C ₂₂	1.39	1.44
C ₂₂ -C ₂₄	1.39	1.42
C ₂₄ -C ₂₃	1.39	1.42
C ₂₃ -C ₂₁	1.39	1.43
C ₂₁ -C ₁₉	1.40	1.38

Bond Angles (°)	
O ₁ -C ₂ -C ₃	126.20
C ₂ -C ₃ -C ₄	123.90
C ₄ -C ₆ -C ₈	122.00
C ₆ -C ₈ -C ₁₉	122.70
C ₈ -C ₁₉ -C ₂₀	119.60
C ₂₀ -C ₂₂ -C ₂₄	120.20

Dihedral Angels (°)	
C ₃₂ -C ₁₁ -C ₁₀ -C ₉	0.25
C ₁₄ -C ₁₃ -C ₁₂ -C ₁₁	0.07
C ₂₈ -C ₆ -C ₄ -C ₃	-0.30
C ₂₁ -C ₁₉ -C ₈ -C ₆	-0.08

Atomic Charges	
O ₁	-0.03
C ₂	0.36
C ₃	-0.20
C ₄	-0.02
C ₅	-0.05
C ₆	-0.14
C ₇	-0.05
C ₈	-0.06
C ₉	-0.20
C ₁₀	-0.02
C ₁₁	-0.14
C ₁₂	-0.06
C ₁₃	-0.06
C ₁₄	-0.09
C ₁₅	-0.08
C ₁₆	-0.10
C ₁₇	-0.10
C ₁₈	-0.09

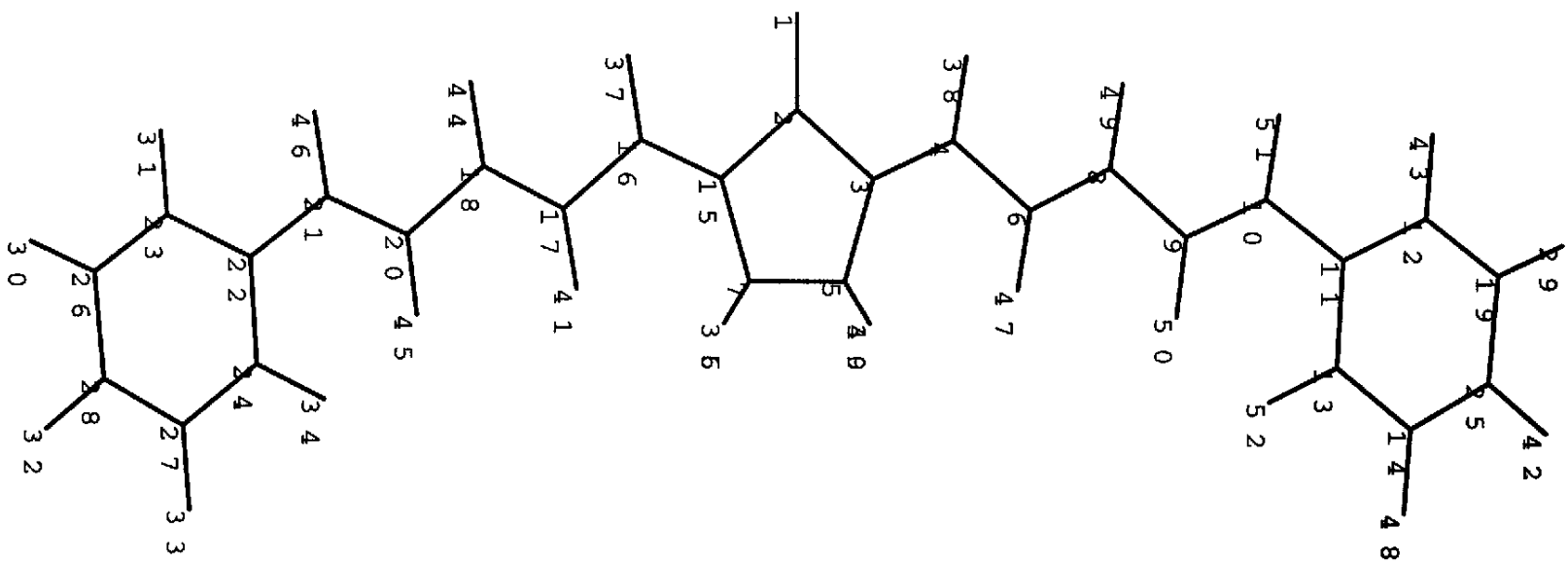


Figure 20: Optimized geometry of 3dbcp ($\Delta H_f = 89.85$ kcal/mol).

Table 9 Calculated Ground State Equilibrium Geometry of 3dbcp by PM3 Method.

	Bond Lengths (Å)	Bond Orders
O ₁ -C ₂	1.22	1.88
C ₂ -C ₃	1.49	0.95
C ₃ -C ₅	1.49	0.99
C ₅ -C ₇	1.53	0.99
C ₇ -C ₁₅	1.49	0.99
C ₃ -C ₄	1.34	1.82
C ₄ -C ₆	1.45	1.06
C ₆ -C ₈	1.34	1.82
C ₈ -C ₉	1.45	1.06
C ₉ -C ₁₀	1.34	1.83
C ₁₀ -C ₁₁	1.46	1.04
C ₁₁ -C ₁₂	1.40	1.38
C ₁₂ -C ₁₉	1.39	1.44
C ₁₉ -C ₂₅	1.39	1.42
C ₂₅ -C ₁₄	1.39	1.42
C ₁₄ -C ₁₃	1.39	1.43
C ₁₃ -C ₁₁	1.40	1.38

Bond Angles (°)	
O ₁ -C ₂ -C ₃	126.10
C ₂ -C ₃ -C ₄	123.80
C ₃ -C ₄ -C ₆	123.60
C ₄ -C ₆ -C ₈	121.60
C ₆ -C ₈ -C ₉	121.80
C ₈ -C ₉ -C ₁₀	121.80
C ₉ -C ₁₀ -C ₁₁	122.70
C ₁₀ -C ₁₁ -C ₁₂	119.60
C ₁₁ -C ₁₂ -C ₁₉	119.90

Dihedral Angels (°)	
C ₄₁ -C ₁₇ -C ₁₆ -C ₁₅	-0.23
C ₄₅ -C ₂₀ -C ₁₈ -C ₁₇	-0.12
C ₂₄ -C ₂₂ -C ₂₁ -C ₂₀	-0.07
C ₄₇ -C ₆ -C ₄ -C ₃	0.28
C ₅₀ -C ₉ -C ₈ -C ₆	0.15
C ₁₃ -C ₁₁ -C ₁₀ -C ₉	0.08

Atomic Charges	
O ₁	-0.31
C ₂	0.36
C ₃	-0.20
C ₄	-0.02
C ₅	-0.05
C ₆	-0.13
C ₇	-0.05
C ₈	-0.07
C ₉	-0.13
C ₁₀	-0.07
C ₁₁	-0.05
C ₁₂	-0.09
C ₁₃	-0.10
C ₁₄	-0.09
C ₁₉	-0.10
C ₂₅	-0.10

4.1.3 Absorption Spectra and INDO/S Calculations

The room temperature absorption spectra of 1dbcp, 2dbcp, and 3dbcp in cyclohexane are shown in Figure 21 - Figure 23 along with the results of INDO/S-CIS calculations. The spectra are similar in their gross appearance. The dominant feature is a strong structured band found between 270 and 370 nm for 1dbcp that moves to longer wavelength and becomes more intense as the polyene chain length increases: 320-420 nm for 2dbcp; 360-470 nm for 3dbcp. The low resolution spacing between the apparent 0-0 and 0-1 vibronic bands of the strong transition falls in the range $1300 - 1440 \text{ cm}^{-1}$ for these compounds. Oscillator strengths (f), uncorrected for solvent index of refraction, have been determined by measuring the area under the strong transition. On the long wavelength side of the strong transition for 1dbcp a series of weak bands with an average spacing of 1280 cm^{-1} is observed between 370 and 460 nm. This band system merges into the long wavelength shoulder of the strong structured transition. For 2dbcp, less resolved weak shoulders are observed between 430 and 490 nm on the long wavelength side of the strong band system. These weak long wavelength bands disappear for 1dbcp and 2dbcp when methanol is used as the solvent. Although no clearly resolved bands are observed for 3dbcp on the long wavelength side of the strong transition. It will be argued later that there is a separate unresolved transition in this region that is masked by the tail of the intense absorption. Turning to the short wavelength side of the strong transition, moderate absorption is observed to fall between 215 and 260 nm for 1dbcp, 230 and 290 nm for 2dbcp, and 260 and 320 nm for 3dbcp. Absorption is seen to rise again near the 200 nm cutoff for all three compounds.

INDO/S calculations provide insight as to the nature of the long wavelength electronic transitions. The INDO/S energies and symmetries of molecular orbitals important in configuration interaction (CI) along with INDO/S – CIS computed singlet state excitations are presented in Table 10 and Table 11 for 1dbcp; Table 12 and Table 13 for 2dbcp; and Table 14 and Table 15 for 3dbcp. Specific comments will be restricted to excitations terminating at the lowest three excited singlet states, S_1 - S_3 . For 1dbcp, 2dbcp, and 3dbcp, S_1 is computed to be a symmetry forbidden $A_2 \leftarrow A_1$ transition (under C_{2v} point group) of the $n \rightarrow \pi^*$ type, arising primarily from the orbital excitation $b_2(n) \rightarrow b_1(\pi^*)$, where $b_1(\pi^*)$ is the LUMO and $b_2(n)$ is HOMO-6 for 3dbcp and HOMO-4 for 1dbcp and 2dbcp. The weak bands observed between 370 and 460 nm for 1dbcp and between 430 and 490 nm for 2dbcp are assigned to this transition. Their position, intensity, and disappearance in alcohol solvent are entirely consistent with $n \rightarrow \pi^*$ behavior.²⁸ Although not separately resolved from the neighboring strong transition, it is believed that S_1 is also $n \rightarrow \pi^*$ ($A_2 \leftarrow A_1$) for 3dbcp in cyclohexane. Fluorescence data presented below support this assignment. According to the INDO/S calculations, S_2 is a strong, y-polarized $B_2 \leftarrow A_1$ transition corresponding primarily to the HOMO \rightarrow LUMO, $a_2(\pi) \rightarrow b_1(\pi^*)$ configuration. Clearly the strong structured transition that dominates the spectra of the three compounds can be assigned with confidence to this excitation. This transition correlates with the $1^1B_u \leftarrow 1^1A_g$ transition of an idealized polyene under the C_{2h} point group. The transition to S_3 is computed by INDO/S-SCI to be a weak, z-polarized $A_1 \leftarrow A_1$ excitation with primary configurations HOMO-1 \rightarrow LUMO, $a_2(\pi) \rightarrow a_2(\pi^*)$ and HOMO \rightarrow LUMO+1, $b_1(\pi) \rightarrow b_1(\pi^*)$. When the calculation is repeated to include doubly excited configurations additional important configurations are found to be HOMO-1,

HOMO \rightarrow LUMO, LUMO+1 and HOMO, HOMO \rightarrow LUMO, LUMO. It appears from the doubly excited configurations that this state correlates with the forbidden idealized polyene $2^1A_g \leftarrow 1^1A_g$ transition, which is known to be S_1 for longer polyene molecules. It would be difficult to observe this relatively weak transition directly in absorption since it is predicted to overlap the short wavelength tail of the much stronger $B_2 \leftarrow A_1$ transition for 1dbcp, 2dbcp, and 3dbcp. However, results from polarized fluorescence excitation spectra (see below) are consistent with the INDO/S prediction that there is a weak transition underlying the tail of the strong band system. Extinction coefficients have been reported for 1dbcp and 2dbcp in cyclohexane as $32,000 \text{ M}^{-1}\text{cm}^{-1}$ (337 nm) and $58,000 \text{ M}^{-1}\text{cm}^{-1}$ (380 nm), respectively.¹⁵ Table 16 summarizes experimental and computed results for electronic transitions between the ground state and the excited states S_1 - S_3 of 1dbcp, 2dbcp, and 3dbcp. Extinction coefficients of these compounds in cyclohexane and methanol are shown in Table 17.

Figure 21: Room temperature absorption spectra of 1dbcp in cyclohexane and INDO/S-CIS calculated results. The diamond on the wavelength axis indicates the computed location of the forbidden ${}^1A_2 \leftarrow {}^1A_1$ transition.

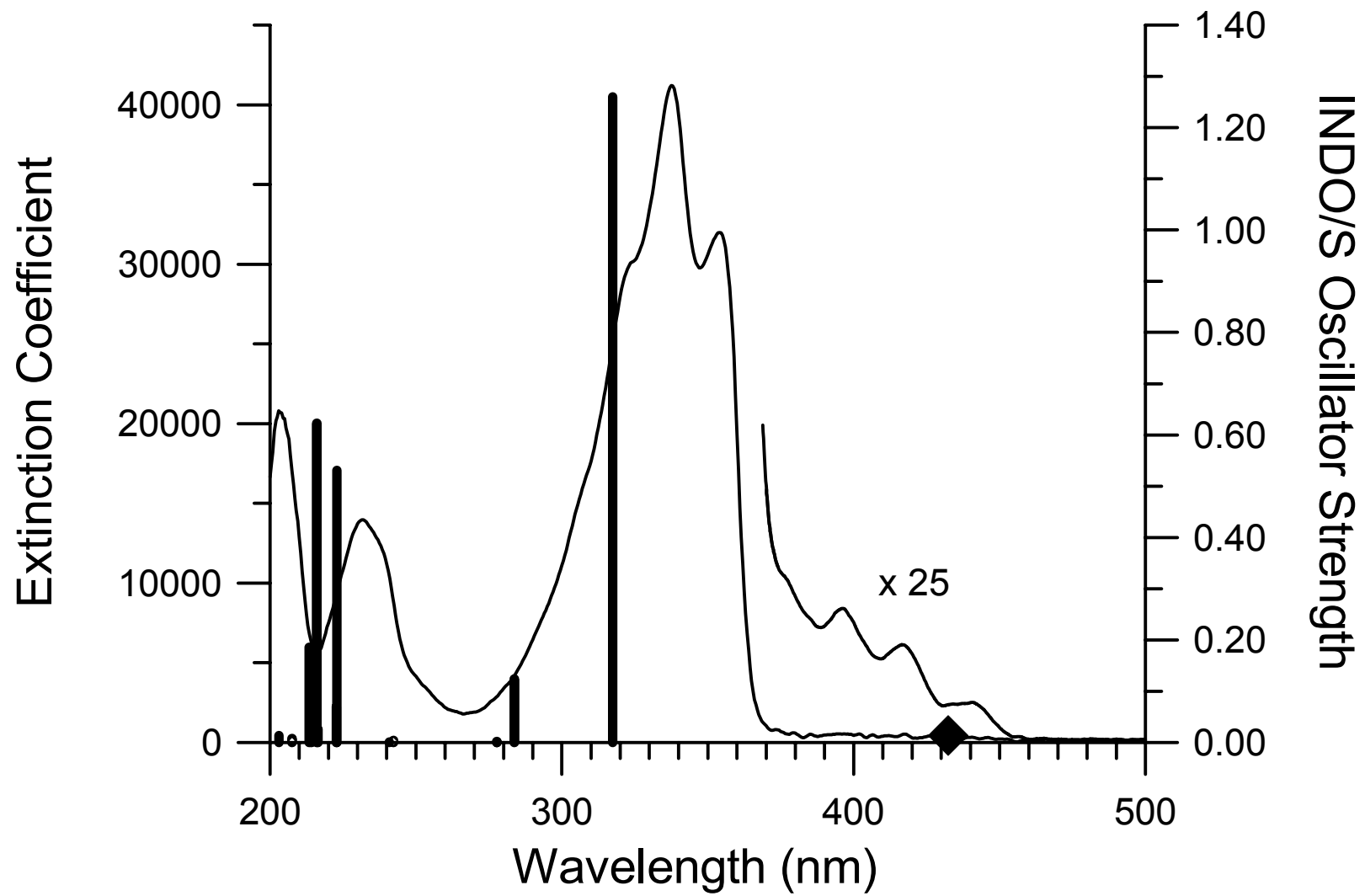


Figure 22: Room temperature absorption spectra of 2dbcp in cyclohexane and INDO/S-CIS calculated results. The diamond on the wavelength axis indicates the computed location of the forbidden ${}^1A_2 \leftarrow {}^1A_1$ transition.

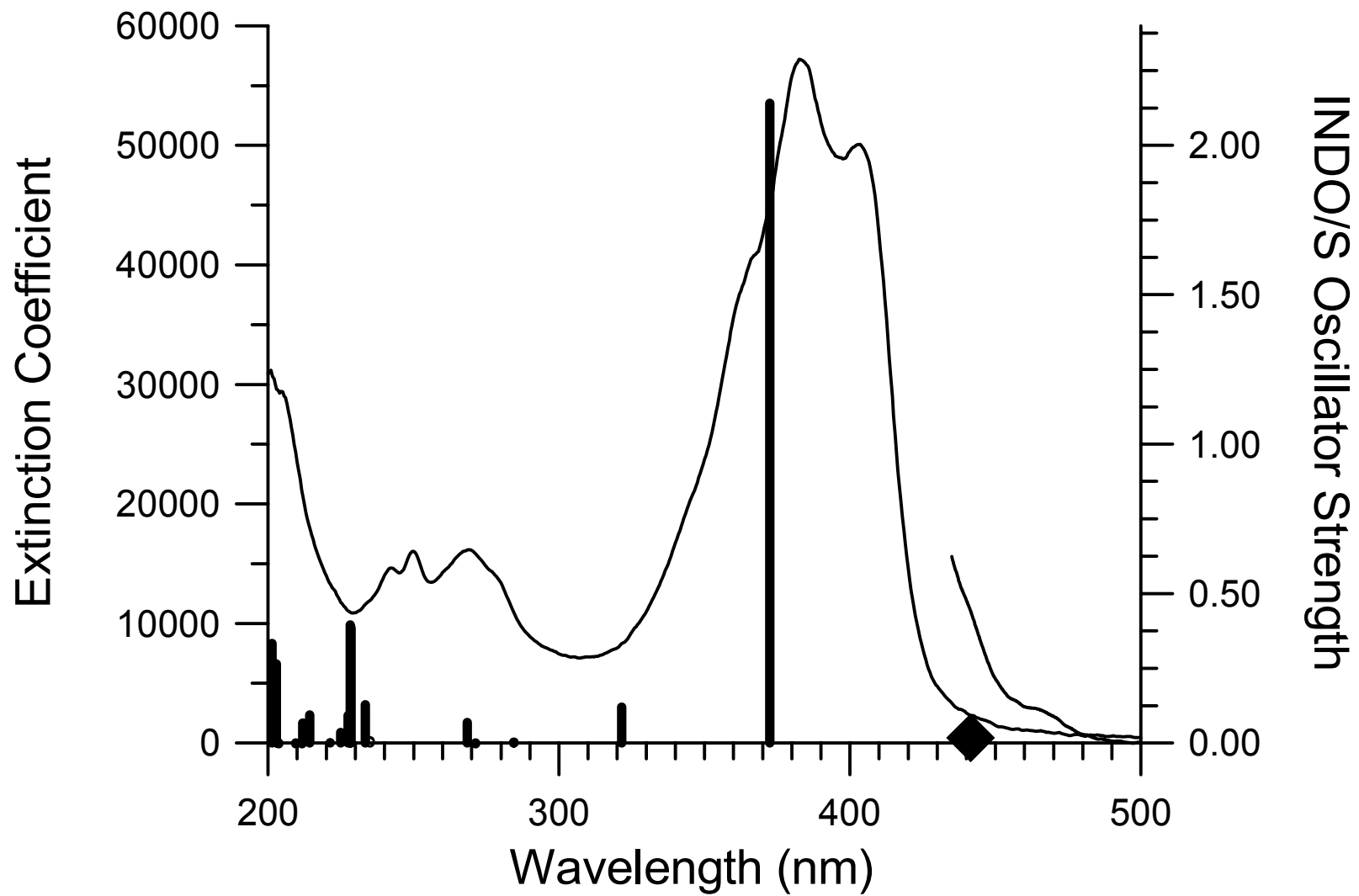


Figure 23: Room temperature absorption spectra of 3dbcp in cyclohexane and INDO/S-CIS calculated results. The diamond on the wavelength axis indicates the computed location of the forbidden ${}^1A_2 \leftarrow {}^1A_1$ transition.

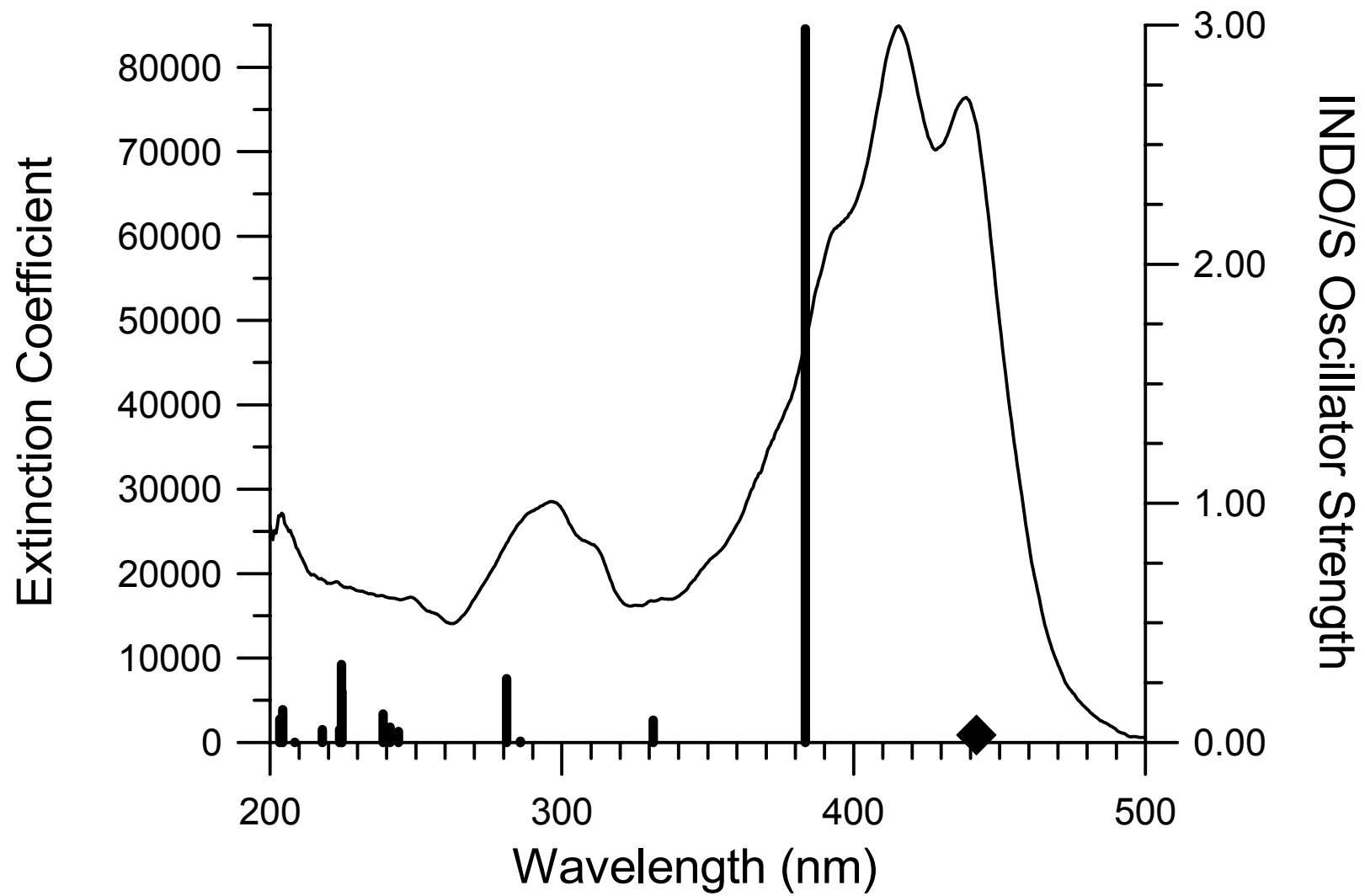


Table 10 INDO/S Energies (eV) and Symmetries of MO's Important in Configuration Interaction (CI) for 1dbcp.

58	2.7378	a'' (b ₂)	
57	2.6094	a' (b ₁)	
56	2.5410	a' (a ₁)	
55	1.7280	a'' (a ₂)	
54	1.0336	a' (b ₁)	
53	0.7434	a' (b ₁)	
52	0.7365	a'' (a ₂)	
51	0.3110	a'' (a ₂)	
50	-0.6624	a' (b ₁)	LUMO
49	-8.0850	a'' (a ₂)	HOMO
48	-8.4097	a' (b ₁)	
47	-9.1332	a' (b ₁)	
46	-9.1449	a'' (a ₂)	
45	-9.4322	a'' (b ₂)	
44	-10.0581	a'' (a ₂)	
43	-10.1098	a' (b ₁)	

Table 11 INDO/S-CIS Computed Singlet State Excitations for 1dbcp.

State		Transition Energy		Oscillator Strength	MO	CI Coef.	
C _s	(C _{2v})	cm ⁻¹	nm				
1 A''	(A ₂)	23166.67	431.655	0.001569	45 → 50	0.82633	(68%)
					45 → 54	0.35155	(12%)
					45 → 47	0.30011	(9%)
2 A''	(B ₂)	31501.76	317.443	1.262325	49 → 50	0.91785	(84%)
3 A'	(A ₁)	35240.50	283.764	0.124080	48 → 50	0.87085	(76%)
					49 → 51	0.39911	(16%)
4 A'	(A ₁)	36002.52	277.758	0.000375	49 → 52	0.50537	(26%)
					48 → 53	0.46278	(21%)
					46 → 51	0.42491	(18%)
					47 → 50	0.41062	(17%)
5 A''	(B ₂)	36008.27	277.714	0.001658	49 → 53	0.50738	(26%)
					48 → 52	0.46753	(22%)
					47 → 51	0.42678	(18%)
					46 → 50	0.40670	(17%)
6 A'	(A ₁)	41268.58	242.315	0.003807	49 → 51	0.66145	(44%)
					48 → 54	0.48146	(23%)
					48 → 50	0.31814	(10%)
					43 → 50	0.24366	(6%)
7 A''	(B ₂)	41516.66	240.867	0.000886	48 → 51	0.58031	(34%)
					49 → 54	0.57768	(33%)
					47 → 52	0.29248	(9%)
					46 → 53	0.29049	(8%)
8 A'	(A ₁)	44861.76	222.907	0.530744	47 → 50	0.63395	(40%)
					49 → 52	-0.44848	(20%)
					48 → 53	0.35328	(12%)
					46 → 51	0.31293	(10%)
9 A''	(B ₂)	44895.16	222.741	0.070334	46 → 50	0.65489	(43%)
					49 → 53	-0.46643	(22%)
					48 → 52	0.37701	(14%)
					47 → 51	0.34430	(12%)
10 A'	(B ₁)	46201.45	216.443	0.026018	45 → 51	-0.42796	(18%)
					43 → 50	-0.42207	(18%)
					47 → 53	0.33777	(11%)
					49 → 51	0.33672	(11%)
					46 → 52	0.33664	(11%)

Table 11 Cont'd. INDO/S-CIS Computed Singlet State Excitations for 1dbcp.

State		Transition Energy		Oscillator Strength	MO	CI Coef.	
C _s	(C _{2v})	cm ⁻¹	nm				
11 A''	(B ₂)	46297.17	215.996	0.623062	44 → 50	-0.45217	(20%)
					47 → 52	0.40556	(16%)
					46 → 53	0.40322	(16%)
					43 → 51	-0.35169	(12%)
					48 → 51	-0.30057	(9%)
12 A'	(B ₁)	46694.65	214.157	0.006390	45 → 51	-0.48305	(23%)
					49 → 55	0.41938	(18%)
					47 → 53	-0.32819	(11%)
					46 → 52	-0.32638	(11%)
					45 → 55	0.30631	(9%)
13 A''	(B ₂)	46856.02	213.420	0.185514	44 → 50	0.49814	(25%)
					48 → 55	0.45730	(21%)
					48 → 51	-0.33344	(11%)
					47 → 52	0.29364	(9%)
					46 → 53	0.29211	(9%)
14 A'	(B ₁)	48182.67	207.544	0.007423	43 → 50	-0.54362	(30%)
					45 → 51	0.47982	(23%)
					49 → 55	0.35019	(12%)
					45 → 55	-0.32502	(11%)
					44 → 51	-0.27093	(7%)
15 A''	(A ₂)	49244.15	203.070	0.013482	49 → 56	-0.73476	(54%)
					48 → 58	0.43766	(19%)
					45 → 57	-0.15355	(2%)
					48 → 63	0.14542	(2%)
					49 → 54	-0.14502	(2%)

Table 12 INDO/S Energies (eV) and Symmetries of MO's Important in Configuration Interaction (CI) for 2dbcp.

70	2.8683	b ₁	
69	2.8658	b ₂	
68	2.6425	a ₁	
67	2.3997	a ₂	
66	1.9033	b ₁	
65	1.2642	a ₂	
64	0.7803	b ₁	
63	0.7796	a ₂	
62	0.6620	b ₁	
61	-0.1900	a ₂	
60	-0.9518	b ₁	LUMO
59	-7.5224	a ₂	HOMO
58	-7.8288	b ₁	
57	-9.1189	a ₂	
56	-9.1190	b ₁	
55	-9.4092	b ₂	
54	-9.4919	a ₂	
53	-9.6088	b ₁	

Table 13 INDO/S-CIS Computed Singlet State Excitations for 2dbcp.

State C _s	Transition Energy			Oscillator Strength	MO	CI Coef.	
	eV	cm ⁻¹	nm				
1 A ₂	2.82355	22773.44	439.108	0.000001	55 → 60	0.81373	(66%)
					55 → 62	0.42124	(18%)
2 B ₂	3.32927	26852.40	372.406	2.141273	59 → 60	-0.89547	(80%)
					58 → 61	0.38501	(15%)
3 A ₁	3.85589	31099.83	321.545	0.120202	58 → 60	0.83285	(69%)
					59 → 61	-0.48680	(24%)
4 B ₂	4.35886	35156.58	284.442	0.002182	59 → 64	-0.49055	(24%)
					58 → 63	-0.47363	(22%)
					56 → 61	0.32504	(11%)
					57 → 60	0.29907	(9%)
					57 → 62	0.28200	(8%)
5 A ₁	4.35901	35157.75	284.432	0.002461	59 → 63	0.49358	(24%)
					58 → 64	0.46886	(22%)
					57 → 61	0.32545	(11%)
					56 → 60	0.29958	(9%)
					56 → 62	0.28263	(8%)
6 A ₁	4.57031	36861.99	271.282	0.000118	59 → 61	-0.67900	(46%)
					58 → 62	0.49183	(24%)
					58 → 60	-0.40814	(17%)
7 B ₂	4.61819	37248.24	268.469	0.068234	58 → 61	-0.62904	(40%)
					59 → 62	0.61338	(38%)
					59 → 60	-0.24002	(6%)
8 A ₁	5.27624	42555.76	234.986	0.006976	59 → 65	0.54491	(30%)
					59 → 61	0.34794	(12%)
					58 → 62	0.34401	(12%)
					54 → 61	0.32667	(11%)
					56 → 64	-0.27185	(7%)
9 B ₂	5.31219	42845.66	233.396	0.128217	58 → 65	0.56066	(31%)
					58 → 61	0.42556	(18%)
					59 → 62	0.34567	(12%)
					59 → 66	-0.24972	(6%)
					57 → 64	0.24270	(6%)
10 B ₂	5.42675	43769.70	228.469	0.384602	57 → 60	-0.50020	(25%)
					59 → 64	-0.45551	(21%)
					56 → 61	-0.40024	(16%)
					58 → 63	-0.38565	(15%)
					56 → 60	-0.26364	(7%)
11 A ₁	5.43282	43818.63	228.213	0.395627	56 → 60	0.49702	(25%)
					59 → 63	-0.45072	(20%)
					57 → 61	0.39482	(16%)
					58 → 64	-0.37932	(14%)
					57 → 60	-0.26192	(7%)

Table 13 Cont'd. INDO/S-CIS Computed Singlet State Excitations for 2dbcp.

State C _s	Transition Energy			Oscillator Strength	MO	CI Coef.	
	eV	cm ⁻¹	nm				
12 B ₂	5.44870	43946.74	227.548	0.092424	54 → 60 53 → 61 59 → 62 57 → 64	0.70230 0.42471 0.32115 -0.19173	(49%) (18%) (10%) (4%)
13 A ₁	5.51040	44444.34	225.001	0.035238	53 → 60 59 → 65 54 → 61	-0.71446 0.39852 -0.37129	(51%) (16%) (14%)
14 B ₁	5.60215	45184.39	221.315	0.000310	55 → 61 55 → 65	-0.82581 -0.45644	(68%) (21%)
15 B ₂	5.78549	46663.08	214.302	0.094064	59 → 66 54 → 60 59 → 62 58 → 61 56 → 63	0.45469 -0.35688 0.31187 0.30926 0.28417	(21%) (13%) (10%) (10%) (8%)
16 A ₁	5.85074	47189.42	211.912	0.066787	57 → 63 56 → 64 59 → 67 58 → 62 58 → 66	0.39154 -0.39019 0.35942 -0.34301 -0.33078	(15%) (15%) (13%) (12%) (11%)
17 A ₂	5.85979	47262.39	211.585	0.000007	59 → 68 58 → 69 58 → 75 58 → 72	0.75090 0.41497 0.25474 0.22192	(56%) (17%) (6%) (5%)
18 B ₁	5.91638	47718.81	209.561	0.000033	58 → 68 59 → 69 59 → 75 59 → 72	-0.62197 -0.53035 -0.31267 -0.27942	(39%) (28%) (10%) (8%)
19 A ₂	6.08612	49087.85	203.716	0.000047	55 → 70 55 → 60 55 → 66 55 → 62	-0.52198 0.50615 0.44435 0.30952	(27%) (26%) (20%) (10%)
20 B ₂	6.11309	49305.35	202.818	0.264197	59 → 66 56 → 63 57 → 64 58 → 65 57 → 63	-0.51728 0.41459 -0.41230 0.30647 -0.21307	(27%) (17%) (17%) (9%) (5%)
21 A ₁	6.15709	49660.23	201.368	0.333373	58 → 66 59 → 67 57 → 63 56 → 64 59 → 65	-0.50265 0.44146 -0.32916 0.32549 0.28429	(25%) (19%) (11%) (11%) (8%)

Table 14 INDO/S Energies (eV) and Symmetries of MO's Important in Configuration

Interaction (CI) for 3dbcp.

80	2.6678	a ₁	
79	2.6558	a ₂	
78	2.3466	b ₁	
77	1.8867	a ₂	
76	1.4348	b ₁	
75	0.8667	a ₂	
74	0.8135	b ₁	
73	0.8125	a ₂	
72	0.3130	b ₁	
71	-0.4297	a ₂	
70	-1.0338	b ₁	LUMO
69	-7.2463	a ₂	HOMO
68	-7.4924	b ₁	
67	-8.8709	a ₂	
66	-9.0321	b ₁	
65	-9.0858	a ₂	
64	-9.0866	b ₁	
63	-9.3780	b ₂	
62	-10.5546	a ₂	
61	-10.5664	b ₁	
60	-11.9301	b ₂	

Table 15 INDO/S-CIS Computed Singlet State Excitations for 3dbcp.

State C _s	Transition Energy			Oscillator Strength	MO	CI Coef	
	eV	cm ⁻¹	nm				
1 A ₂	2.82441	22780.41	438.974	0.000004	63 → 70	0.77289	(60%)
					63 → 72	0.45016	(20%)
					63 → 76	0.29220	(9%)
2 B ₂	3.23331	26078.41	383.459	2.984100	69 → 70	-0.88060	(78%)
					68 → 71	0.40386	(16%)
3 A ₁	3.74224	30183.22	331.310	0.092547	68 → 70	0.82052	(67%)
					69 → 71	-0.50584	(26%)
4 A ₁	4.33899	34996.28	285.745	0.004721	68 → 74	-0.44534	(20%)
					69 → 73	0.44224	(20%)
					65 → 71	0.31653	(10%)
					67 → 73	-0.30296	(9%)
					64 → 72	0.29807	(9%)
5 B ₂	4.33926	34998.49	285.727	0.001396	68 → 73	0.45641	(21%)
					69 → 74	-0.44541	(20%)
					64 → 71	0.31886	(10%)
					65 → 72	0.30898	(10%)
					67 → 74	0.30812	(9%)
6 A ₁	4.38751	35387.61	282.585	0.000003	69 → 71	0.63079	(40%)
					68 → 72	0.51111	(26%)
					68 → 70	0.38234	(15%)
7 B ₂	4.41176	35583.19	281.032	0.266741	69 → 72	-0.63230	(40%)
					68 → 71	-0.59948	(36%)
					67 → 70	-0.25266	(6%)
8 B ₂	4.99723	40305.35	248.106	0.000055	67 → 70	-0.59444	(35%)
					68 → 75	0.45644	(21%)
					69 → 72	0.40023	(16%)
					68 → 71	-0.27005	(7%)
					66 → 71	-0.23150	(5%)
9 A ₁	5.08094	40980.54	244.018	0.045136	69 → 75	0.64757	(42%)
					66 → 70	0.41990	(18%)
					68 → 72	0.36681	(13%)
					69 → 71	-0.25372	(6%)
					68 → 76	-0.24849	(6%)
10 A ₁	5.14027	41459.08	241.202	0.063062	66 → 70	0.61435	(38%)
					67 → 71	0.55108	(30%)
					69 → 71	0.29329	(9%)
					69 → 75	-0.23930	(6%)

Table 15 Cont'd. INDO/S-CIS Computed Singlet State Excitations for 3dbcp.

State C _s	Transition Energy			Oscillator Strength	MO	CI Coef	
	eV	cm ⁻¹	nm				
11 B ₂	5.19371	41890.04	238.720	0.119095	66 → 71	-0.50594	(26%)
					67 → 70	-0.46375	(22%)
					68 → 75	-0.40116	(16%)
					68 → 71	0.37329	(14%)
					69 → 70	0.23838	(6%)
12 B ₂	5.51851	44509.76	224.670	0.212561	65 → 70	0.45983	(21%)
					64 → 71	-0.44131	(19%)
					69 → 74	-0.41959	(18%)
					68 → 73	0.35476	(13%)
					65 → 72	-0.27436	(8%)
13 A ₁	5.52302	44546.13	224.486	0.326013	64 → 70	0.49344	(24%)
					65 → 71	-0.47164	(22%)
					69 → 73	0.43650	(19%)
					68 → 74	-0.39656	(16%)
14 B ₂	5.53849	44670.88	223.859	0.053279	69 → 76	0.57858	(33%)
					68 → 71	-0.30982	(10%)
					69 → 72	0.27904	(8%)
					68 → 77	0.27373	(7%)
					67 → 72	0.27207	(7%)
15 B ₁	5.55692	44819.56	223.117	0.000249	63 → 71	-0.77536	(60%)
					63 → 75	0.48196	(23%)
16 A ₁	5.68941	45888.17	217.921	0.053491	68 → 76	-0.56930	(32%)
					69 → 77	-0.49437	(24%)
					68 → 72	-0.29470	(9%)
					66 → 72	0.24076	(6%)
					69 → 71	0.22738	(5%)
17 A ₂	5.73998	46296.03	216.001	0.000000	69 → 80	0.68174	(46%)
					68 → 81	0.47304	(22%)
					68 → 84	0.25578	(7%)
					69 → 86	-0.25215	(6%)
18 B ₁	5.76962	46535.14	214.891	0.000013	68 → 80	-0.56306	(32%)
					69 → 81	-0.55593	(31%)
					69 → 84	-0.30443	(9%)
					68 → 86	0.28274	(8%)
					69 → 85	0.24197	(6%)
19 B ₂	5.94680	47964.15	208.489	0.000864	68 → 77	-0.44692	(20%)
					62 → 70	-0.37489	(14%)
					66 → 71	-0.34652	(12%)
					67 → 72	0.34588	(12%)
					69 → 78	-0.30539	(9%)

Table 15 Cont'd. INDO/S-CIS Computed Singlet State Excitations for 3dbcp.

State C _s	Transition Energy			Oscillator Strength	MO	CI Coef	
	eV	cm ⁻¹	nm				
20 A ₁	6.00801	478457.85	206.365	0.000099	61 → 70	-0.43755	(19%)
					66 → 72	0.41974	(18%)
					67 → 71	-0.39479	(16%)
					69 → 77	0.28347	(8%)
					64 → 74	0.22591	(5%)
21 A ₂	6.02865	48624.35	205.658	0.000015	63 → 70	0.52742	(28%)
					63 → 83	-0.44251	(20%)
					63 → 78	0.37193	(14%)
					63 → 76	-0.35771	(13%)
					63 → 72	-0.22244	(5%)
22 B ₂	6.06687	48932.60	204.363	0.137440	65 → 74	-0.46222	(21%)
					64 → 73	0.44565	(20%)
					69 → 78	0.41735	(17%)
					68 → 79	0.27046	(7%)
					62 → 70	-0.20048	(4%)
23 A ₁	6.09560	49164.30	203.400	0.095822	68 → 78	-0.41961	(18%)
					64 → 74	0.35722	(13%)
					65 → 73	-0.35525	(13%)
					69 → 79	-0.34082	(12%)
					68 → 72	0.27005	(7%)
24 A ₂	6.10541	49.243	203.073	0.000007	60 → 82	0.54496	(30%)
					68 → 81	0.32797	(11%)
					67 → 80	-0.31021	(10%)
					68 → 84	-0.29315	(9%)
					68 → 89	0.26702	(7%)
25 B ₂	6.14299	49546.54	201.830	0.000312	69 → 82	-0.53205	(28%)
					69 → 84	0.44313	(20%)
					69 → 89	-0.31616	(10%)
					66 → 80	-0.29482	(9%)
					67 → 81	0.28661	(8%)

Table 16 Absorption Spectral Data for 1dbcp, 2dbcp, and 3dbcp in Cyclohexane at Room Temperature and INDO/S Calculated Results.

	1dbcp	2dbcp	3dbcp
S₁ (A₂)			
λ (nm), exp	370-460	430-490	---
ϵ (M ⁻¹ cm ⁻¹)	~10 ²	~10 ²	---
λ_{max} (nm), calc	432	439	439
f, calc	0.00	0.00	0.00
S₂ (B₂)			
λ_{max} (nm), exp	337	382	415
ϵ_{max} (M ⁻¹ cm ⁻¹)	41.2 x 10 ³	57.2 x 10 ³	84.9 x 10 ³
f, exp	0.76	1.05	1.64
λ_{max} (nm), calc	317	372	383
f, calc	1.26	2.14	2.98
S₃ (A₁)			
λ_{max} (nm), calc	284	321	331
f, calc	0.12	0.12	0.09

Table 17 Extinction Coefficients of Compounds in Cyclohexane and Methanol.

Compound	Solvent	λ_{max} (nm)	ϵ ($\text{M}^{-1}\text{cm}^{-1}$)
1dbcp	Cyclohexane	337	41,214
	Methanol	354	42,248
2dbcp	Cyclohexane	382	57,208
	Methanol	408	61,029
3dbcp	Cyclohexane	415	84,905
	Methanol	445	83,586

4.1.4 Fluorescence Properties

In examining the fluorescence properties of these compounds it is found that each behaves differently with respect to changes in solvent polarity and hydrogen bonding strength. The pKa values of the alcohol solvents used are presented in Table 18. No fluorescence has been observed for 1dbcp in any of the solvents studied (nonpolar, polar aprotic or protic solvents). Fluorescence is observed for 2dbcp in alcohols but not in nonpolar nor in aprotic polar solvents. For 3dbcp, fluorescence is observed in a variety of solvents including polar protic and aprotic solvents and some aprotic nonpolar solvents. However, no fluorescence has been observed for 3dbcp in alkane solvents. In situations where fluorescence has not been observed for 1dbcp, 2dbcp, or 3dbcp, it is believed that S_1 is $n\pi^*$ and S_2 is $\pi\pi^*$. The absence of measurable fluorescence when S_1 is $n\pi^*$ is attributed to efficient $^1(n\pi^*) \rightarrow ^3(\pi\pi^*)$ intersystem crossing which, as noted by El-Sayed, is a direct consequence of the strong spin-orbit coupling that exists between singlet and triplet states of different orbital configurations.³⁹ A solvent induced inversion of state order such that S_1 becomes $\pi\pi^*$ is believed to occur in those situations where fluorescence is observed. The inversion of $n\pi^*$ and $\pi\pi^*$ states when $n\pi^*$ lies lower in energy in nonpolar solvents is due to the well known shift to higher energy experienced by $n\pi^*$ states and the shift to lower energy experienced by $\pi\pi^*$ states on going from nonpolar to polar solvents. Hydrogen bonding solvents generally cause the largest blue shift for $n\pi^*$ transitions and the magnitude of the shift has been correlated with the hydrogen bonding strength of the solvent.^{27,40,41} As the INDO/S calculations indicate, and has been found for short polyene ketones and aldehydes where $n\pi^*$ is lower in energy than $\pi\pi^*$, the energy of the $n\pi^*$ state decreases less rapidly than that of the $\pi\pi^*$ state as

the number of conjugated double bonds increases.^{24,42} Thus in environments where S_1 is $n\pi^*$ for 1dbcp, 2dbcp, and 3dbcp, the $S_1(n\pi^*)$ - $S_2(\pi\pi^*)$ energy gap is expected to decrease in going from 1dbcp to 3dbcp.

Figure 24 and Figure 25 present the room temperature fluorescence, fluorescence excitation, and absorption spectra of 2dbcp and 3dbcp in the alcohol series 1-octanol, 1-butanol, 1-propanol, ethanol, methanol, 2,2,2,-trifluoroethanol (TFE), and hexafluoroisopropanol (HFIP). Features to note are that the fluorescence spectra red shift to a greater extent than do the absorption spectra as the solvent pKa decreases. The excitation spectra and absorption spectra for 2dbcp do not overlap completely; whereas there is reasonably good overlap of excitation and absorption spectra for 3dbcp in the series of alcohols. Specifically, it is found that the excitation spectra of 2dbcp in alcohols are red shifted relative to the absorption spectra, resulting in an apparent dependence of ϕ_f on the S_1 excitation wavelength. The effect is far less pronounced for 2dbcp in strongly hydrogen bonding solvents of TFE and HFIP. The results for 2dbcp in alcohols are strongly reminiscent of the 77 K results reported by Becker^{25,43} for certain polyene ketones and aldehydes, including retinals, in EPA (ether/ isopentane/ ethanol) and by Christensen and coworkers for 2,4,6,8-decatetraenal in methanol/ ethanol at 10 K.²⁷ The explanation provided in these previous studies is applicable to the results presented here. Within the alcohol solution a mixture of hydrogen bonded and non-hydrogen bonded molecules of 2dbcp exists. For the non-hydrogen bonded members, $n\pi^*$ remains below $\pi\pi^*$ and does not fluoresce. Hydrogen bonding inverts the order of these states and induces fluorescence from S_1 ($\pi\pi^*$). Presumably the failure of the nonfluorinated alcohols to completely hydrogen bond with 2dbcp is because much of the solvent is tied

up in self-association.^{27,44,45} As with 2,4,6,8-decatetraenal, the extent of complex formation for 2dbcp with the stronger hydrogen-bonding solvents TFE and HFIP appears to be complete as witnessed by the good agreement between excitation and absorption spectra.²⁷ Unlike decatetraenal, however, a strong enhancement in fluorescence intensity is not observed for 2dbcp in TFE when the temperature is lowered from 100 K to 10 K. Contrary to the situation for 2dbcp, it is found that there is generally good agreement between the excitation and absorption spectra of 3dbcp in alcohols. The conclusion here is that although there is a distribution of hydrogen bonded and nonhydrogen bonded molecules of 3dbcp, the nonhydrogen bonded molecules find themselves in a polar solvent environment that is sufficient to invert $n\pi^*$ and $\pi\pi^*$ and induce fluorescence. The observation of fluorescence from 3dbcp in aprotic polar solvents such as acetonitrile shows that it is possible to achieve state inversion in 3dbcp without forming a hydrogen bonded complex with the solvent.

Since, 3dbcp is found to fluoresce in a number of aprotic solvents as well as protic solvents, a more complete study of solvent effects on absorption and fluorescence spectra was carried out as shown in Figure 27 and Figure 28. The fluorescence spectra were found to be independent of the excitation wavelength, and similarly, the excitation spectra were found to be independent of the wavelength of fluorescence that was monitored.

3dbcp in protic and aprotic solvents are plotted separately in Figure 29 to determine the solvent sensitivity by using Lippert plots and to calculate the dipole moment of the compound. In general, solvent effects may occur due to electronic polarizability of solvent (n) and molecular polarizability (as a function of ϵ , resulting

from reorientation of solvent molecules).²⁹ Besides the general effects, specific solvent effects may also take place due to interactions between the solvent and the fluorophore, such as; hydrogen bonding, acid-base chemistry, charge transfer reactions. If there is high sensitivity to solvent, upon excitation, large changes in dipole moment may occur. 3dbcp exhibits Stokes' shifts proportional to that of orientation polarizability in protic and aprotic polar solvents. Figure 29-c shows similar slopes for protic and aprotic solvents indicating similar mechanism, due to specific solvent effects. It is also observed that in strong hydrogen bonding solvents, specific solvent fluorophore interaction takes place and results in larger Stokes' shift.²⁹ Besides the specific solvent effects, linearity of plots provides important evidence to general solvent effects in the spectral shifts.

Due to the assumptions that are used in the Lippert method, the excited state dipole moment upon excitation can only be approximated. Using the Ratio method a more reliable excited state dipole moment calculation can be obtained, since only measured parameters are used in this equation. Despite to the parameter difference of these methods, the order of magnitude can be determined reliably from both methods and dipole moment can be estimated. In the next paragraph a discussion on the calculations of dipole moments will be given along with their calculated values.

Although not in a perfectly linear manner, it is found that the absorption and fluorescence band maxima shift to lower energy; whereas the difference, the Stokes' shift, moves to higher energy when plotted against Δf , the solvent's orientation polarization. The orientation polarization is defined as $\Delta f = \frac{(\epsilon - 1)}{(2\epsilon + 1)} - \frac{(n^2 - 1)}{(2n^2 + 1)}$, where, ϵ is the dielectric constant and n is the index of refraction for the solvent. The positive slope for the Stokes' shift vs. Δf plot is evidence that the dipole moment is larger for 3dbcp in

the excited state than in the ground state.²⁹ It is possible to calculate the dipole moment of 3dbcp in S₁ from the solvent induced shifts in the absorption and fluorescence spectra by means of the ratio method given in Eq. (4-1)⁴⁶

$$\mu_e = \mu_g \frac{\Delta E_f}{\Delta E_a} \quad (4-1)$$

where, μ_e and μ_g are the excited state and ground state dipole moments and ΔE_f and ΔE_a are the solvatochromic shifts for fluorescence and absorption. The major advantage of using this method over the Lippert-Mataga method^{47,48} is that it is not necessary to assume a cavity radius for the solute. In employing Eq. (4-1) to determine μ_e the underlying assumptions are that μ_e and μ_g are collinear and that the cavity radius is about the same in both states. Using the PM3 computed value for μ_g (2.79 D), μ_e is calculated to be 6.4 D from the aprotic solvent data and 6.6 D from the protic solvent data. The gas phase INDO/S calculation gives a slightly higher dipole moment of 7.2 D for 3dbcp in the B₂ state.

Fluorescence quantum yields have also been measured for 3dbcp and are plotted against the fluorescence frequency in Figure 30. It is observed that the quantum yield is approximately 10⁻³ when the fluorescence maximum occurs above 19,000 cm⁻¹ (nonpolar solvents), increases sharply to 0.04±0.01 between 19,000 and 17,000 cm⁻¹ (polar solvents) and decreases gradually (0.03-0.01) below 17,000 cm⁻¹ (alcohols). The radiative rate constants k_f can be determined from a knowledge of ϕ_f and the measured fluorescence lifetime τ , according to $k_f = \phi_f/\tau$. The rate of nonradiative decay from S₁ can be calculated from

$$k_{nr} = (1/\phi_f - 1) k_f \quad (4-2)$$

In the absence of experimental values for τ , it is necessary to rely on the method of Strickler and Berg⁴⁹ to estimate k_f from the integrated absorption spectra. The radiative rates of decay for 3dbcp in CCl_4 and methanol are calculated by the Strickler and Berg method to be 5×10^8 and $4 \times 10^8 \text{ s}^{-1}$, respectively. From these values of k_f and the measured ϕ_f , the k_{nr} values are calculated from Eq. (4-2) to be 6×10^{11} (CCl_4) and $1 \times 10^{10} \text{ s}^{-1}$ (methanol) for 3dbcp. Limited as it may be⁵⁰, the data obtained in these two solvents suggest that the order of magnitude decrease in ϕ_f for 3dbcp in solvents where emission occurs above $19,000 \text{ cm}^{-1}$ compared to its value in those solvents where the fluorescence occurs at lower frequencies is due primarily to a larger value for k_{nr} . This is contrary to the trend expected from the energy gap law for internal conversion, which predicts that the rate of internal conversion should increase as the energy gap between S_1 and S_0 decreases.⁵¹ Explanations for the enhanced rate of nonradiative decay for 3dbcp in solvents where emission occurs at frequencies above $19,000 \text{ cm}^{-1}$ can be found by considering that it is in these nonpolar solvents (CS_2 , CCl_4 , toluene) that 3dbcp is expected to have the smallest $S_1(\pi\pi^*)$ - $S_2(n\pi^*)$ energy gap. There are two pathways by which this small energy gap could result in efficient nonradiative decay of S_1 . One is through an enhancement in the rate of intersystem crossing and the other is through an enhancement of the rate of internal conversion. If ${}^3n\pi^*$ lies between $S_1(\pi\pi^*)$ and $T_1(\pi\pi^*)$, efficient intersystem crossing could account for the weak fluorescence. Because of the dramatic difference in oscillator strengths, k_f for $S_1(\pi\pi^*)$ is expected to be much larger than for $S_1(n\pi^*)$. Hence a small amount of fluorescence can be observed for 3dbcp in these solvents compared to alkane solvents where no fluorescence has been observed and where S_1 is $n\pi^*$. A blue shift of the ${}^3n\pi^*$ state in polar or hydrogen bonding solvents

could shift it above $S_1(\pi\pi^*)$ and cutoff this path for intersystem crossing. An alternative mechanism for solvent dependent intersystem crossing that does not require $^3n\pi^*$ to be located below $S_1(\pi\pi^*)$ is second-order vibronic spin-orbit coupling.^{52,53} Here increasing the $n\pi^* - \pi\pi^*$ energy gap with solvent diminishes the degree of state mixing which in turn reduces the rate of intersystem crossing.

The enhanced internal conversion pathway involves the “proximity effect” where vibronic interaction between closely spaced $n\pi^*$ and $\pi\pi^*$ states is expected to lead to the distortion and displacement of the potential energy surfaces of the coupled states. Lim has argued through theory and experiment that such distortion/displacement of S_1 can dramatically increase the rate of internal conversion.⁵⁴ Any influence (solvent, substituents) that increases the $n\pi^* - \pi\pi^*$ energy gap between strongly coupled states would reduce the vibronic coupling between them and the associated distortion/displacement of potential energy surfaces, thus decreasing the rate of internal conversion. For many nitrogen heterocyclic and aromatic carbonyl compounds that do not fluoresce or fluoresce weakly in nonpolar aprotic solvents, it has been observed that a switch to protic solvents greatly increases ϕ_f . Studies indicate that for some of these molecules the change in fluorescence behavior can not be attributed to a change in singlet-triplet intersystem crossing.⁵⁵ The extent to which each of these pathways contributes to k_{nr} when S_1 of 3dbcp is above $19,000\text{ cm}^{-1}$ awaits further investigation. The rate that ϕ_f drops off with decreasing energy when S_1 of 3dbcp is below $17,000\text{ cm}^{-1}$ appears to be consistent with the energy gap law for internal conversion which predicts an exponential dependence of k_{ic} on ΔE , the $S_1 - S_0$ energy gap⁴²:

$$k_{ic} = Ce^{-\alpha\Delta E} \quad (4-3)$$

The room temperature fluorescence properties of 2dbcp and 3dbcp are summarized in Table 19 and Table 20. Fluorescence, fluorescence excitation, and polarized excitation spectra were measured for 2dbcp and 3dbcp at 77 K in an ethanol/methanol (4:1) glass and are shown in Figure 31. In comparing the room temperature spectra of 2dbcp and 3dbcp in ethanol with the 77 K spectra in ethanol/methanol, it is observed that the spectra change from broad featureless bands to spectra exhibiting well-resolved vibronic structure. It is also seen that the low temperature absorption spectra are red shifted and the fluorescence spectra blue shifted relative to the room temperature spectra, resulting in a much smaller Stokes' shift. Small Stokes' shifts are commonly observed for molecules in low temperature glasses and are attributed to the inability of the solvent matrix to reorient and stabilize the molecule during the excited state lifetime. The red shift of the absorption spectrum in going from a room temperature liquid to a low temperature glass for a polar molecule in a polar solvent is also frequently observed and may be related to the thermochromic shift discussed by Suppan.³⁰ The decrease in the degree of positive polarization observed towards the short wavelength tail of the strong $B_2(y) \leftarrow A_1$ transition for 2dbcp and 3dbcp may be due to the presence of a weak underlying transition of perpendicular polarization. As noted earlier, the INDO/S calculations do predict a weak $A_1(z) \leftarrow A_1$ transition (S_3) to occur in this region.

Table 18 Alcohol Acidity.

Alcohol	pKa
n_Octanol	
t_Butanol	18.0
n_propanol	16.2
Ethanol	15.9
Methanol	15.5
2,2,2_Trifluoroethanol	12.4
Hexafluoroisopropanol	9.3

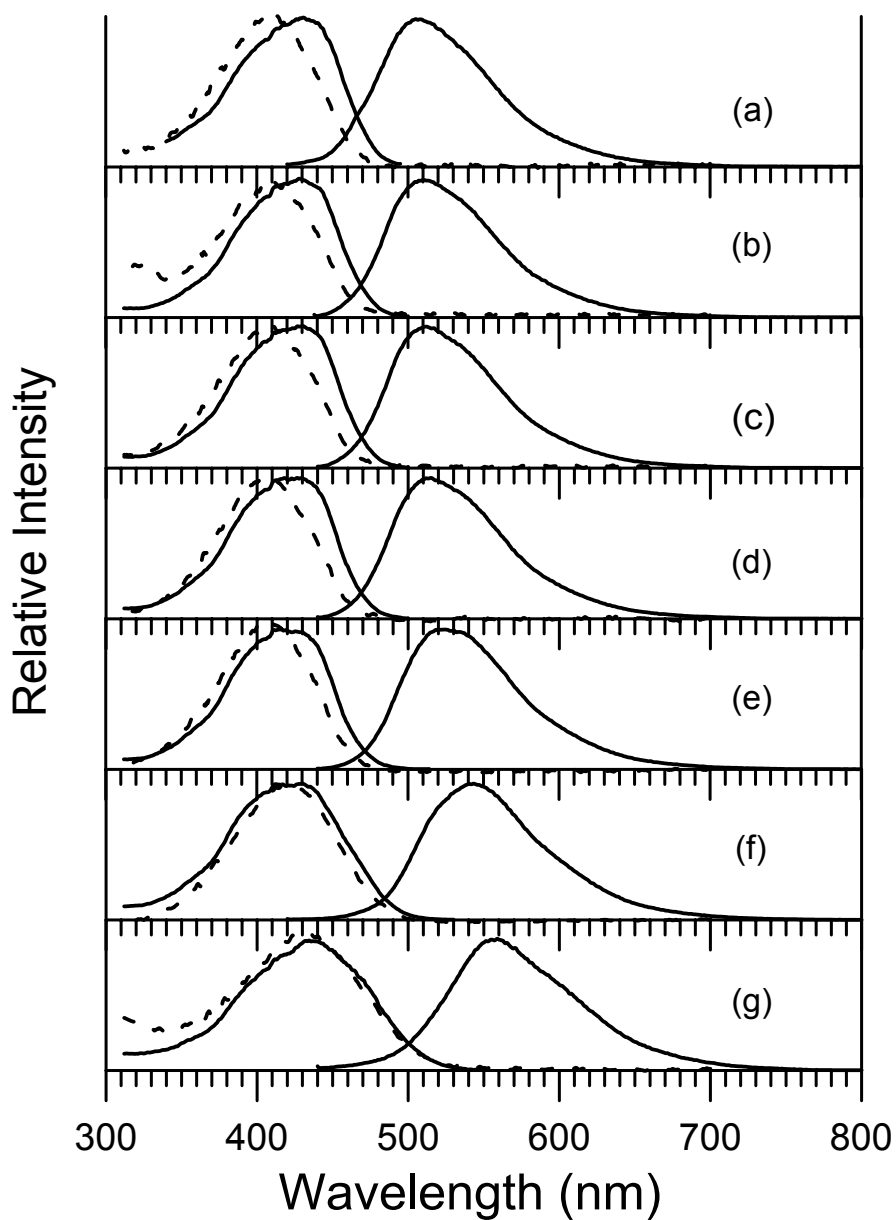


Figure 24: Absorption (dashed line), excitation (left), and fluorescence (right) spectra of 2dbcp in alcohols: (a) 1-octanol ($\lambda_{\text{Ex max}}$: 431 nm); (b) 1-butanol ($\lambda_{\text{Ex max}}$: 428 nm); (c) 1-propanol ($\lambda_{\text{Ex max}}$: 430 nm); (d) ethanol ($\lambda_{\text{Ex max}}$: 420 nm); (e) methanol ($\lambda_{\text{Ex max}}$: 416 nm); (f) TFE ($\lambda_{\text{Ex max}}$: 430 nm); (g) HFIP ($\lambda_{\text{Ex max}}$: 434 nm).

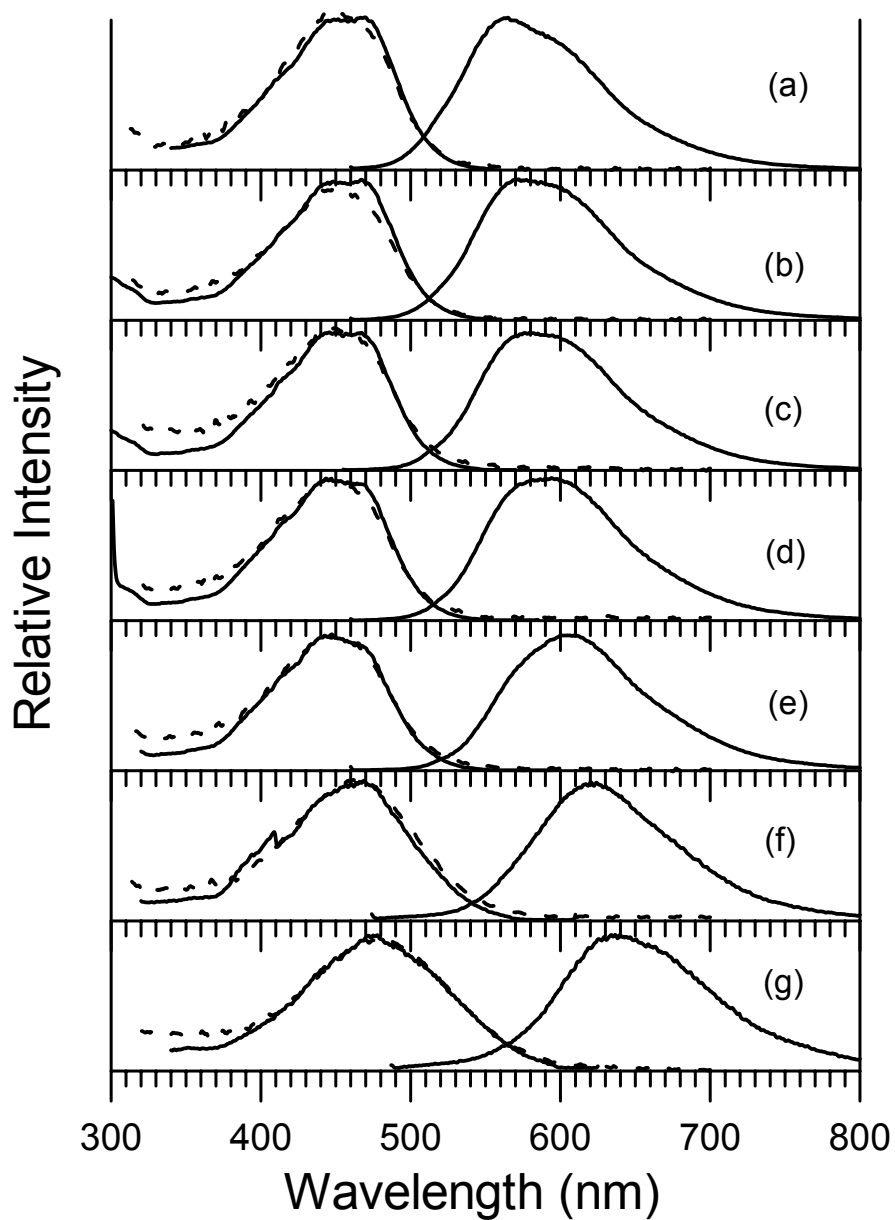


Figure 25: Absorption (dashed line), excitation (left), and fluorescence (right) spectra of 3dbcp in alcohols: (a) 1-octanol ($\lambda_{\text{Ex max}}$: 452 nm); (b) 1-butanol ($\lambda_{\text{Ex max}}$: 450 nm); (c) 1-propanol ($\lambda_{\text{Ex max}}$: 445 nm); (d) ethanol ($\lambda_{\text{Ex max}}$: 445 nm); (e) methanol ($\lambda_{\text{Ex max}}$: 451 nm); (f) TFE ($\lambda_{\text{Ex max}}$: 464 nm); (g) HFIP ($\lambda_{\text{Ex max}}$: 477 nm).

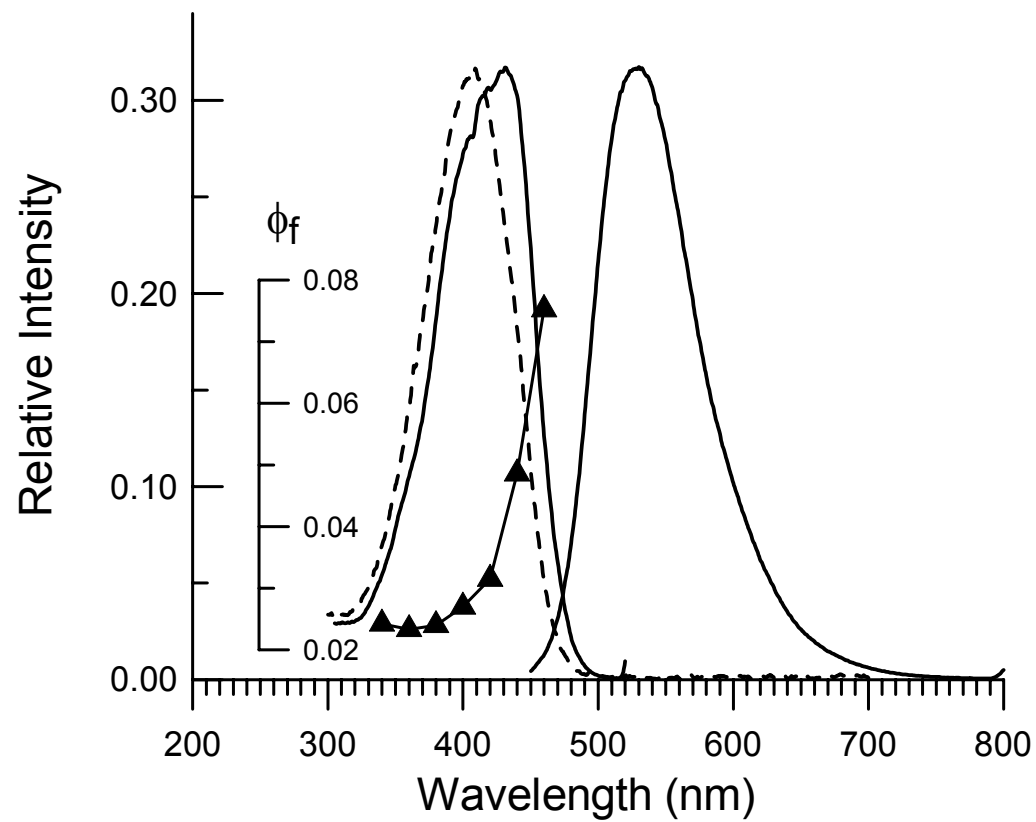


Figure 26: Absorption (dashed line), excitation (left), and fluorescence (right) spectra and fluorescence quantum yield as a function of excitation wavelength for 2dbcp in methanol (multiple excitation from 340 nm to 460 nm with increments of 20 nm).

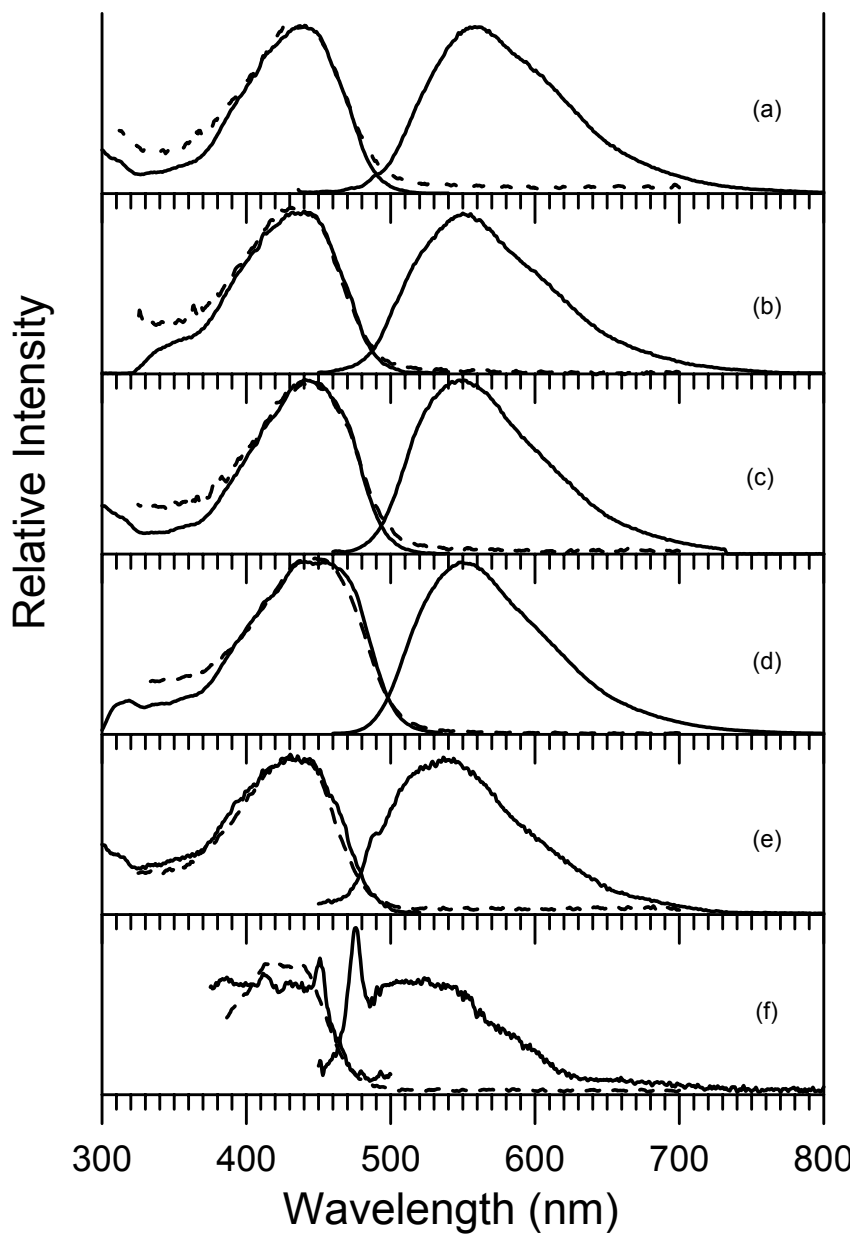


Figure 27: Absorption (dashed line), excitation (left), and fluorescence (right) spectra of 3dbcp in various solvents I: (a) acetonitrile ($\lambda_{\text{Ex max}}$: 434 nm); (b) acetone ($\lambda_{\text{Ex max}}$: 435 nm); (c) dichloromethane ($\lambda_{\text{Ex max}}$: 447 nm); (d) pyridine ($\lambda_{\text{Ex max}}$: 449 nm); (e) ethyl acetate ($\lambda_{\text{Ex max}}$: 425 nm); (f) ether ($\lambda_{\text{Ex max}}$: 409 nm).

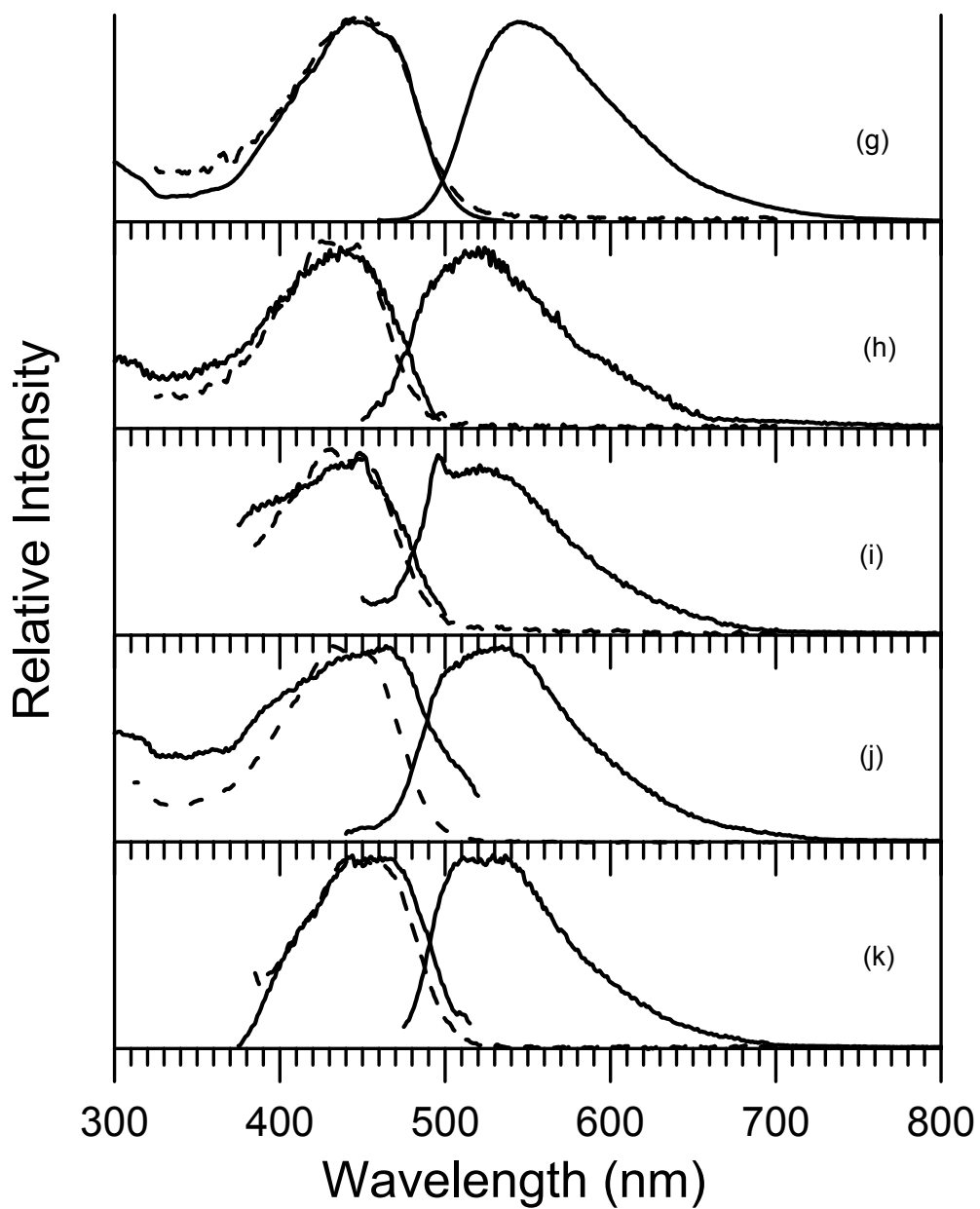


Figure 28: Absorption (dashed line), excitation (left), and fluorescence (right) spectra of 3dbcp in various solvents II: (g) chloroform ($\lambda_{\text{Ex max}}$: 450 nm); (h) carbon tetrachloride ($\lambda_{\text{Ex max}}$: 427 nm); (i) toluene ($\lambda_{\text{Ex max}}$: 445 nm); (j) benzene ($\lambda_{\text{Ex max}}$: 480 nm); (k) carbon disulfide ($\lambda_{\text{Ex max}}$: 443 nm).

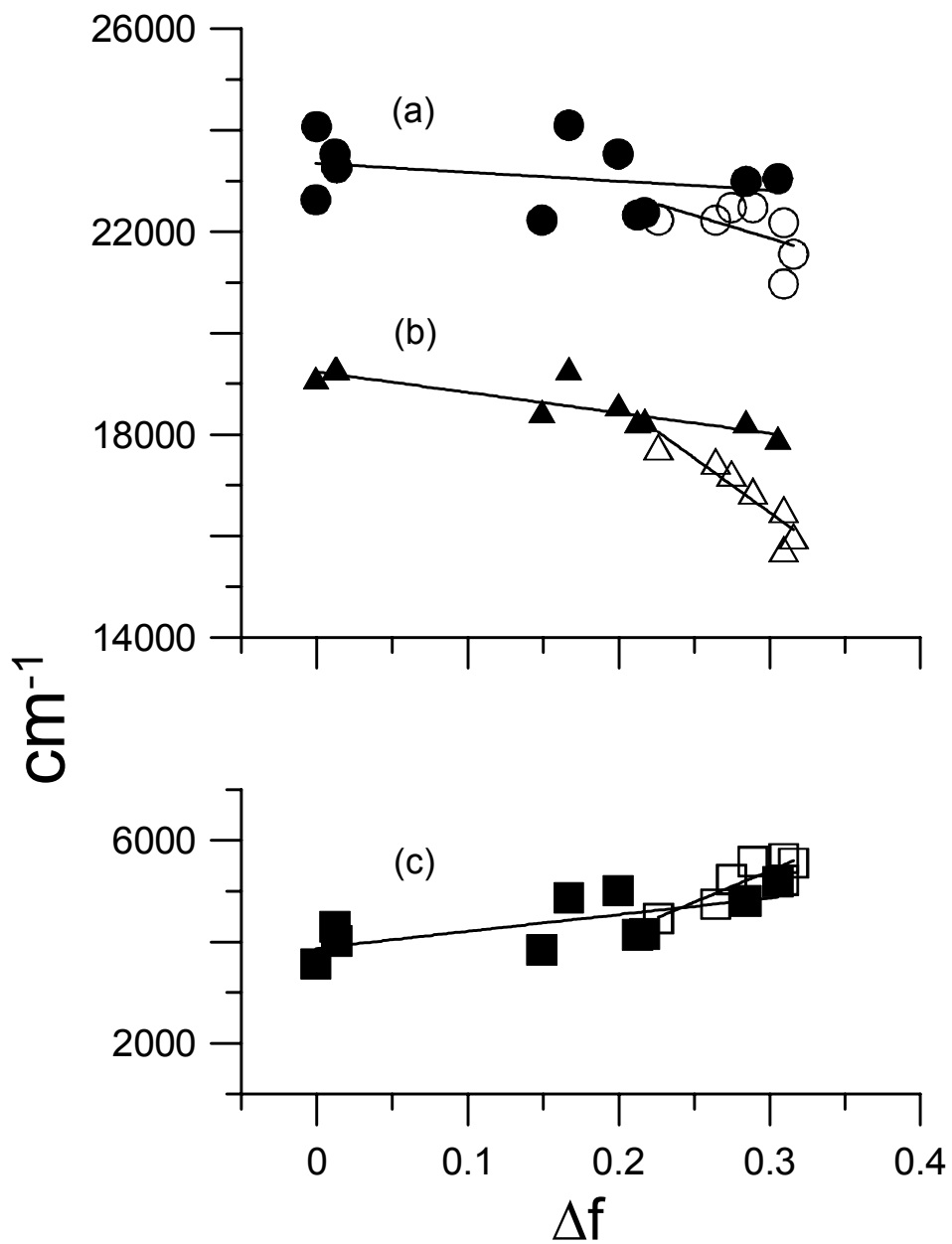


Figure 29: Plot of (a) absorption frequency; (b) fluorescence frequency; (c) Stokes' shift against solvent orientation polarization of 3dbcp. Open symbols for protic solvents; solid symbols for aprotic solvents.

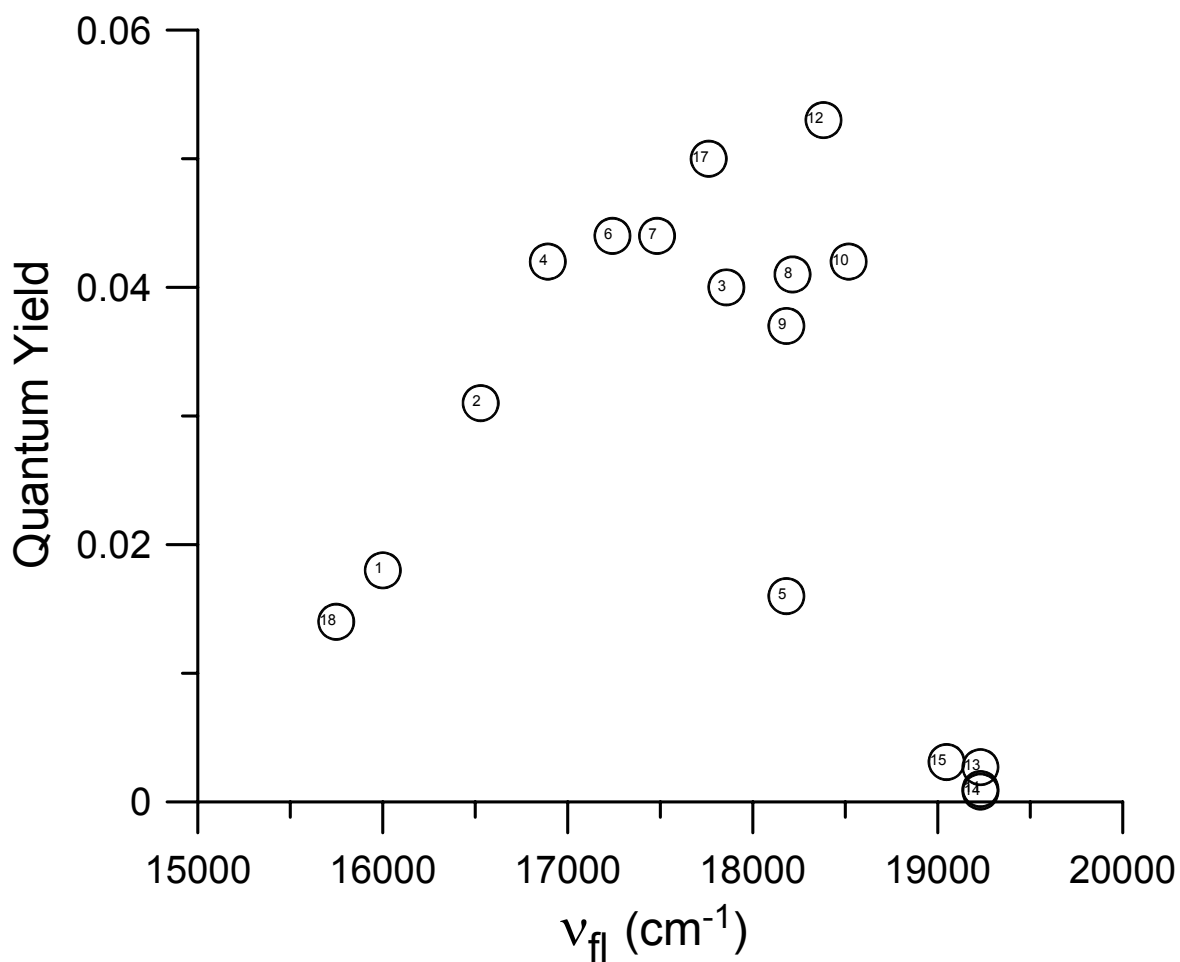


Figure 30: Fluorescence quantum yield of 3dbcp in different solvents plotted against the frequency of fluorescence.

The solvents used are shown by numbers: 1) TFE, 2) MeOH, 3) ACN, 4) EtOH, 5) acetone, 6) n_propanol, 7) n_butanol, 8) CH₂Cl₂, 9) pyridine, 10) ethyl acetate, 11) ether, 12) CHCl₃, 13) toluene, 14) CCl₄, 15) CS₂, 16) cyclohexane, 17) n_octanol, 18) HFIP.

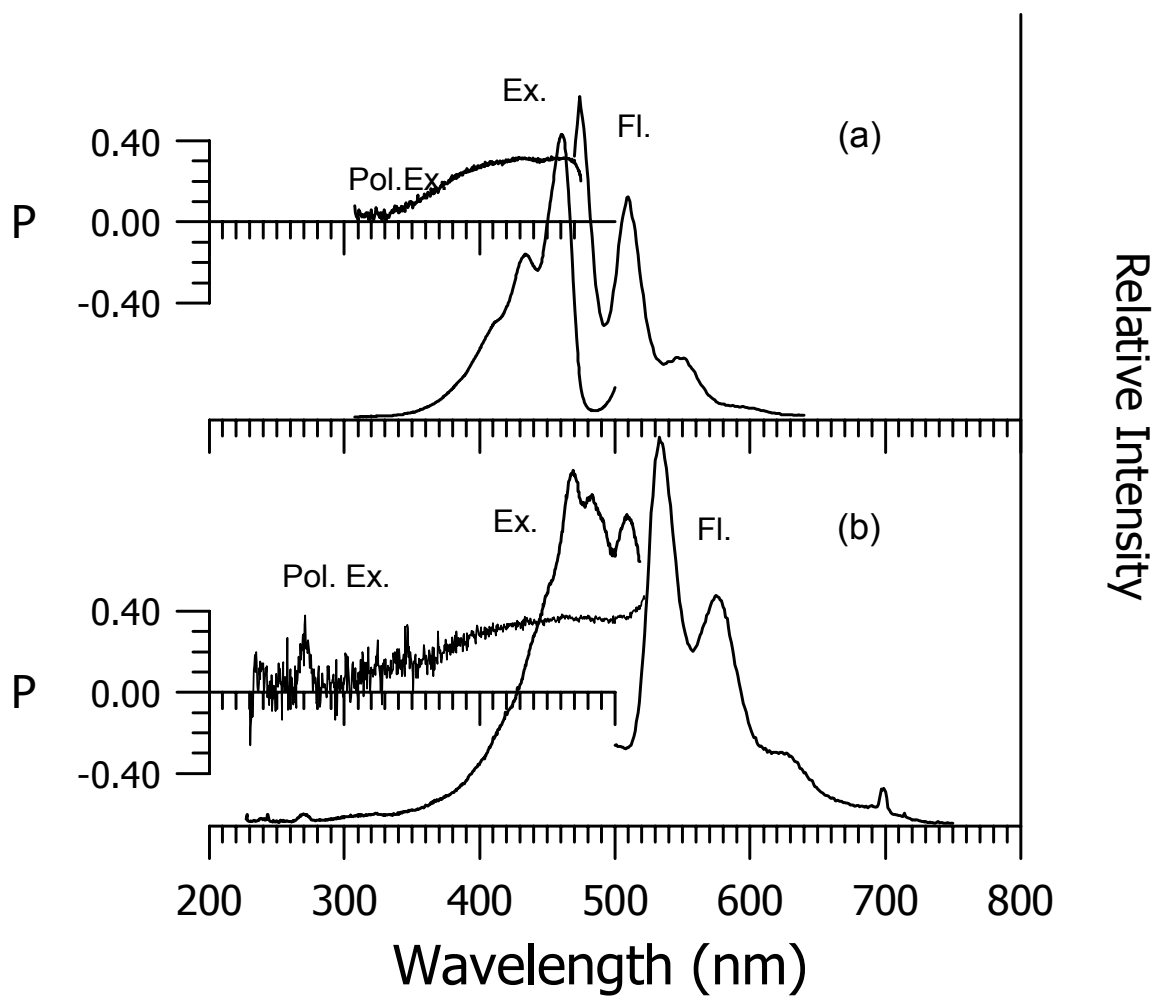


Figure 31: (a) Fluorescence, fluorescence excitation, and polarized excitation spectra of 2dbcp in ethanol/methanol (4:1) glass at 77 K ($\lambda_{\text{Ex max}}$: 460 nm) (b) Fluorescence, fluorescence excitation, and polarized excitation spectra of 3dbcp in ethanol/methanol (4:1) glass at 77 K ($\lambda_{\text{Ex max}}$: 470 nm).

Table 19 Absorption, Excitation, and Fluorescence Spectral Data and Fluorescence

Quantum Yields for 2dbcp in Alcohols.

Solvent	abs. λ_{\max} (nm)	exc. λ_{\max} (nm)	flu. λ_{\max} (nm)	abs. ν_{\max} (cm^{-1})	exc. ν_{\max} (cm^{-1})	flu. ν_{\max} (cm^{-1})	pKa	ϕ_f	λ_{ex} for ϕ_f (nm)
1-octanol	412	431	505	24272	23202	19802		0.020	409
1-butanol	412	428	510	24272	23364	19608		0.018	409
1-propanol	409	430	512	24450	23256	19531	16.2	0.020	409
ethanol	410	420	515	24390	23810	19417	15.9	0.027	405
methanol	408	416	522	24510	24038	19517	15.5	0.026	400
TFE	420	430	542	23810	23256	18450	12.4	0.035	409
HFIP	432	434	558	23148	23041	17921	9.3	0.013	409

Table 20 Absorption and Fluorescence Spectral Data and Fluorescence Quantum Yields for 3dbcp.

Solvent	abs. λ_{max} (nm)	flu. λ_{max} (nm)	abs. ν_{max} (cm^{-1})	flu. ν_{max} (cm^{-1})	Stokes' shift (cm^{-1})	Δf^*	ϕ_f	λ_{ex} for ϕ_f (nm)
carbon disulfide	442	525	22624	19048	3577	0.0007	0.0031	400
cyclohexane	415		24067			0.0002		
carbon tetrachloride	425	520	23529	19231	4299	0.0119	0.0008	400
toluene	430	520	23256	19231	4025	0.0131	0.0027	400
chloroform	450	544	22222	18382	3840	0.1491	0.053	400
ethyl ether	415	520	24096	19231	4866	0.1669	0.001	400
ethyl acetate	425	540	23529	18519	5011	0.1996	0.042	400
pyridine	448	550	22321	18182	4140	0.2124	0.037	400
dichloromethane	447	549	22371	18215	4156	0.2171	0.041	410
1-octanol	450	563	22222	17762	4460	0.2263	0.050	400
1-butanol	450	572	22222	17483	4740	0.2642	0.044	400
1-propanol	445	580	22472	17241	5231	0.2746	0.044	410
acetone	435	550	22989	18182	4807	0.2843	0.016	415
ethanol	445	592	22472	16892	5580	0.2887	0.042	400
acetonitrile	434	560	23041	17857	5184	0.3054	0.040	400
HFIP	477	635	20964	15748	5216	0.3092	0.014	410
methanol	451	605	22173	16529	5644	0.3093	0.031	400
TFE	464	625	21552	16000	5552	0.3159	0.018	405

*⁵⁶ Solvent polarity constants used for polarity function calculations are taken from Suppan, P. and Ghoneim, N., in Solvatochromism, The Royal Society of Chemistry, Cambridge, 1997.

4.1.5 Additional Spectral Data

In the remainder of Section 1, additional absorption properties of 1dbcp and 2dbcp along with 1dbcp_u will be presented. As mentioned earlier, 1dbcp does not fluoresce in any of the solvents. To investigate the possibility of fluorescence activation through extending the path of double bond conjugation through the cyclopentanone ring, 1dbcp_u was synthesized (see Chapter 3). However, 1dbcp_u did not show any fluorescence. Furthermore, 2dbcp, as mentioned earlier, fluoresces only in polar protic (alcohols) solvents. Therefore, only these absorption properties of the compounds will be presented in hydrocarbon (cyclohexane), aprotic polar (acetonitrile), and polar protic (methanol) solvents. The absorption measurements of 1dbcp_u, 1dbcp, and 2dbcp, are shown in Figure 32 through Figure 34, respectively.

1dbcp_u has two bands in the absorption spectra as shown in Figure 32. The lower wavelength band in cyclohexane appears to be sensitive to solvent polarity. This band shifts to the red with increasing solvent polarity from cyclohexane (300 nm and 342 nm) to methanol (310 nm and 342 nm). The higher wavelength band seems to be solvent independent with changing polarity. This observation has also been reported in the literature.³⁶ The existence of two different bands in 1dbcp_u was attributed to the geometrical structure of this compound. The upper part of 1dbcp_u possesses a solvent sensitive carbonyl group with conjugation of exocyclic double bonds, whereas the lower part is like *cis* 1,6-diphenylhexatriene and less sensitive to solvent polarity. The two bands have been attributed to excitations involving these two regions of the molecule. The comparison of 1dbcp and 2dbcp (1dbch and 2dbch can be seen in Appendix E) absorption spectra shows that increasing number of double bonds within the polyene

chain leads to a shift towards lower energy. The measurements have been conducted according to the increasing polarity of solvents: cyclohexane, acetonitrile, and methanol and shown in Figure 33 and Figure 34 for 1dbcp and 2dbcp, respectively. These figures show that the $\pi\pi^*$ transition is shifted towards the red with increasing solvent polarity order. Vibronic structure can be resolved only with the hydrocarbon solvent for both of the compounds. The wavelengths at the maximum absorption bands of ndbcp, 1dbch, 2dbch, and 1dbcp_u are shown in Table 21.

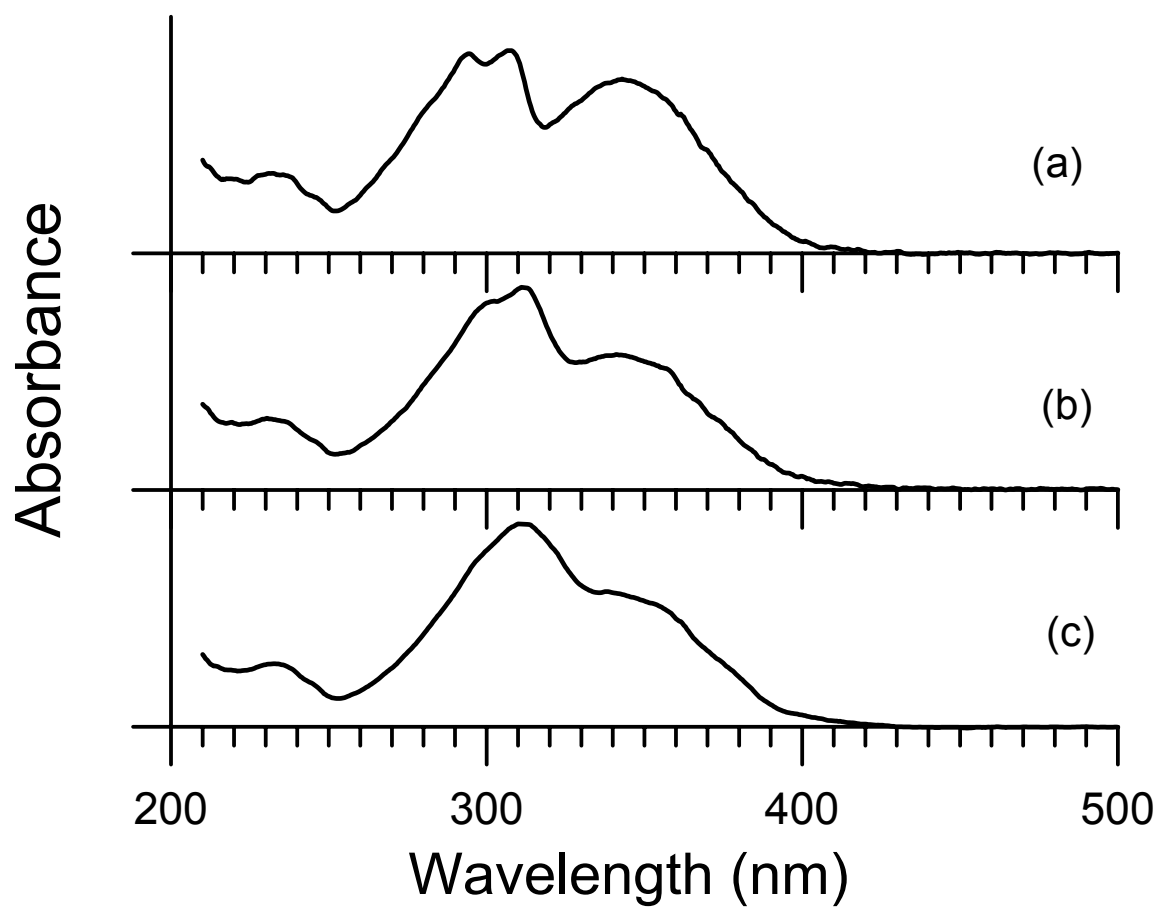


Figure 32: Absorption spectra of 1dbcp_u in solvents: (a) cyclohexane; (b) acetonitrile; (c) methanol.

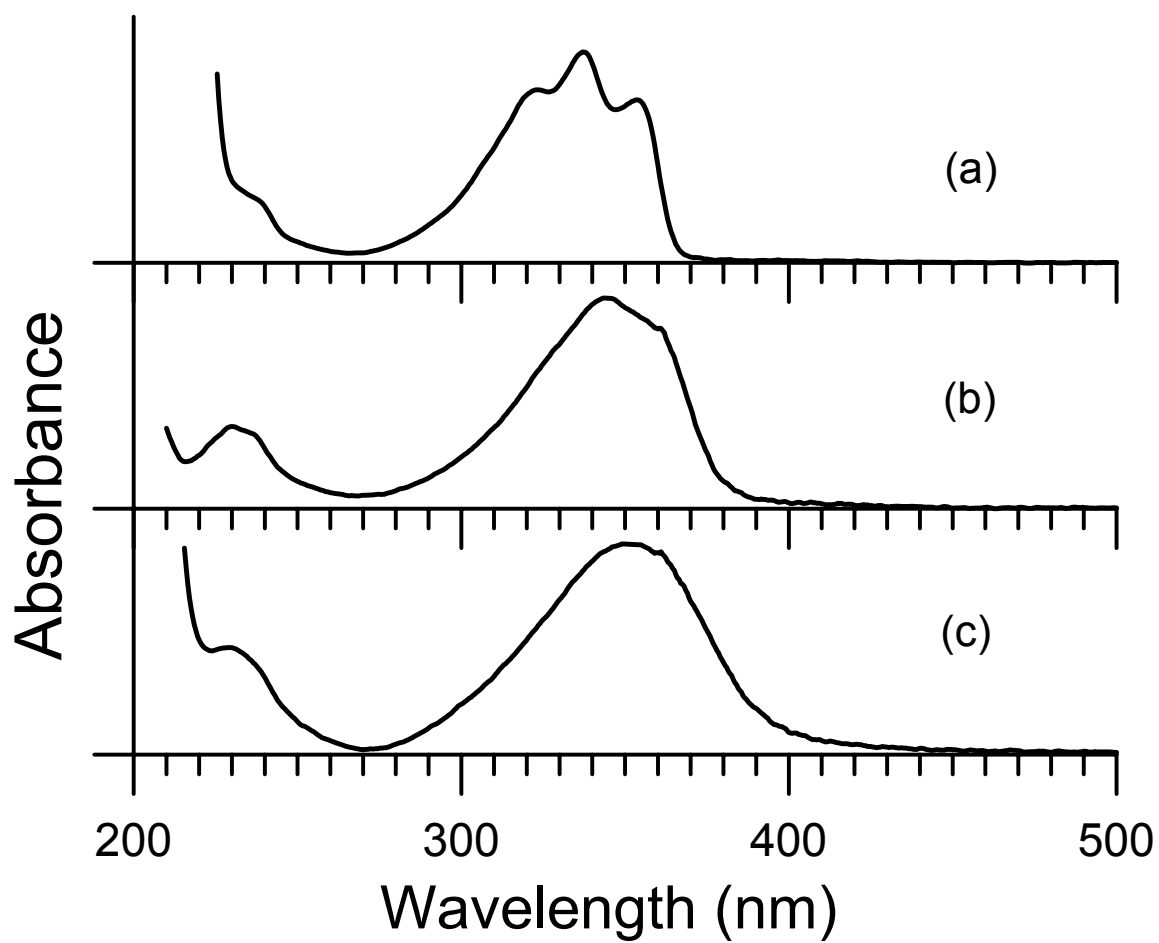


Figure 33: Absorption spectra of 1dbc in solvents: (a) cyclohexane; (b) acetonitrile, and (c) methanol.

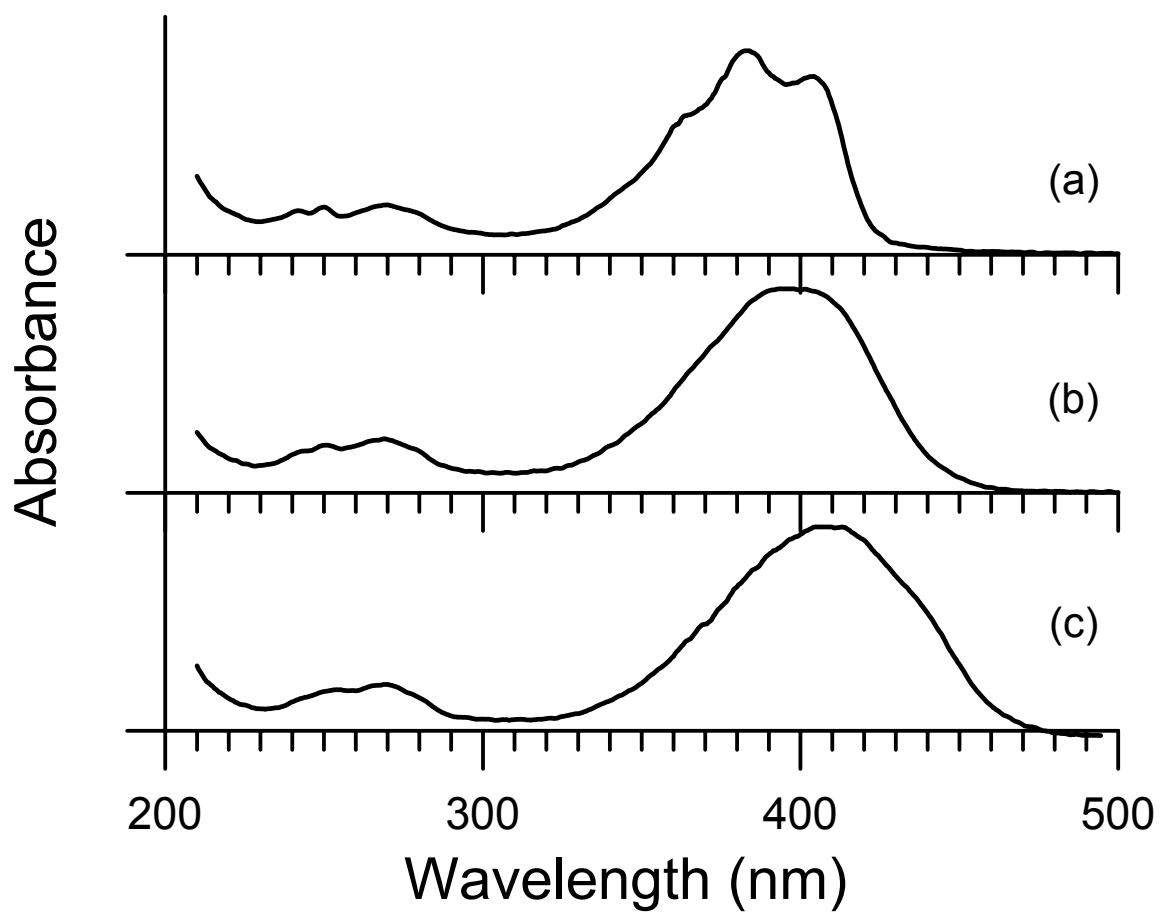


Figure 34: Absorption spectra of 2dbc in solvents: (a) cyclohexane; (c) acetonitrile, and (c) methanol.

Table 21 Maximum Absorption Energy of Compounds in Various Solvents.

Solvent	Compound					
	Maximum Absorption Energy (cm ⁻¹)					
	1dbcp	2dbcp	3dbcp	1dbcp_u	1dbch	2dbch
CH	29674 (337 nm)	26316, 25000 (380, 400 nm)	24272, 22883 (412, 437 nm)	29412, 33333 (342, 300nm)	31446 (318nm)	27027, 25641 (370, 390 nm)
ACN	29240 (342 nm)	25316 (395 nm)	23041 (434 nm)	32051, 29412 (312, 340 nm)	30864 (324 nm)	26316 (380 nm)
Me	28571 (350 nm)	24510 (408 nm)	22173 (451 nm)	28571, 32258 (350, 310 nm)	30769 (325 nm)	25974 (385 nm)

4.1.6 Summary

Spectroscopic properties for a series of 2,5-diarylidene-cyclopentanones have been presented. Electronic absorption and fluorescence spectra have been measured for the all-*E* configurations of 2,5-dibenzylidene-cyclopentanone (1dbcp), 2,5-bis-(3-phenylallylidene)-cyclopentanone (2dbcp), and 2,5-bis-(5-phenyl-penta-2,4-dienylidene)-cyclopentanone (3dbcp).

The absorption spectra have been assigned with the aid of INDO/S calculations. Molecular structures used for the INDO/S calculations were computed with the PM3 Hamiltonian. Agreement between absorption spectra obtained in cyclohexane at room temperature and the theoretical predictions is good. For 1dbcp, 2dbcp, and 3dbcp the general features of the spectra are similar. The transition to S_1 (weak) is assigned as $n \rightarrow \pi^*$ ($A_2 \leftarrow A_1$), to S_2 (strong) as $\pi \rightarrow \pi^*$ ($B_2 \leftarrow A_1$), and to S_3 (moderate) as $\pi \rightarrow \pi^*$ ($A_1 \leftarrow A_1$). The energy gap between S_1 and S_2 is seen to decrease as the length of the polyene chain increases in going from 1dbcp to 3dbcp.

Fluorescence is not observed for 1dbcp in any of the solvents studied (protic and aprotic). Fluorescence is observed for 2dbcp in protic solvents only. For 3dbcp, fluorescence is observed in a number of protic and aprotic solvents. Solvents, which are able to induce fluorescence, are believed to do so by inverting the order of $^1(n\pi^*)$ and $^1(\pi\pi^*)$ states. The influence of hydrogen bonding on the excitation spectra of 2dbcp and 3dbcp has been explored.

Solvent induced shifts in the absorption and fluorescence spectra of 3dbcp in combination with the PM3 calculated ground state dipole moment (2.8 D) have been used

to determine the excited state dipole moment of 3dbcp (6.4 D/protic solvents; 6.6 D/aprotic solvents).

Fluorescence quantum yields are found to vary with the frequency of emission for 3dbcp, going through a maximum in the mid-frequency range. The variation in quantum yields with frequency is attributed primarily to changes in the nonradiative rate of decay from S_1 . Excitation, polarized excitation, and fluorescence spectra have been measured for 2dbcp and 3dbcp at 77 K in ethanol/methanol glass. Vibronic features not observed in the broad spectra obtained in alcohols at room temperature become clearly resolved at 77 K.

4.2 Section 2: Ground and Excited State Properties in Acidic Media : Excited State Proton Transfer for 2,5-Diarylidene-Cyclopentanones

4.2.1 Introduction

The preliminary observations in acetic acid and the findings in alcohols as discussed in the previous section, suggest further investigation of the ground and excited state properties of the 2,5-diarylidene-cyclopentanones in acidic media. These studies include: gradually diluting with water, solutions of the compounds in strong and weak acids, deuterium isotope effects on spectra, concentration dependence studies of the spectral properties, and low temperature measurements. A brief photochemical study of 1dbcp and 1dbcp-H⁺ has been carried out and analyzed by HPLC to determine if E → Z photoisomerization takes place in acid solution as it does in organic solvents. The PM3 optimized structures of the protonated 2,5-diarylidene-cyclopentanones along with INDO/S calculations have been performed to further understand the effect of acidic media on the compounds and their electronic structure and spectra.

4.2.2 Spectroscopic Investigations in Acidic Media

In the investigation of the spectroscopic behavior of the compounds in acidic media, first acetic acid was used. The room temperature absorption, fluorescence, and fluorescence excitation spectra of 2dbcp and 3dbcp in glacial acetic acid are presented in Figure 35. Fluorescence is not observed for 1dbcp in acetic acid, whereas the fluorescence spectra of 2dbcp and 3dbcp consist of two overlapping bands (535, 615 nm for 2dbcp; 606, 685 nm for 3dbcp). The excitation spectrum of each compound does not

change when the monitoring wavelength is moved from the shorter wavelength fluorescence band to the longer wavelength band.

Further studies of the affect of pH on the spectroscopic properties of 2dbcp were carried out. First spectra were recorded for 2dbcp in acetic acid solutions of various dilutions with water. Spectra corresponding to 2dbcp in acetic acid at pH values of (a) 1.8 and (b) 2.5 are shown in Figure 36. In the fluorescence spectra, the relative intensity of the band at 615 nm decreases in going from pH=1.8 to pH=2.5. This band eventually disappears when the solution is diluted further with water. The lack of complete overlap of the absorption and excitation spectra at pH=1.8 suggests that under these conditions more than one species exists in solution e.g. strongly hydrogen bonded (or hydrogen bonded) and non-hydrogen bonded (or weakly hydrogen bonded) forms of 2dbcp. At the higher pH of 2.5, better overlap of the absorption and excitation spectra suggests a more homogeneous solution.

In the next spectroscopic study of 2dbcp, various strengths of sulfuric acid solutions were used. Figure 37 presents absorption and fluorescence data for 2dbcp in (a) 96% sulfuric acid and diluted sulfuric acid solutions with pH equal to approximately (b) 1.0, (c) 1.4, and (d) 1.6. In 96% sulfuric acid, broad absorption and fluorescence bands are observed for 2dbcp at approximately 570 and 630 nm, respectively. Upon dilution with water, a new absorption band is seen to grow in at approximately 440 nm while the absorption at 570 nm decreases in relative intensity. The fluorescence band at 630 nm remains relatively unchanged in appearance for the range of dilutions (pH) studied. Fluorescence excitation spectra are in reasonable agreement with the absorption spectra measured in this study. From the studies of 2dbcp in acidic media a fairly clear picture

arises. In 96% sulfuric acid there is essentially complete protonation of the ketone, both in the ground state and the excited state. As the sulfuric acid solution is diluted and the pH increases, the growth of the absorption band at 440 nm is attributed to absorption by ground state unprotonated 2dbcp. An equilibrium is established between ground state protonated and unprotonated 2dbcp that can be shifted from one form to the other by altering the pH through dilution. The fact that fluorescence is observed only at 630 nm for the range of sulfuric acid strengths studied indicates that in all cases emission is observed only from protonated 2dbcp. The absence of fluorescence from unprotonated 2dbcp in diluted sulfuric acid solutions where it is known to be present in significant amounts relative to protonated 2dbcp, e.g. pH=1.4, 1.6, indicates that under these conditions 2dbcp undergoes a highly efficient excited state proton transfer reaction on the S_1 surface forming the protonated cation prior to emission.

In acetic acid solutions the situation is somewhat different in that there is no evidence of ground state protonation of 2dbcp in the absorption spectra; however the fluorescence spectra shown in Figure 35 and Figure 36 show two bands consistent with emission from both unprotonated (535 nm) and protonated (615 nm) 2dbcp. In this case protonation is occurring only on the excited state surface, but to a lesser degree than for the sulfuric acid solutions discussed previously. As a result, emission from unprotonated and protonated species contributes to the fluorescence spectra in acetic acid solutions. Room temperature absorption, fluorescence and fluorescence excitation spectra of 1dbcp and 2dbcp in 96% sulfuric acid, and 3dbcp in 96% sulfuric acid: glacial acetic acid (1:3) are shown in Figure 38. In all cases the absorption and fluorescence maxima are shifted considerably to the red relative to spectra recorded in alcohol or aprotic organic solvents.

It is assumed that in these strongly acidic solvents all three of the ketones exist as protonated species, both in the ground state and in the excited state. From here on, ground state protonated species are indicated as 1dbcp-H⁺, 2dbcp-H⁺ and 3dbcp-H⁺. From Figure 35 (b) and Figure 38, it is seen that results similar to those found for 2dbcp are observed for 3dbcp. In acidic acid media a single absorption band is observed; whereas two emission bands exist. The similarity of these spectra to those of 2dbcp in acetic acid suggests that excited state proton transfer also takes place for 3dbcp in this solvent. For 3dbcp in sulfuric acid: acetic acid it is seen that, although appearing in the same general spectral region, there is significant deviation between the absorption spectrum and the excitation spectrum. Other species such as ring protonated cations may be contributing to the absorption in this region; however there is insufficient data to make a definitive assignment.

The observation of excited state proton transfer in acetic acid and diluted sulfuric acid for 2dbcp and 3dbcp but not for 1dbcp can be understood by considering that the transfer of electron charge density to the carbonyl oxygen atom upon excitation from S₀ to S₁($\pi\pi^*$) makes 2dbcp and 3dbcp stronger bases in the excited state, thus promoting excited state proton transfer from the acid. Conversely, a reduction in electron charge density on the oxygen atom occurs when S₁ is $n\pi^*$, making a molecule a weaker base in S₁.⁵⁷ Just as with alcohol solvents, it appears that S₁ remains $n\pi^*$ for 1dbcp in acetic acid; whereas a state inversion occurs for 2dbcp and 3dbcp.

Figure 39 and Figure 40 show the absorption, excitation, and fluorescence spectra of 2dbcp and 3dbcp in (a) methanol, (b) acetic acid, and (c) sulfuric acid (for 2dbcp) and sulfuric acid: acetic acid (1:4) (for 3dbcp) solvents, respectively. As the acidity of the

solvents increases a progression is observed from absorption and emission of hydrogen bonded but not protonated species (methanol), followed by absorption by hydrogen bonded and emission from hydrogen bonded and protonated molecules (acetic acid), finally to absorption and emission from protonated species (sulfuric acid).

Comparisons of the absorption and fluorescence properties of 2dbcp and 3dbcp in acetic acid and acetic acid-d₁ are shown in Figure 41 and Figure 42, although the spectra are very similar in the undeuterated and deuterated solvents, it is seen that the ratio of unprotonated to protonated emission is significantly greater for 2dbcp but essentially unchanged for 3dbcp when these molecules are placed in deuterated acetic acid. For 2dbcp this observation is consistent with a kinetic isotope decrease in the rate of excited state proton transfer prior to emission; however, equilibrium considerations can not be ruled out as a contributing factor to the observed phenomenon.

To eliminate the possibility that the longer wavelength band observed in the fluorescence spectra of 2dbcp in acetic acid is not due to ground state aggregation or excited state excimer formation³², a concentration study of 2dbcp in acetic acid has been conducted and is shown in Figure 43. A stock solution of the compound was prepared in acetic acid and spectra were recorded at various dilutions by taking an aliquot of the stock solution and adding acetic acid. If aggregation/ excimer effects were contributing to the long wavelength band, the band should diminish in intensity relative to the shorter wavelength band upon dilution. It is observed that the intensities of the two bands remain constant relative to each other, thus eliminating aggregation/ excimer formation as an explanation for the observed spectral features.

Low temperature, 77K, fluorescence and fluorescence excitation spectra have been measured for 1dbcp, 2dbcp, and 3dbcp in acidic media. Figure 44 shows spectra at 77K using acetic acid solvent for (a) 2dbcp and (b) 3dbcp. It is seen that some vibronic structure is resolved in the fluorescence and excitation spectra for 2dbcp. The apparent 0-0 bands occur at 484 nm in fluorescence and 452 nm in the excitation spectrum. This is a blue shift from the fluorescence maximum of 535 nm and a red shift from the 484 nm excitation maximum observed at room temperature in this solvent. As a result, there is a considerably smaller Stokes' shift at low temperature. A shoulder in the fluorescence spectrum at 600-610 nm may be from the protonated cation suggesting that the degree of excited state protonation has been quenched considerably compared to room temperature. For 3dbcp in acetic acid the shift from room temperature to low temperature follows a similar pattern from 606 to 560 nm in fluorescence and from 449 to 470 nm in the excitation spectrum. There is no clearly resolved indication of emission that can be assigned to the protonated cation. However the spectrum is broad and a small amount of cation emission, if present, may not be resolvable. Figure 45 presents the fluorescence and fluorescence excitation spectra of (a) 1dbcp-H⁺ and (b) 2dbcp-H⁺ in 96% sulfuric acid and (c) 3dbcp in sulfuric acid: acetic acid: (1:4) at 77K. Resolved vibronic structure is observed for 1dbcp-H⁺ and 2dbcp-H⁺ with red shifts in fluorescence and blue shifts in absorption relative to room temperature for both species resulting in small Stokes' shifts relative to room temperature. In the case of 3dbcp-H⁺ the spectra remain broad at low temperature and the shifts smaller between room temperature and low temperature. As mentioned in the first Section of the Results and Discussion chapter, small Stokes' shifts are commonly observed for molecules in low temperature glasses and are attributed to the

inability of the solvent matrix to reorient and stabilize the molecule during the excited state lifetime.

Table 22 shows a summary of absorption (excitation) and fluorescence wavelengths, and the Stokes' shifts of the compounds in acids along with ΔpK_a between their ground and the excited states. The transition energies of acid and its conjugated base are used in the ΔpK_a estimation. However, the assumption of no entropy change for dissociation in the ground and excited states may not be satisfactory for a precise calculation of the pK_a change between the electronic states. Therefore, these values should be considered only in the order of magnitudes. Nevertheless, Table 22 shows the changes in electronic state pK_a values of 2dbcp and 3dbcp by using Forster cycle.

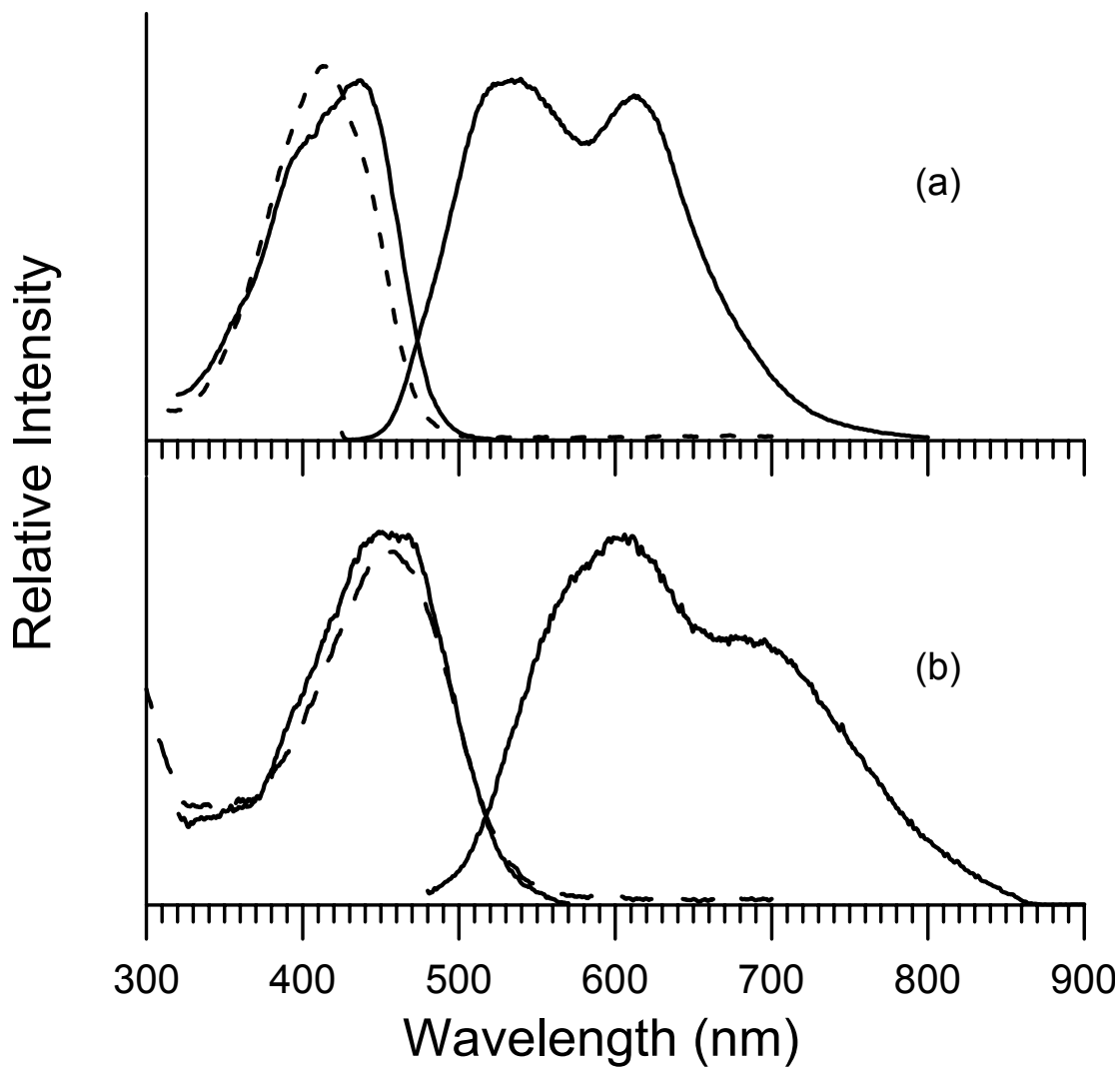


Figure 35: Absorption (dashed line), excitation (left), and fluorescence (right) spectra of (a) 2dbcp ($\lambda_{\text{Ex max}}$: 415 nm) and (b) 3dbcp in acetic acid ($\lambda_{\text{Ex max}}$: 455 nm).

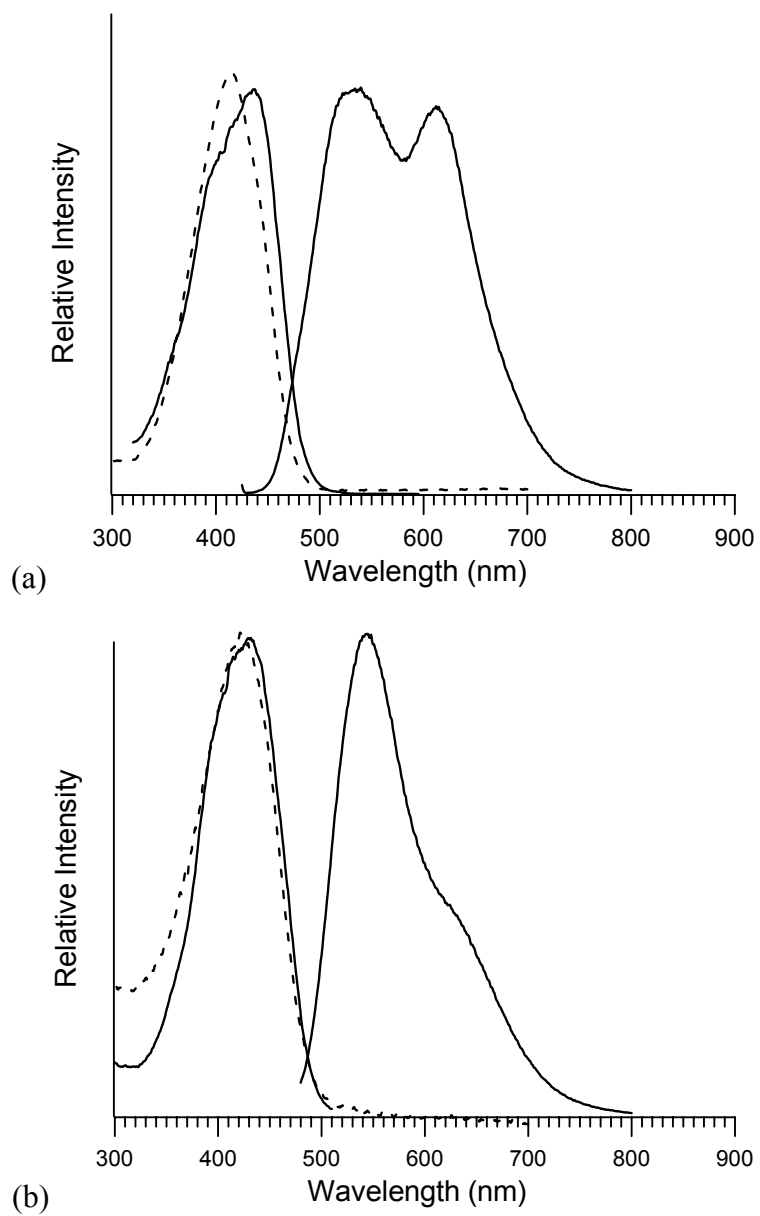


Figure 36: Titration study of 2dbcp in acetic acid: absorption (dashed line), fluorescence, and fluorescence excitation spectra (solid lines): (a) pH=1.8 and (b) pH=2.5 (in each case, excitation wavelengths: 415 nm).

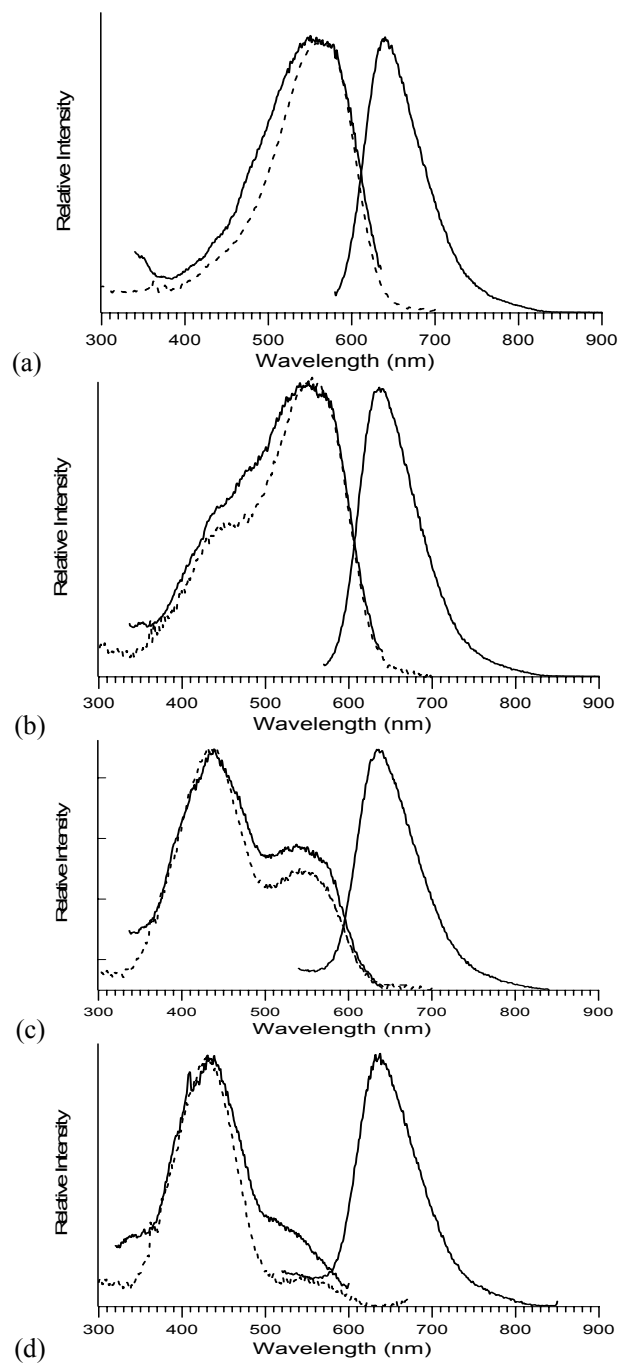


Figure 37: Titration study of 2dbcp in sulfuric acid: absorption (dashed line), fluorescence, and fluorescence excitation spectra (solid lines): (a) pH=96%; (b) pH=1; (c) pH=1.4; and (d) pH=1.6 (in each case, excitation wavelengths: 580 and 430 nm).

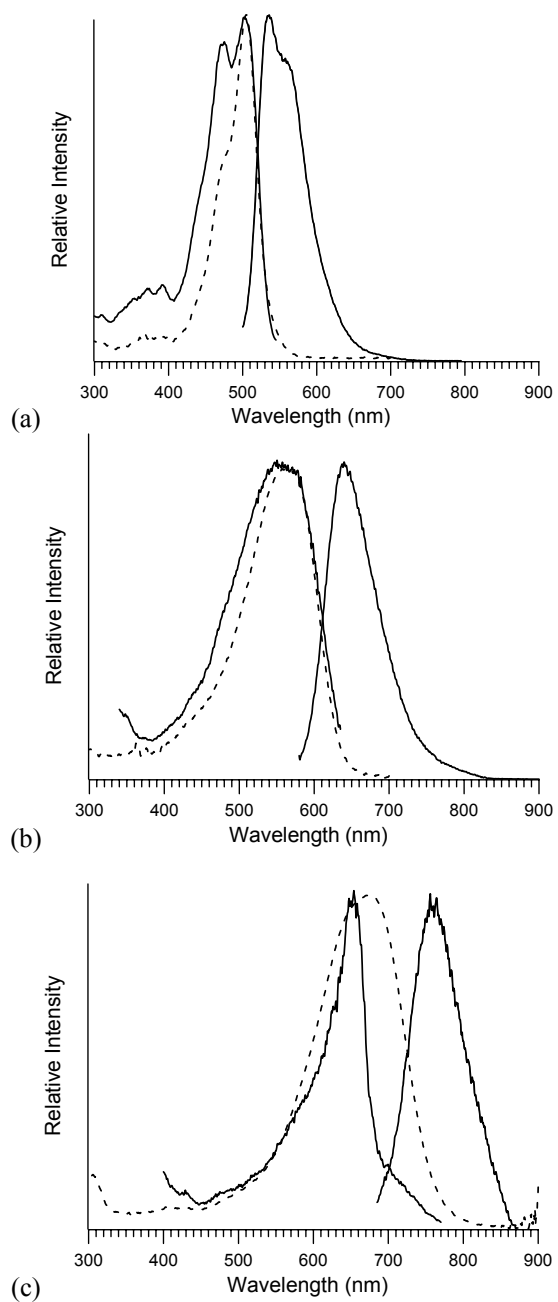


Figure 38: Absorption (dashed line), fluorescence, and fluorescence excitation spectra of (a) 1dbcp-H⁺ ($\lambda_{\text{Ex max}}$: 475 nm) and (b) 2dbcp-H⁺ in sulfuric acid ($\lambda_{\text{Ex max}}$: 580 nm and (c) 3dbcp-H⁺ ($\lambda_{\text{Ex max}}$: 660 nm) in sulfuric acid/acetic acid (1:3) mixture.

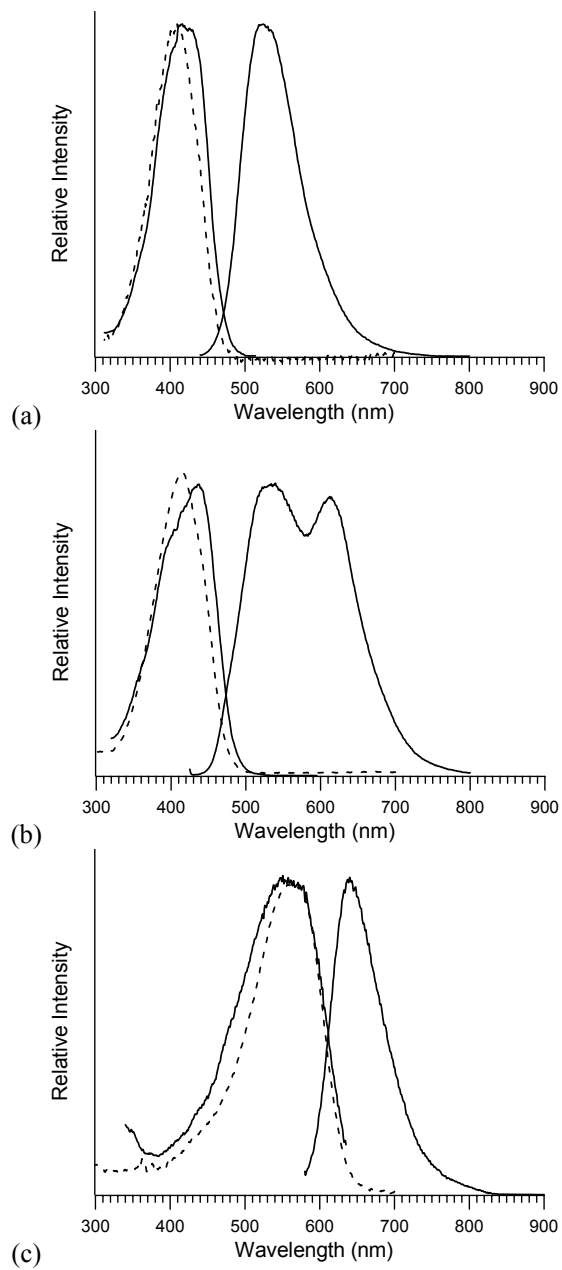


Figure 39: Absorption (dashed line), fluorescence, and fluorescence excitation spectra (solid lines) of 2dbcp in solvents: (a) methanol; (b) acetic acid; and (c) sulfuric acid.

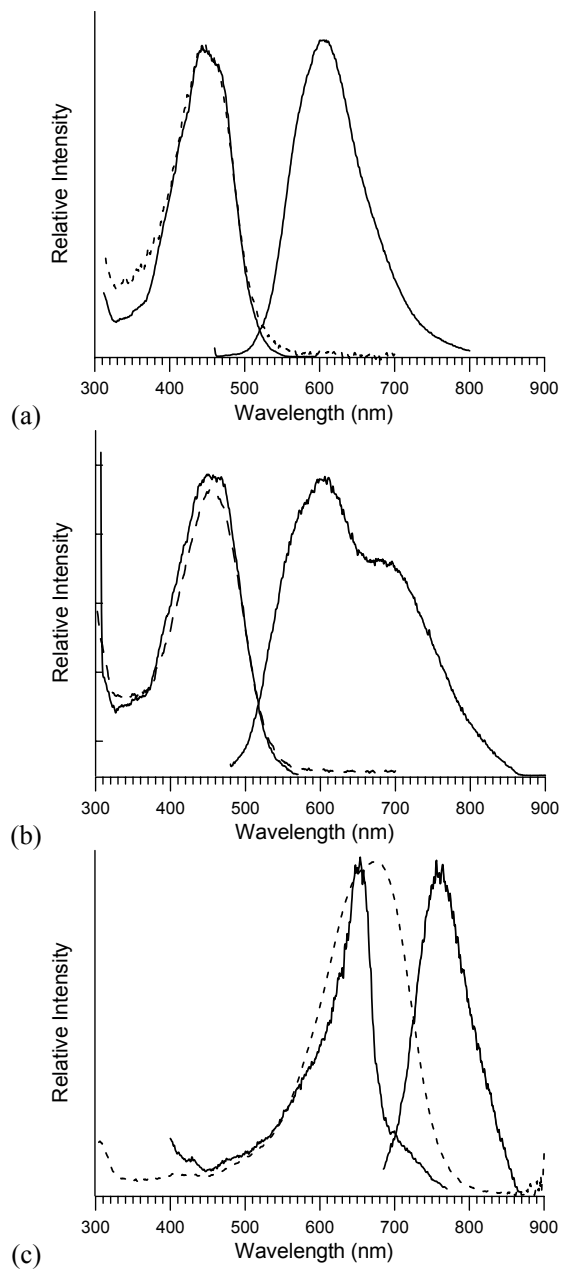


Figure 40: Absorption (dashed line), fluorescence, and fluorescence excitation spectra (solid lines) 3dbcp in solvents: (a) methanol; (b) acetic acid; and (c) sulfuric acid.

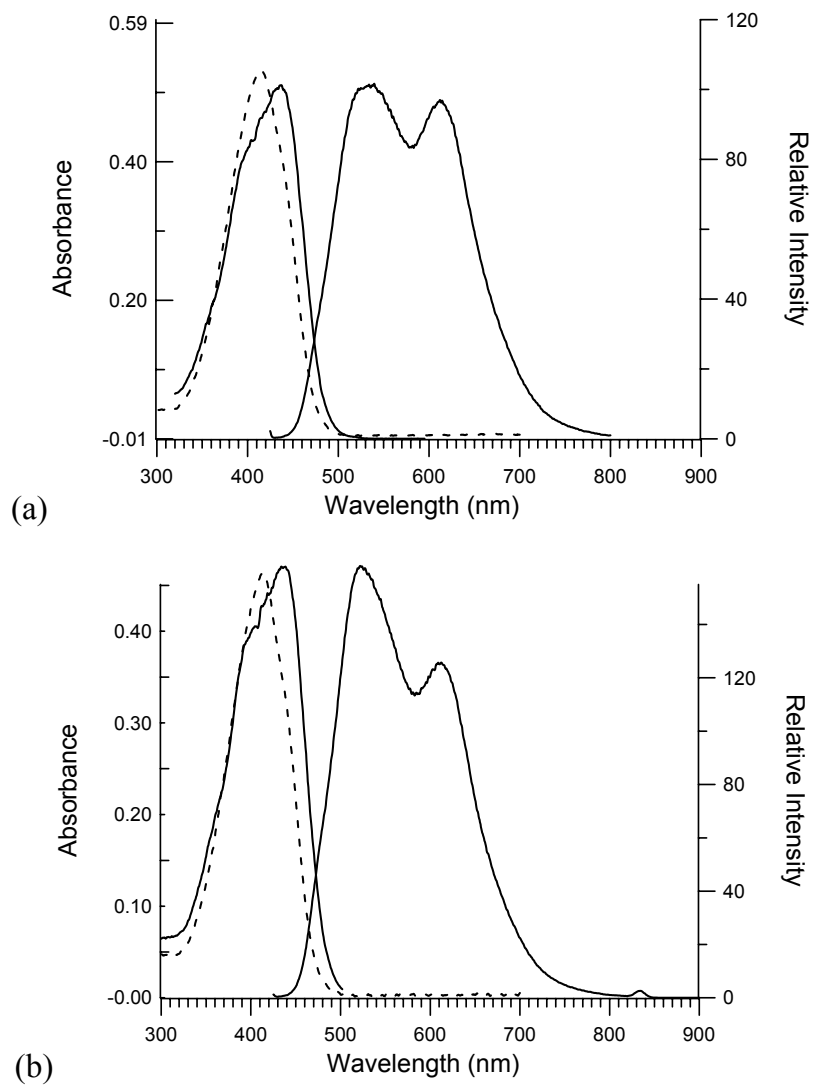


Figure 41: Fluorescence and fluorescence excitation spectra (solid lines) of 2dbcp in (a) acetic and (b) deuterated acetic acid (in each case, excitation wavelength: 415 nm)

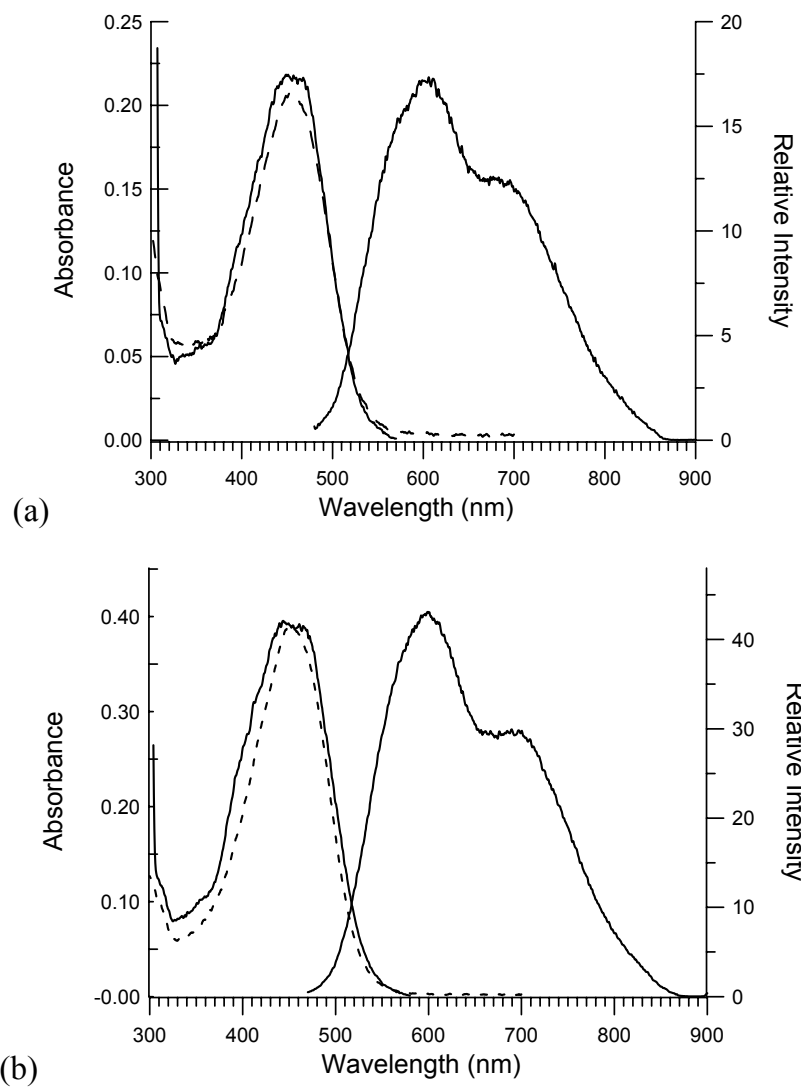


Figure 42: Fluorescence and fluorescence excitation spectra (solid lines) of 3dbcp in (a) acetic and (b) deuterated acetic acid (in each case, excitation wavelength: 455 nm).

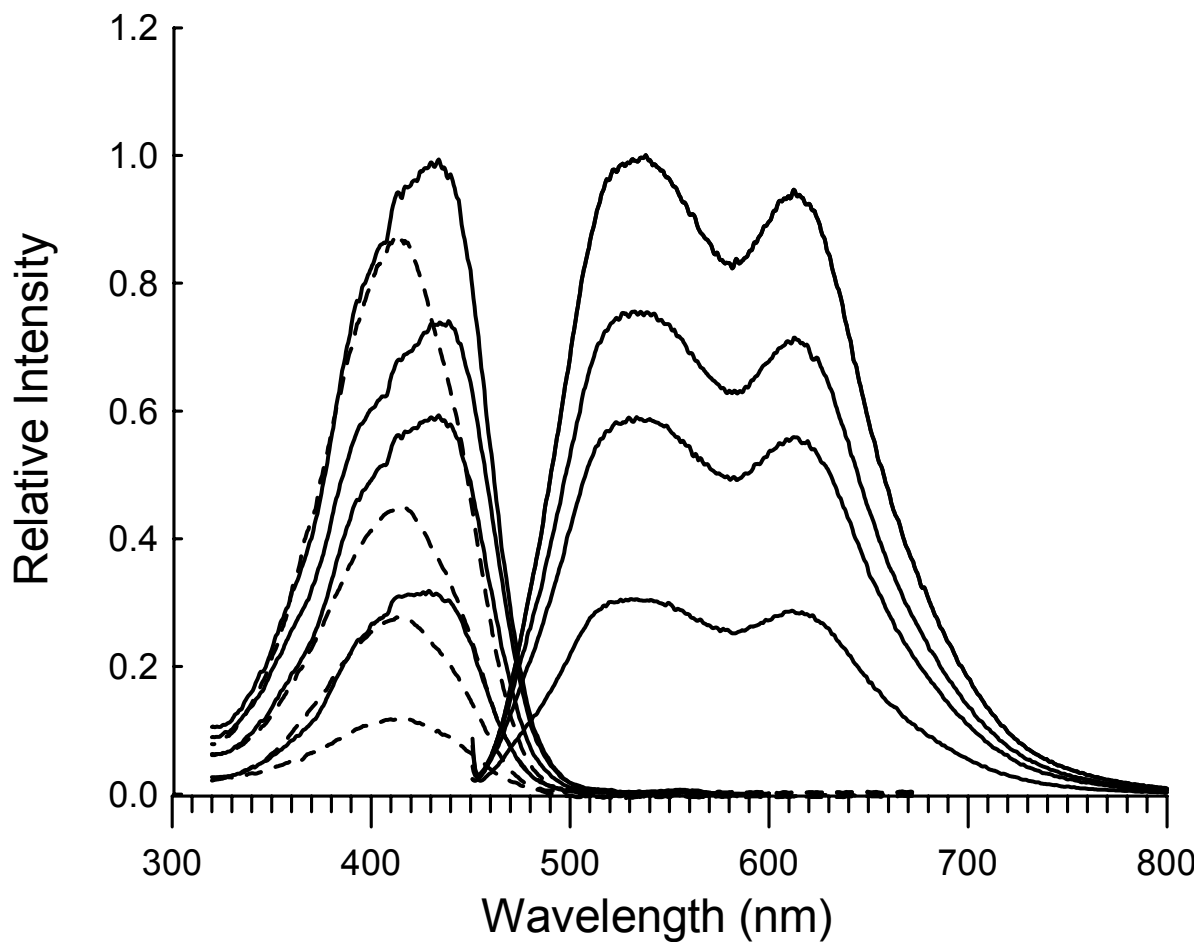


Figure 43: Concentration study of 2dbcp in acetic acid (concentrations from top to bottom: 4.79×10^{-4} M, 2.39×10^{-4} M, 1.20×10^{-4} M, 5.99×10^{-5} M).

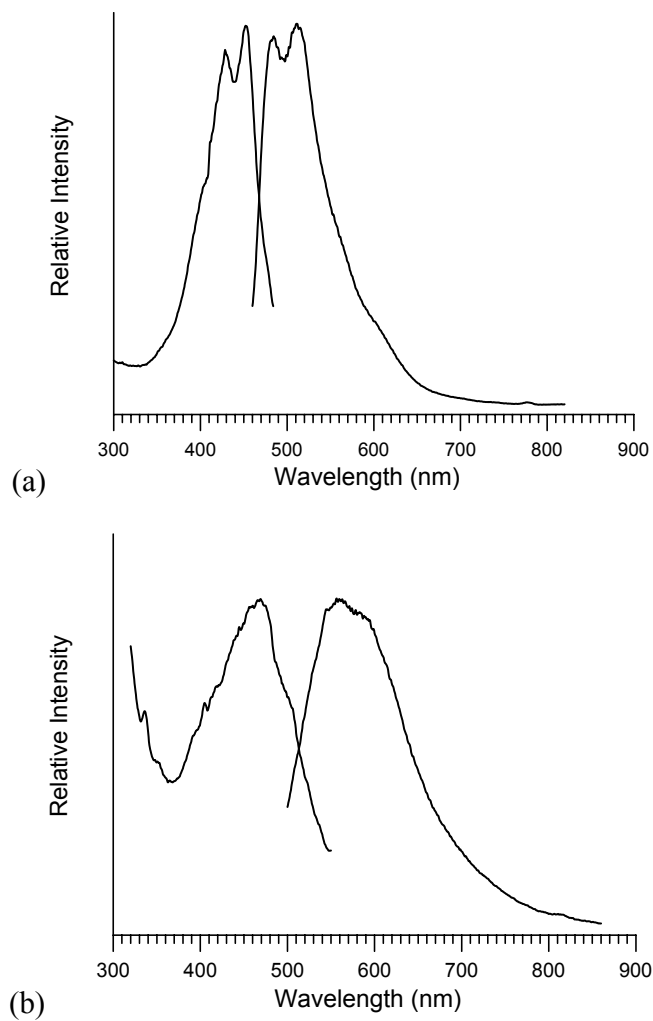


Figure 44: Fluorescence and fluorescence excitation spectra of (a) 2dbcp ($\lambda_{\text{Ex max}}$: 430 nm) and (b) 3dbcp in acetic acid ($\lambda_{\text{Ex max}}$: 455 nm) at 77K.

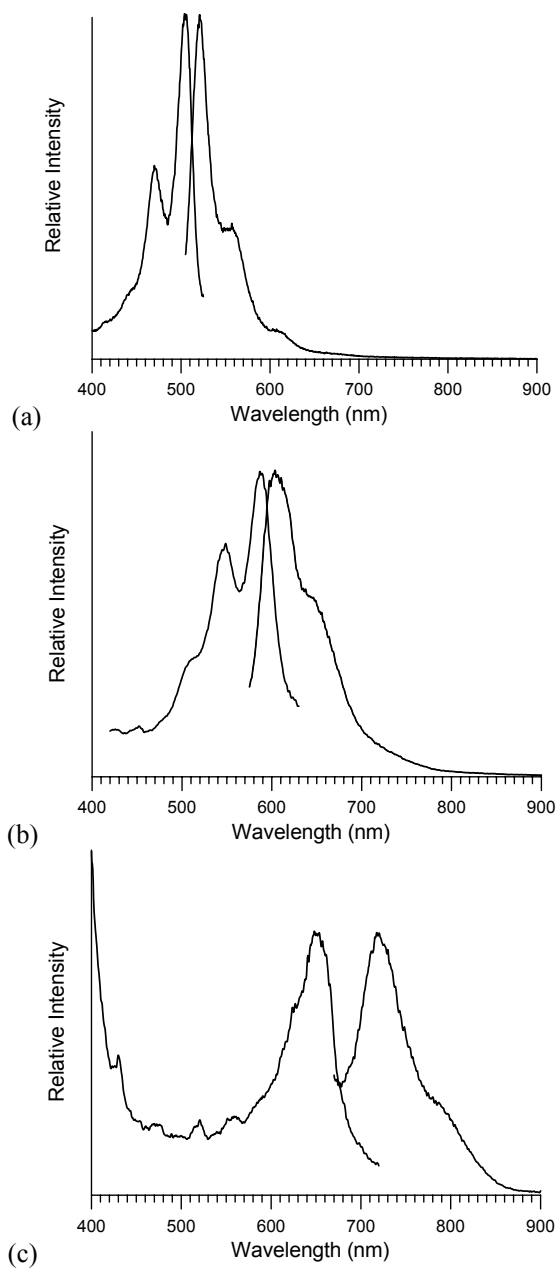


Figure 45: Fluorescence and fluorescence excitation spectra of (a) 1dbcp-H^+ ($\lambda_{\text{Ex max}}$: 505 nm) and (b) 2bcp-H^+ in sulfuric acid ($\lambda_{\text{Ex max}}$: 585 nm) and (c) 3dbcp-H^+ in sulfuric/ acetic acid mixture (1:3) ($\lambda_{\text{Ex max}}$: 630 nm) at 77K.

Table 22 Properties of 2,5-diarylidene Cyclopentanones in Acidic Media and Differences in the Electronic State Acidities in Acetic Acid at Room Temperature.

Solvents	Compounds	ν flu (cm^{-1})	ν abs (cm^{-1})	$\Delta\nu$ (abs-flu) (cm^{-1})	ΔpKa ($\text{pKa}-\text{pKa}^*$) Forster
Sulfuric Acid	1dbcp	18692, 17889 535, 559 nm	19802 505 nm	1110	
	2dbcp	14925 670 nm	17182 582 nm	2257	
	3dbcp	13333 750 nm	14598 685 nm	1265	
Acetic Acid	1dbcp	-	27778 360 nm	-	-6.2
	2dbcp	19231, 16260 520, 615 nm	24271 412 nm	5041	
	3dbcp	16556, 14598 604, 685 nm	22222 450 nm	5666	
Methanol	1dbcp	-	28249 354	-	
	2dbcp	19157 522	24510 408	5353	
	3dbcp	16529 605	22173 451	5644	

4.2.3 PM3 Optimized Geometries of Protonated Cations

For geometry optimization, initial structures of 1dbcp-H⁺, 2dbcp-H⁺, and 3dbcp-H⁺ were drawn with all carbon, oxygen, and hydrogen atoms in or nearly in the same plane. The PM3 optimized structures of 1dbcp-H⁺, 2dbcp-H⁺, and 3dbcp-H⁺ are shown in Figure 46-Figure 48. The calculated ground state geometric parameters for these compounds are given in Table 23 - Table 25, respectively.

All three compounds are predicted to have a C-O bond length of 1.32 Å. The O-H bond length is predicted to be 0.96 Å for all three compounds. The single bond connected to the phenyl group is predicted to have a bond length of 1.44 Å for 1dbcp-H⁺, 2dbcp-H⁺ and 1.45 Å for 3dbcp-H⁺. For 2dbcp-H⁺ and 3dbcp-H⁺, the exocyclic C-C single bond lengths fall in the range of 1.42-1.45 Å and the exocyclic double bond lengths fall in the range of 1.35-1.36 Å. The phenyl group rotations of 1dbcp-H⁺ are predicted to be 20° out of plane relative to cyclopentanone ring. Nearly planar structures are predicted for 2dbcp-H⁺ and 3dbcp-H⁺ with phenyl group rotation angles of 0.03° and 0.02°, respectively. The C-O-H bond angles are calculated to be 109.5° for 1dbcp-H⁺, 109.2° for 2dbcp-H⁺, and 109.0° for 3dbcp-H⁺.

The atomic charges of the H connected to O are predicted to be in the range of 0.23-0.24 for all three compounds. The atomic charge on the C atom bonded to O is predicted to decrease with increasing bond length, as 0.36, 0.35, and 0.34 for 1dbcp-H⁺, 2dbcp-H⁺, and 3dbcp-H⁺, respectively. The O atomic charges are predicted to be -0.15 for 1dbcp-H⁺, 2dbcp-H⁺ and -0.16 for 3dbcp-H⁺.

In Figure 49 and Figure 50, 3D rendering of optimized structures of 1dbcp/ 1dbcp-H⁺ and 2dbcp/ 2dbcp-H⁺ are presented for a better geometrical visualization of the

compounds. The investigation on the similarities and differences of the structural properties of unprotonated and protonated forms of 1dbcp are summarized in: Figure 51 (atomic charges), Figure 52 (bond lengths), and Figure 53 (bond orders). It is appealing to note that the changes observed in bond lengths, bond orders and atomic charges in going from the neutral compound to the protonated compound are consistent with the resonance structures presented in Figure 54 for 1dbcp-H⁺. In addition to the expected changes in the C-O bond, it is observed that the exocyclic double bond shows a decrease in bond order and an increase in bond length in going from neutral to protonated cation; whereas the opposite is observed for the single bond connected to the phenyl group. The redistribution of charge upon protonation is also consistent with the resonance structures. For example the charge on the benzylidene carbon increases from -0.01 to 0.15 upon protonation.

In the alternation of double and single bonds of 1dbcp and 1dbcp-H⁺, the difference in alternating bonds are found to be 0.12 Å and 0.08 Å, respectively. The difference in the lengths of alternating bonds is found to be in an excellent agreement for 1dbcp-H⁺ with the reported linear longer polyene alternation (C_nH_{2n+2}, where n is up to 22), which is 0.08 Å.⁵⁸ To have a better understanding in bond alternation, the electronic interactions in π electron systems must be investigated.⁵⁸ The single bond lengths of 1dbcp and 1dbcp-H⁺ are found to be shorter than the normal alkane C-C bond length (1.54Å), which is consistent with the idea of the delocalization of π-electrons. Nevertheless, alternating double and single bond orders are found to be quite different than the bond orders of normal alkane and alkene, which necessitates further investigation.

4.2.4 Absorption Spectra and INDO/S Calculations

The room temperature absorption spectrum of 1dbcp-H⁺, 2dbcp-H⁺, and 3dbcp-H⁺ in sulfuric acid are shown in Figure 55 - Figure 57 along with the results of INDO/S calculations. As seen from these figures, the experimental absorption spectra of protonated compounds exhibited excellent agreement with the INDO/S calculations. The absorption spectrum of 1dbcp-H⁺ shows a strong band between 410-570 nm along with a resolved shoulder at 470 nm. It is observed that with increasing polyene chain length a shift towards longer wavelengths takes place and the absorption spectra become broader. The strong absorption bands for 2dbcp-H⁺ and 3dbcp-H⁺ are observed between 410-680 nm and 450-850 nm, respectively. On the shorter wavelength side of the strong transition, a moderate absorption band for 1dbcp-H⁺ is observed between 340-400 nm; whereas, weak absorption bands of 2dbcp-H⁺ and 3dbcp-H⁺ fall between 300-390 nm and 370-430 nm, respectively. A weak absorption band between 220-250 nm is observed for 1dbcp-H⁺, moderate absorption bands are found between 250-300 nm for 2dbcp-H⁺ and 270-350 nm for 3dbcp-H⁺. Absorption is seen to rise near the 200 nm cut-off for all three protonated compounds.

The INDO/S calculations were carried out to understand the nature of long wavelength electronic transitions. Specific comments will be restricted to excitations terminating at the lowest three excited states: S₁-S₃. These calculations show that transition to S₁ corresponds to the HOMO → LUMO excitation for all three protonated compounds which are predicted to be ππ* in nature. The strong long wavelength transition observed for 1dbcp-H⁺, 2dbcp-H⁺, and 3dbcp-H⁺ can be assigned to this excitation. This transition correlates with S₀ → S₂ for the unprotonated compounds. The

primary configurations for the transition to S_2 are found as follows: 1dbcp- H^+ : HOMO-4 \rightarrow LUMO (342 nm); 2dbcp- H^+ and 3dbcp- H^+ : HOMO-1 \rightarrow LUMO (382 and 418 nm, respectively). The computed transition to S_2 shows a weak transition for 1dbcp- H^+ and moderate transitions for 2dbcp- H^+ and 3dbcp- H^+ . The S_3 calculations reveal transitions with the primary configurations of 1dbcp- H^+ to be moderate: HOMO-1 \rightarrow LUMO (338 nm); 2dbcp- H^+ and 3dbcp- H^+ to be weak: HOMO-3 \rightarrow LUMO (328 nm) and HOMO \rightarrow LUMO+1 (329 nm), respectively. Figure 59 shows the LUMO, HOMO, and HOMO-1 for 3dbcp- H^+ as calculated by INDO/S. Table 26 - Table 28 show the calculated excitations above 200 nm.

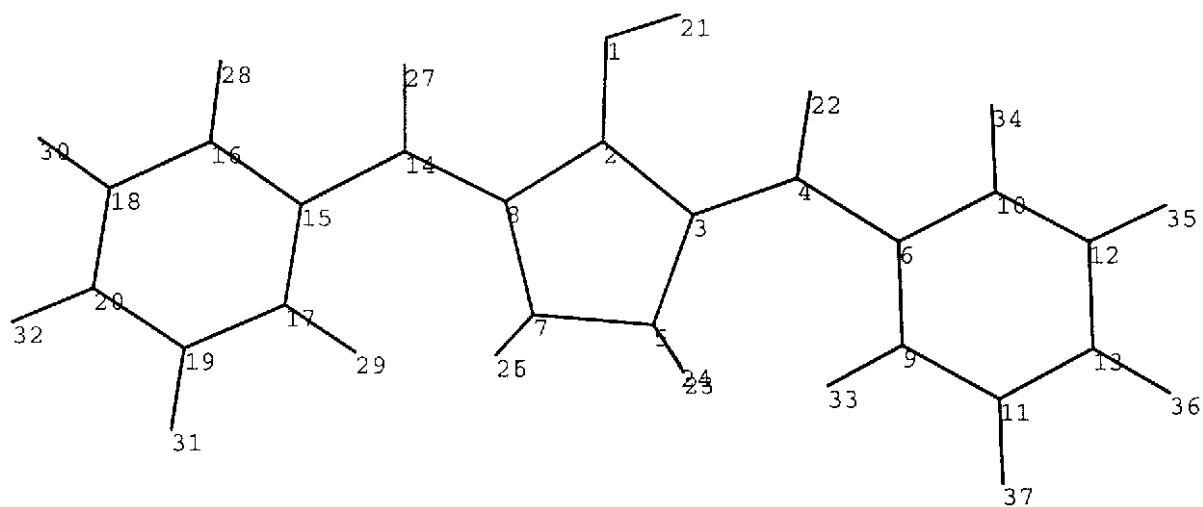


Figure 46: Optimized geometry of 1dbcp-H⁺ ($\Delta H_f = 196.71$ kcal/mol).

Table 23 Calculated Ground State Equilibrium Geometry of ldbcp-H⁺ by PM3 Method.

	Bond Lengths (Å)	Bond Orders
H ₂₁ -O ₁	0.96	0.91
O ₁ -C ₂	1.32	1.25
C ₂ -C ₃	1.44	1.14
C ₂ -C ₈	1.43	1.20
C ₃ -C ₅	1.50	0.98
C ₇ -C ₈	1.50	0.98
C ₅ -C ₇	1.54	0.99
C ₃ -C ₄	1.36	1.63
C ₈ -C ₁₄	1.37	1.56
C ₄ -C ₆	1.44	1.11
C ₁₄ -C ₁₅	1.44	1.13
C ₆ -C ₁₀	1.41	1.33
C ₁₅ -C ₁₆	1.41	1.32
C ₁₀ -C ₁₂	1.39	1.46
C ₁₆ -C ₁₈	1.39	1.46
C ₁₂ -C ₁₃	1.39	1.39
C ₁₈ -C ₂₀	1.39	1.39
C ₁₃ -C ₁₁	1.39	1.41
C ₂₀ -C ₁₉	1.39	1.41
C ₁₁ -C ₉	1.39	1.44
C ₁₉ -C ₁₇	1.39	1.45
C ₉ -C ₆	1.40	1.34
C ₁₇ -C ₁₅	1.40	1.33

Bond Angles (°)	
H ₂₁ -O ₁ -C ₂	109.20
O ₁ -C ₂ -C ₈	126.30
C ₃ -C ₅ -C ₇	105.80
C ₅ -C ₇ -C ₈	106.10
C ₂ -C ₃ -C ₄	124.60
C ₇ -C ₈ -C ₁₄	123.70
C ₃ -C ₄ -C ₆	123.00
C ₈ -C ₁₄ -C ₁₅	122.10
C ₄ -C ₆ -C ₁₀	121.80
C ₁₄ -C ₁₅ -C ₁₆	122.70
C ₆ -C ₁₀ -C ₁₂	122.70
C ₁₅ -C ₁₆ -C ₁₈	119.50
C ₁₀ -C ₁₂ -C ₁₃	119.50
C ₁₆ -C ₁₈ -C ₂₀	120.20
C ₆ -C ₉ -C ₁₁	120.00
C ₁₅ -C ₁₇ -C ₁₉	120.00

Dihedral Angels (°)	
C ₁₇ -C ₁₅ -C ₁₄ -C ₈	-20.30
C ₉ -C ₆ -C ₄ -C ₃	19.60

Atomic Charges	
H ₂₁	0.24
O ₁	-0.15
C ₂	0.36
C ₃	-0.28
C ₄	0.15
C ₅	-0.04
C ₆	-0.15
C ₇	-0.04
C ₈	-0.24
C ₉	-0.04
C ₁₀	-0.03
C ₁₁	-0.11
C ₁₂	-0.11
C ₁₃	-0.02
C ₁₄	0.20
C ₁₅	-0.16
C ₁₆	-0.02
C ₁₇	-0.03
C ₁₈	-0.11
C ₁₉	-0.11
C ₂₀	-0.01

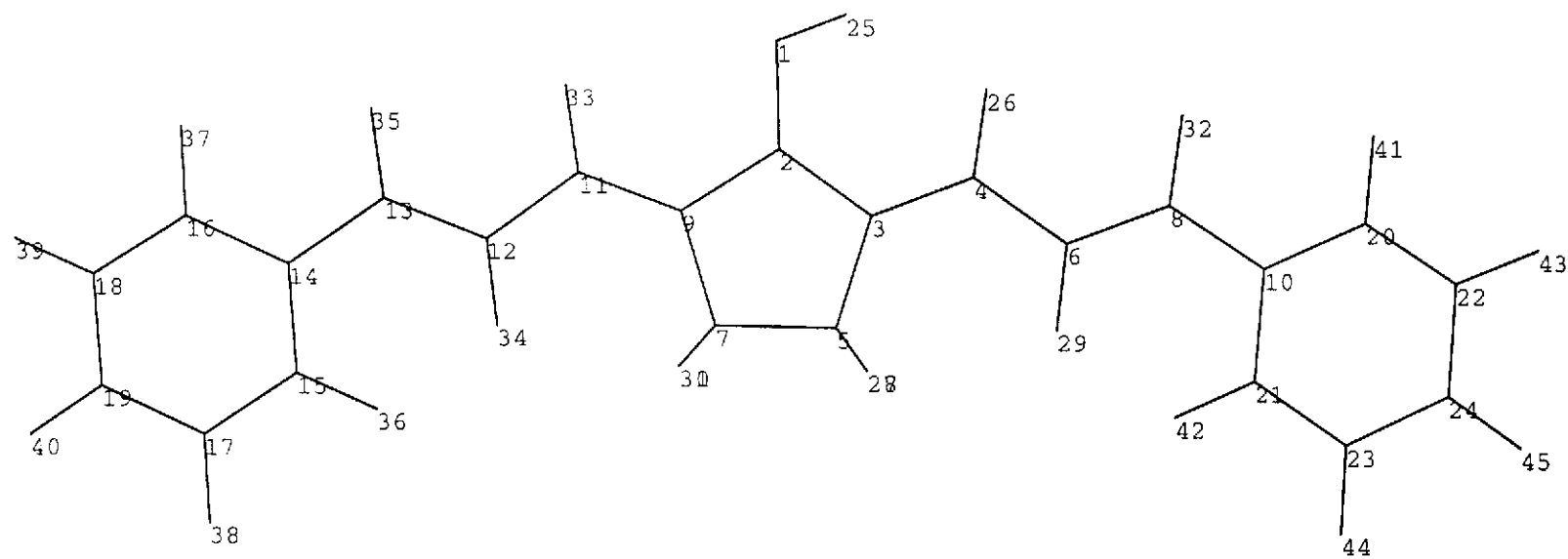


Figure 47: Optimized geometry of 2dbcp-H⁺ ($\Delta H_f = 217.55$ kcal/mol).

Table 24 Calculated Ground State Equilibrium Geometry of 2dbcp-H⁺ by PM3 Method.

	Bond Lengths (Å)	Bond Orders
H ₂₅ -O ₁	0.96	0.91
O ₁ -C ₂	1.32	1.23
C ₂ -C ₃	1.44	1.15
C ₂ -C ₉	1.42	1.23
C ₃ -C ₅	1.50	0.98
C ₇ -C ₉	1.50	0.98
C ₅ -C ₇	1.54	0.99
C ₃ -C ₄	1.36	1.60
C ₉ -C ₁₁	1.42	1.52
C ₄ -C ₆	1.42	1.16
C ₁₁ -C ₁₂	1.42	1.19
C ₆ -C ₈	1.36	1.69
C ₁₂ -C ₁₃	1.36	1.66
C ₈ -C ₁₀	1.45	1.08
C ₁₃ -C ₁₄	1.44	1.09
C ₁₀ -C ₂₀	1.40	1.35
C ₁₄ -C ₁₆	1.40	1.35
C ₂₀ -C ₂₂	1.39	1.45
C ₁₆ -C ₁₈	1.39	1.45
C ₂₂ -C ₂₄	1.39	1.41
C ₁₈ -C ₁₉	1.39	1.41
C ₂₃ -C ₂₄	1.39	1.41
C ₁₇ -C ₁₉	1.39	1.41
C ₂₁ -C ₂₃	1.39	1.45
C ₁₅ -C ₁₇	1.39	1.45
C ₁₀ -C ₂₁	1.40	1.35
C ₁₄ -C ₁₅	1.40	1.35

Bond Angles (°)	
H ₂₅ -O ₁ -C ₂	109.20
O ₁ -C ₂ -C ₃	126.30
C ₃ -C ₅ -C ₇	105.80
C ₅ -C ₇ -C ₉	106.10
C ₂ -C ₃ -C ₄	124.60
C ₃ -C ₄ -C ₆	123.70
C ₉ -C ₁₁ -C ₁₂	123.00
C ₄ -C ₆ -C ₈	122.10
C ₁₁ -C ₁₂ -C ₁₃	121.80
C ₆ -C ₈ -C ₁₀	122.70
C ₁₂ -C ₁₃ -C ₁₄	122.70
C ₈ -C ₁₀ -C ₂₀	119.50
C ₁₃ -C ₁₄ -C ₁₆	119.50
C ₂₀ -C ₂₂ -C ₂₄	120.20
C ₂₄ -C ₂₃ -C ₂₁	120.00
C ₁₅ -C ₁₇ -C ₁₉	120.00
C ₂₃ -C ₂₁ -C ₁₀	120.30

Dihedral Angles (°)	
C ₃₄ -C ₁₂ -C ₁₁ -C ₉	0.02
C ₁₅ -C ₁₄ -C ₁₃ -C ₁₂	0.03
C ₂₉ -C ₆ -C ₄ -C ₃	-0.04
C ₂₁ -C ₁₀ -C ₈ -C ₆	-0.03

Atomic Charges	
H ₂₅	0.24
O ₁	-0.15
C ₂	0.35
C ₃	-0.28
C ₄	-0.04
C ₅	-0.03
C ₆	-0.25
C ₇	-0.04
C ₈	0.11
C ₉	-0.26
C ₁₀	-0.14
C ₁₁	0.18
C ₁₂	-0.27
C ₁₃	0.13
C ₁₄	-0.15
C ₁₅	-0.04
C ₁₆	-0.04
C ₁₇	-0.11
C ₁₈	-0.11
C ₁₉	-0.03
C ₂₀	-0.04
C ₂₁	-0.05
C ₂₂	-0.11
C ₂₃	-0.11
C ₂₄	-0.04

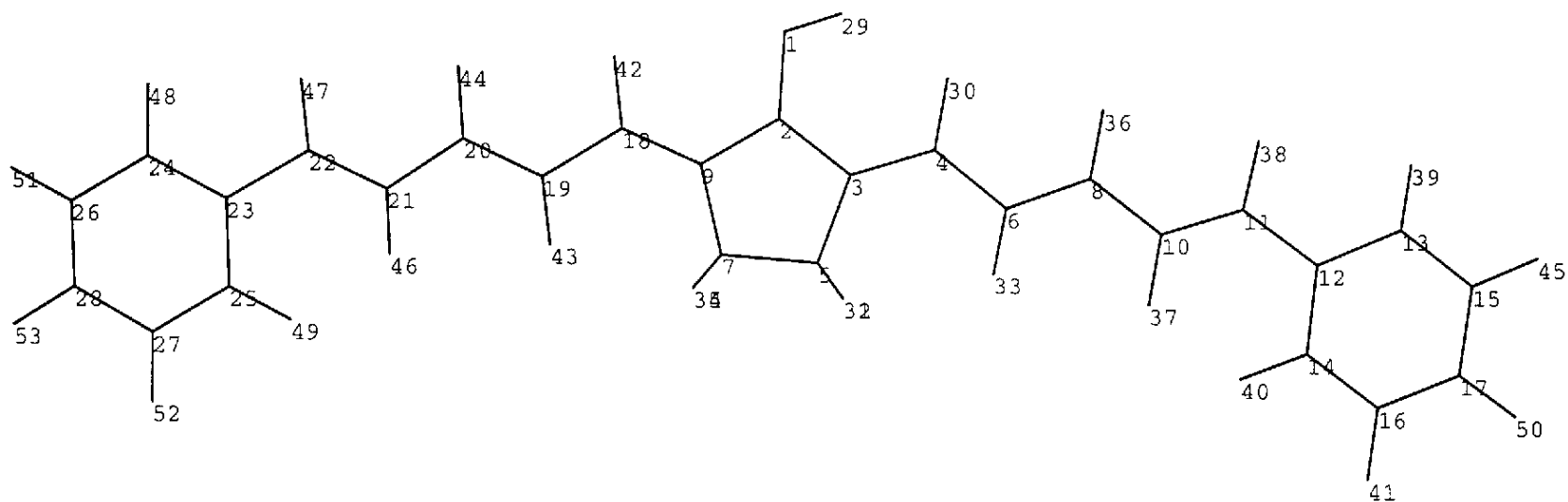


Figure 48: Optimized geometry of 3dbcp-H⁺ ($\Delta H_f = 243.35$ kcal/mol).

Table 25 Calculated Ground State Equilibrium Geometry of 3dbcp-H⁺ by PM3 Method.

	Bond Lengths (Å)	Bond Orders
H ₂₉ -O ₁	0.96	0.91
O ₁ -C ₂	1.32	1.22
C ₂ -C ₃	1.44	1.16
C ₂ -C ₉	1.42	1.24
C ₃ -C ₅	1.50	0.98
C ₇ -C ₉	1.50	0.98
C ₅ -C ₇	1.54	0.99
C ₃ -C ₄	1.36	1.59
C ₉ -C ₁₈	1.37	1.50
C ₄ -C ₆	1.42	1.17
C ₁₈ -C ₁₉	1.42	1.21
C ₆ -C ₈	1.36	1.67
C ₁₉ -C ₂₀	1.36	1.62
C ₈ -C ₁₀	1.43	1.12
C ₂₀ -C ₂₁	1.43	1.14
C ₁₀ -C ₁₁	1.35	1.75
C ₂₁ -C ₂₂	1.35	1.72
C ₁₁ -C ₁₂	1.45	1.06
C ₂₂ -C ₂₃	1.45	1.07
C ₁₂ -C ₁₃	1.40	1.36
C ₂₃ -C ₂₄	1.40	1.36
C ₁₃ -C ₁₅	1.39	1.44
C ₂₄ -C ₂₆	1.39	1.44
C ₁₅ -C ₁₇	1.39	1.41
C ₂₆ -C ₂₈	1.39	1.41
C ₁₆ -C ₁₇	1.39	1.41
C ₂₇ -C ₂₈	1.39	1.41
C ₁₄ -C ₁₆	1.39	1.44
C ₂₅ -C ₂₇	1.39	1.44
C ₁₂ -C ₁₄	1.40	1.36
C ₂₃ -C ₂₅	1.40	1.36

Bond Angles (°)	
H ₂₉ -O ₁ -C ₂	109.00
O ₁ -C ₂ -C ₃	126.20
C ₂ -C ₃ -C ₅	108.20
C ₅ -C ₇ -C ₉	106.10
C ₂ -C ₃ -C ₄	124.60
C ₂ -C ₉ -C ₁₈	118.90
C ₃ -C ₄ -C ₆	123.70
C ₉ -C ₁₈ -C ₁₉	123.10
C ₄ -C ₆ -C ₈	121.70
C ₁₈ -C ₁₉ -C ₂₀	121.40
C ₆ -C ₈ -C ₁₀	121.80
C ₁₉ -C ₂₀ -C ₂₁	121.80
C ₈ -C ₁₀ -C ₁₁	122.10
C ₂₀ -C ₂₁ -C ₂₂	122.00
C ₁₀ -C ₁₁ -C ₁₂	122.80
C ₂₁ -C ₂₂ -C ₂₃	122.80
C ₁₁ -C ₁₂ -C ₁₃	119.50
C ₂₂ -C ₂₃ -C ₂₄	119.50
C ₁₂ -C ₁₃ -C ₁₅	120.00
C ₂₃ -C ₂₄ -C ₂₆	120.00
C ₁₇ -C ₁₆ -C ₁₄	120.00
C ₁₆ -C ₁₄ -C ₁₂	120.30
C ₂₃ -C ₂₄ -C ₂₆	120.20

Dihedral Angels (°)	
C ₄₃ -C ₁₉ -C ₁₈ -C ₉	0.00
C ₄₆ -C ₂₁ -C ₂₀ -C ₁₉	-0.01
C ₂₅ -C ₂₃ -C ₂₂ -C ₂₁	-0.01
C ₃₃ -C ₆ -C ₄ -C ₃	0.02
C ₃₇ -C ₁₀ -C ₈ -C ₆	0.04
C ₁₄ -C ₁₂ -C ₁₁ -C ₁₀	0.02

Atomic Charges	
H ₂₉	0.23
O ₁	-0.16
C ₂	0.34
C ₃	-0.28
C ₄	0.12
C ₅	-0.03
C ₆	-0.24
C ₇	-0.04
C ₈	0.09
C ₉	-0.27
C ₁₀	-0.23
C ₁₁	0.06
C ₁₂	-0.12
C ₁₃	-0.06
C ₁₄	-0.06
C ₁₅	-0.10
C ₁₆	-0.10
C ₁₇	-0.06
C ₁₈	0.17
C ₁₉	-0.26
C ₂₀	0.12
C ₂₁	-0.24
C ₂₂	0.08
C ₂₃	-0.12
C ₂₄	-0.05
C ₂₅	-0.06
C ₂₆	-0.11
C ₂₇	-0.10
C ₂₈	-0.05

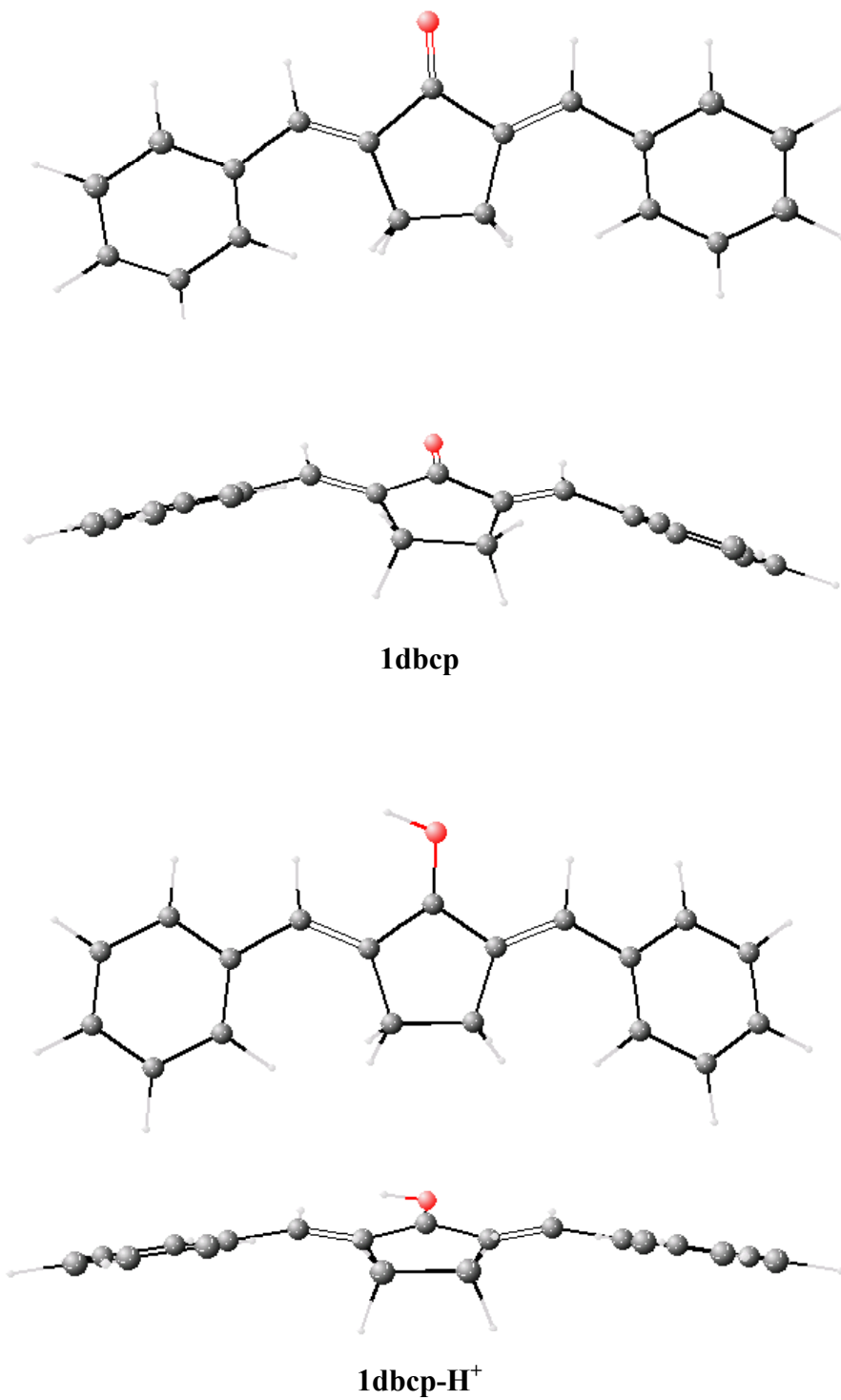
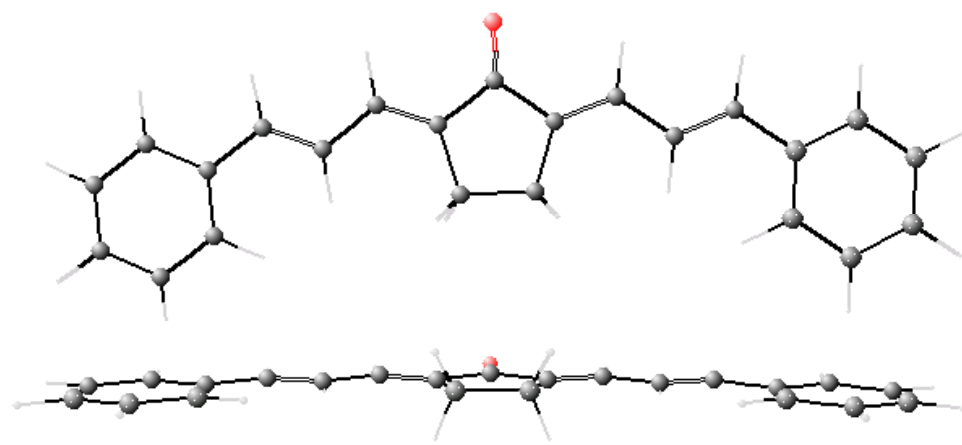
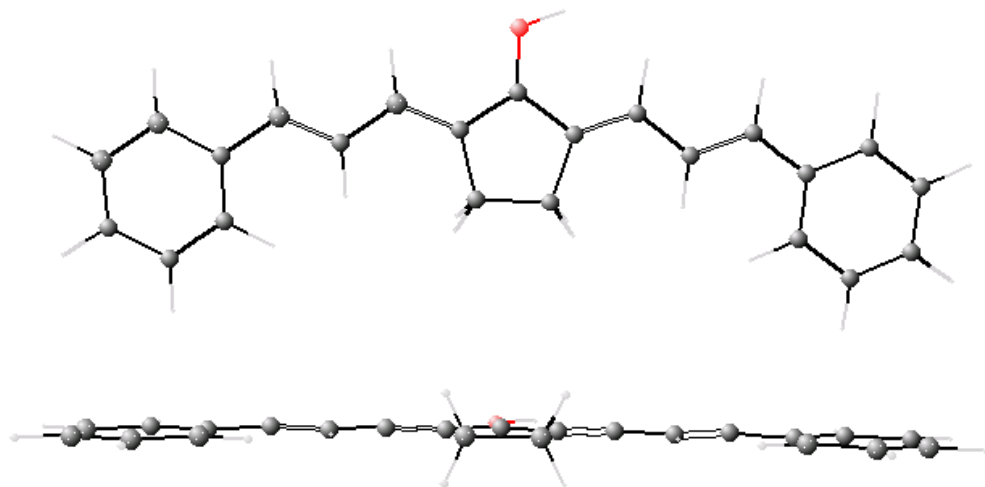


Figure 49: Three-dimensional optimized geometry of 1dbcp and 1dbcp-H⁺.



2dbcp



2dbcp-H⁺

Figure 50: Three-dimensional optimized geometry of 2dbcp and 2dbcp-H⁺.

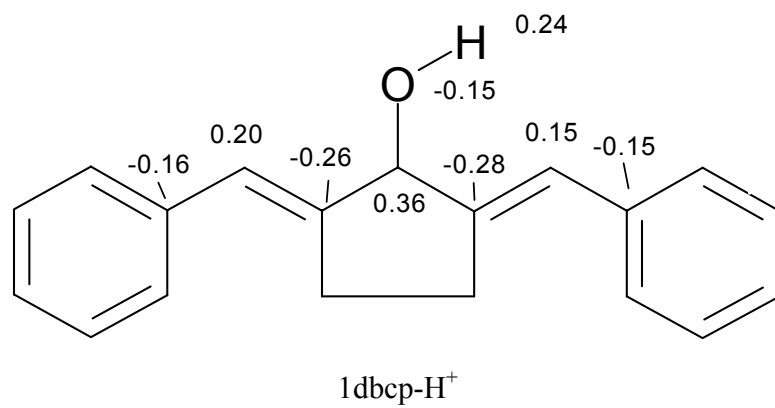
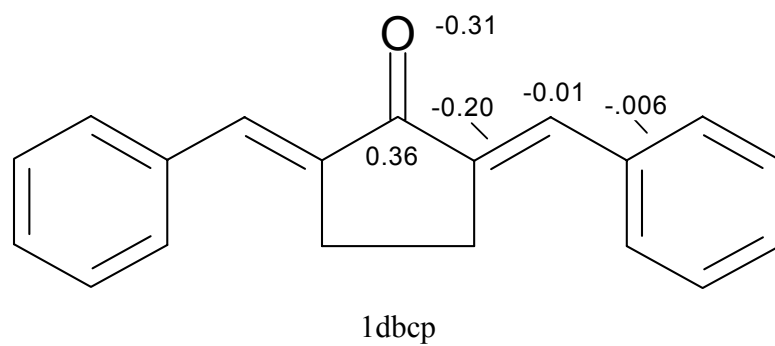
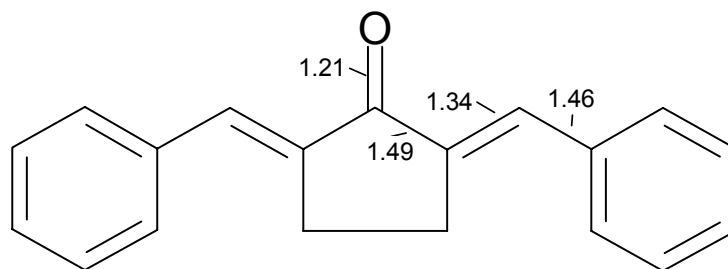
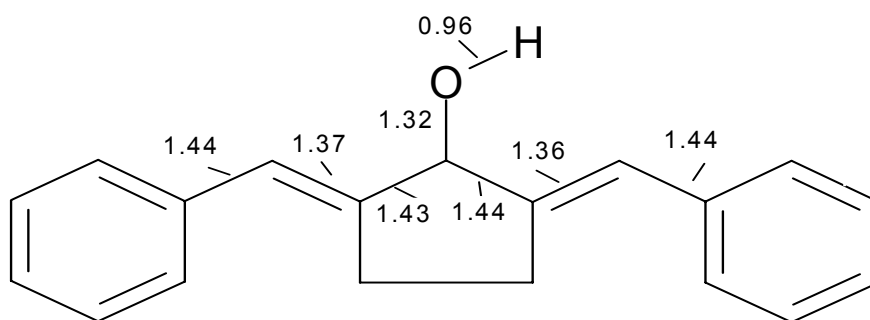


Figure 51: Atomic charges of 1dbcp and 1dbcp-H⁺.



1dbcp



1dbcp-H⁺

Figure 52: Bond lengths of 1dbcp and 1dbcp-H⁺.

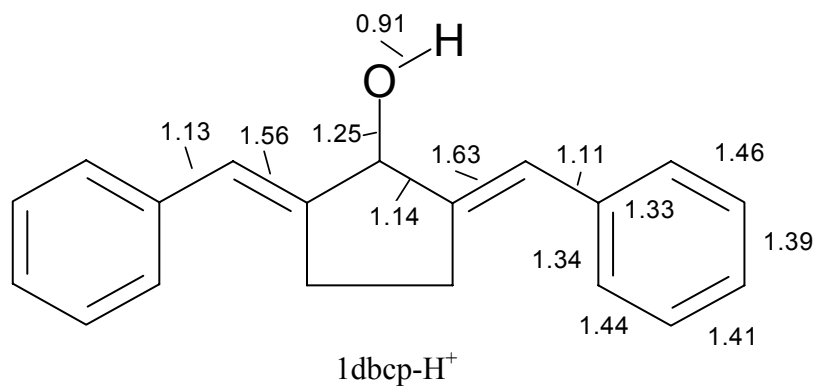
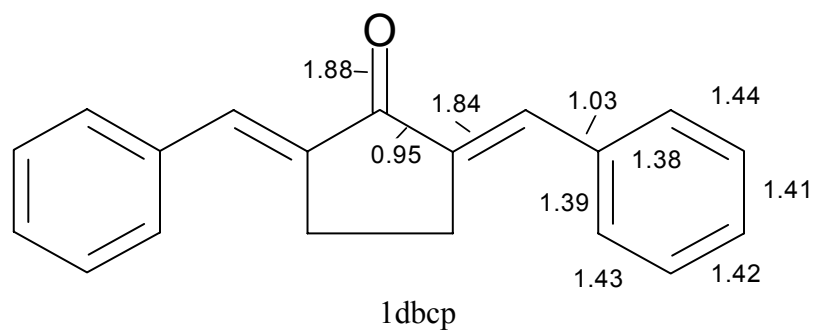


Figure 53: Bond orders of 1dbcp and 1dbcp-H⁺.

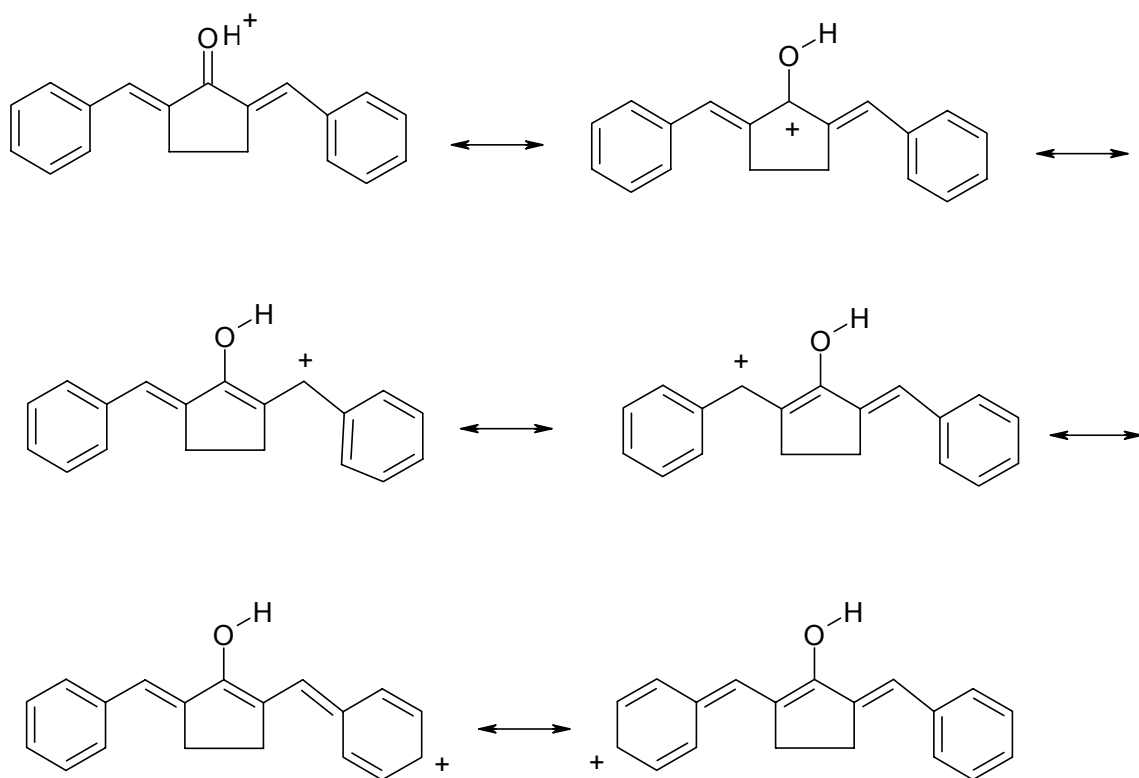


Figure 54: Resonance structures of 1dbcp- H^+ .

Figure 55: Room temperature absorption spectra of 1dbcp-H⁺ in sulfuric acid and INDO/S-CIS calculated results.

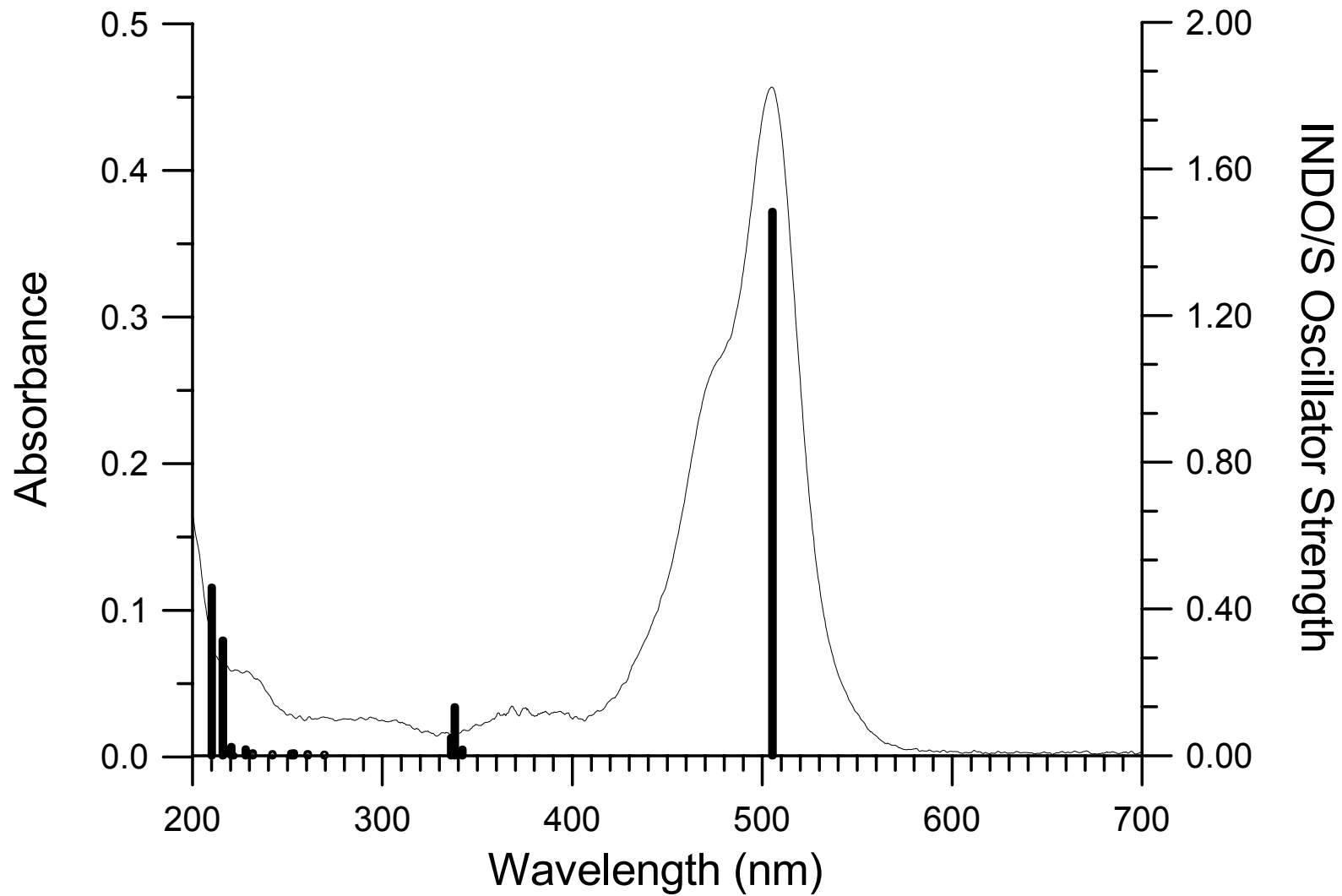


Figure 56: Room temperature absorption spectra of 2bcp-H⁺ in sulfuric acid and INDO/S-CIS calculated results.

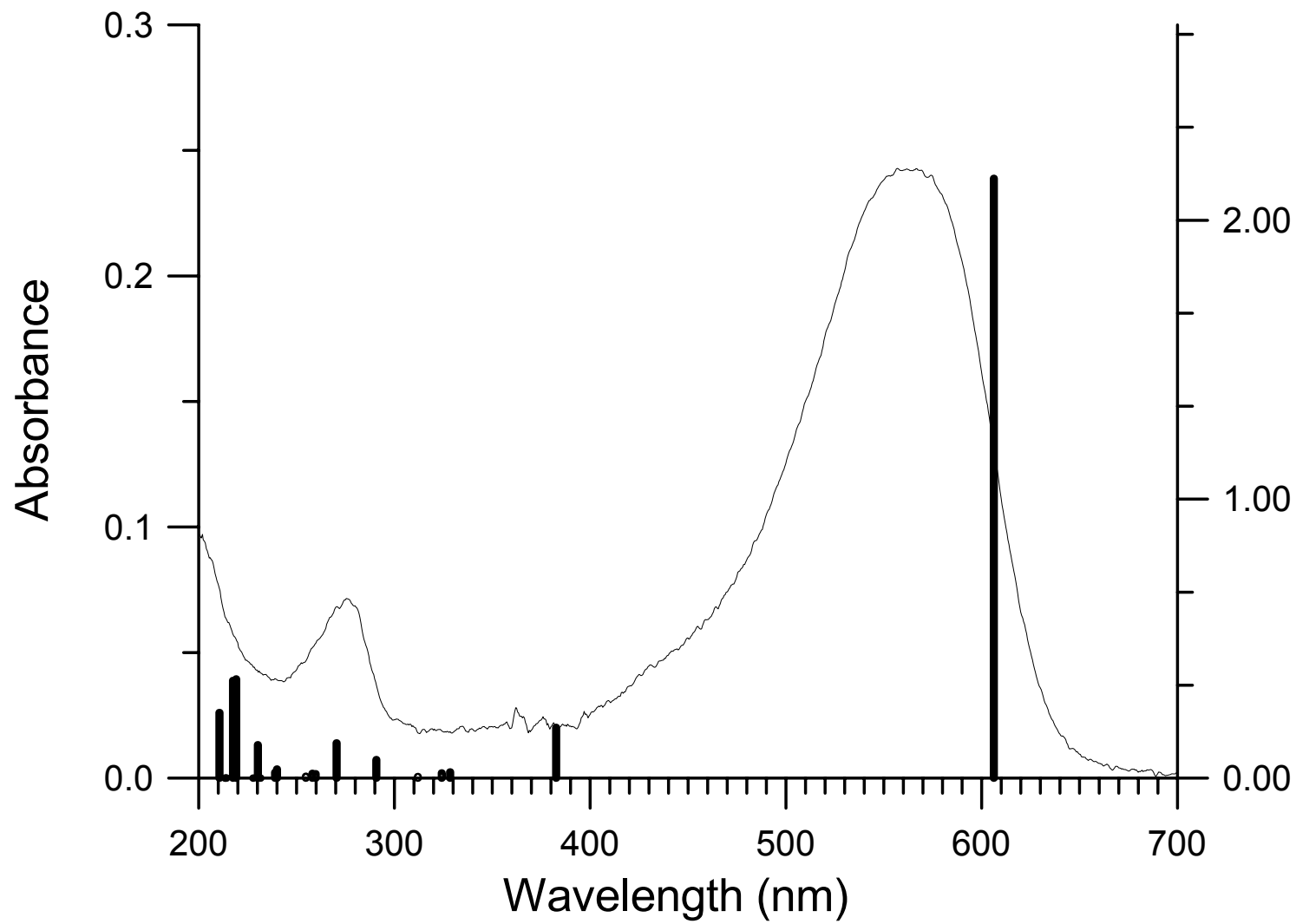


Figure 57: Room temperature absorption spectra of 3dbcp-H⁺ in sulfuric acid/ acetic acid (1:3) and INDO/S-CIS calculated results.

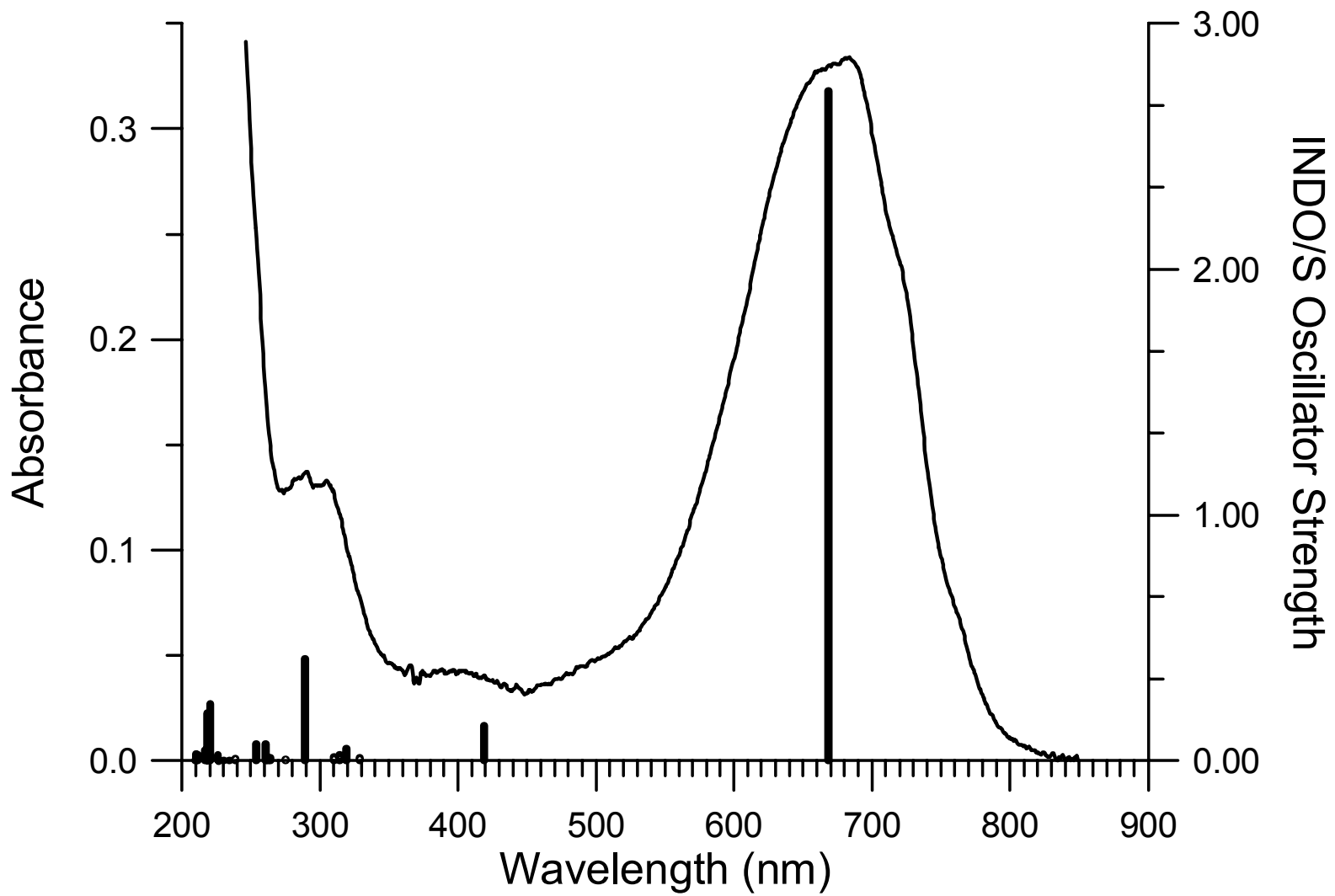
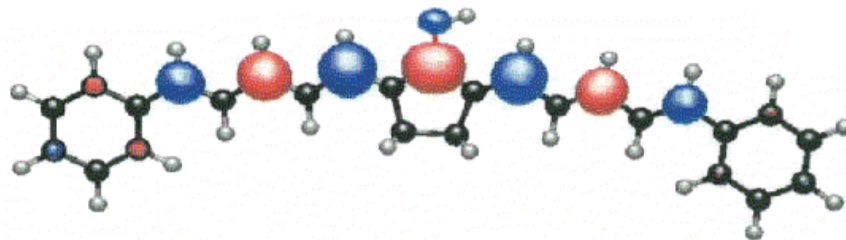
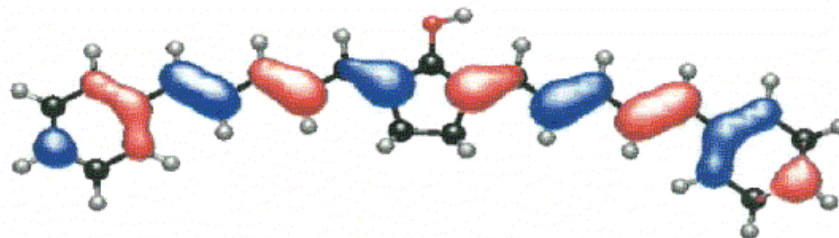


Figure 58: LUMO, HOMO, and HOMO-1 for 3dbcp-H⁺ as calculated by INDO/S.

Molecular orbital 70(Alpha) -4.9157 eV



Molecular orbital 69(Alpha) -9.3955 eV



Molecular orbital 68(Alpha) -10.1273 eV

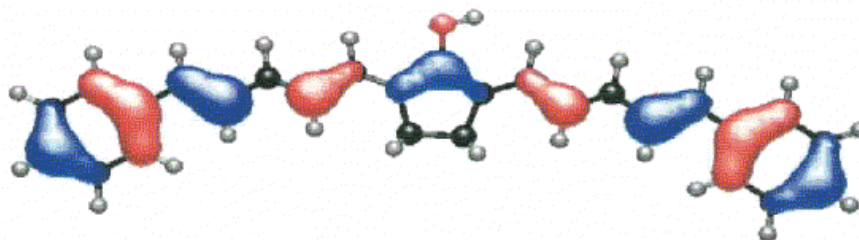


Table 26 INDO/S-CIS Computed Singlet State Excitations for 1dbcp-H⁺.

State	Transition energy			Oscillator Strength	MO	CI Coef.	
	eV	cm ⁻¹	nm				
1	2.45327	19786.91	505.385	1.484035	49 → 50	-0.96677	(93%)
2	3.62323	29223.35	342.192	0.017395	46 → 50	-0.7738	(60%)
					48 → 50	-0.4496	(20%)
					46 → 51	0.27107	(7%)
3	3.66675	29574.32	338.131	0.132771	48 → 50	-0.79908	(64%)
					46 → 50	0.48673	(24%)
4	3.68863	29750.79	336.126	0.048987	47 → 50	-0.88031	(77%)
					47 → 51	-0.29444	(9%)
5	4.60187	37116.59	269.421	0.003982	49 → 51	0.90847	(83%)
6	4.75584	38358.41	260.699	0.005138	45 → 50	0.82998	(69%)
					49 → 52	0.26586	(7%)
					48 → 51	0.24283	(6%)
7	4.89322	39466.48	253.38	0.007285	49 → 54	0.41394	(17%)
					49 → 53	0.36607	(13%)
					47 → 52	-0.36037	(13%)
					47 → 50	0.32398	(10%)
					47 → 51	-0.31131	(10%)
8	4.92023	39684.31	251.989	0.006399	49 → 53	0.4067	(17%)
					46 → 52	0.37288	(14%)
					49 → 54	-0.36564	(13%)
					46 → 51	-0.29918	(9%)
					46 → 50	-0.297	(9%)
9	5.12155	41308.04	242.084	0.049465	49 → 52	-0.68366	(47%)
					45 → 50	0.31062	(10%)
					48 → 51	-0.30949	(10%)
					43 → 50	-0.29161	(9%)
					46 → 51	0.20609	(4%)
10	5.35118	43160.14	231.695	0.007268	44 → 50	0.85738	(74%)
					45 → 51	0.24323	(6%)
					47 → 53	0.14442	(2%)
11	5.43703	43852.57	228.037	0.017842	43 → 50	0.70804	(50%)
					38 → 50	0.32188	(10%)
					45 → 50	0.30323	(9%)
					41 → 50	-0.25312	(6%)
					49 → 52	-0.24058	(6%)
12	5.59473	45124.54	221.609	0.000022	49 → 56	-0.71073	(51%)
					49 → 57	0.56632	(32%)

Table 26 Cont'd. INDO/S-CIS Computed Singlet State Excitations for 1dbcp-H⁺.

State	Transition energy			Oscillator Strength	MO	CI Coef.	
13	5.62392	45359.95	220.459	0.024691	49 → 55	-0.56828	(32%)
					47 → 53	-0.36145	(13%)
					44 → 50	0.27603	(8%)
					48 → 54	0.26232	(7%)
					48 → 52	-0.26079	(7%)
14	5.74237	46315.33	215.911	0.314916	49 → 57	-0.41333	(17%)
					47 → 54	0.37944	(14%)
					46 → 53	-0.34471	(12%)
					48 → 53	-0.31534	(10%)
					46 → 54	0.3058	(9%)
15	5.90053	47590.93	210.124	0.458804	47 → 51	0.4896	(24%)
					49 → 54	0.4769	(23%)
					47 → 52	0.34494	(12%)
					48 → 51	-0.29405	(9%)
					49 → 53	0.24959	(6%)

Table 27 INDO/S-CIS Computed Singlet State Excitations for 2dbcp-H⁺.

State	Transition energy			Oscillator Strength	MO	CI Coef.	
	eV	cm ⁻¹	nm				
1	2.0452	16495.66	606.22	2.149701	59 → 60	0.95259	(91%)
2	3.2404	26135.57	382.62	0.181268	58 → 60	0.92944	(86%)
3	3.77491	30446.66	328.443	0.022102	56 → 60 56 → 61	-0.8554 0.37795	(73%) (14%)
4	3.82486	30849.53	324.154	0.01824	57 → 60 57 → 61	0.8385 0.39582	(70%) (16%)
5	3.97408	32053.08	311.983	0.005273	59 → 61	0.90356	(82%)
6	4.26358	34388.08	290.798	0.066269	55 → 60 59 → 62 58 → 61	-0.76386 -0.41813 -0.37158	(58%) (17%) (14%)
7	4.58448	36976.28	270.444	0.125939	59 → 62 55 → 60 58 → 61	0.68143 -0.545 0.32479	(46%) (30%) (11%)
8	4.7723	38491.21	259.8	0.015409	59 → 65 57 → 60 58 → 65 57 → 62 57 → 64	0.48341 0.44855 -0.41329 0.31085 0.25148	(23%) (20%) (17%) (10%) (6%)
9	4.80444	38750.37	258.062	0.016823	59 → 63 56 → 60 58 → 63 56 → 62 56 → 64	0.42629 -0.42322 0.37498 -0.32216 0.25435	(18%) (18%) (14%) (10%) (6%)
10	4.86594	39246.45	254.8	0.006366	54 → 60 55 → 61 48 → 60	-0.8374 -0.28369 -0.21887	(70%) (8%) (5%)
11	5.16603	41666.82	239.999	0.032588	59 → 64 59 → 63 58 → 62 54 → 60 58 → 66	-0.60043 -0.36784 0.36409 0.29373 -0.25369	(36%) (14%) (13%) (9%) (6%)
12	5.18788	41843.03	238.988	0.020556	58 → 61 59 → 62 59 → 60	0.75215 -0.43752 0.24531	(57%) (19%) (6%)

Table 27 Cont'd. INDO/S-CIS Computed Singlet State Excitations for 2dbcp-H⁺.

State	Transition energy			Oscillator Strength	MO	CI Coef.	
	eV	cm ⁻¹	nm				
13	5.35528	43193.22	231.518	0.000005	59 → 67	-0.79877	(64%)
					55 → 67	-0.28061	(8%)
					53 → 60	0.25653	(7%)
					47 → 60	0.25358	(6%)
14	5.3856	43437.79	230.214	0.119524	59 → 66	0.63989	(41%)
					57 → 65	0.32619	(11%)
					56 → 63	-0.31804	(10%)
					58 → 64	0.31258	(10%)
					55 → 62	0.25704	(7%)
15	5.44012	43877.55	227.907	0.000145	47 → 60	-0.51662	(27%)
					53 → 60	-0.49832	(25%)
					59 → 67	-0.41266	(17%)
					50 → 60	0.28702	(8%)
					45 → 60	-0.21324	(5%)
16	5.65801	45634.93	219.13	0.355356	57 → 61	-0.55746	(31%)
					59 → 65	-0.46359	(21%)
					57 → 62	0.38191	(15%)
					58 → 65	0.30165	(9%)
					57 → 60	0.23341	(5%)
17	5.70011	45974.44	217.512	0.349978	56 → 61	0.5314	(28%)
					59 → 63	0.4202	(18%)
					56 → 62	0.38889	(15%)
					58 → 63	0.27551	(8%)
					56 → 64	-0.2445	(6%)
18	5.789	46691.43	214.172	0.000636	57 → 65	0.47239	(22%)
					59 → 68	0.42866	(18%)
					56 → 63	0.35247	(12%)
					59 → 64	0.32809	(11%)
					58 → 69	-0.20448	(4%)
19	5.80602	46828.67	213.544	0.000013	59 → 70	-0.7896	(62%)
					58 → 67	-0.38294	(15%)
					54 → 67	0.23755	(6%)
20	5.88643	47477.25	210.627	0.23501	59 → 69	0.57584	(33%)
					56 → 63	-0.40266	(16%)
					57 → 65	0.34753	(12%)
					59 → 66	-0.27871	(8%)
					58 → 68	-0.26488	(7%)

Table 28 INDO/S-CIS Computed Singlet State Excitations for 3dbcp-H⁺.

State	Transition energy			Oscillator Strength	MO	CI Coef.	
	eV	cm ⁻¹	nm				
1	1.85472	14959.35	668.478	2.727067	69 → 70	0.93725	(88%)
2	2.95909	23866.69	418.994	0.142993	68 → 70	-0.92008	(85%)
3	3.77148	30419.05	328.741	0.013601	69 → 71	-0.89447	(80%)
					68 → 72	0.30053	(9%)
4	3.88356	31322.99	319.254	0.047811	65 → 70	-0.82012	(67%)
					68 → 71	0.27312	(7%)
					69 → 72	-0.25339	(6%)
					66 → 70	-0.218	(5%)
5	3.94352	31806.65	314.4	0.021754	66 → 70	0.76352	(58%)
					66 → 71	0.38127	(15%)
					66 → 72	-0.26163	(7%)
					65 → 70	-0.22548	(5%)
6	3.99637	32232.86	310.242	0.015769	67 → 70	0.76267	(58%)
					67 → 71	-0.39873	(16%)
					67 → 72	-0.27734	(8%)
7	4.28718	34578.4	289.198	0.413541	69 → 72	-0.7188	(52%)
					68 → 71	0.47382	(22%)
					65 → 70	0.34951	(12%)
8	4.50847	36363.26	275.003	0.004285	64 → 70	-0.85584	(73%)
					62 → 70	0.27799	(8%)
9	4.69356	37856.09	264.158	0.010965	67 → 70	-0.54607	(30%)
					69 → 76	-0.41314	(17%)
					68 → 76	0.39105	(15%)
					67 → 73	-0.2705	(7%)
					65 → 76	0.2554	(7%)
10	4.72525	38111.71	262.387	0.011817	66 → 70	0.5103	(26%)
					68 → 75	0.40764	(17%)
					69 → 75	0.36862	(14%)
					66 → 73	-0.2753	(8%)
					65 → 75	-0.25995	(7%)
11	4.75722	38369.59	260.623	0.068878	68 → 71	-0.69093	(48%)
					69 → 72	-0.48613	(24%)
					69 → 70	0.26014	(7%)
					65 → 72	-0.25463	(6%)
12	4.88943	39435.89	253.576	0.069296	69 → 73	-0.74634	(56%)
					68 → 72	0.44686	(20%)
					68 → 74	-0.23364	(5%)

Table 28 Cont'd. INDO/S-CIS Computed Singlet State Excitations for 3dbcp-H⁺.

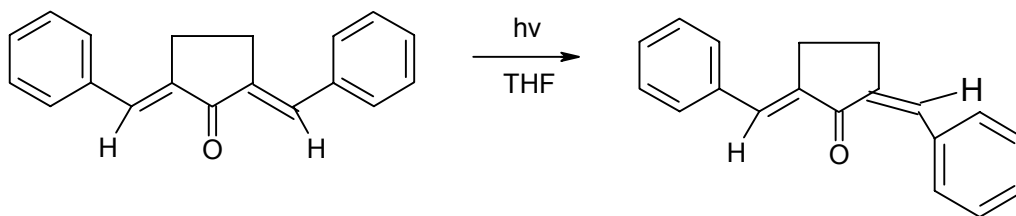
State	Transition energy			Oscillator Strength	MO	CI Coef.	
	eV	cm ⁻¹	nm				
13	5.18906	41852.6	238.934	0.008807	69 → 74	0.62633	(39%)
					68 → 73	0.39525	(16%)
					63 → 70	0.31674	(10%)
					65 → 72	0.30001	(9%)
					64 → 71	0.22226	(5%)
14	5.28498	42626.24	234.597	0.000004	69 → 78	0.8506	(72%)
					65 → 78	0.36779	(14%)
15	5.38255	43413.15	230.345	0.000535	65 → 71	-0.61778	(38%)
					68 → 72	-0.39571	(16%)
					69 → 73	-0.37533	(14%)
					68 → 74	-0.26495	(7%)
					68 → 70	-0.22032	(5%)
16	5.47109	44127.34	226.617	0.000115	56 → 70	-0.69838	(49%)
					61 → 70	-0.38786	(15%)
					60 → 70	-0.27876	(8%)
					59 → 70	-0.21544	(5%)
					58 → 70	0.20492	(4%)
17	5.48454	44235.77	226.061	0.022048	63 → 70	-0.71795	(52%)
					69 → 74	0.41009	(17%)
					68 → 77	0.241	(6%)
					64 → 71	-0.23036	(5%)
					57 → 70	-0.19725	(4%)
18	5.62155	45340.85	220.552	0.233962	67 → 71	-0.59236	(35%)
					69 → 76	0.42197	(18%)
					67 → 72	-0.41364	(17%)
					68 → 76	-0.31795	(10%)
					67 → 70	-0.28449	(8%)
19	5.66402	45683.39	218.898	0.000027	69 → 81	0.73801	(54%)
					68 → 78	0.3543	(13%)
					69 → 84	0.25568	(7%)
					64 → 78	-0.24305	(6%)
					68 → 83	0.23561	(6%)
20	5.67656	45784.56	218.414	0.193915	66 → 71	-0.46739	(22%)
					69 → 77	0.43188	(19%)
					66 → 72	0.33874	(11%)
					69 → 75	-0.31965	(10%)
					68 → 74	0.25403	(6%)

Table 28 Cont'd. INDO/S-CIS Computed Singlet State Excitations for 3dbcp-H⁺.

State	Transition energy			Oscillator Strength	MO	CI Coef.	
	eV	cm ⁻¹	nm				
21	5.68699	45868.61	218.014	0.050956	69 → 77	0.57425	(33%)
					66 → 71	0.33079	(11%)
					68 → 75	0.27597	(8%)
					66 → 72	-0.23974	(6%)
					69 → 75	0.23958	(6%)
22	5.71837	46121.77	216.817	0.041471	62 → 70	0.72548	(53%)
					63 → 71	0.25788	(7%)
					64 → 72	-0.24725	(6%)
					55 → 70	-0.22709	(5%)
					64 → 70	0.22044	(5%)
23	5.86577	47310.58	211.369	0.022268	69 → 79	0.661	(44%)
					68 → 77	-0.36587	(13%)
					63 → 70	-0.3238	(10%)
					67 → 76	-0.21707	(5%)
					66 → 75	-0.21681	(5%)
24	5.89937	47581.63	210.165	0.027592	64 → 71	-0.52067	(27%)
					65 → 72	-0.46671	(22%)
					69 → 74	0.29811	(9%)
					63 → 70	0.29621	(9%)
					68 → 73	-0.26129	(7%)
25	5.91336	47694.47	209.668	0.000063	69 → 83	0.63406	(40%)
					69 → 84	-0.40322	(16%)
					68 → 84	0.31883	(10%)
					68 → 81	0.28052	(8%)
					68 → 83	0.22831	(5%)

4.2.5 Photochemistry Studies of 1dbcp and 1dbcp-H⁺

George and Roth⁵⁹ have studied the photochemistry of 1dbcp in THF. In their study, 1dbcp was irradiated using a high pressure mercury lamp filtered by a cobalt (II) chloride solution. Their fractional crystallization and NMR studies revealed an E → Z photoisomerization of 1dbcp as shown below.



In our studies, 1dbcp in THF was irradiated for various intervals (5, 15, 45, 60 min) with a 150W xenon arc lamp filtered through 15 cm of distilled water. Irradiations were also carried out for 1dbcp-H⁺ (1dbcp dissolved in 96 % H₂SO₄) followed by neutralization, recovery of solid material, and redissolving the solid in THF. The reversibility of protonation was studied by taking IR spectra of material that is recovered after acidification followed by neutralization. It is found that the spectra agree with the spectra of the compounds prior to treatment with acid as shown in Appendix B.

The photochemical behavior of the compounds were analyzed using HPLC by comparing each peaks retention time, absorption spectra (obtained from 360 nm, where 1dbcp does maximum absorption), and the percent area of each peak to find out the relative amount of a particular compound. The results of the photochemistry studies of 1dbcp and 1dbcp-H⁺ are given in Figure 59 and Figure 60, respectively. Figure 59-a shows that prior to irradiation in THF, 99.0 % of the compound is found to be 1dbcp and 1 % is the minor product, namely the photoisomer product of 1dbcp (1 %). This

photoisomer product (34.6 %) grows after 5 min irradiation (Figure 59-b) and reaches photoequilibrium with the major product after 45 min (52.0 % major, 48.0 % minor), and remains unchanged after 60 min (51 % and 49 % minor) irradiations (Figure 59-c,d). The major product and its photoisomer are further analyzed by comparing their UV-VIS absorption spectra obtained by utilizing HPLC and are presented in Appendix F. Photoisomer product is shifted slightly to shorter wavelength and a slight shoulder beginning to appear at about 420nm. The absorption spectra of major product and its photoisomer are similar in shape and their absorption intensities vary at different periods of irradiation.

The photochemistry study of 1dbcp-H⁺ shown in Figure 60-a reveals that prior to irradiation 97.6 % 1dbcp (after neutralization) and 2.4 % of minor photoisomer product of 1dbcp was obtained. The entire irradiation study shows no growth of 1dbcp photoproduct(s) (minor products at 45 min: 2.4 % and 60 min 3.1 %). Besides the minor photoisomer product, at retention time below 2 min, growing peaks are observed with longer irradiation, which are shown in Appendix G - (A) for different durations of irradiation. These peaks may be occurring due to breaking down of the compound at higher energy. Compared to major product, the chromatographs of the peaks observed below 2 min retention time appear to be quite different in shape with a three-peak band system instead of one peak. Another significant difference is found from the comparison of the absorption spectra of these peaks, which are shown in Appendix G - (B). While the maximum of compound is near 360 nm, the products eluting before two minutes appear to have their maxima below 300 nm, with the 380 nm peak being only a minor shoulder.

In summary, the photochemistry studies show that, unlike 1dbcp, irradiation of 1dbcp-H⁺ does not produce photoproducts under the conditions of these experiments. The decomposition products of 1dbcp-H⁺ at retention time below 2 min can be further investigated. Other than noting that S₁ is nπ* for 1dbcp in THF; whereas S₁ is ππ* for 1dbcp-H⁺, a detailed explanation for this difference in photochemical behavior awaits further experimental and theoretical work.

4.2.6 Summary

Spectroscopic evidence has been provided that indicates that 2dbcp and 3dbcp undergo S₁ excited state proton transfer in acetic acid at room temperature. The absence of observable fluorescence from 1dbcp in acetic acid indicates that S₁ is nπ*; whereas the observation of fluorescence from 2dbcp and 3dbcp is consistent with S₁ being ππ*. All three compounds are protonated on the ground and excited states in 96 % sulfuric acid. A comparative study of calculated properties for the PM3 optimized structures of the neutral and protonated compounds has been made. Remarkably good agreement has been achieved between the experimental absorption spectra of 1dbcp-H⁺, 2dbcp-H⁺ and 3dbcp-H⁺ and INDO/S molecular orbital calculations. Photochemical studies indicate that 1dbcp-H⁺ does not undergo E → Z photoisomerization under conditions that induce photoisomerization for 1dbcp.

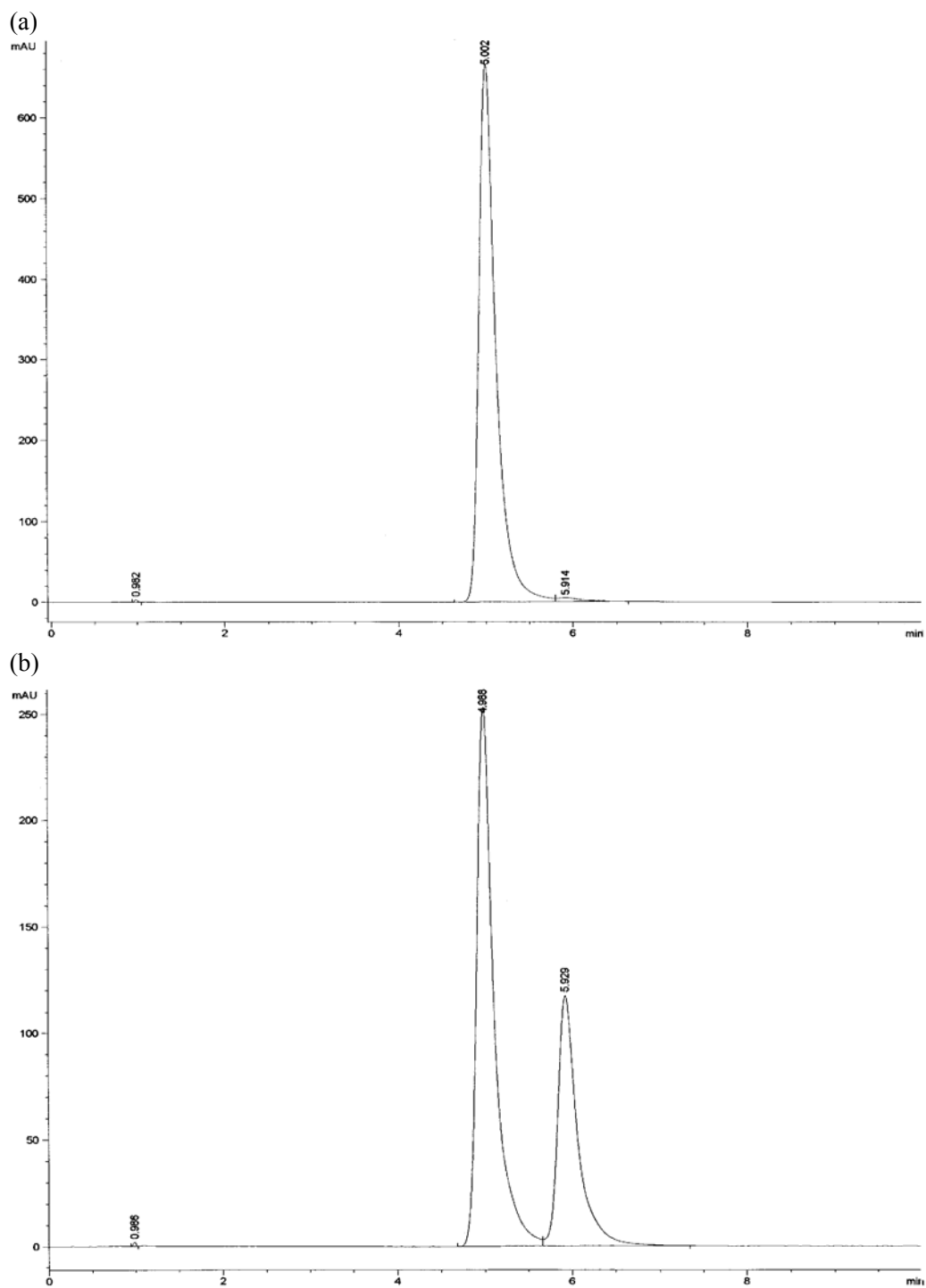


Figure 59: HPLC of 1dbcp in THF: (a) 0 and (b) 5 min irradiation.

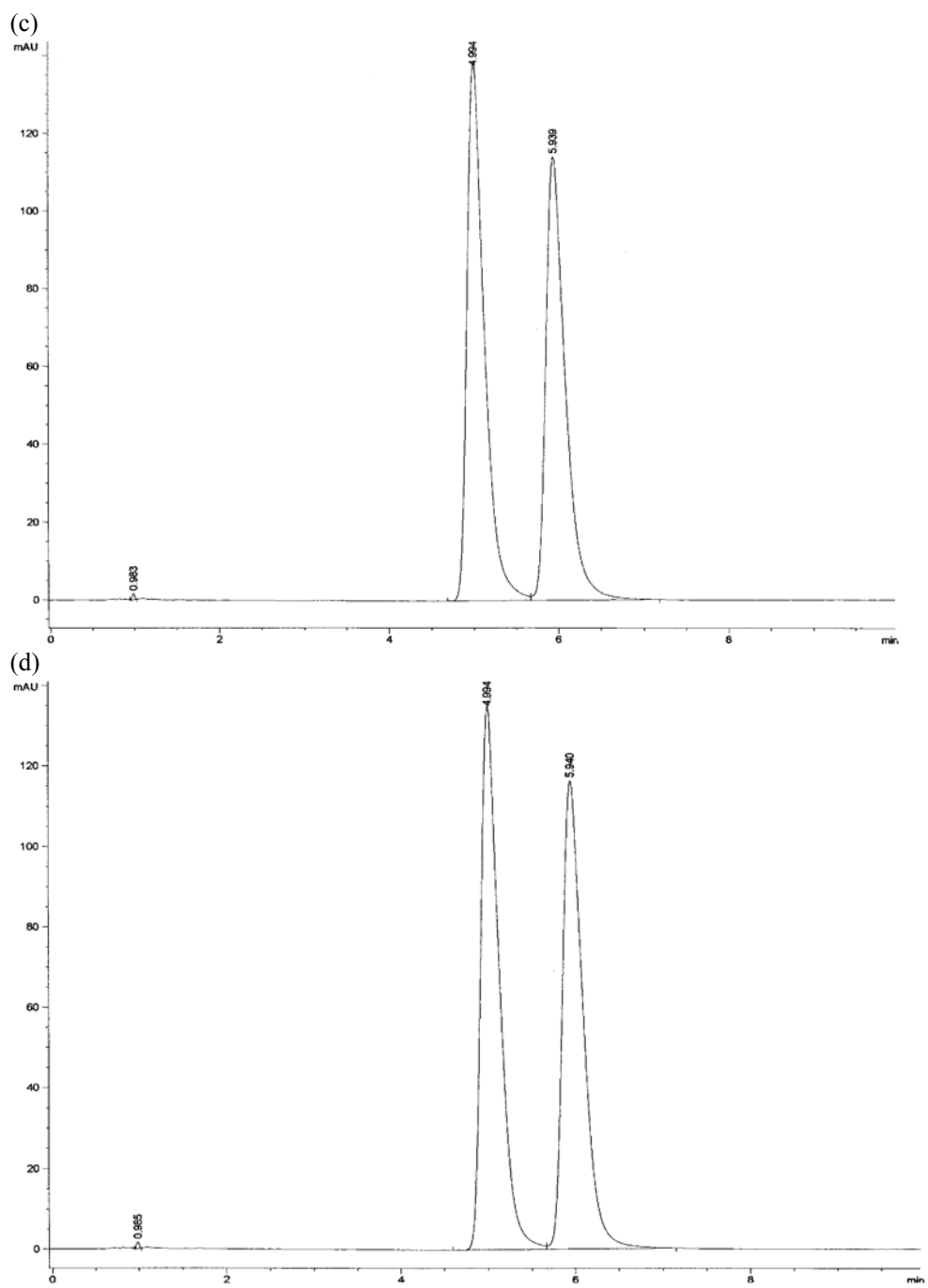


Figure 57 Cont'd. HPLC of 1dbcp in THF: (c) 45 min and (d) 1h irradiation.

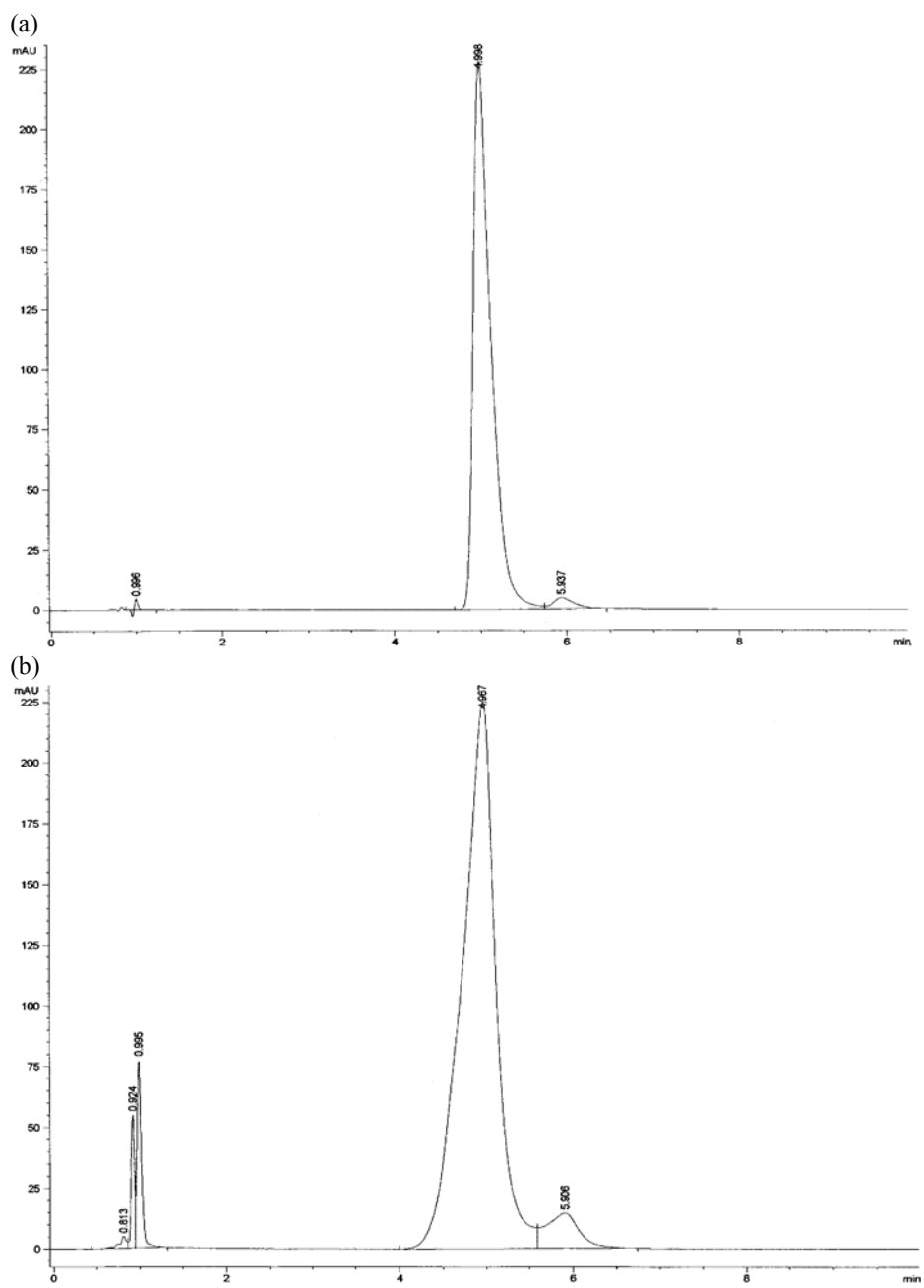


Figure 60: HPLC of 1dbcp-H⁺ in THF: (a) 0 and (b) 5 min irradiation.

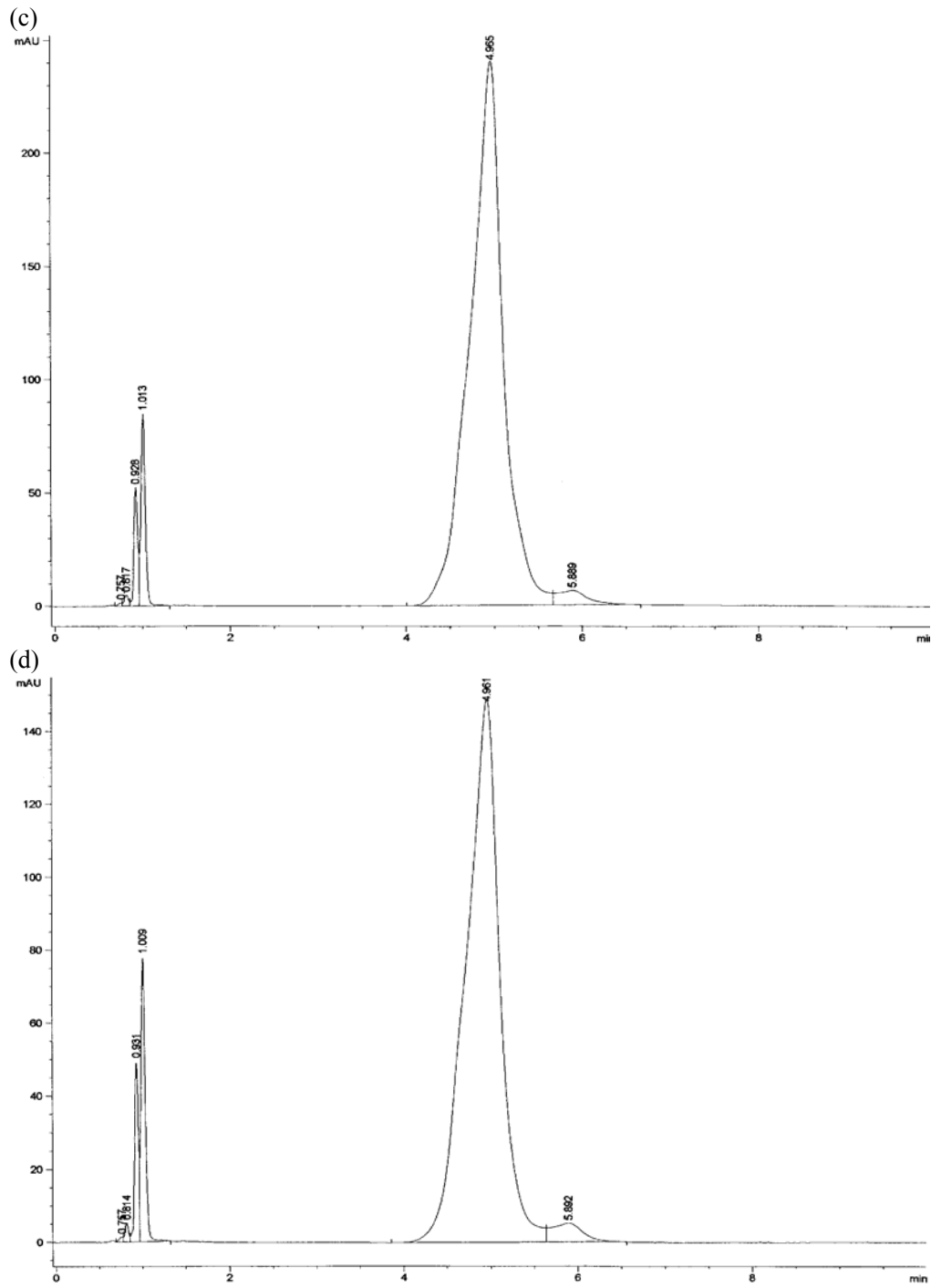


Figure 58 Cont'd. HPLC of 1dbcp-H⁺ in THF: (c) 45 min and (d) 1h irradiation.

4.3 Section 3: Absorption and Fluorescence Properties of 2,5-bis-[3-(4-dimethylamino-phenyl)-allylidene-cyclopentanone

4.3.1 Introduction

A substituted 2,5-diarylidene-cyclopentanone, namely, 2,5-bis-[3-(4-dimethylamino-phenyl)-allylidene-cyclopentanone (2dbma) has been studied briefly to understand the effects that an electron donating group bonded to each of the phenyl rings of 2dbcp has on the spectroscopic properties. This dimethyl amino substituted ketone is an example of a ketocyanine dye. Similar dyes have been shown to have useful applications in photopolymer imaging^{3,60} and in probing the polarity of the dye's environment.

4.3.2 Absorption Properties

The electronic absorption properties of this molecule show a dramatic dependence on solvent. Solutions vary in color from light yellow → orange → red → purple as the polarity of the solvent increases. The absorption spectra of 2dbma in solvents of decreasing polarity, from top to bottom, are shown in Figure 61. The solvents start with the most polar TFE, followed by methanol, n_butanol, 1,2_dichlorobenzene, acetonitrile, ether, and the least polar, cyclohexane. It is observed that, in addition to shifting to lower energy, the strong long wavelength band becomes broader with increasing solvent polarity. Some vibronic structure is observed in cyclohexane but all structure is lost in polar solvents. These solvent shifts and broadening effects are consistent with an internal charge transfer (ICT) transition, presumably from the nitrogen of the dimethylamino group (donor) to the carbonyl oxygen (acceptor).³ The wavelengths at the maximum

absorption bands vary from the least polar, cyclohexane 480 nm (Lippert polarity: ~ 0) to the most polar solvent, TFE 536 nm (Lippert polarity: 0.3159) as shown in Table 29 and Figure 61.

4.3.3 Fluorescence Properties

The absorption, fluorescence excitation, and fluorescence spectra of 2dbma in various solvents were investigated and the spectra are shown in Figure 62 - Figure 64. As with the absorption spectra, it is observed that 2dbma exhibits a significant broadening in the absorption and the fluorescence excitation spectra as the polarity of the solvent increases or with decreasing pK_a in the case of alcohols, as shown in Figure 62 (polarity and acid strength decrease from top to bottom). The order of decreasing broadening from left to right is: TFE, methanol, ethanol, 2-propanol, n-propanol, n-butanol. In the fluorescence spectra, a large shift towards the red is observed from the least polar (n-butanol), 690 nm to the most polar (TFE), 764 nm. However, such a large change is not observed for the wavelength maxima in the absorption and the excitation spectra. The difference between the wavelengths of maximum absorption for TFE and n-butanol is found to be 20 nm. In Figure 63, absorption, fluorescence excitation, and fluorescence spectra of 2dbma in various polar aprotic solvents are shown. In these solvents, the broadening observed in absorption and fluorescence excitation spectra are less pronounced and a better overlap of absorption and excitation spectra exists compared to protic solvents. In Figure 64, absorption, fluorescence excitation, and fluorescence spectra of 2dbma in various aromatic and aprotic solvents are shown. Similar to what is observed in polar protic and polar aprotic solvents, fluorescence spectra exhibited a red shift with increasing solvent polarity.

Fluorescence and fluorescence excitation spectra are measured for 2dbma in ethanol/ methanol mixture (4:1) at 77K and shown in Figure 65. In ethanol at room temperature, 2dbma exhibits broader fluorescence and fluorescence excitation spectra compared to the well-resolved vibronic structure at 77 K in ethanol/methanol. At low temperature, the fluorescence excitation spectrum is found to shift towards the red and the fluorescence spectra shift towards the blue compared to the room temperature spectra, resulting in a much smaller Stokes' shift. Small Stokes' shifts were seen previously for the 2,5-diarylidene-cyclopentanone compounds at 77K, as discussed in Section 1 and are attributed to the inability of the solvent matrix to reorient and stabilize the molecule during its excited state lifetime. The red shift of the excitation spectrum in going from a room temperature liquid to a low temperature glass for a polar molecule in a polar solvent is also frequently observed and may be related to the thermochromic shift as discussed by Suppan.³⁰

The observed red shift with increasing solvent polarity indicates an increase in the dipole moment upon excitation. A similar finding is reported for the analog with one double bond (1dbma) by Das.³ Figure 66 shows the plots of 2dbma (a) absorption and (b) fluorescence frequency along with (c) Stokes' shift against solvent orientation polarization in a number of protic and aprotic solvents. Since, 2dbma fluoresces in protic and aprotic solvents; plots are drawn for both categories of solvents. The ground state dipole moment was calculated by PM3 to be 4.3 D. Using both the Lippert method (Onsager cavity radius =6.01Å, calculated by Gaussian98) and the ratio method, excited state dipole moments were calculated to be 13.1 D (Lippert), 8.8 D (ratio) for alcohols and 10.5 D (Lippert), 9.8 (ratio) for aprotic solvents. INDO/S predicts a gas phase

excited state dipole moment of 10.1 D for this state. It is seen that Lippert, ratio, and theoretical methods yield an excited state dipole moment in the range of 9 to 13 D. Given the uncertainties inherent in these methods, e.g. Onsager cavity radius, the agreement is reasonably good.

2dbma presents somewhat similar slopes for protic and aprotic polar solvents, indicating general solvent effects. However, for nonpolar solvents, a deviation from the linear plot is observed. These behaviors indicate different excited state dipole moments, due to the presence of two different excited states, such as in nonpolar solvents weakly emissive LE state and in protic and aprotic polar solvents ICT state.²⁹ In LE state, electronic distribution may not change upon excitation. As ICT state forms complete charge transfer from amino group to carbonyl group takes place, which may even necessitate twisting of dimethylamino group to allow the nitrogen atoms to be in an easier conjugation with the phenyl ring. Therefore, part of the shift maybe due to LE and ICT/TICT states.

Absorption and fluorescence characteristics of 2dbma in various solvents along with Lippert solvent polarity functions are shown in Table 29. As seen from this Table, ϕ_f in various solvents shows considerable variation from 0.004 in TFE to 0.443 in CH_2Cl_2 . Figure 67 presents ϕ_f 's of 2dbma plotted against orientation polarization. In hydrocarbon solvents the 2dbma ϕ_f values are found to be small ($\sim 10^{-2}$). Emission in these solvents occurs at energies above $20,000 \text{ cm}^{-1}$ and the spectra are characterized by resolved vibronic structure. The low ϕ_f 's may be the result of the proximity of a nearby $n\pi^*$ state as was suggested for 3dbcp in nonpolar solvents or it may be an indication that the emitting state is described as a weakly emissive locally excited (LE) state with little

CT character. The presence of vibronic structure in the emission spectrum and the small Stokes shift is consistent with LE behavior. There is an increase in ϕ_f (0.35-0.44) in nonpolar-moderately polar solvents. In polar solvents ϕ_f is found to drop off steadily with increasing solvent polarity. This drop in ϕ_f at lower emission frequencies may be a manifestation of the energy gap law mentioned in the case of 3dbcp. However, an alternative explanation for the trend in ϕ_f may be found in the work of Rettig and co workers⁶¹ who also find a maximum in the ϕ_f vs. solvent polarity plot for the structurally similar amino substituted chalcones. Without going into the details, they have explained this behavior in terms of a somewhat complex equilibrium between twisted excited states (TICT) and planar excited states. TICT is a special excited state where, the plane of the dimethyl amino group is at an angle with the rest of the molecule.⁶² Due to twisted dimethyl amino group, conjugation is lost and total charge is separated between the dimethyl amino group and aromatic ring. TICT state can not be directly observed by absorption of light, since its geometry is not planar as is the case for the ground state. Briefly, TICT state forms from the S_1 state due to slow twisting of the two parts of the molecule, where polarity of solvent plays a very important role in stabilizing the dipolar TICT state in such a way to make it below the S_1 state.

A more complete explanation of the ϕ_f results found for 2dbma awaits further computational and experimental work.

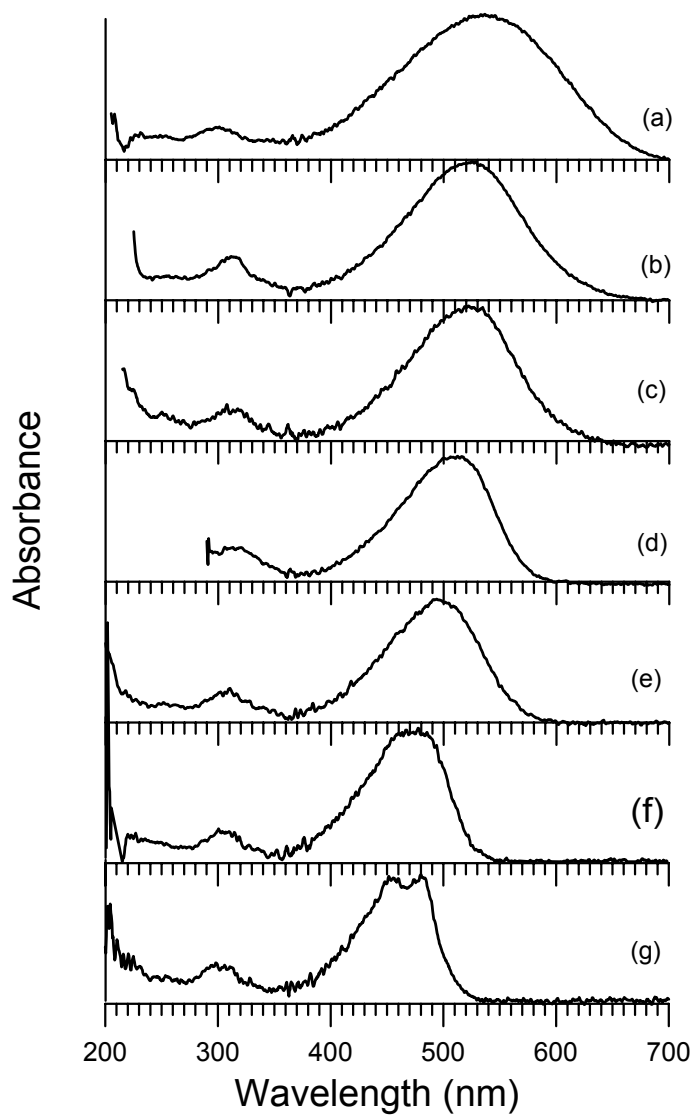


Figure 61: Absorption spectra of 2dbma in various solvents: (a) 2,2,2_trifluoroethanol; (b) methanol; (c) n_butanol; (d) 1,2_dichlorobenzene; (e) acetonitrile; (f) ether; (g) cyclohexane.

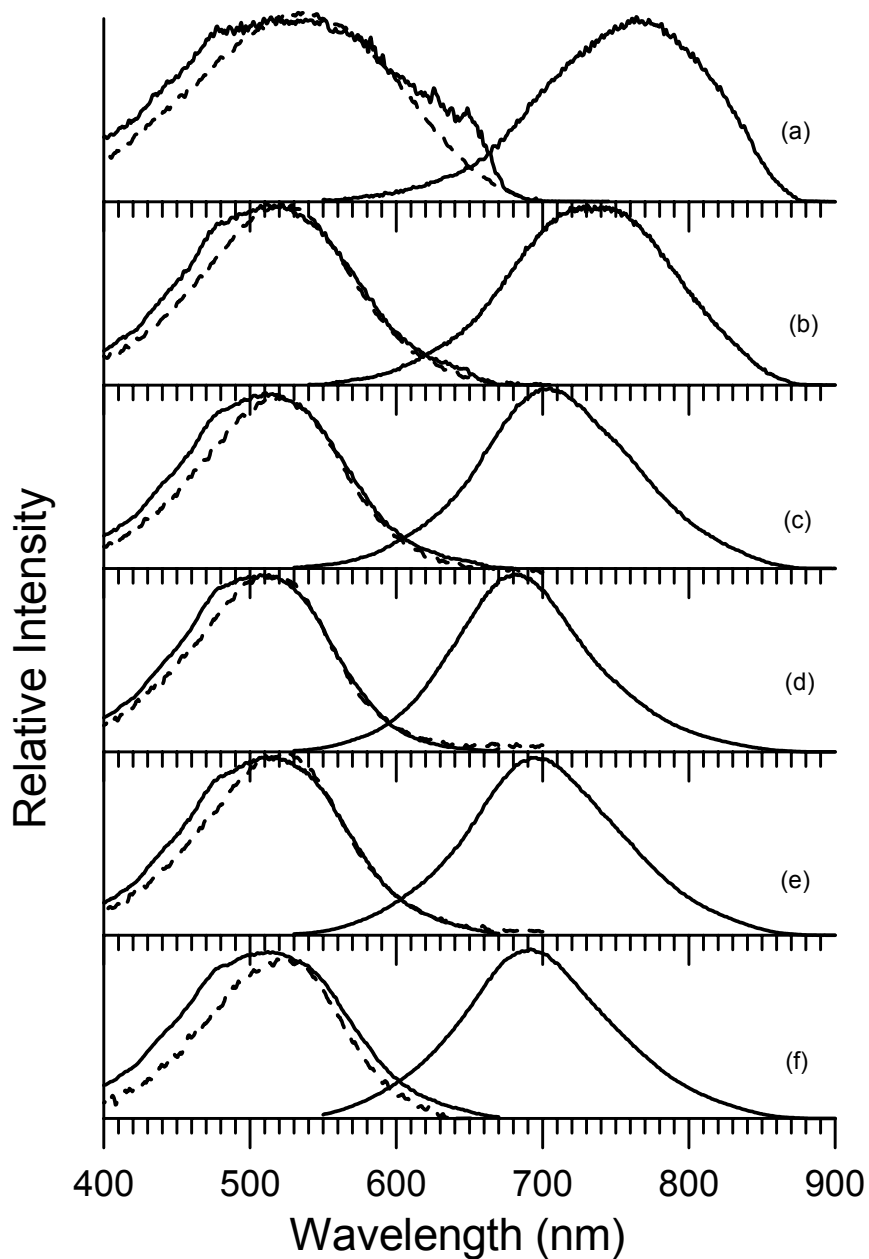


Figure 62: Absorption (dashed line), fluorescence, and fluorescence excitation spectra (solid lines) of 2dbma in alcohols: (a) 2,2,2-trifluoroethanol ($\lambda_{\text{Ex max}}$: 535 nm); (b) methanol ($\lambda_{\text{Ex max}}$: 525 nm); (c) ethanol ($\lambda_{\text{Ex max}}$: 510 nm); (d) isopropanol ($\lambda_{\text{Ex max}}$: 510 nm); (e) n-propanol ($\lambda_{\text{Ex max}}$: 515 nm); (f) n-butanol ($\lambda_{\text{Ex max}}$: 515 nm).

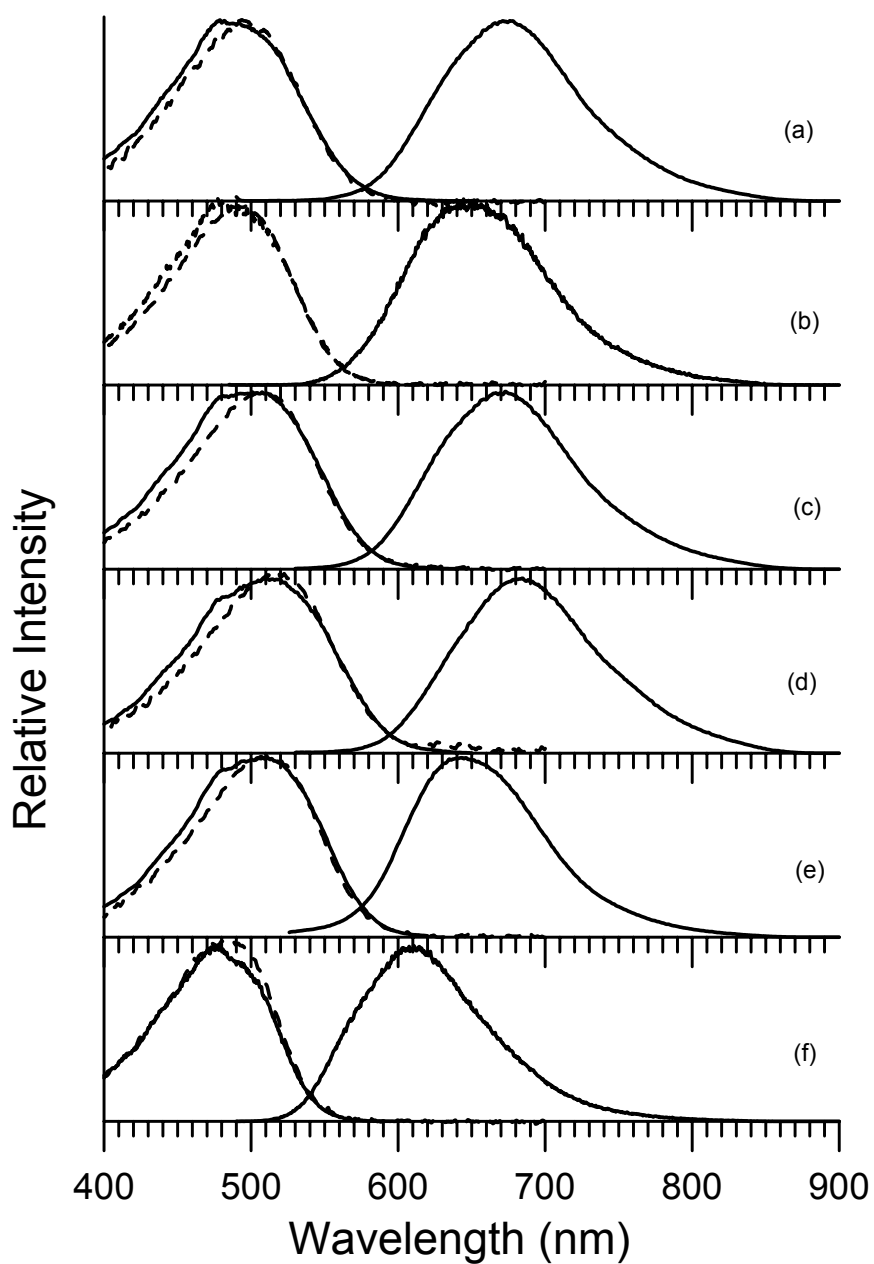


Figure 63: Absorption (dashed line), fluorescence, and fluorescence excitation spectra (solid lines) of 2dbma in solvents I: (a) acetonitrile ($\lambda_{\text{Ex max}}$: 478 nm); (b) acetone ($\lambda_{\text{Ex max}}$: 475 nm); (c) n,n_dimethylformamide ($\lambda_{\text{Ex max}}$: 507 nm); (d) dimethyl sulfoxide ($\lambda_{\text{Ex max}}$: 515 nm); (e) pyridine ($\lambda_{\text{Ex max}}$: 506 nm); (f) ethyl acetate ($\lambda_{\text{Ex max}}$: 480 nm).

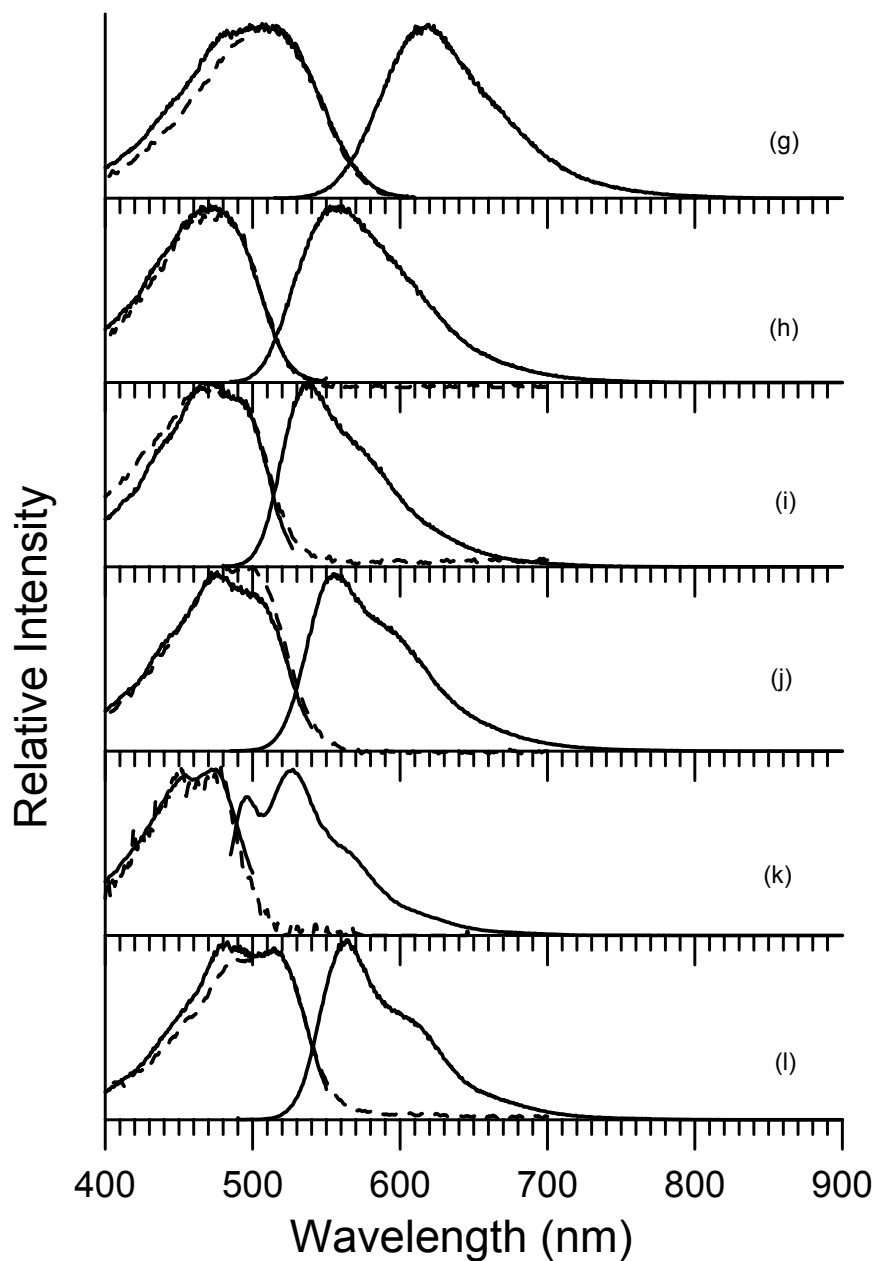


Figure 64: Absorption (dashed line), fluorescence, and fluorescence excitation spectra (solid lines) of 2dbma in solvents II: (g) 1,2_dichlorobenzene ($\lambda_{\text{Ex max}}$: 505 nm); (h) ether ($\lambda_{\text{Ex max}}$: 475 nm); (i) carbon tetrachloride ($\lambda_{\text{Ex max}}$: 470 nm); (j) benzene ($\lambda_{\text{Ex max}}$: 474 nm); (k) hexane ($\lambda_{\text{Ex max}}$: 480 nm); (l) carbon disulfide ($\lambda_{\text{Ex max}}$: 480 nm).

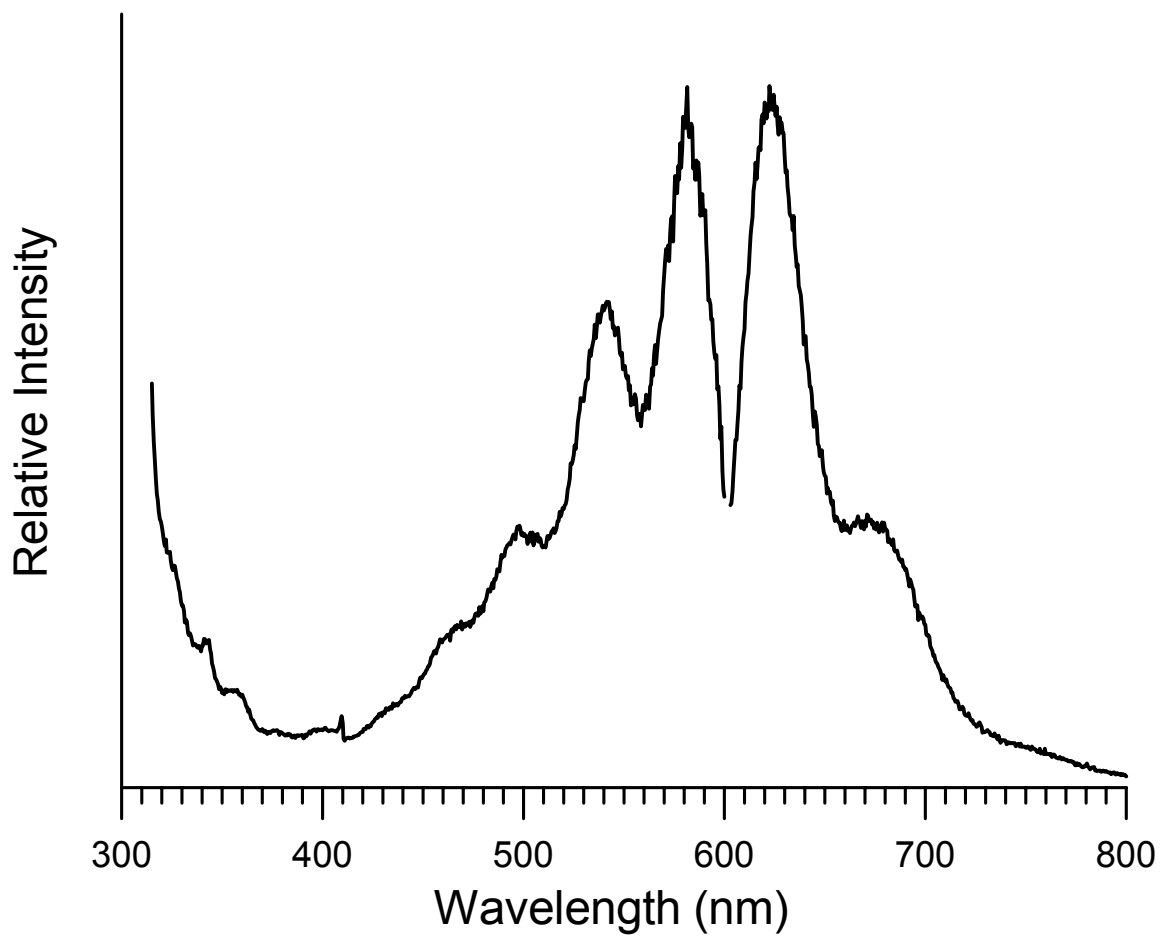


Figure 65: Fluorescence and fluorescence excitation spectra of 2dbma in ethanol/methanol (4:1) ($\lambda_{\text{Ex max}}$: 580 nm) at 77K.

Table 29 2dbma Absorption and Fluorescence Characteristics in Various Solvents and Solvent Polarity Functions.

Solvents	ν_{flu} (cm^{-1})	ν_{abs} (cm^{-1})	$\Delta\nu_{(\text{abs-flu})}$ (cm^{-1})	* $\Delta f_{\text{Lippert}}$	Quantum Yield
TFE	13089 (764 nm)	18657 (536 nm)	5568	0.3159	0.004
Methanol	13605 (735 nm)	19048 (525 nm)	5442	0.3093	0.016
ACN	14837 (674 nm)	20408 (490 nm)	5571	0.3054	0.065
Ethanol	14184 (705 nm)	19608 (510 nm)	5423	0.2887	0.061
Acetone	15504 (645 nm)	20367 (491 nm)	4863	0.2843	0.215
2_Propanol	14684 (681 nm)	19417 (515 nm)	4733	0.2769	0.134
N,N_Dimethylformamide	14859 (673 nm)	19724 (507 nm)	4865	0.2752	0.155
n_Propanol	14388 (695 nm)	19417 (515 nm)	5029	0.2746	0.093
n_Butanol	14493 (690 nm)	19417 (515 nm)	4925	0.2642	0.147
DMSO	14620 (684 nm)	19417 (515 nm)	4798	0.2637	0.116
CH ₂ Cl ₂	15748 (635 nm)	19920 (502 nm)	4172	0.2171	0.443
Pyridine	15552 (643 nm)	19763 (506 nm)	4211	0.2124	0.362
Ethyl Acetate	16287 (614 nm)	20833 (480 nm)	4547	0.1996	0.330
1,2_DiClBenzene	16129 (620 nm)	19802 (505 nm)	3673	0.1867	0.394
Ether	17857 (560 nm)	21053 (475 nm)	3195	0.1669	0.247
CHCl ₃	15552 (643 nm)	20000 (500 nm)	4448	0.1491	0.329
Toluene	18182 (550 nm)	20202 (495 nm)	2020	0.0131	0.390
CCl ₄	18622 (537 nm)	21505 (465 nm)	2883	0.0119	0.229

Table 29 Con't. 2dbma Absorption and Fluorescence Characteristics in Various Solvents and Solvent Polarity Functions.

Solvents	ν_{flu} (cm^{-1})	ν_{abs} (cm^{-1})	$\Delta\nu_{(\text{abs-flu})}$ (cm^{-1})	* $\Delta f_{\text{Lippert}}$	Quantum Yield
Benzene	18018 (555 nm)	21053 (475 nm)	3035	0.0031	0.378
Heptane	20121 (497 nm)	21053 (475 nm)	932	0.0007	0.042
Hexane	20161 (496 nm)	20921 (478 nm)	759	-0.0004	0.038
Cyclohexane	20000 (500 nm)	20833 (480 nm)	833	-0.0004	0.064
CS ₂	17699 (565 nm)	20833 (480 nm)	3134	-0.0007	0.415

*⁵⁶ Solvent polarity constants used for polarity function calculations are taken from Suppan, P. and

Ghoneim, N., in Solvatochromism, The Royal Society of Chemistry, Cambridge, 1997.

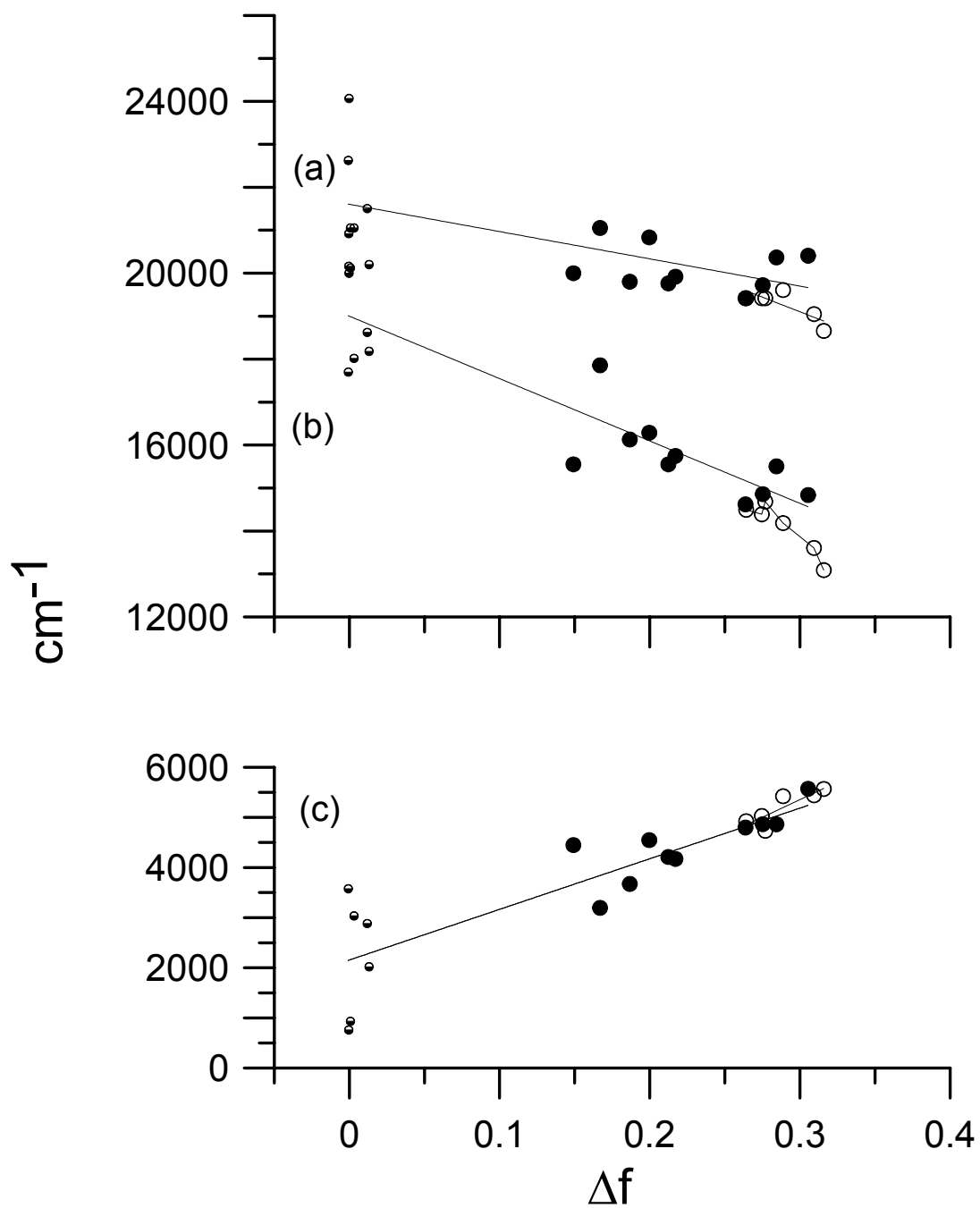


Figure 66: 2dbma plot of (a) absorption frequency, (b) fluorescence frequency, (c) Stokes' shift against solvent orientation polarization. Open symbols for protic solvents, solid symbols for aprotic polar solvents, and semi-filled symbols for nonpolar solvents.

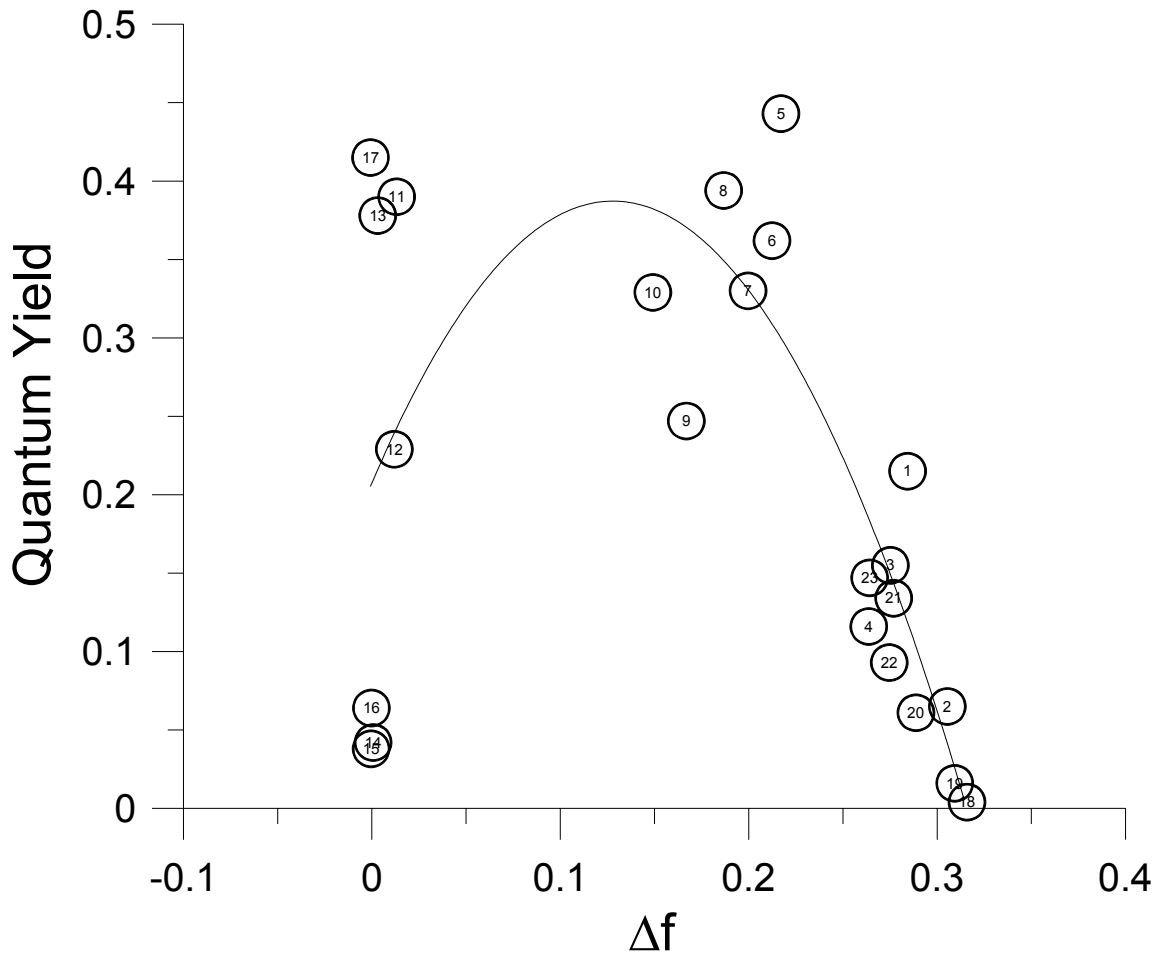


Figure 67: Fluorescence quantum yield of 2dbma plotted against orientation polarization.

The solvents used are shown by the numbers: 1) Acetone, 2) ACN, 3)

N,N_dimethylformamide, 4) DMSO, 5) CH₂Cl₂, 6) pyridine, 7) ethyl acetate, 8)

1,2_dichloro benzene, 9) ether, 10) CHCl₃, 11) toluene, 12) CCl₄, 13) benzene, 14)

heptane, 15) hexane, 16) cyclohexane, 17) CS₂, 18) TFE, 19) MeOH, 20) EtOH, 21)

isopropanol, 22) n_propanol, 23) n_butanol

4.3.4 Summary

The effects of an electron donating group substituted on the phenyl rings of a diarylidene-cyclopentanone have been investigated. The absorption bands of dimethylamino substituted diarylidene-cyclopentanone have been assigned to an internal charge transfer (ICT) from the nitrogen of the dimethylamino group to the carbonyl oxygen. This compound has found to display fluorescence in protic, polar aprotic, nonpolar, and aromatic solvents.

The spectral shifts observed with increasing solvent polarity indicate an increase in the dipole moment of 2dbma upon excitation. The Lippert and ratio methods yield an excited state dipole moment in the range 9-13 D when combined with the PM3 calculated ground state dipole moment of 4.3 D.

Quantum yields in various solvents show variation from 0.004 in TFE to 0.443 in CH_2Cl_2 . A detailed explanation for the trend found in ϕ_f is a subject for future investigation.

5 SUMMARY AND RECOMMENDATIONS FOR FUTURE WORK

5.1 Summary

1) Electronic absorption and fluorescence spectra have been measured for the all E configurations of 2,5-dibenzylidene-cyclopentanone (1dbcp), 2,5-bis-(3-phenylallylidene)-cyclopentanone (2dbcp), and 2,5-bis-(5-phenyl-penta-2,4-dienylidene)-cyclopentanone (3dbcp). The absorption spectra have been assigned with the aid of INDO/S calculations. Agreement between absorption spectra obtained in cyclohexane at room temperature and the theoretical predictions is good. For 1dbcp, 2dbcp, and 3dbcp the general features of the spectra are similar. The transition to S_1 (weak) is assigned as $n \rightarrow \pi^*$ ($A_2 \leftarrow A_1$), to S_2 (strong) as $\pi \rightarrow \pi^*$ ($B_2 \leftarrow A_1$), and to S_3 (moderate) as $\pi \rightarrow \pi^*$ ($A_1 \leftarrow A_1$). The energy gap between S_1 and S_2 is seen to decrease as the length of the polyene chain increases in going from 1dbcp to 3dbcp.

2) Fluorescence has not been observed for 1dbcp in any of the solvents studied (protic and aprotic). Fluorescence has been observed for 2dbcp in protic solvents only. For 3dbcp, fluorescence has been observed in a number of protic and aprotic solvents. Environments that are able to induce fluorescence are believed to do so by inverting the order of $^1(n\pi^*)$ and $^1(\pi\pi^*)$ states.

3) Solvent induced shifts in the absorption and fluorescence spectra of 3dbcp in combination with the PM3 calculated ground state dipole moment (2.8 D) have been used to determine the excited state dipole moment of 3dbcp (6.4 D/protic solvents; 6.6 D/aprotic solvents).

4) Fluorescence quantum yields have been found to vary with the frequency of emission for 3dbcp, going through a maximum in the mid-frequency range. The variation in

quantum yields with frequency is attributed primarily to changes in the nonradiative rate of decay from S_1 .

5) No fluorescence has been observed for 1dbcp in acetic acid, where, it is believed that S_1 is $n\pi^*$. Fluorescence has been observed for 2dbcp and 3dbcp in acetic acid where, it is believed that S_1 is $\pi\pi^*$.

6) Fluorescence spectra of 2dbcp and 3dbcp show two bands, one due to emission of unprotonated (at the shorter wavelength) and the other to protonated (at the longer wavelength) molecules. The experimental data indicate that protonation takes place on the excited state surface.

7) A concentration study of 2dbcp in acetic acid was conducted to investigate the possibility of aggregation or excimer formation that may result in the observed spectral features. In the fluorescence spectra, no intensity reduction has been observed in the long wavelength band relative to the short wavelength band, indicating that the observed features are not related to concentration dependent phenomena.

8) Isotope studies have been conducted to enlighten the equilibrium considerations of unprotonated and protonated 2dbcp and 3dbcp in acetic and deuterated acetic acid. Similar spectra of 2dbcp and 3dbcp have been observed in both solvents. 2dbcp exhibited behavior consistent with a kinetic isotope decrease in the rate of excited state proton transfer prior to emission.

9) Protonated cations exhibit excellent agreement between INDO/S calculations and experimental absorption spectra. The calculations reveal that the transition to S_1 corresponds to HOMO \rightarrow LUMO excitation for all three protonated compounds and is $\pi\pi^*$ in nature.

10) Photochemistry studies indicate that under similar experimental conditions $E \rightarrow Z$ photoisomerization does not occur for 1dbcp-H^+ , whereas it does occur for 1dbcp .

11) The long wavelength absorption band of 2dbma has been assigned to an internal charge transfer (ICT) transition from the nitrogen of the dimethylamino group to the carbonyl oxygen. The excited state dipole moment has been determined to be 9-13 D, based on a combination of experimental and theoretical data. Fluorescence quantum yields are found to vary considerably with changes in solvent.

5.2 Recommendation for Future Research

Future studies on the electronic structure and spectroscopic properties of diarylidene-cycloalkanones and their protonated cations should benefit from the experiences acquired in this study. A discussion on the recommendations for future research is presented in the following sections.

5.2.1 Experimental Investigations of Lifetimes

As previously presented in Section 4.2, 3dbcp was found to fluoresce in a number of aprotic and protic solvents. Using the Strickler and Berg method radiative rates were calculated for 3dbcp only in methanol and CCl_4 . This limited number of data show a drastic drop in the order of magnitude in ϕ_f for 3dbcp in these solvents where emission occurs above $19,000\text{ cm}^{-1}$ due to a higher k_{nr} in this region, which is a contradictory situation to energy gap law. This contradiction may be arising due to enhancement in the rate of intersystem crossing and enhancement of the rate of internal conversion.

Therefore, using single photon counting technique emission lifetimes of 3dbcp should be determined in a number of solvents to understand the extent to which of these pathways

contributes to k_{nr} when S_1 of 3dbcp is above $19,000 \text{ cm}^{-1}$. In the next paragraph the principles of time correlated single photon counting is summarized.

Photons are counted in a time-correlated relation to the excitation pulse using the laser flash photolysis system shown in Figure 68.^{29,63} Employing laser as a pulse light source, sample is repetitively excited and each pulse is optically monitored by a photomultiplier. By this way, a start signal, is produced to trigger the voltage ramp, of time-to-amplitude converter (TAC) is initiated. The TAC can be considered as a stopwatch and provides an output pulse that indicates voltage, which is proportional to the start and stop signals (at the detection time of the first photon). Using a multichannel analyzer (MCA) this voltage is converted to a time channel by an analog to digital converter. MCA build up a probability histogram of counts vs. time channels by summing over the pulses. The intensity of the decay of the sample is found from the histogram of photon arrival times.

In the experimental stage, samples will be prepared for TCSPC analysis by dissolving the 3dbcp in a number of solvents. The concentration of sample should be such that its absorbance will be around 0.6 at the laser excitation wavelength. Placing the sample in a quartz cell, its absorbance will be measured with a Shimadzu UV2100 UV-visible. The solution should be degassed by N_2 bubbling and capped with a rubber septum and a parafilm wrapped around it.

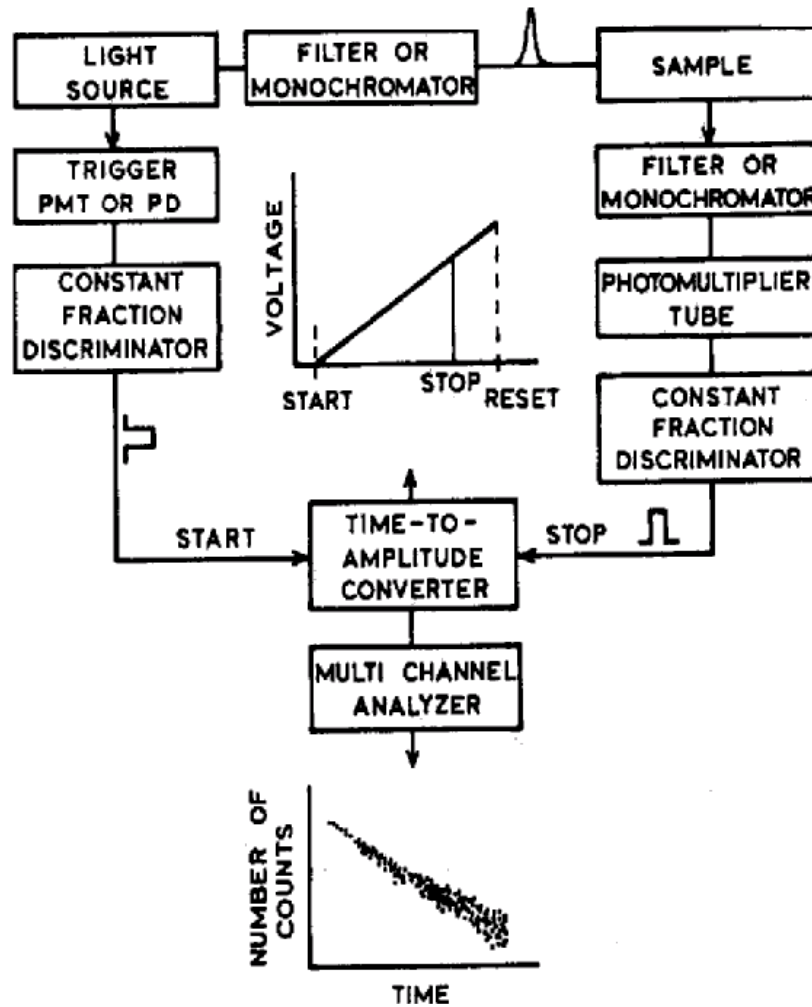


Figure 68: Schematic for time-correlated single photon counting.²⁹

5.2.2 Photochemistry Study

1dbcp-H⁺ photochemistry studies indicated no photoisomerization and indication of cleavage (breaking down) of the molecule at higher energies. However, in 1dbcp photochemistry study, a photoisomer was formed with no cleavage of the product. The cleavage products from 1dbcp-H⁺ and the photoisomer observed from 1dbcp needs to be further analyzed. For this purpose, preparative HPLC can be used to collect the products and NMR spectroscopy to characterize them.

5.2.3 Optimized Geometry of 2dbma

Determining the optimized geometry of 2dbma was not within the scope of this thesis. However, it would be beneficial to investigate the effects of the electron donor and electron acceptor groups on the bond length, bond order, and bond angle of 2dbma, which may be directly compared to the calculated 2dbcp structure properties for a better understanding of electron delocalization. To achieve this objective PM3 method and MOPAC 2000 should be used.

REFERENCES

- (1) Barnabus, M. V.; Liu, A.; Trifunac, A. D.; Krongauz, V. V.; and Chang, C. T. *J. Phys. Chem.* **1992**, *96*, 212.
- (2) Pivovarenko, V. G.; Klueva, A. V.; Doroshenko, A. O.; and Demchenko, A. P. *Chem. Phys. Lett.* **2000**, *325*, 389.
- (3) Das, P. K.; Pramanik, R.; Banerjee, D.; and Bagchi, S. *Spectrochim. Acta A* **2000**, *56*, 2763.
- (4) Doroshenko, A. O.; Grigorovich, A. V.; Posokhov, E. A.; Pivovarenko, V. G.; and Demchenko, A. P. *Mol. Eng.* **1999**, *8*, 199.
- (5) Kawamata, J.; Inoue, K.; and Inabe, T. *Bull. Chem. Soc. Jpn.* **1998**, *71*, 2777.
- (6) Kawamata, J.; Inoue, K.; Inabe, T.; M., K.; Kato, M.; and Taniguchi, Y. *Chem. Phys. Lett.* **1996**, *249*, 29.
- (7) Theocharis, C. R.; Alison, M. C.; Hopkin, S. E.; Jones, P.; Perryman, A. C.; and Usanga, F. *Mol. Cryst. Liq. Cryst. Inc. Nonlin. Opt.* **1998**, *156*, 85.
- (8) Frey, H.; Behmann, G.; and Kaupp, G. *Chem. Ber.* **1987**, *120*, 387.
- (9) Theocharis, C. R.; Jones, W.; Thomas, J. M.; Montevalli, M.; and Hursthouse, B. *J. Chem. Soc. Perkin Trans. II* **1984**, *71*.
- (10) Theocharis, C. R.; Thomas, J. M.; and Jones, W. *Mol. Cryst. Liq. Cryst. Inc. Nonlin. Opt.* **1983**, *93*, 53.
- (11) Brannon, J. H.; Magde, D. *J. Phys. Chem. A* **1978**, *82*, 705.
- (12) Fujitsu. MOPAC2000, 1999; Vol. 1.0.
- (13) Sanford, E. M.; Paulisse, K. W.; and Reeves, J. T. *J. Appl. Polym. Sci.* **1999**, *74*, 2255.
- (14) Issa, R. M.; Etaiw, S. H.; Issa, I. M.; and El-Shafie, A. K. *Acta Chim. Acad. Sci. Hung., Tomus* **1976**, *89*, 381.
- (15) Farrel, P. G.; Read, B. A. *Can. J. Chem.* **1968**, *46*, 3685.
- (16) Hudson, B. S.; Kohler, B. E.; and Shulten, K. In *Excited States*; Lim, E. C., Ed.; Academic Press: New York, 1982; Vol. 6; pp 1.
- (17) Christensen, R. L. The Photochemistry of Carotenoids. In *Advances in Photosynthesis*; Frank H. A.; Young, A. J. B., G.; Cogdell, R. J, Ed.; Kluwer Academic Publishers: Dordrecht, The Netherlands, 1999; Vol. 8; pp 137.
- (18) Levine, I. N. *Quantum chemistry*, 4th ed.; Prentice Hall: Englewood Cliffs, N.J., 1991.
- (19) Turro, N., J. *Modern Molecular Photochemistry*; University Science Books: Sausalito, California, 1991.
- (20) Marcotte, N.; Ferry-Forgues, S. *J. Chem. Soc., Perkin Trans. 2* **2000**, 1711.
- (21) Marcotte, N., Ferry-Forgues, S. *J. Photochem. Photobiol. A Chemistry* **2000**, *130*, 133
- (22) Reichardt, R. *Chem. Rev.* **1994**, *94*, 2319.
- (23) Marcotte, N.; Ferry-Forgues, S.; and Lavabre, D. *J. Phys. Chem. A* **1999**, *103*, 3163
- (24) Das, P. K.; Becker, R. S. *J. Phys. Chem.* **1978**, *82*, 2081.
- (25) Das, P. K.; Becker, R. S. *J. Phys. Chem.* **1978**, *82*, 2093.

- (26) Petek, H.; Bell, A. J.; Christensen, R. L.; Yoshihara, K. *J. Chem. Phys.* **1992**, *96*, 2412.
- (27) Papanikolas, J.; Walker, G. C.; Shamamian, V. A.; Christensen, R. L.; and Baum, J. C. *J. Am. Chem. Soc.* **1990**, *112*, 1912.
- (28) Baltrop, J.; Coyle, J. D. *Principles of Photochemistry*; Wiley & Sons, Inc: New York, 1978.
- (29) Lakowicz, J. R. *Principles of fluorescence spectroscopy*, 2nd ed.; Kluwer Academic/Plenum: New York, 1999.
- (30) Suppan, P. *J. Photochem. Photobiol. A* **1990**, *50*, 293.
- (31) Pierola, I. F.; Turro, J. N.; and Kuo, P. K. *Macromolecules* **1985**, *18*, 508.
- (32) Sharma, A. S., G. S. *Introduction to Fluorescence Spectroscopy*; Wiley-Interscience Publication: Canada, 1999.
- (33) Iranpoor, N.; Kazemi, F. *Tetrahedron* **1998**, *54*, 9475.
- (34) Olomuchi; Gall, L. *J. Bull. Soc. Chim. France (Chim. Mol)* **1976**, 1467.
- (35) Maeta, H.; Suzuki, K. *Tetrahedron Lett.* **1993**, *34*, 341.
- (36) Desiraju, G. R.; Kishan, K. V. R. *Indian J. Chem.* **1988**, *27B*, 953.
- (37) Chynwat, V. An investigation of the electronic structure, spectroscopy, and photochemistry of aromatic butatrienes, Worcester Polytechnic Institute, 1992.
- (38) Rechthaler, K.; Kohler, G. *Chem. Phys. Lett.* **1994**, *189*, 99.
- (39) El-Sayed, M. A. *J. Chem. Phys.* **1963**, *38*, 2834.
- (40) Jaffe', H. H.; Orchin, M. *Theory and Applications of Ultraviolet Spectroscopy*; John Wiley & Sons, Inc.: New York, 1962.
- (41) Brealey, G. J.; Kasha, M. *J. Am. Chem. Soc.* **1955**, *77*, 4462.
- (42) Klessinger, M.; Michl, J. *Excited States and Photochemistry of Organic Molecules*; VCH Publishers, Inc.: New York, 1995.
- (43) Takemura, T.; Das, P. K.; Hug, G.; Becker, R. S. *J. Am. Chem. Soc.* **1976**, *98*, 7099.
- (44) Fletcher, A. N. *J. Phys. Chem.* **1972**, *76*, 2562.
- (45) Kuhn, L. P. *J. Am. Chem. Soc.* **1952**, *74*, 2492.
- (46) Suppan, P. *Chem. Phys. Lett.* **1983**, *94*, 272.
- (47) Lippert, E. Z. *Electrochem.* **1957**, *61*, 962.
- (48) Mataga, N.; Kaifu, Y.; and Koizumi, M. *Bull. Chem. Soc. Jpn.* **1956**, *29*, 465.
- (49) Strickler, S. J.; Berg, R. A. *J. Chem. Phys.* **1962**, *37*, 814.
- (50) Connors, R. E.; Ucak-Astarlioglu, M. G. *A limited supply of 3 prevents us from obtaining the extinction coefficients in a wide variety of solvents.*
- (51) Siebrand, W. J. *J. Chem. Phys.* **1967**, *46*, 2411.
- (52) Lim, E. C.; Yu, J. M. H. *J. Chem. Phys.* **1967**, *47*, 3270.
- (53) Lim, E. C.; Yu, J. M. H. *J. Chem. Phys.* **1966**, *45*, 4742.
- (54) Lim, E. C. *J. Phys. Chem.* **1986**, *90*, 6770.
- (55) Madej, S. L.; Okajima, S.; Lim, E. C. *J. Chem. Phys.* **1976**, *65*, 1219.
- (56) Suppan, P.; Ghoneim, N. *Solvatochromism*; Royal Society of Chemistry: Cambridge, 1997.
- (57) Moomaw, W. R.; Anton, M. F. *J. Phys. Chem.* **1976**, *80*, 2243.
- (58) Orlandi, G.; Zerbetto, F.; and Zgierski, M. Z. *Chem. Rev.* **1991**, *91*, 867.
- (59) George, H.; Roth, R. J. *Tetrahedron Letters* **1971**, *43*, 4057.

(60) Chang, B. T.-L. Photopolymerizable Compositions Containing cis-a-dicarbonyl Compounds and Selected Sensitizers. In *Wilmington, Delaware*; E. I. du Pont de Nemours and Company: Claymont, Delaware, 1973.

(61) Rurack, K.; Dekhtyar, M. L.; Bricks, J. L.; Resch-Genger, U.; and Rettig, W. *J. Phys. Chem.A* **1999**, *103*, 9626

(62) Suppan, P. *Chemistry and Light*; The Royal Society of Chemistry: Cambridge, 1994.

(63) Wang, Z.; Weininger, S. J.; and McGimpsey, W. G. *J. of Phys. Chem.* **1993**, *97*, 374.

APPENDIX

APPENDIX A

¹H_NMR AND ¹³C_NMR SPECTRA OF COMPOUNDS

Figure A 1 1dbcp

Figure A 2 2dbcp

Figure A 3 3dbcp

Figure A 4 1dbch

Figure A 5 2dbch

Figure A 6 1dbcp_u

Figure A 7 2dbma

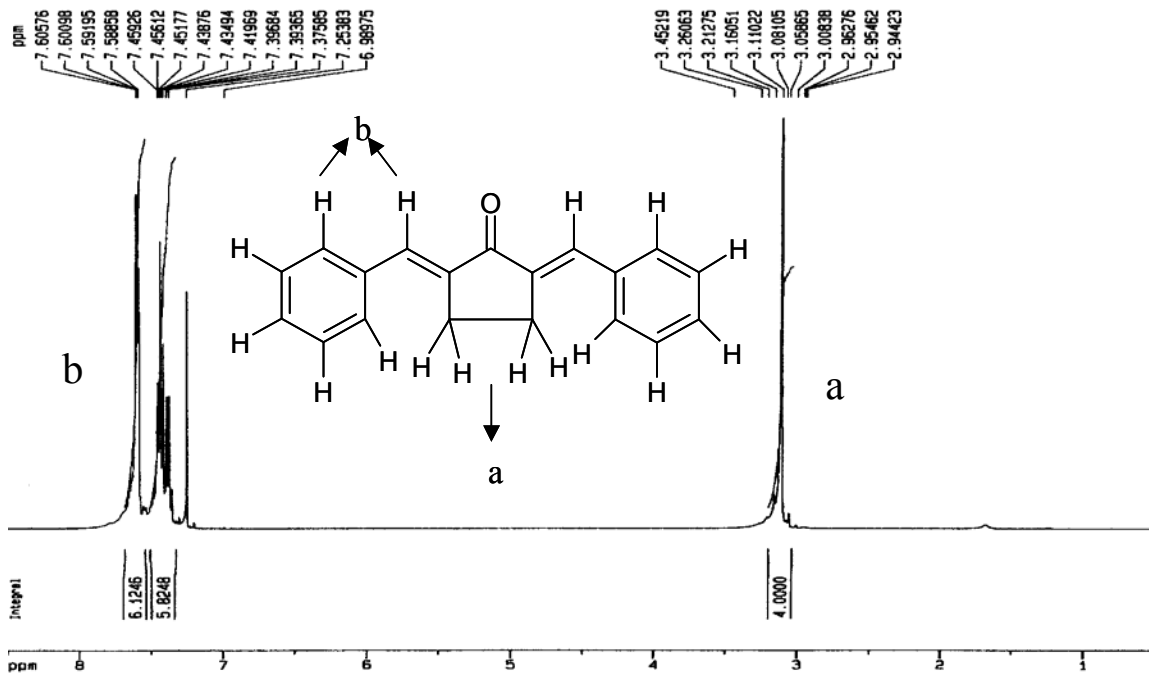


Figure A-1. a) ¹H NMR 1dbcp

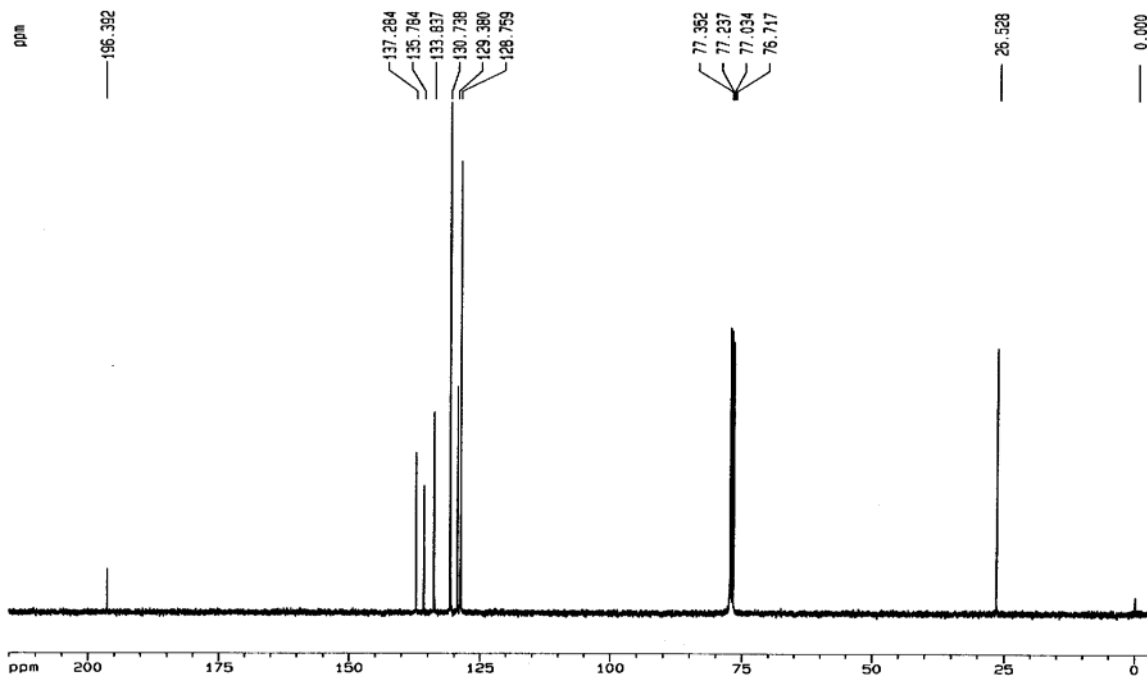


Figure A-1. b) ¹³C NMR 1dbcp

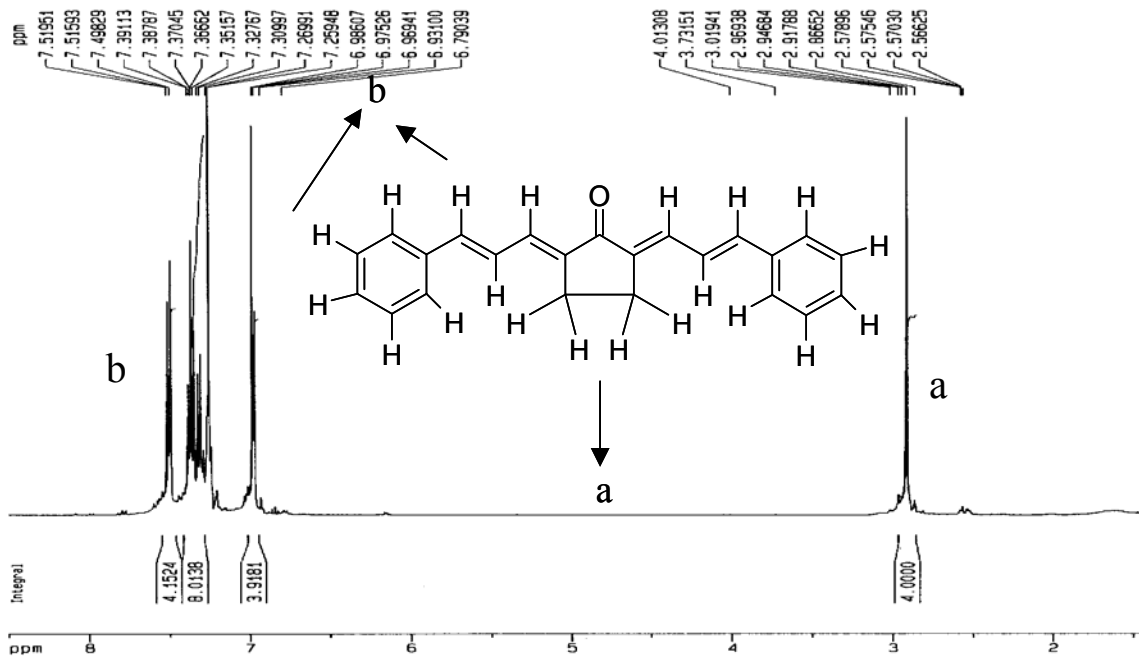


Figure A-2. a) ^1H NMR 2dbcpc

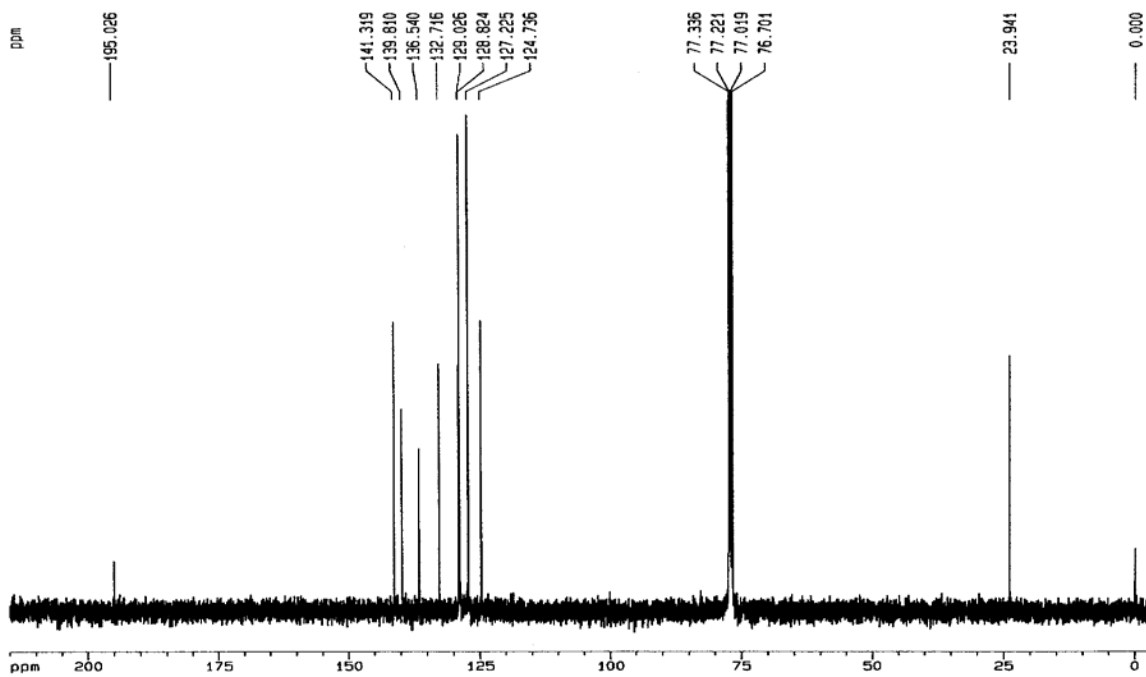


Figure A-2. b) ^{13}C NMR 2dbcpc

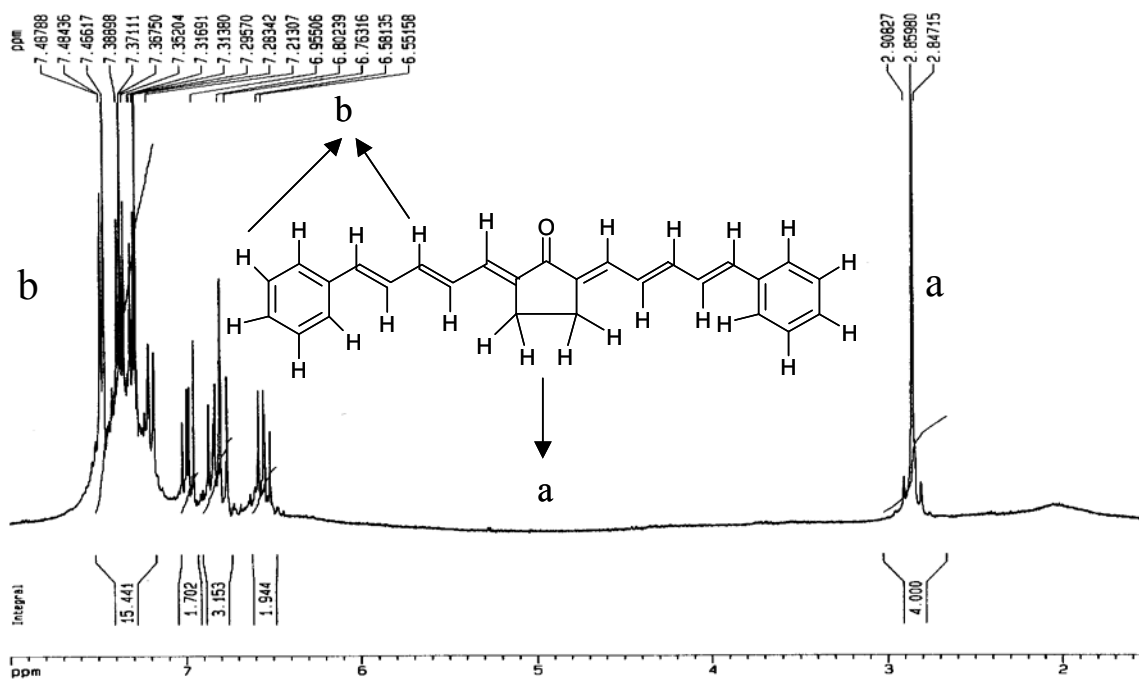


Figure A-3. a) ^1H -NMR 3dbcp

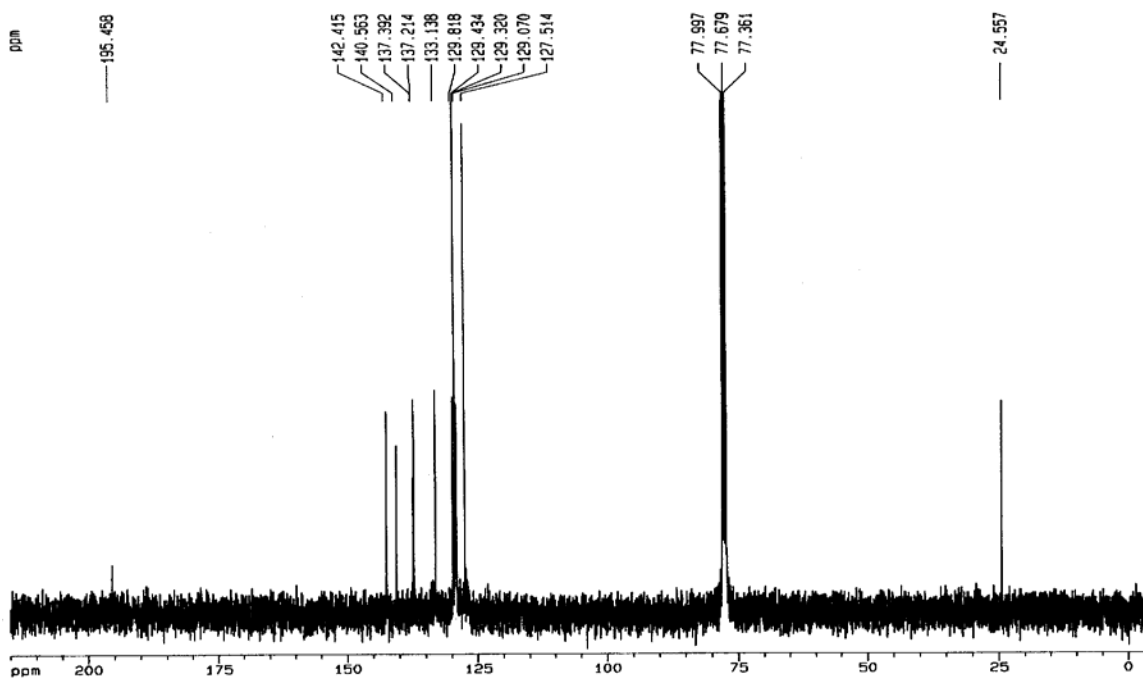


Figure A-3. b) ^{13}C -NMR 3dbcp

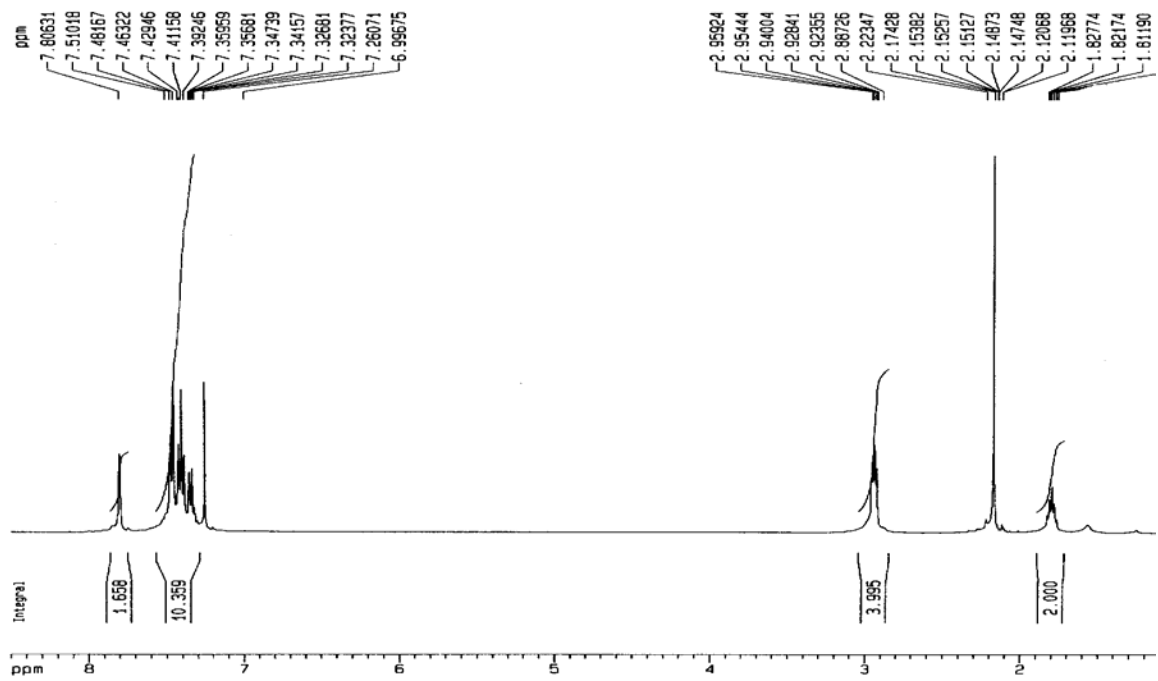


Figure A-4. a) ¹H_NMR 1dbch

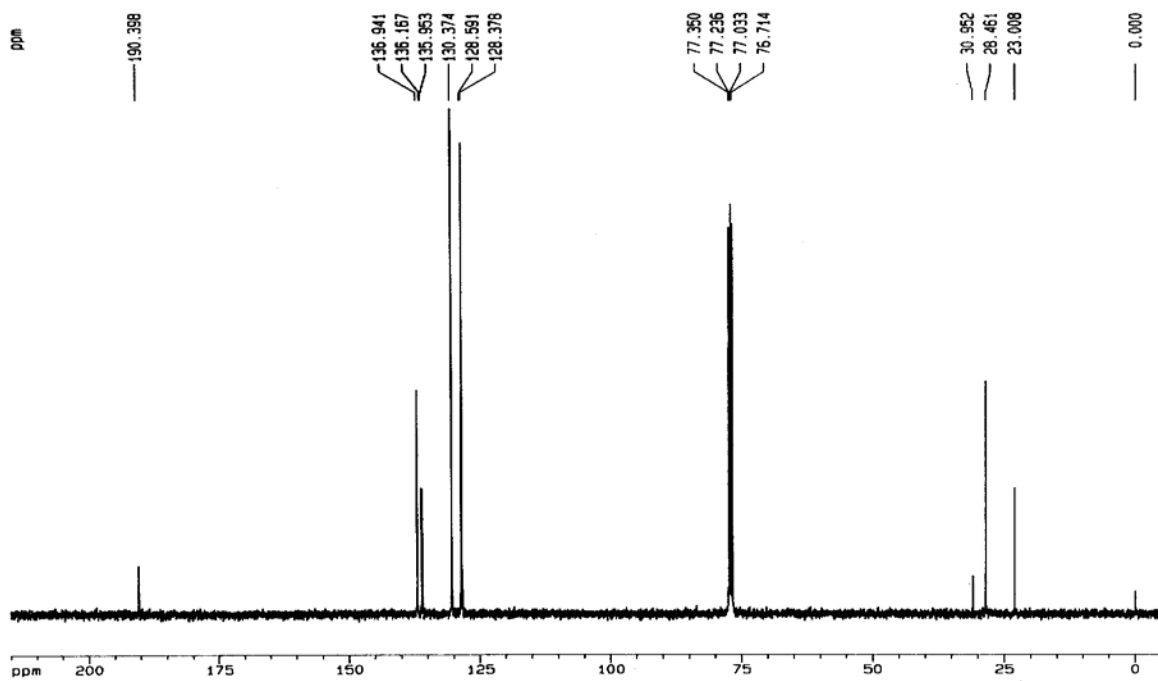


Figure A-4. b) ¹³C_NMR 1dbch

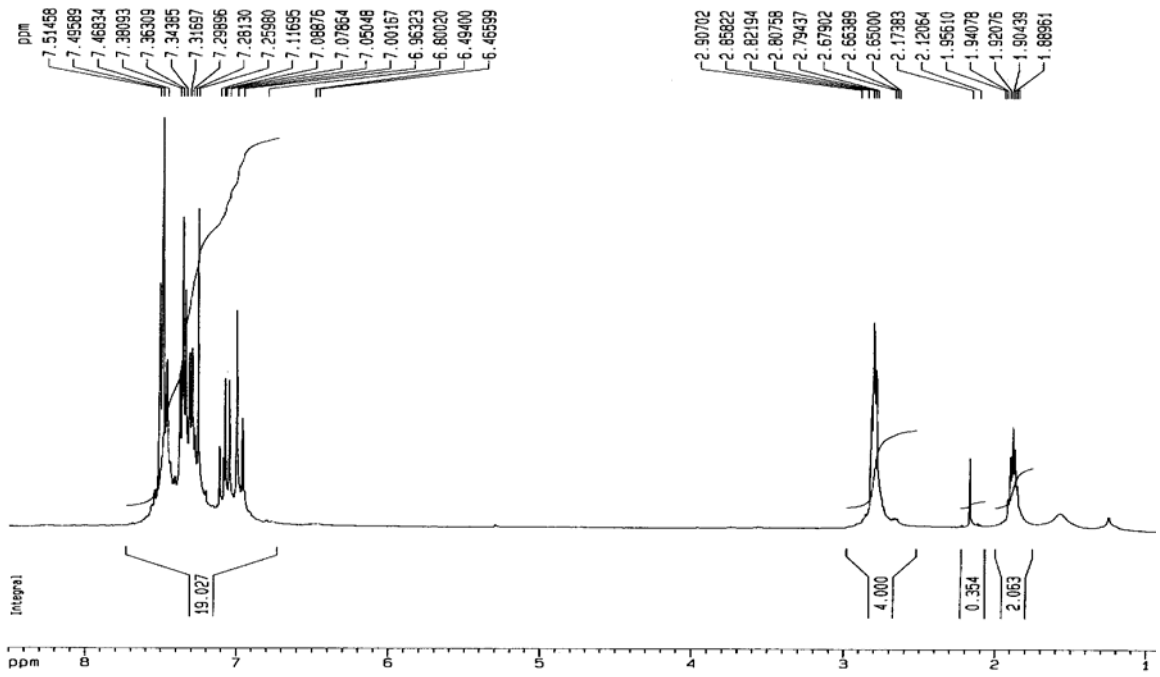


Figure A-5. a) 1H_NMR 2dbch

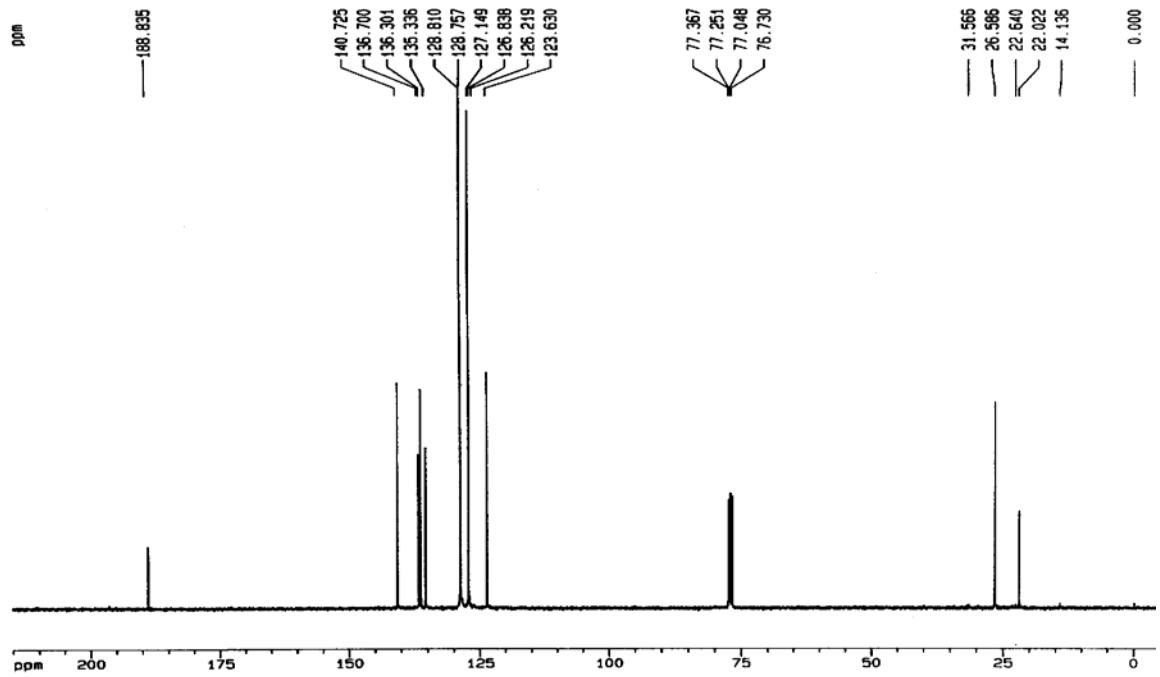


Figure A-5. b) 13C_NMR 2dbch

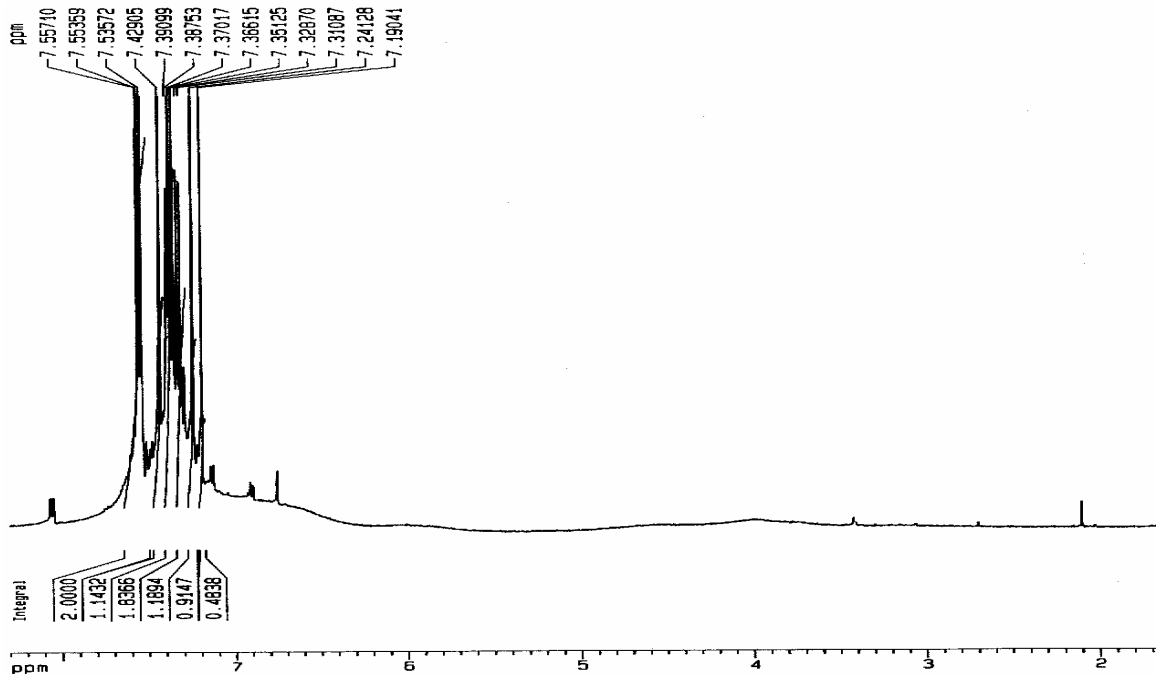


Figure A-6. a) 1H_NMR 1dbcp_u

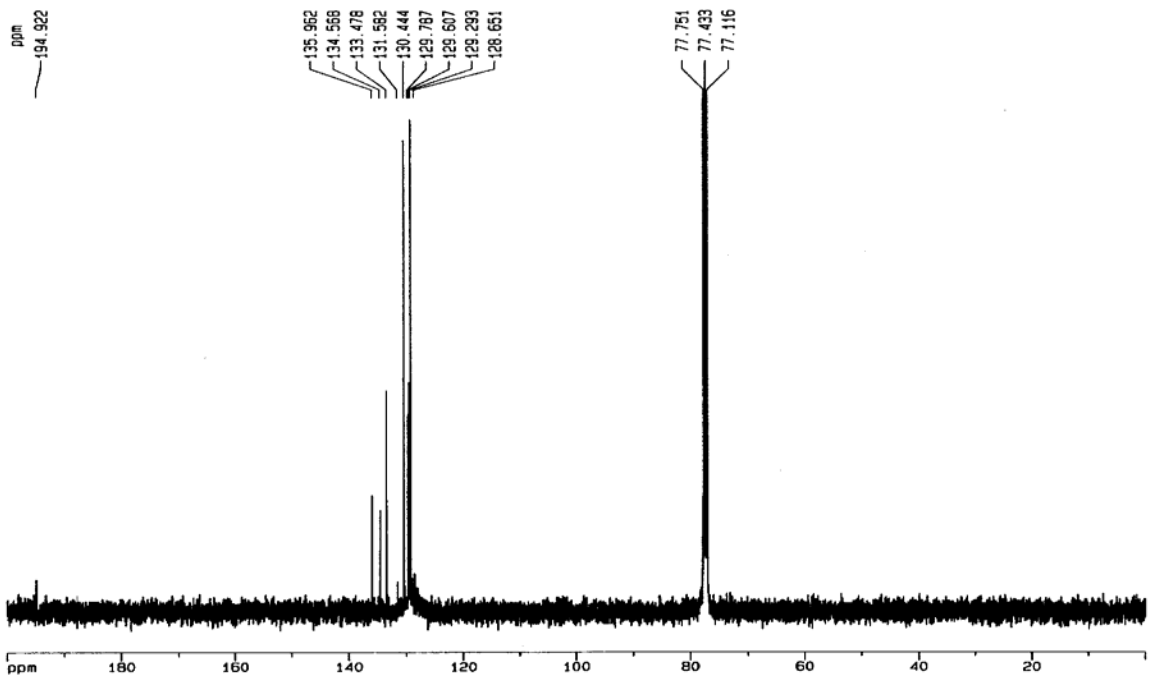


Figure A-6. b) 13C_NMR 1dbcp_u

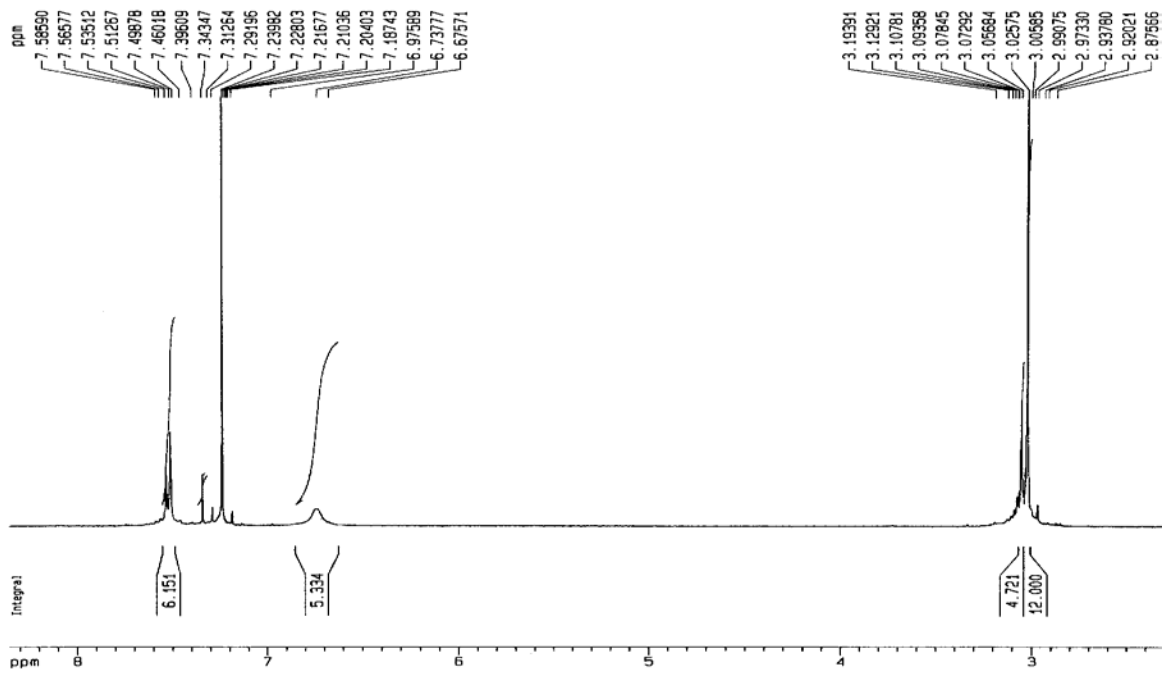


Figure A-7. a) 1H_NMR 2dbma

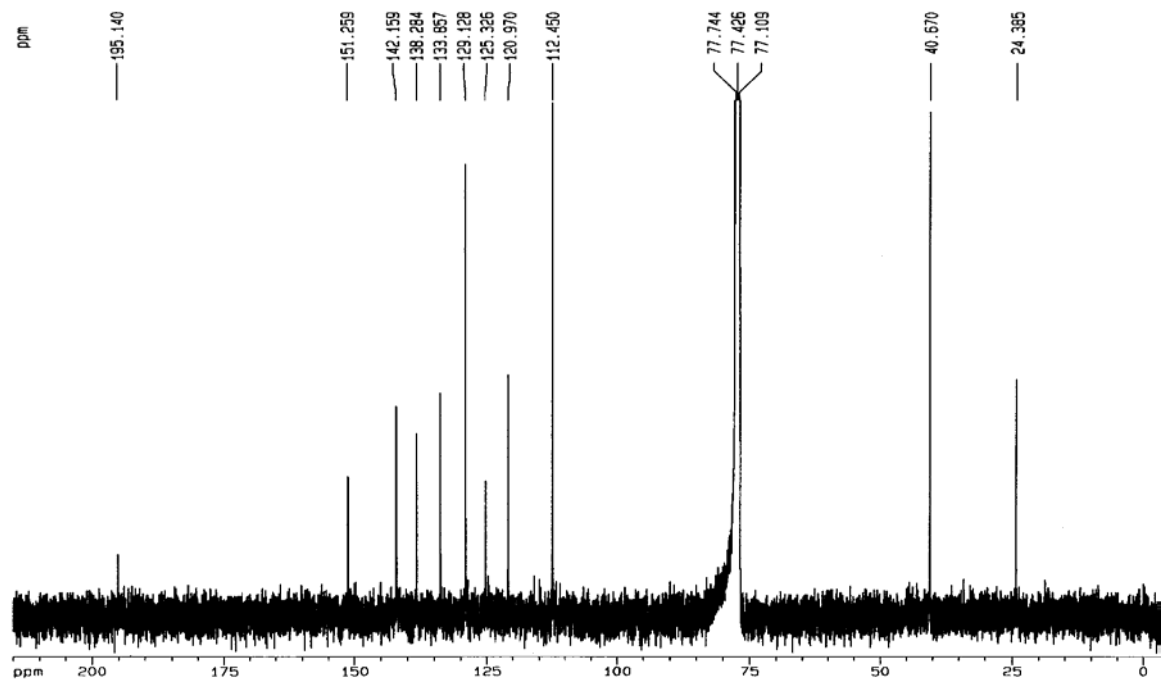


Figure A-7. b) 13C_NMR 2dbma

APPENDIX B

IR SPECTRA OF NEUTRAL COMPOUNDS

Figure B 1 1dbcp

Figure B 2 2dbcp

Figure B 3 3dbcp

Figure B 4 1dbch

Figure B 5 2dbch

Figure B 6 1dbcp_u

Figure B 7 2dbma

IR SPECTRA OF NEUTRALIZED PROTONATED CATIONS

Figure B 8 1dbcp of neutralized protonated cation

Figure B 9 2dbcp of neutralized protonated cation

Figure B 10 3dbcp of neutralized protonated cation

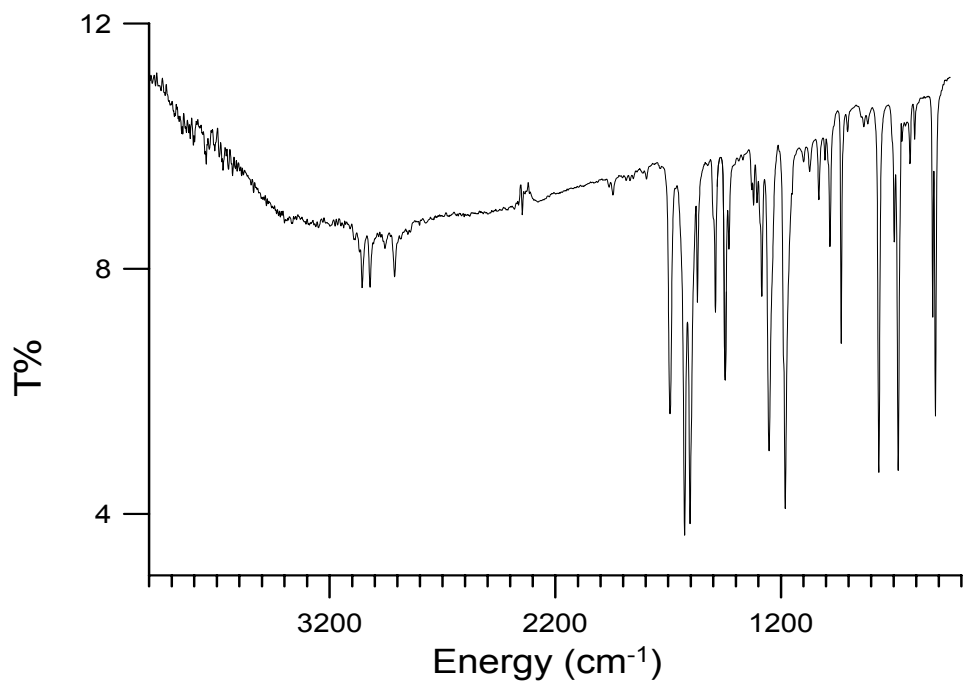


Figure B-1. 1dbcp

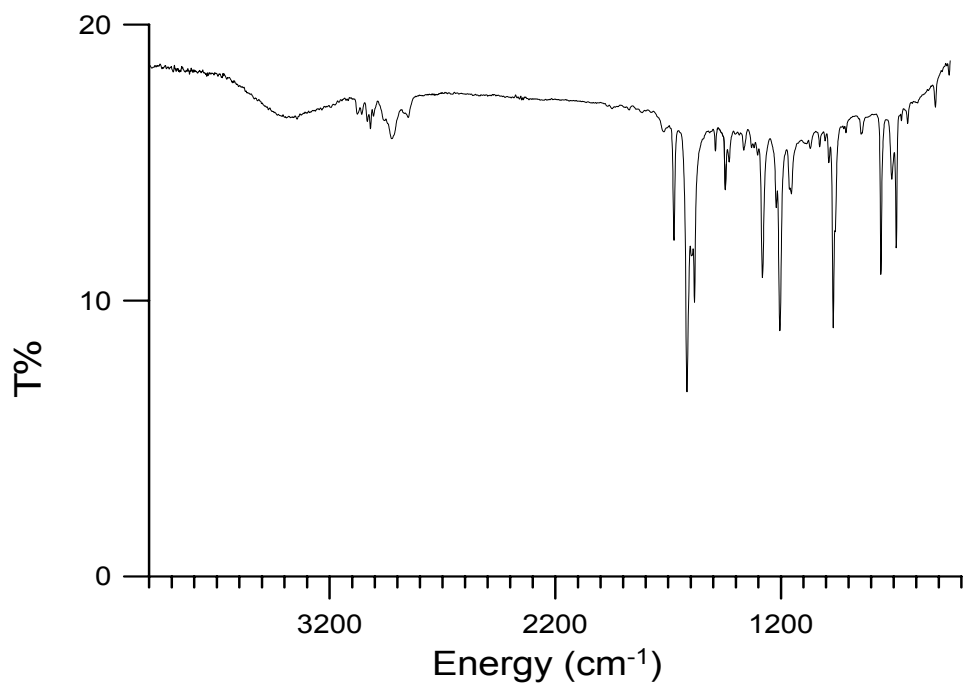


Figure B-2. 2dbcp

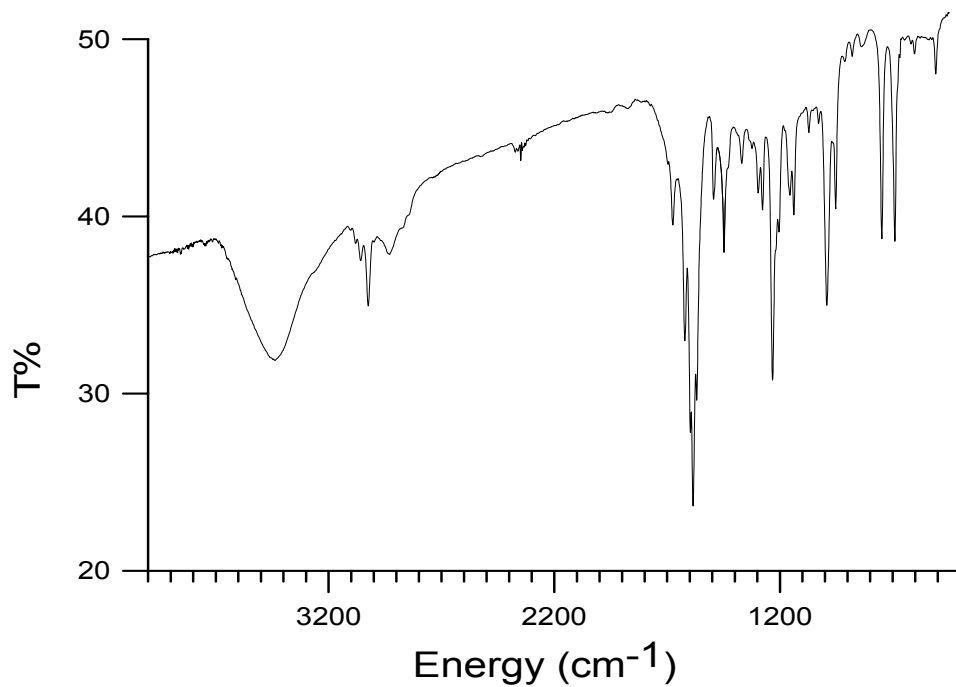


Figure B-3. 3dbcp

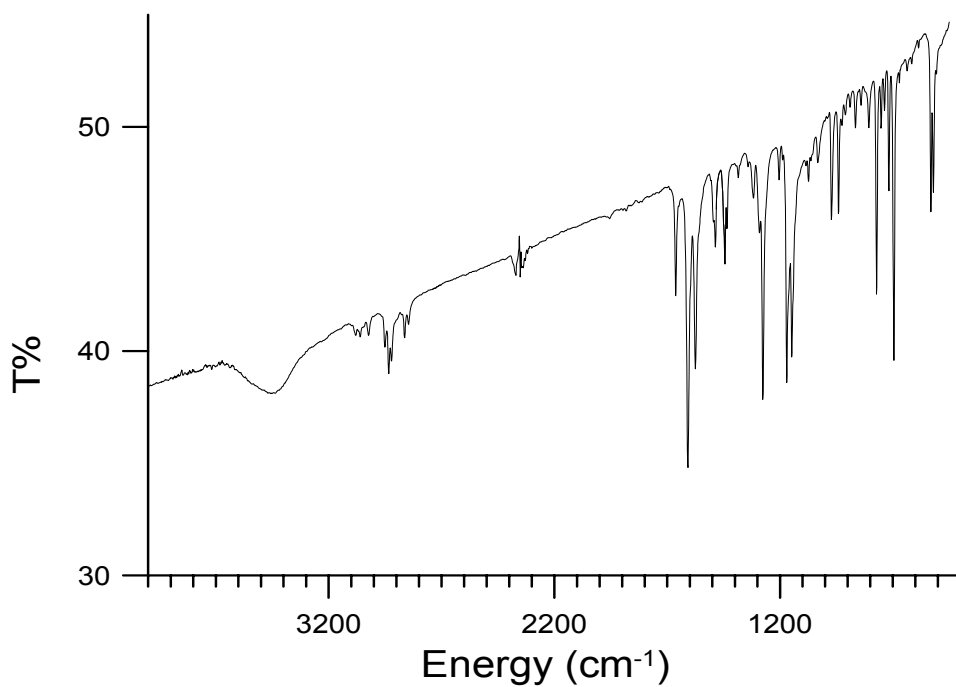


Figure B-4. 1dbch

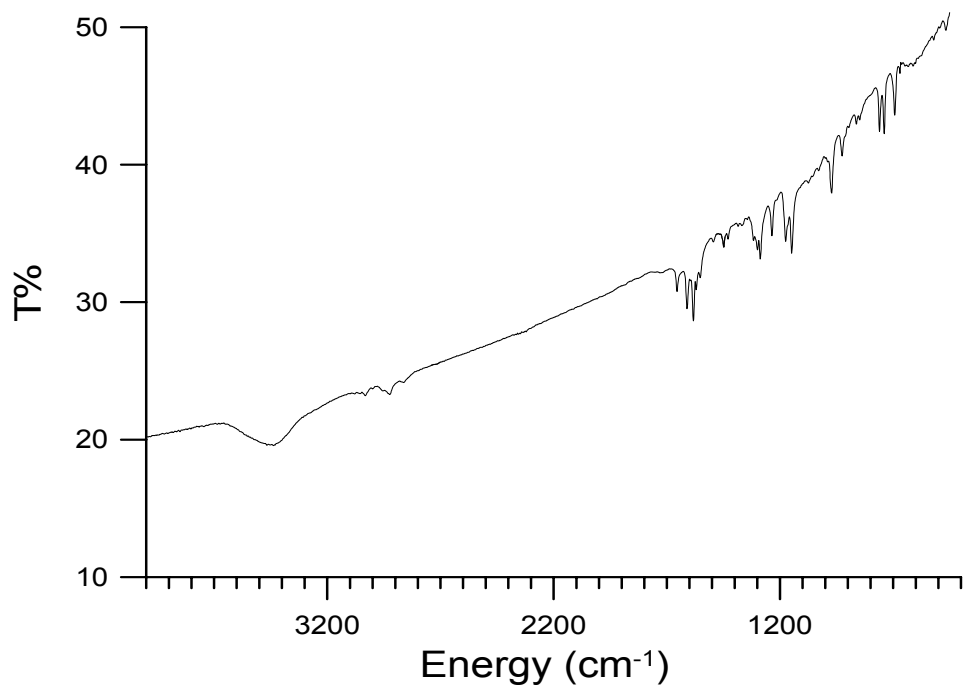


Figure B-5. 2dbch

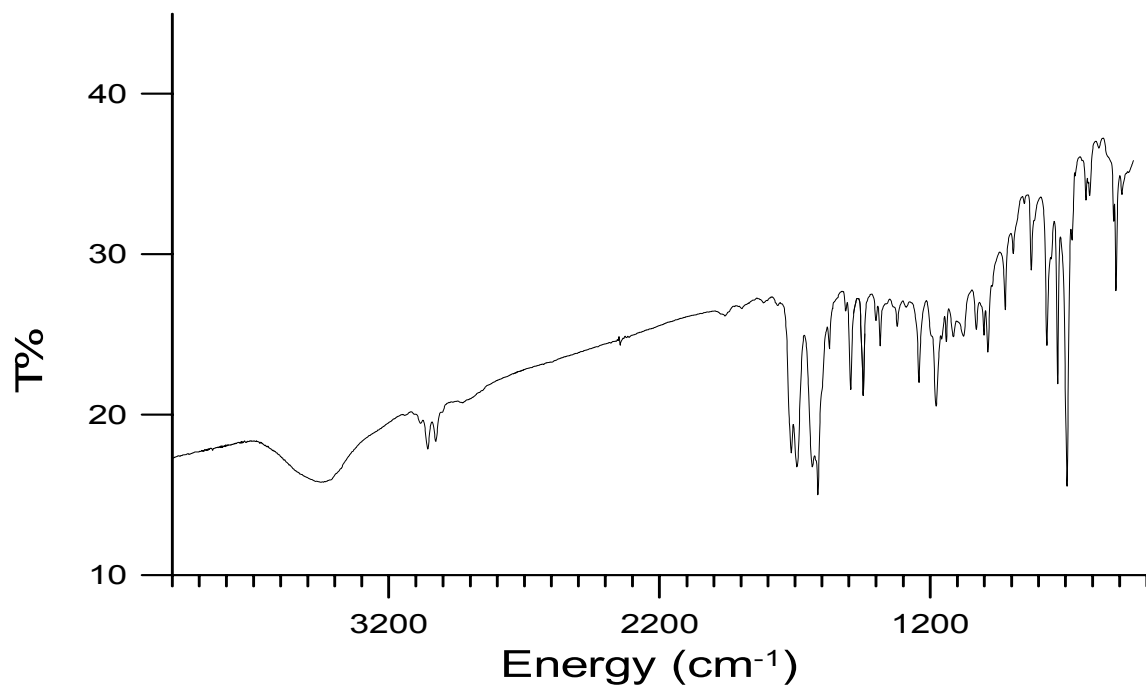


Figure B-6. 1dbcp_u

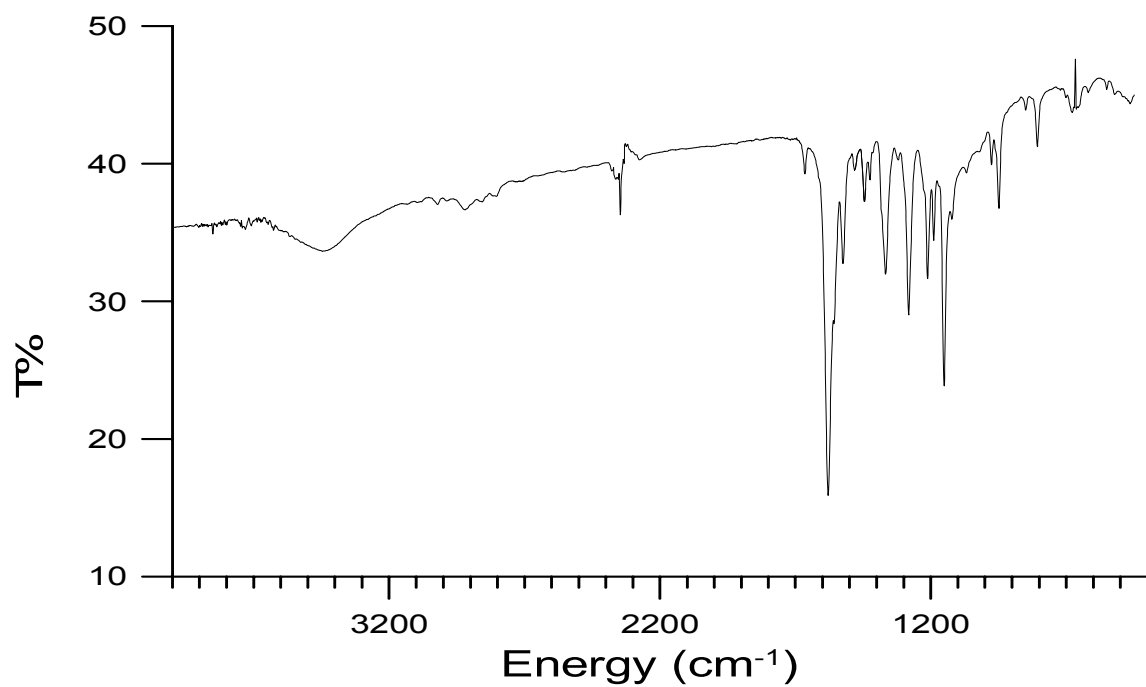


Figure B-7. 2dbma

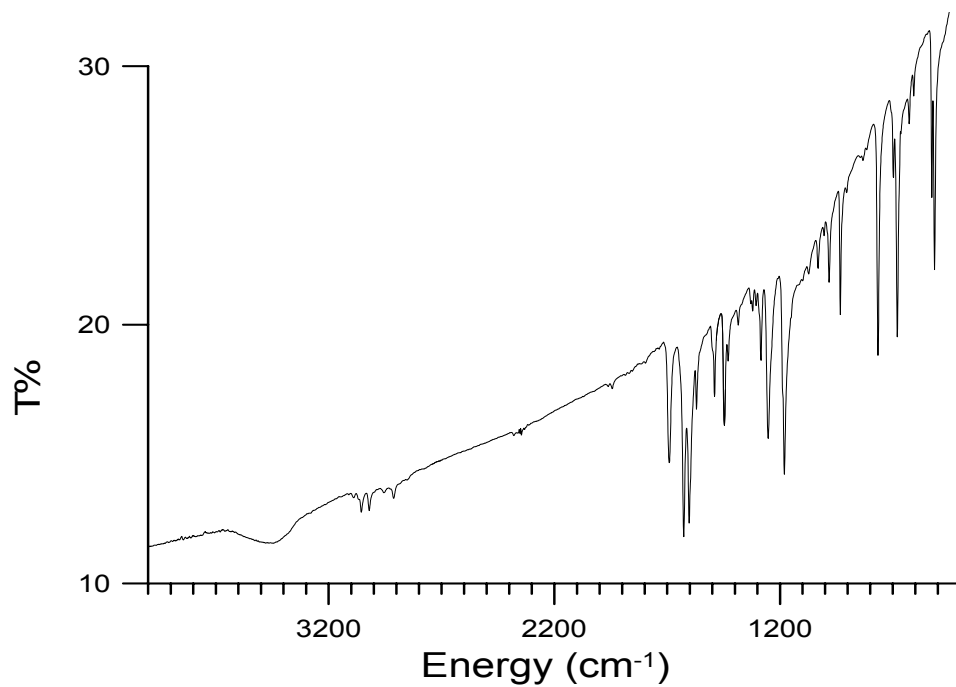


Figure B-8. 1dbcp of neutralized protonated cation

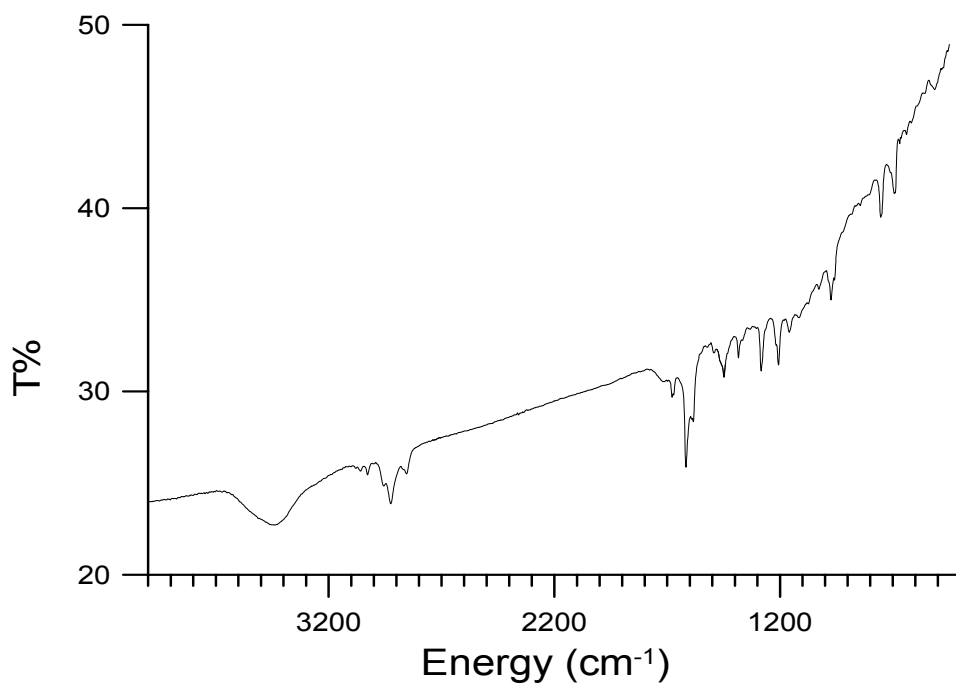


Figure B-9. 2dbcp of neutralized protonated cation

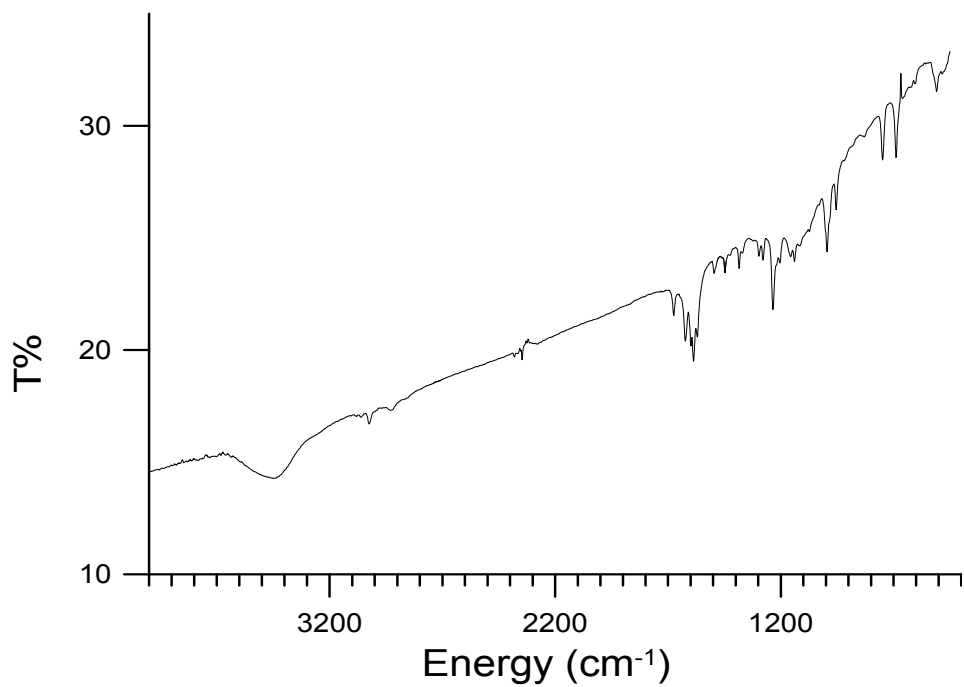


Figure B-10. 3dbcp of neutralized protonated cation

APPENDIX C

FLUORESCENCE SPECTRA CORRECTION FACTOR CALCULATION



DATA ANALYSIS

Cubic Spline Interpolation

N,N'-DMANB Corrected Fluorescence Standard For LS50B with RED Sensitive Phototube

This QuickSheet demonstrates Mathcad's **cspline**
and **interp** functions for connecting X-Y data.



Enter a matrix of X-Y data to be interpolated:

Corrected emission spectrum for N,N'-DMANB taken from J.R. Lakowicz, Principles of
Fluorescence Spectroscopy 2nd Ed.

data :=

22502.25	1.49
22251.89	2.01
22002.25	2.98

Click on the **Input Table** above until you see the handles, and
enlarge it to see the matrix **data** used in this example.

data := csort(data, 0) X := data⁽ⁱ⁾ Y := data^(j)

Spline coefficients:

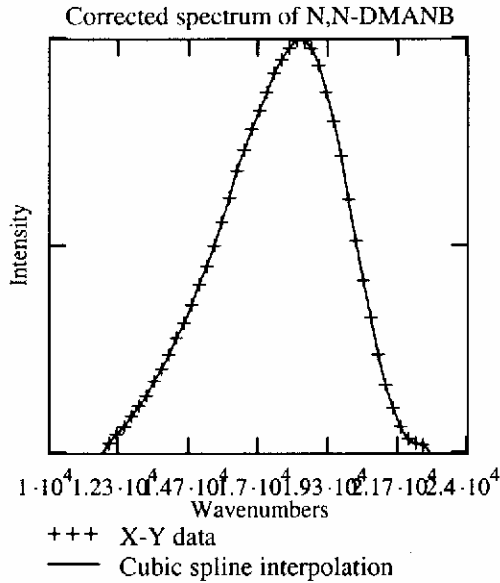
S := cspline(X, Y)

Fitting function:

fit(x) := interp(S, X, Y, x)

Sample interpolated values: $\text{fit}(14000) = 23.455$ $\text{fit}(13) = -1.117$
 $\text{fit}(18400) = 99.781$

$j := 12500, 12550.. 22200$



$j =$

$1.25 \cdot 10^4$
$1.255 \cdot 10^4$
$1.26 \cdot 10^4$
$1.265 \cdot 10^4$
$1.27 \cdot 10^4$
$1.275 \cdot 10^4$
$1.28 \cdot 10^4$
$1.285 \cdot 10^4$
$1.29 \cdot 10^4$
$1.295 \cdot 10^4$
$1.3 \cdot 10^4$
$1.305 \cdot 10^4$
$1.31 \cdot 10^4$
$1.315 \cdot 10^4$
$1.32 \cdot 10^4$
$1.325 \cdot 10^4$

$\text{fit}(j) =$

5.927
6.374
6.861
7.375
7.904
8.437
8.963
9.479
9.984
10.476
10.954
11.419
11.887
12.374
12.898
13.476

$$\int_{12500}^{22000} \text{fit}(x) dx = 4.972 \times 10^5$$

Fluorescence data for N,N-DMANB from LS50B corrected for bandpass by multiplying intensities by λ^2 and normalized to 100. RED sensitive phototube. Data copied from excel and insert>component>input table.. paste table from excel

$xdata :=$

	0	1
0	23529.41	1.05
1	23501.76	1.05

$xdata := \text{csort}(xdata, 0)$

$A := xdata^{(0)}$

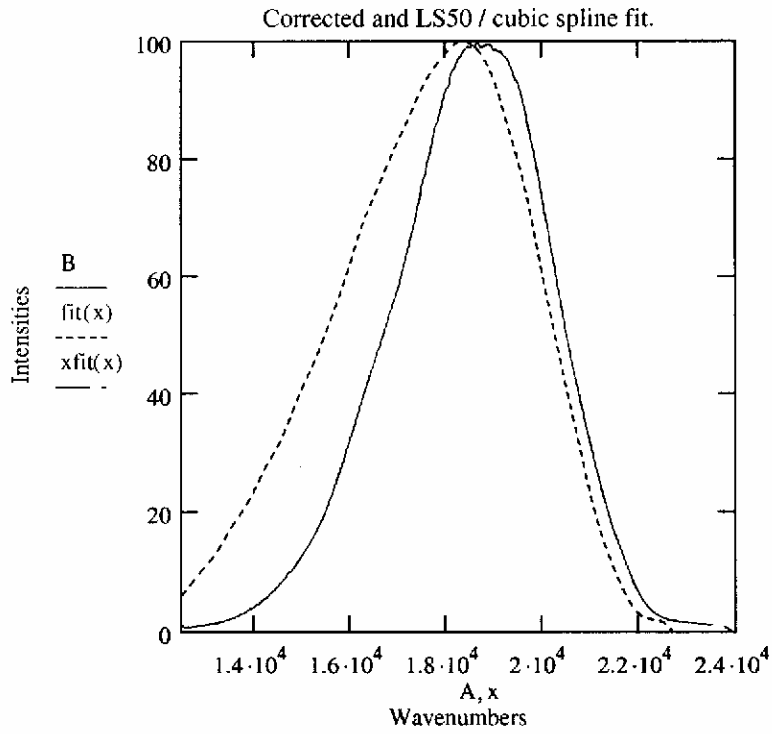
$B := xdata^{(1)}$

Spline coefficients:

$S := \text{cspline}(A, B)$

Fitting function:

$xfit(x) := interp(S, A, B, x)$



Determining correction factors at regular wavenumber intervals by dividing corrected spectral data by uncorrected spectral data.

$l := 13000, 13050..22200$

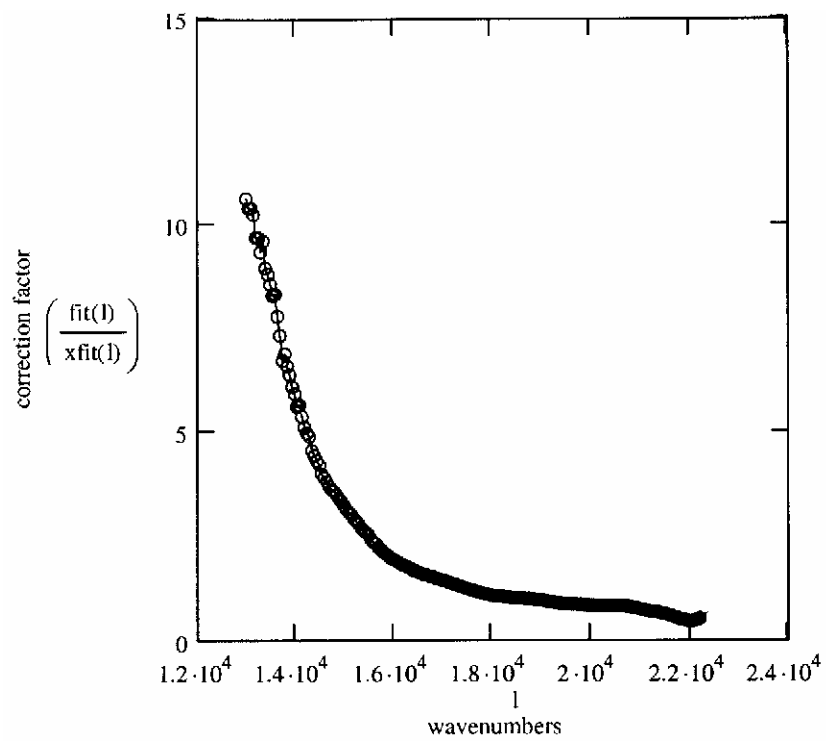
$l =$

$1.3 \cdot 10^4$
$1.305 \cdot 10^4$
$1.31 \cdot 10^4$
$1.315 \cdot 10^4$
$1.32 \cdot 10^4$

$xfit(l) =$

1.03
1.097
1.142
1.207

$\frac{(\text{fit}(l))}{(\text{xfit}(l))} =$
10.64
10.411
10.41
10.254
9.699



APPENDIX D

QUANTUM YIELD CALCULATION

Connors

Quantum yield determination for 2dbcp in Ethanol with
red sensitive tube.
experiment 2

This QuickSheet demonstrates Mathcad's **cspline**
and **interp** functions for connecting X-Y data.



Enter a matrix of X-Y data to be interpolated:

Enter spectral data for compound after converting to wavenumbers, multiplying intensity by
lambda squared DO NOT normalize intensity. Insert data from Excel -right key, paste table.

data :=

24096.39	1.13·10 ⁵
24067.39	1.13·10 ⁵
24038.46	1.15·10 ⁵
24009.6	1.13·10 ⁵

Click on the **Input Table** above until you see the handles, and
enlarge it to see the matrix **data** used in this example.

data := csort(data, 0)

X := data^{<0>}

Y := data^{<1>}

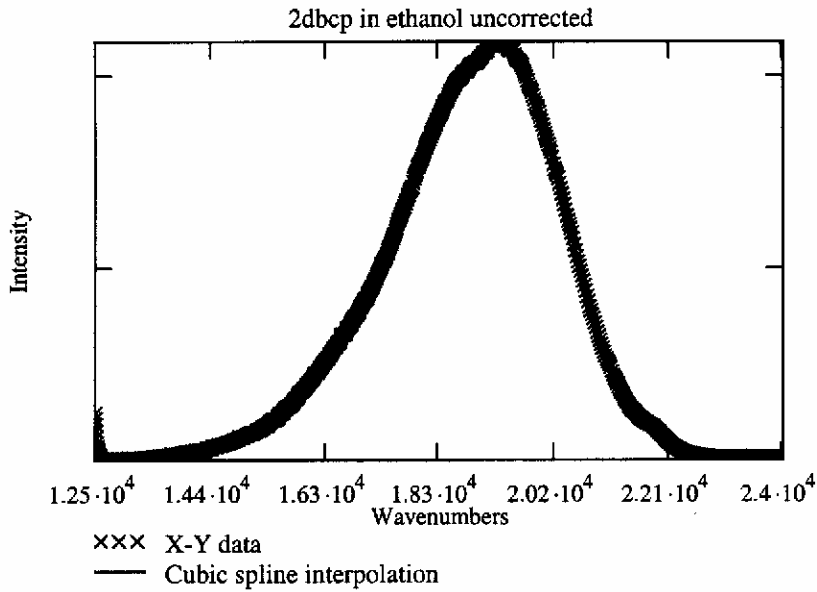
Spline coefficients:

S := cspline(X, Y)

Fitting function:

fit(x) := interp(S, X, Y, x)

Sample interpolated values: $\text{fit}(21000) = 5.735 \times 10^6$
 $\text{fit}(18800) = 2.067 \times 10^7$



Correction factors for LS50B with red sensitive tube

DATA Limits 13,000-22,100 Wavenumbers

corrdata :=

	0	1
0	13000	10.64
1	13050	10.41
2	13100	10.41

xdata := csort(corrdata,0)

A := corrdata⁽⁰⁾ B := corrdata⁽¹⁾

Spline coefficients:

S := cspline(A,B)

Fitting function:

Fitting function:

corrfit(x) := interp(S,A,B,x)

$\text{corrspec}(x) := \text{corrfit}(x) \cdot \text{fit}(x)$

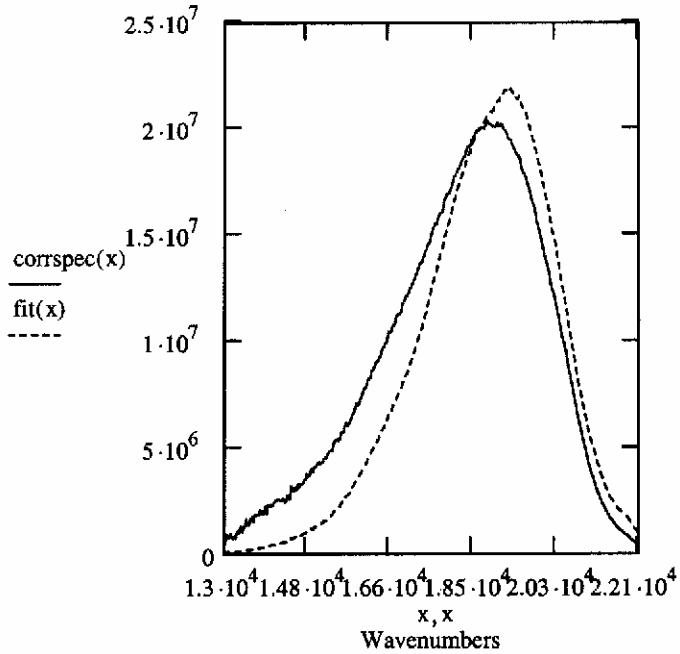
$l := 13000, 13050.. 22100$

$l =$

$1.3 \cdot 10^4$
$1.305 \cdot 10^4$
$1.31 \cdot 10^4$
$1.315 \cdot 10^4$

$\text{corrspec}(l) =$

$7.3 \cdot 10^5$
$8.456 \cdot 10^5$
$7.642 \cdot 10^5$
$8.237 \cdot 10^5$
$7.037 \cdot 10^5$



$$\int_{13000}^{22100} \text{fit}(x) dx = 7.548 \times 10^{10} \quad \int_{13000}^{22100} \text{corrspec}(x) dx = 8.272 \times 10^{10}$$

Enter a matrix of X-Y data to be interpolated:

Enter spectral data for standard (coumarin 481) after converting to wavenumbers, multiplying intensity by lambda squared DO NOT normalize intensities. Insert data from Excel -right key, paste table.

$\text{stdata} :=$

24096.39	$2.25 \cdot 10^5$
24067.39	$1.6 \cdot 10^5$
24038.46	$1.21 \cdot 10^5$

Click on the **Input Table** above until you see the handles, and enlarge it to see the matrix **data** used in this example.

```
stdata := csort(stdata, 0)
```

```
C := stdata<0>
```

```
D := stdata<1>
```

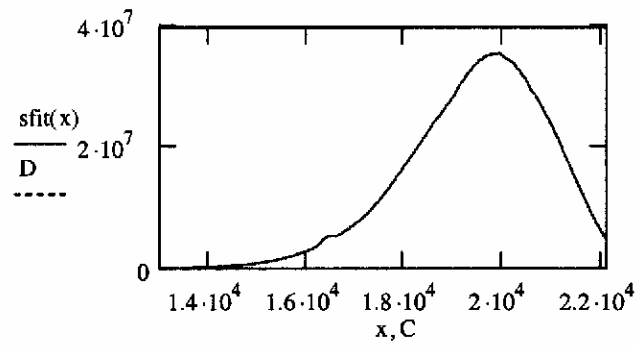
Spline coefficients:

```
S := cspline(C, D)
```

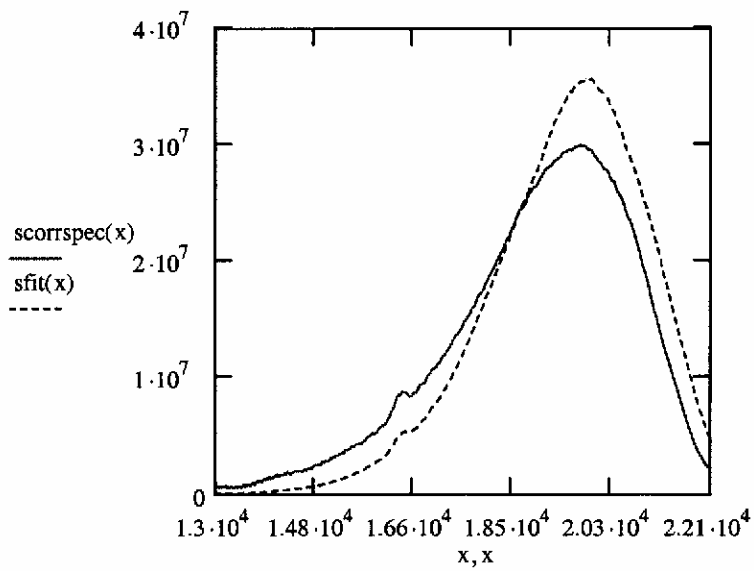
Fitting function:

```
sfit(x) := interp(S, C, D, x)
```

$$\text{sfit}(18000) = 1.708 \times 10^7$$



```
scorrspec(x) := corrfitt(x) \cdot (sfit(x))
```



Compound	Standard
$\int_{13000}^{22100} \text{corrspec}(x) dx = 8.272 \times 10^{10}$	$\int_{13000}^{22100} \text{scorrsec}(x) dx = 1.147 \times 10^{11}$

Area under corrected compound curve

Area under corrected standard curve

$D_c := \int_{13000}^{22100} \text{corrsec}(x) dx$	$D_s := \int_{13000}^{22100} \text{scorrsec}(x) dx$
$D_c = 8.272 \times 10^{10}$	$D_s = 1.147 \times 10^{11}$

	Compound	Standard
Absorbance at $\lambda(\text{ex})$	Ac := 0.057	As := 0.019
Index of refraction	EtOH	acetonitrile
	nc := 1.3614	ns := 1.3441
quantum yield of standard		QYs := 0.11

$$QY_c := QY_s \cdot \left(\frac{A_s}{A_c} \right) \cdot \left(\frac{nc}{ns \cdot ns} \right) \cdot \left(\frac{D_c}{D_s} \right)$$

$$QY_c = 0.027$$

$$QY_{\text{raw}} := QY_s \cdot \left(\frac{A_s}{A_c} \right) \cdot \left(\frac{nc}{ns \cdot ns} \right) \cdot \left(\frac{7561}{12240} \right)$$

$$QY_{\text{raw}} = 0.023$$

APPENDIX E

ABSORPTION SPECTRA

Figure E 1 1dbch

Figure E 2 2dbch

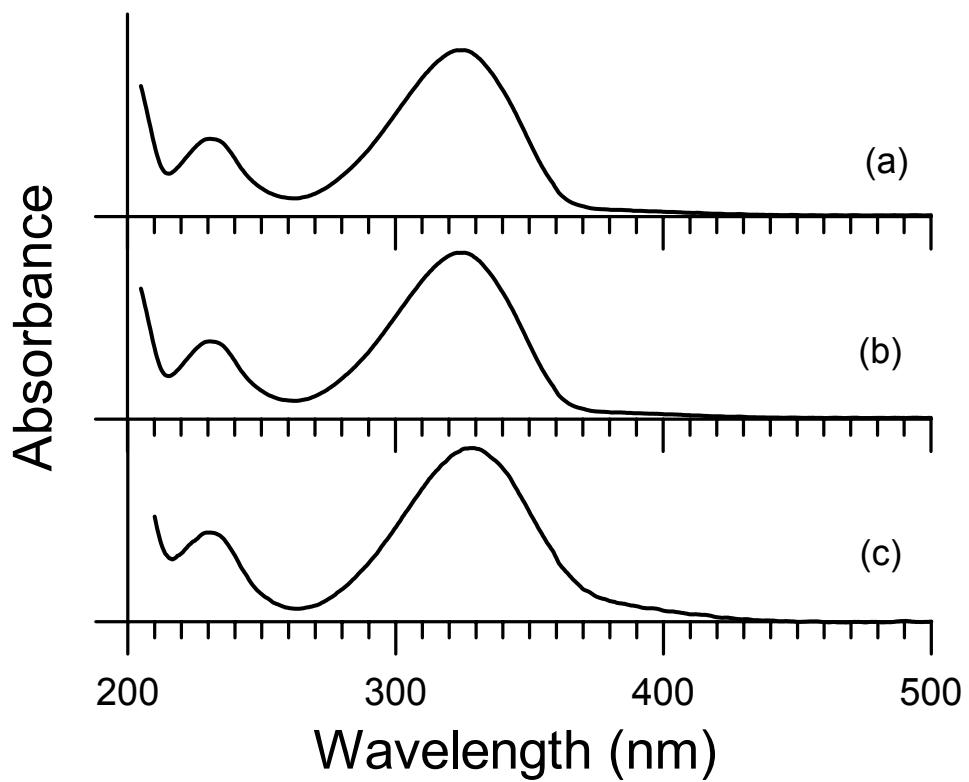


Figure E-1. Absorption spectra of 1dbch in (a) cyclohexane, (b) acetonitrile, (c) methanol.

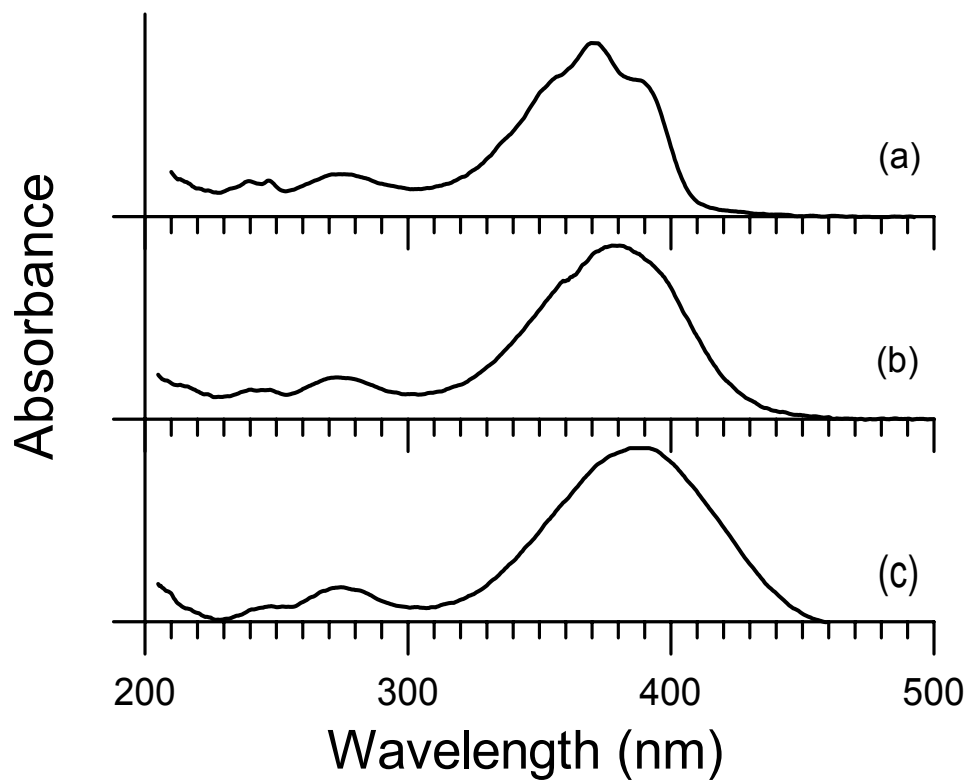


Figure E-2. Absorption spectra of 2dbch in (a) cyclohexane, (b) acetonitrile, (c) methanol.

APPENDIX F

PHOTOCHEMISTRY STUDY: UV-VIS ABSORPTION SPECTRA OF NON-IRRADIATED AND IRRADIATED 1DBCP IN THF BY HPLC

Figure F-1.

(a) Non irradiated, peak 1

(b) Non irradiated, peak 2

Figure F-2.

(a) 5 min irradiated, peak 1

(b) 5 min irradiated, peak2

Figure F-3.

(a) 45 min irradiated, peak 1

(a) 45 min irradiated, peak 2

Figure F-4.

(a) 60 min irradiated, peak 1

(b) 60 min irradiated, peak2

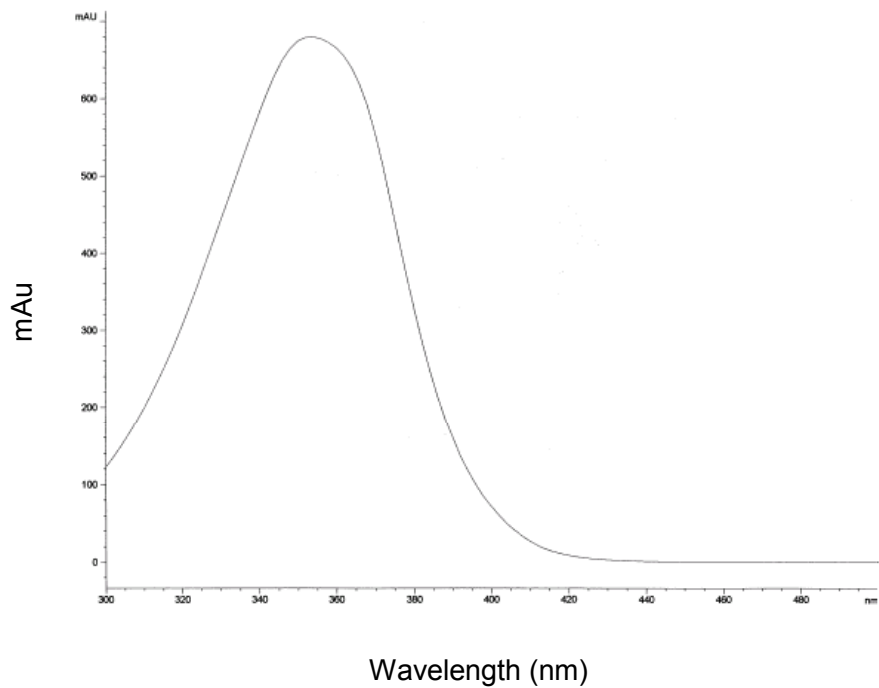


Figure F-1 (a) Non-irradiated. Retention time: 5.005 min, intensity: 679 mAu

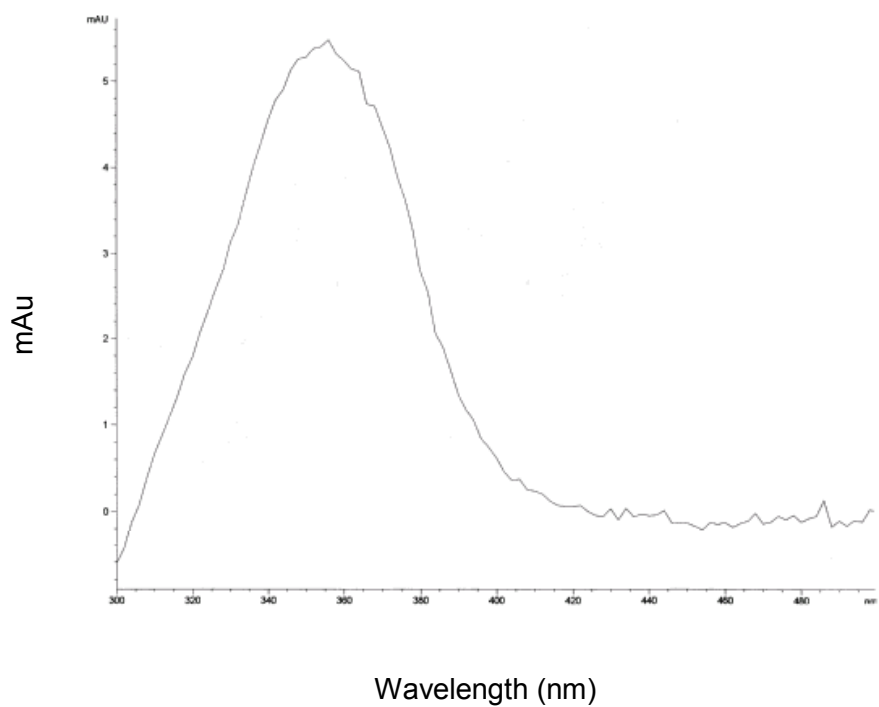


Figure F-1 (b) Non-irradiated. Retention time: 5.932 min, intensity 6.1 mAu

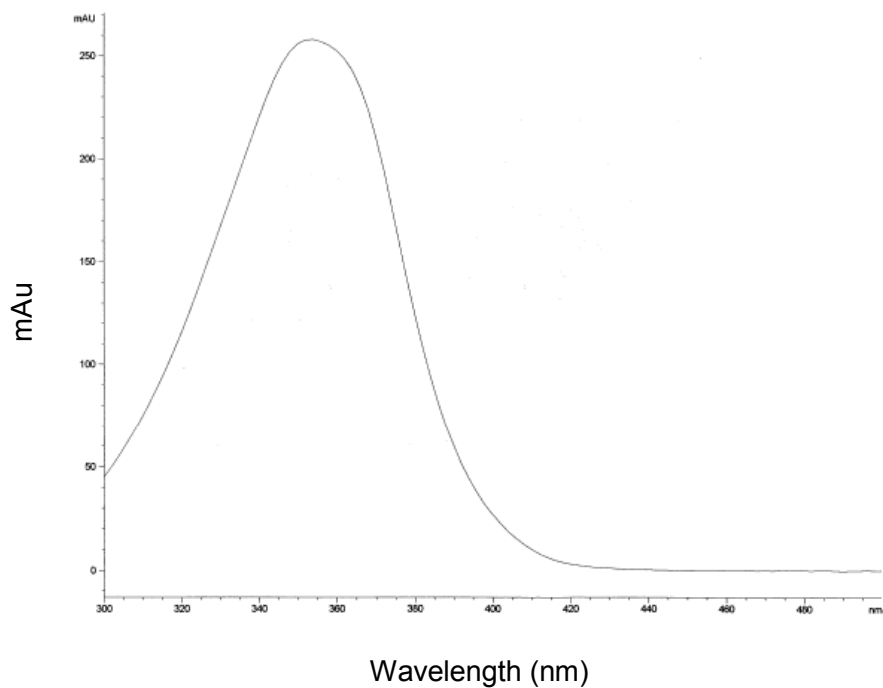


Figure F-2 (a) 5 min irradiated. Retention time: 4.989 min, intensity: 258 mAu

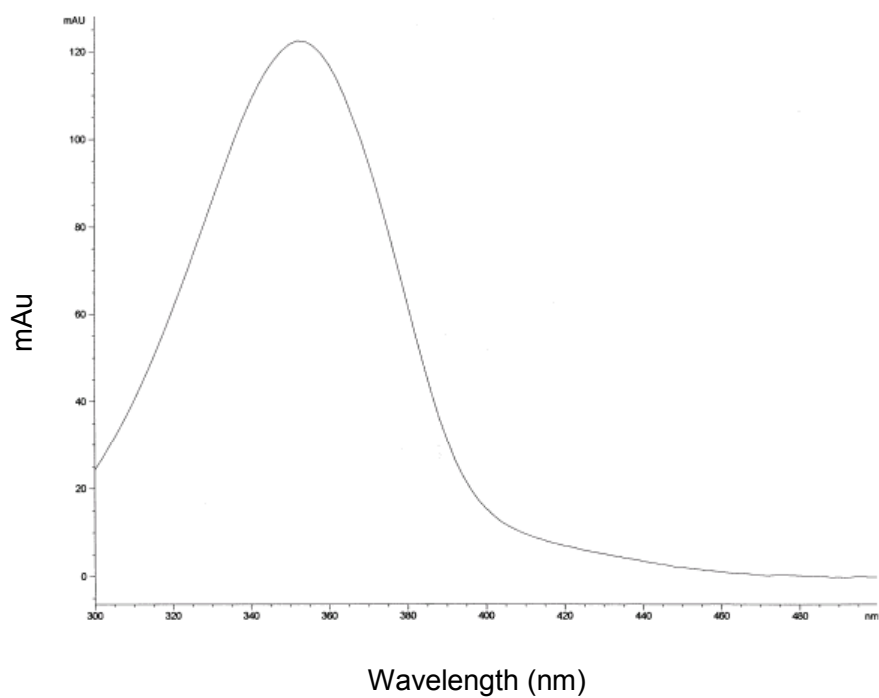


Figure F-2 (b) 5 min irradiated. Retention time: 5.929 min, intensity: 123 mAu

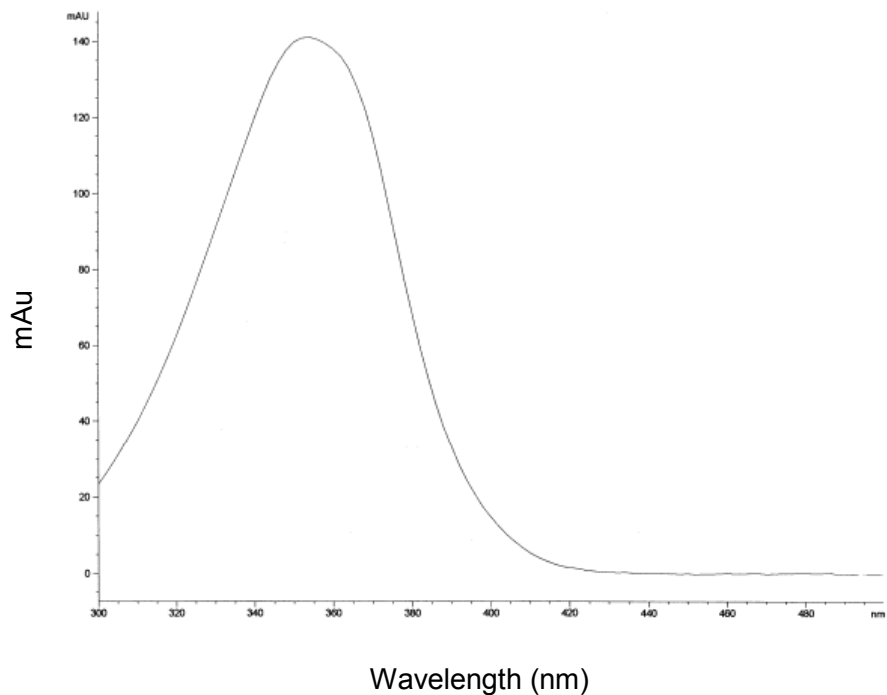


Figure F-3 (a) 45 min irradiated. Retention time: 4.998 min, intensity: 141 mAu

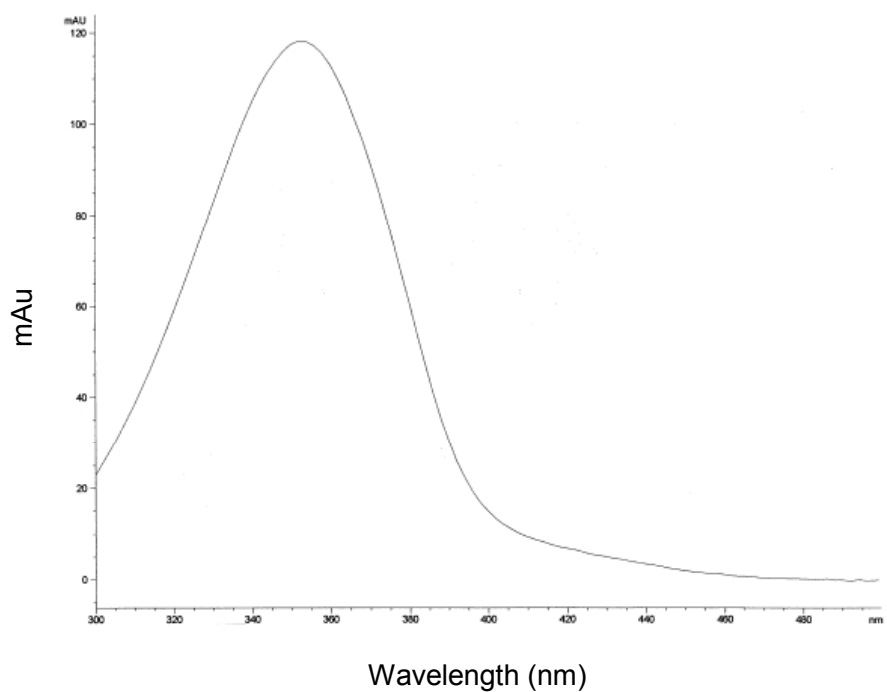


Figure F-3 (b) 45 min irradiated. Retention time: 5.945 min, intensity: 118 mAu

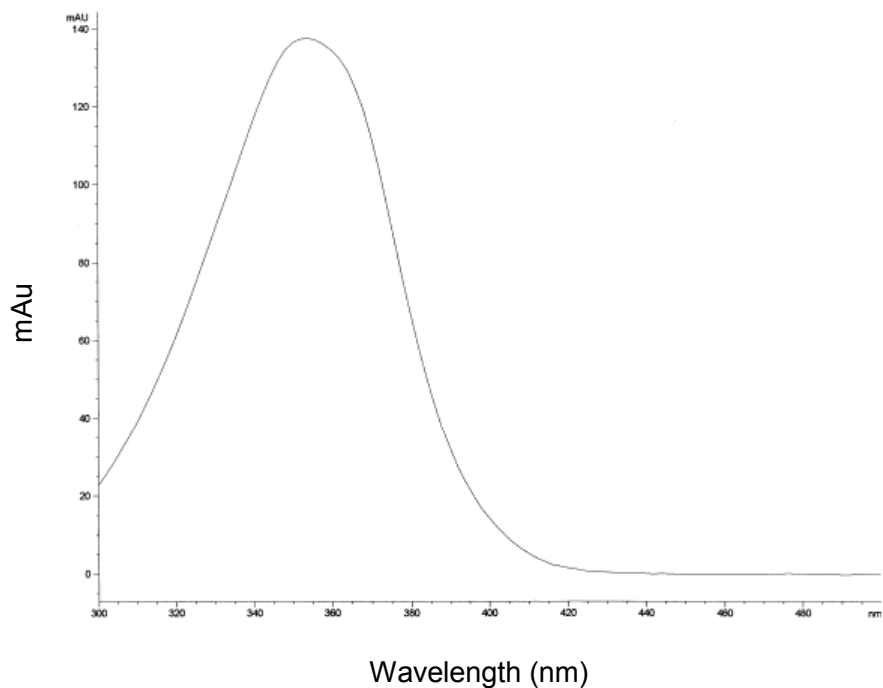


Figure F-4 (a) 60 min irradiated. Retention time: 4.995 min, intensity: 138 mAu

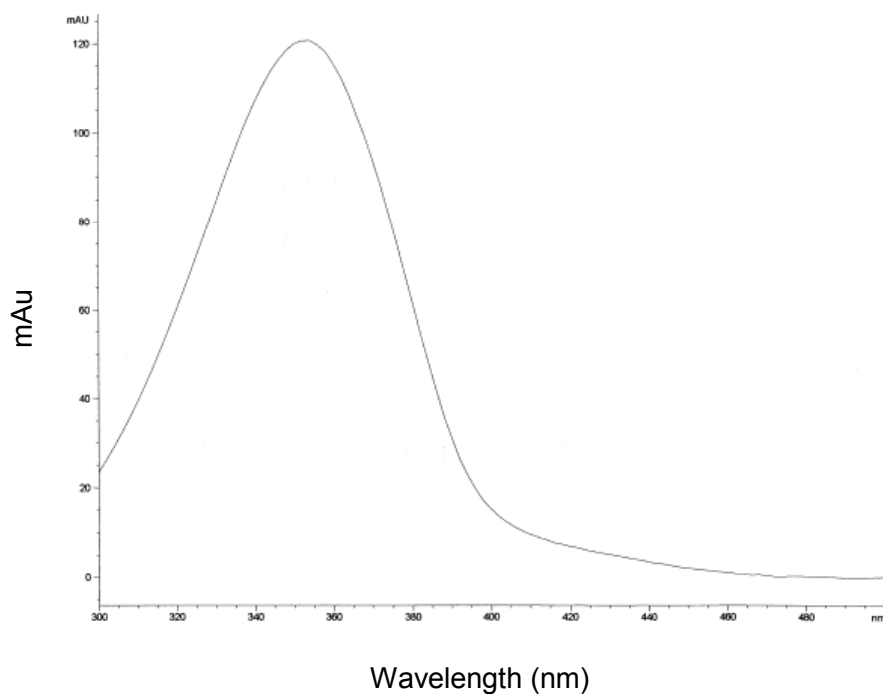


Figure F-4 (b) 60 min irradiated. Retention time: 5.942 min, intensity: 121 mAu

APPENDIX G

PHOTOCHEMISTRY STUDY: NEUTRALIZED 1DBCP-H⁺ IN THF

G-1) Impurity study by HPLC below 2 min retention time

G-2) UV-VIS absorption spectra corresponding to chromatography peaks

G-1) IMPURITY STUDY BY HPLC BELOW 2 MIN RETENTION TIME (294 nm)

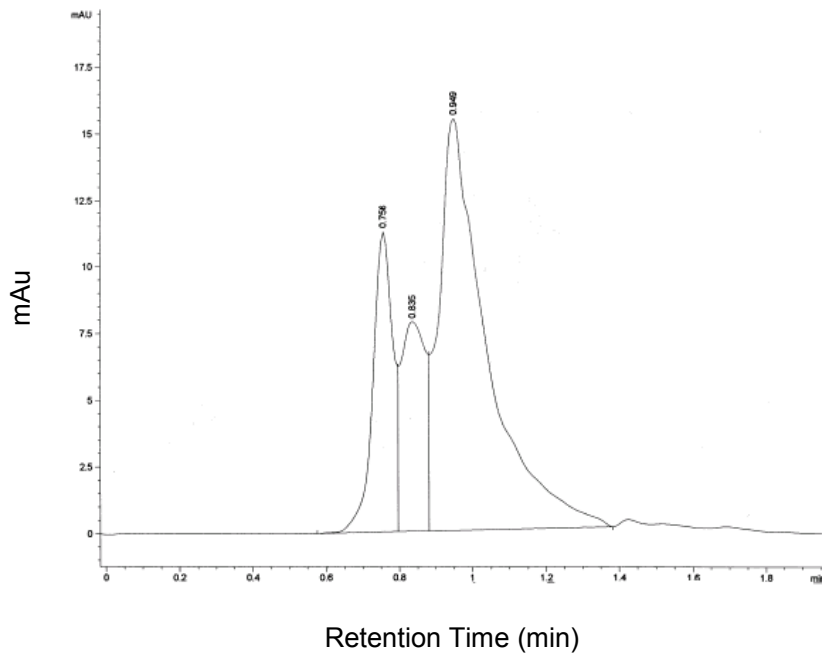


Figure G-1 (a) 1dbcp-H⁺ in THF non irradiated

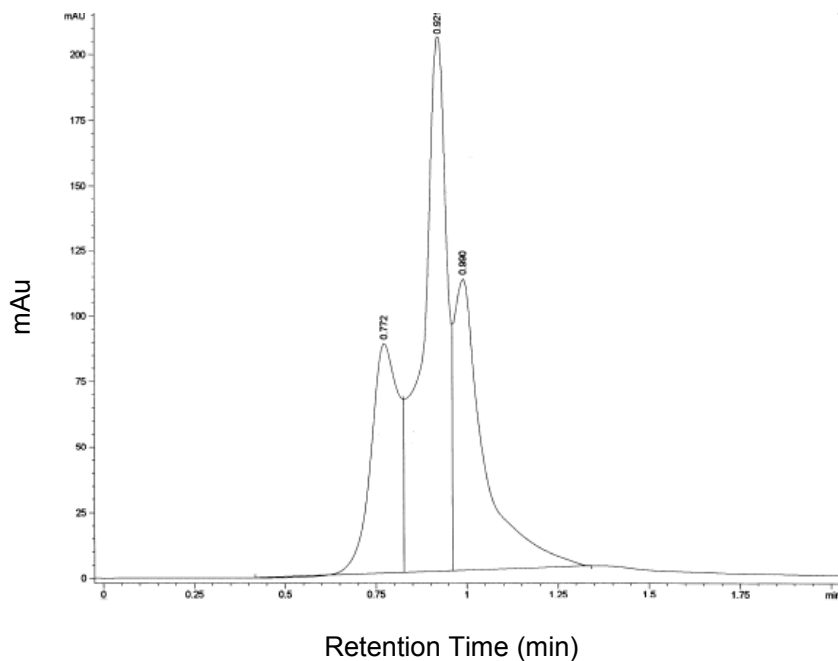


Figure G-1 (b) 1dbcp-H⁺ in THF 5 min irradiated

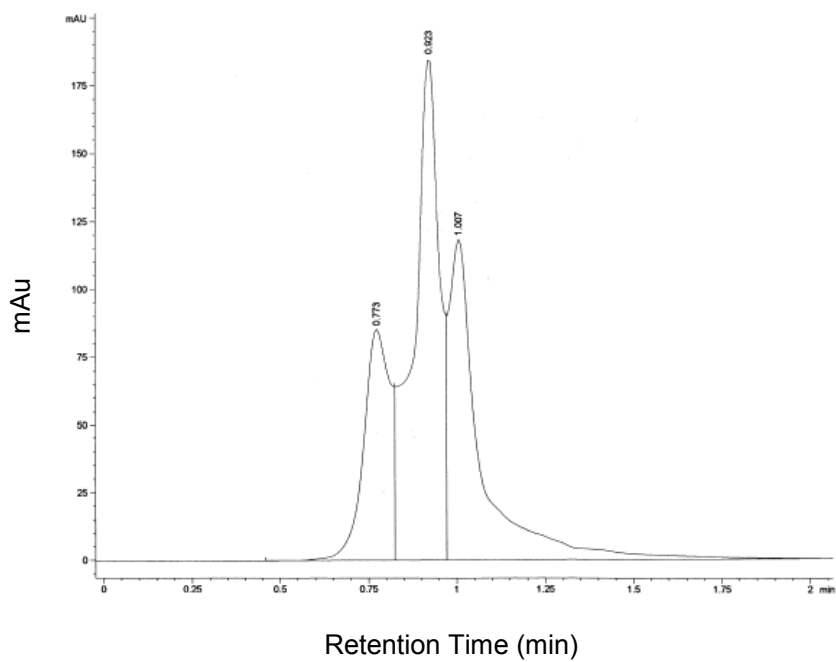


Figure G-1 (c) 1dbcp-H⁺ in THF 45 min irradiated

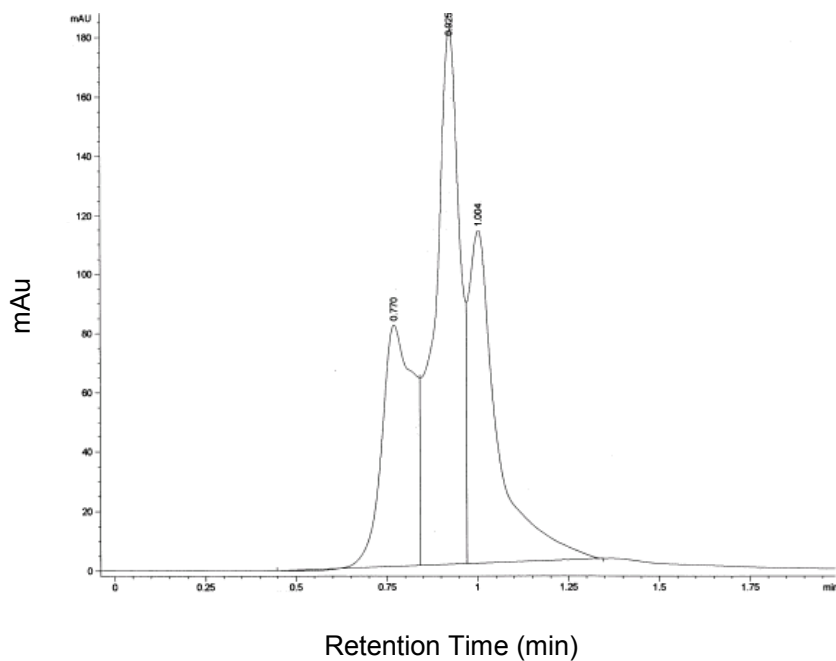


Figure G-1 (d) 1dbcp-H⁺ in THF 60 min irradiated

G-2) UV-VIS ABSORPTION SPECTRA CORRESPONDING TO HPLC PEAKS (60 MIN IRRADIATION, 290 NM)

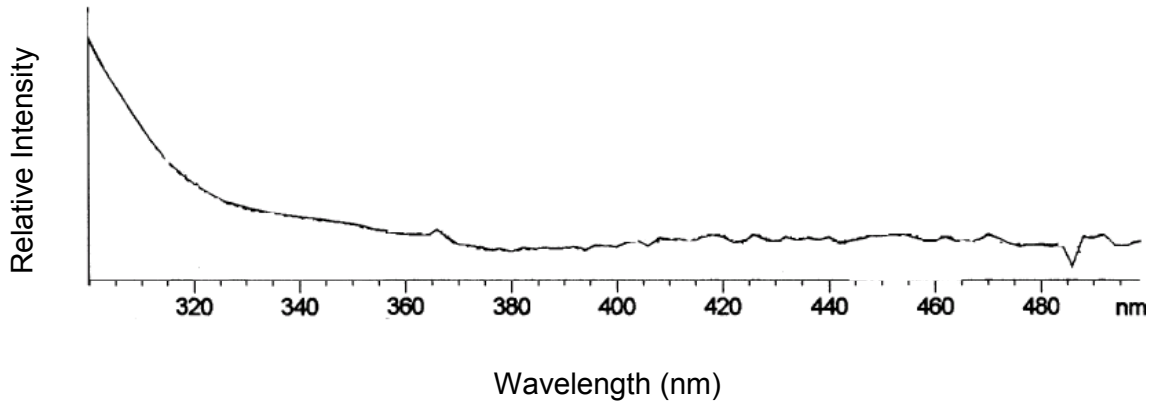


Figure G-2 (a) Peak at 0.770 min

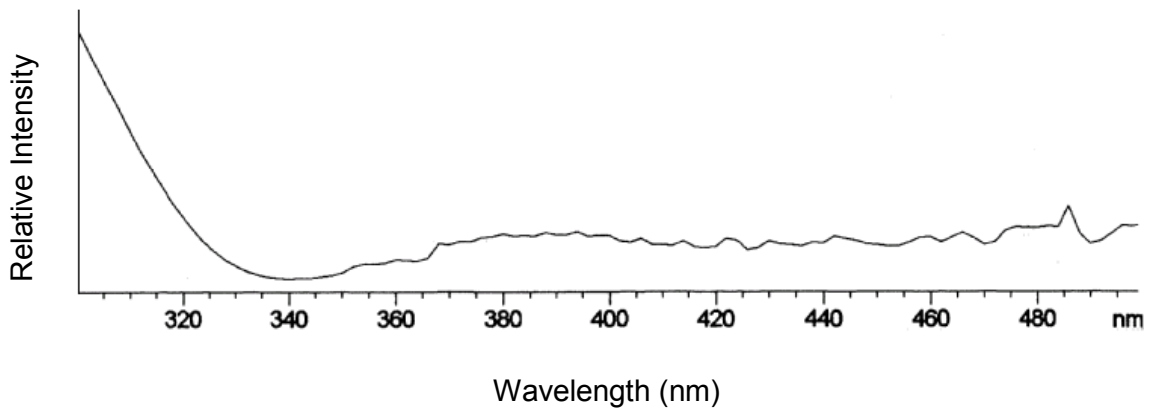


Figure G-2 (b) Peak at 0.925 min

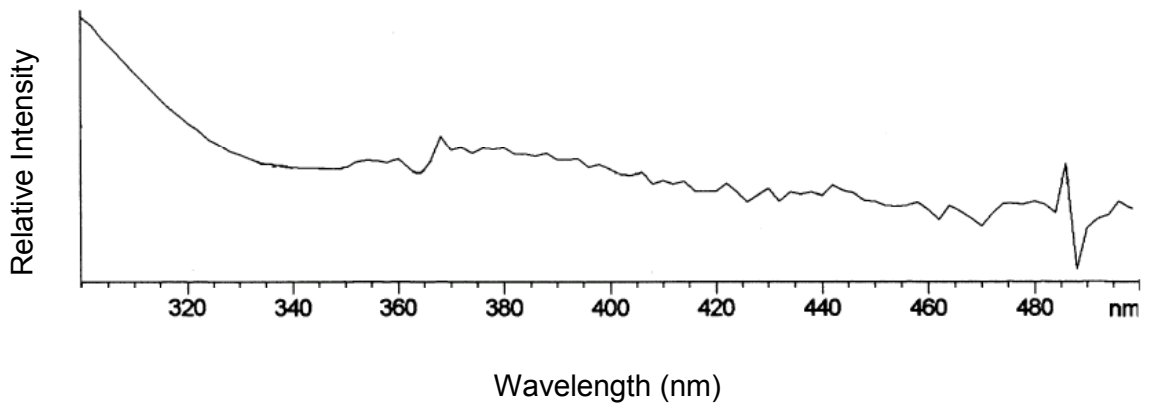


Figure G-2 (c) Peak at 1.004 min

APPENDIX H

HPLC METHOD INFORMATION

Method Information

1dbcp Total of 60 min-irradiated in THF, 3.0ml/min, 65%ACN (neutralized). Filtered through water.

Method Change History

Operator	Date	Change Information
	4/26/2002 9:44:18 PM	

Run Time Checklist

Pre-Run Cmd/Macro: off
Data Acquisition: on
Standard Data Analysis: on
Customized Data Analysis: off
Save GLP Data: on
Post-Run Cmd/Macro: off
Save Method with Data: on

```

=====
HP 1100 High Pressure Gradient Pump 1
=====

```

```

Control
  Flow           :      3.000 ml/min
  Stoptime      :      10.10 min
  Posttime      :      Off

Solvents
  Solvent A     :      35.0 % (Water)
  Solvent B     :      65.0 % (ACN)

PressureLimits
  Minimum Pressure :      0 bar
  Maximum Pressure :      400 bar

Auxiliary
  Maximal Flow Ramp :      100.00 ml/min^2
  Compressibility A :      50*10^-6/bar
  Minimal Stroke A  :      20 ul
  Compressibility B :      115*10^-6/bar
  Minimal Stroke B  :      Auto

Store Parameters
  Store Ratio A    :      Yes
  Store Ratio B    :      Yes
  Store Flow       :      Yes
  Store Pressure   :      Yes

Timetable is empty

```

```

=====
HP 1100 Diode Array Detector 1
=====

```

```

Signals

Signal  Store  Signal,Bw  Reference,Bw  [nm]
A:      Yes   408 4        Off

```

B:	Yes	345	4	600 100
C:	Yes	337	4	Off
D:	Yes	360	4	Off
E:	Yes	294	20	Off

Spectrum

Store Spectra	:	Apex + Baselines
Range from	:	300 nm
Range to	:	500 nm
Range step	:	2.00 nm
Threshold	:	0.00 mAU

Time

Stoptime	:	As pump
Posttime	:	Off

Required Lamps

UV lamp required	:	Yes
Vis lamp required	:	Yes

Autobalance

Prerun balancing	:	Yes
Postrun balancing	:	No
Margin for negative Absorbance: 100 mAU		

Peakwidth	:	> 0.1 min
Slit	:	2 nm

Analog Outputs

Zero offset ana. out. 1:	5 %
Zero offset ana. out. 2:	5 %
Attenuation ana. out. 1:	1000 mAU
Attenuation ana. out. 2:	1000 mAU

Timetable is empty

```

=====
                        HP 1100 Autosampler 1
=====

```

Injection

```

Injection Mode      : Standard
Injector volume    : 40.0 ul

Auxiliary
Drawspeed          : 200 ul/min
Ejectspeed         : 200 ul/min
Draw position      : 0.0 mm

Time
Stoptime           : As Pump
Posttime           : Off

```

```

=====
                        Integration Events
=====

```

Results will be produced with the standard integrator.

```

-----
                        Default Integration Event Table "Event"
-----

```

Event	Value	Time
Initial Area Reject	1.000	Initial
Initial Threshold	-2.000	Initial
Initial Peak Width	0.040	Initial
Initial Shoulders	OFF	Initial

```

-----
                        Signal Specific Integration Event Table "Event_DAD1A"
-----

```

Event	Value	Time
Initial Area Reject	1.000	Initial
Initial Threshold	-2.000	Initial
Initial Peak Width	0.040	Initial
Initial Shoulders	OFF	Initial
Baseline Now	0.000	0.790

 Signal Specific Integration Event Table "Event_DAD1C"

Event	Value	Time
Initial Area Reject	0.422	Initial
Initial Threshold	-1.315	Initial
Initial Peak Width	0.102	Initial
Initial Shoulders	OFF	Initial

 Signal Specific Integration Event Table "Event_DAD1B"

Event	Value	Time
Initial Area Reject	1.895	Initial
Initial Threshold	-1.377	Initial
Initial Peak Width	0.159	Initial
Initial Shoulders	OFF	Initial
Baseline Now	0.000	0.790

Apply Manual Integration Events: No

=====
 Specify Report
 =====

Destination: Printer, Screen
 Quantitative Results sorted by: Signal
 Report Style: Full
 Sample info on each page: Yes
 Add Chromatogram Output: Yes
 Chromatogram Output: Multi-Page (Landscape) on 1 Pages

=====
 Signal Options
 =====

Include: Axes, Retention Times, Baselines, Tick Marks
 Font: Arial, Size: 8

Ranges: Full
Multi Chromatograms: Overlaid, All the same Scale

=====
Calibration Table
=====

isocratic standard calibration

Calib. Data Modified : 4/14/2000 4:28:30 PM
Calculate : Height Percent
Rel. Reference Window : 5.000 %
Abs. Reference Window : 0.000 min
Rel. Non-ref. Window : 2.000 %
Abs. Non-ref. Window : 0.000 min
Uncalibrated Peaks : not reported
Partial Calibration : Yes, identified peaks are recalibrated
Correct All Ret. Times: No, only for identified peaks

Curve Type : Linear
Origin : Included
Weight : Equal

Recalibration Settings:
Average Response : Average all calibrations
Average Retention Time: Floating Average New 75%

Calibration Report Options :
Printout of recalibrations within a sequence:
Calibration Table after Recalibration
Normal Report after Recalibration
If the sequence is done with bracketing:
Results of first cycle (ending previous bracket)

Signal 1: DAD1 A, Sig=408,4 Ref=off
Signal 2: DAD1 B, Sig=345,4 Ref=600,100
Signal 3: DAD1 C, Sig=337,4 Ref=off
Signal 4: DAD1 D, Sig=360,4 Ref=off
Signal 5: DAD1 E, Sig=294,20 Ref=off

Peak Sum Table

=====
No Entries in table
=====

=====
Purity Options - HPLC 1100
=====

Options for enhanced Spectral / Peak Purity method

Reference Spectra

Manual: Ref1: 1.116 min

Wavelength Range

Full Range

Spectrum Normalization

Normalize : All the same Scale

Purity Options for data files with 'Peak Controlled' spectra

Spectra per Peak

All

Threshold : 0.00 mAU

Purity Threshold :

990.0000

Purity Options for data files with 'All' or 'All in Peak' spectra

Spectra per Peak

Automatic : 5

Threshold : 0.00 mAU

Purity Calculation Technique

Simple

Purity factor calculated with - Average Spectrum

Threshold curve

Calculated standard deviation of noise at 0.00 min with
14 spectra